Optimal Energy Management Strategy for a Fuel Cell Hybrid Electric Vehicle

PhD Thesis

by

Tom Fletcher
MEng (Hons) DIS

Submitted in partial fulfilment of the requirements for the award of
Degree of Doctor of Philosophy of Loughborough University

May 2017

Abstract

The Energy Management Strategy (EMS) has a huge effect on the performance of any hybrid vehicle because it determines the operating point of almost every component associated with the powertrain. This means that its optimisation is an incredibly complex task which must consider a number of objectives including the fuel consumption, drive-ability, component degradation and straight-line performance. The EMS is of particular importance for Fuel Cell Hybrid Electric Vehicles (FCHEVs), not only to minimise the fuel consumption, but also to reduce the electrical stress on the fuel cell and maximise its useful lifetime. This is because the durability and cost of the fuel cell stack is one of the major obstacles preventing FCHEVs from being competitive with conventional vehicles.

In this work, a novel EMS is developed, specifically for Fuel Cell Hybrid Electric Vehicles (FCHEVs), which considers not only the fuel consumption, but also the degradation of the fuel cell in order to optimise the overall running cost of the vehicle. This work is believed to be the first of its kind to quantify effect of decisions made by the EMS on the fuel cell degradation, inclusive of multiple causes of voltage degradation. The performance of this new strategy is compared in simulation to a recent strategy from the literature designed solely to optimise the fuel consumption. It is found that the inclusion of the degradation metrics results in a 20% increase in fuel cell lifetime for only a 3.7% increase in the fuel consumption, meaning that the overall running cost is reduced by 9%.

In addition to direct implementation on board a vehicle, this technique for optimising the degradation alongside the fuel consumption also allows alternative vehicle designs to be compared in an unbiased way. In order to demonstrate this, the novel optimisation technique is subsequently used to compare alternative system designs in order to identify the optimal economic sizing of the fuel cell and battery pack. It is found that the overall running cost can be minimised by using the smallest possible fuel cell stack that will satisfy the average power requirement of the duty cycle, and by using an oversized battery pack to maximise the fuel cell efficiency and minimise the transient loading on the stack.

This research was undertaken at Loughborough University as part of the Doctoral Training Centre (DTC) in Hydrogen, Fuel Cells and Their Applications in collaboration with the University of Birmingham and Nottingham University and with sponsorship from HORIBA-MIRA (Nuneaton, UK). A Microcab H4 test vehicle has been made available for use in testing for this research which was previously used for approximately 2 years at the University of Birmingham. The Microcab H4 is a small campus based vehicle designed for passenger transport and mail delivery at low speeds as seen on a university campus. It has a top speed of approximately 30mph, and is fitted with a 1.2kW fuel cell and a 2kWh battery pack.

Acknowledgements

I would like to express my deepest gratitude to my supervisor, Prof. Rob Thring, for his constant guidance and mentoring throughout my time as a research student and for agreeing to continue to supervise me despite his imminent retirement. In particular, I would like to thank Rob for allowing me the freedom to follow through with the ideas that I had during my early research and giving me guidance on how to follow through with the research that I wanted to do.

This work would not have been possible without the guidance, expertise and financial support of my industrial sponsor, HORIBA-MIRA Ltd.. In particular, I would like to thank my industrial supervisor, Martin Watkinson, for his constant feedback and the direction to ensure that my research is still relevant to the real world and ensuring that I do not always constrain myself to the academic "bubble". Martin has constantly provided feedback on all of my research and has had a considerable influence on the direction of my work. In addition to Martin, I would like to express my gratitude to Derek Charters, who sadly passed away early this year. Derek was especially good at thinking outside of the box, and his opinions have certainly influenced the work presented in this thesis.

There are a substantial number of other supporting players in the production of this work and it would not be possible to mention them all by name. However, I would also like to thank Microcab and the University of Birmingham for providing the test vehicle used during the production of my vehicle model, Dr. Matt Lintern, and Dr. Iain Staffell for providing me with drive cycle data, without which this work would not have been possible and Steve Horner for access to the chassis dynamometer and giving me the support I needed to perform vehicle testing. I must also thank Dr. Thomas Steffen and Dr. Christopher Vagg for providing me with their expert opinions on the techniques that I have used.

I would like to express my sincere gratitude the unfaltering moral and emotional support that I have received from my family. My loving parents, David and Linda, have done nothing but nurture and support my inquisitive nature, making any number of personal sacrifices to ensure that I had the best education and a safe and happy upbringing; for this I am enormously grateful. Like my wife, Laura, they have been through all of the highs, and helped me through all of the lows that I have experienced over the past 4 years.

Finally, I must make a special mention for Laura herself for putting up with a boyfriend and now a husband who has insisted on remaining a student until past his 30th birthday. Laura has put up with me working late nights, weekends and even travelling to the other side of the world to present at a conference while she stays at home and looks after our son, Alex. More than anyone, Laura has been with me through the excitement of a successful day, the frustration of a bad one, and most importantly the seemingly unending sleepless nights associated with the final months of my PhD while raising a toddler. Without her support, this work would not have been possible.

Contents

Abstract **i**

Acknowledgements **ii**

Figures **x**

Tables **xi**

Nomenclature **xii**

Acronyms **xv**

1 Introduction **1**
1.1 Overview . . . 2
1.2 The Requirement for Low Carbon Vehicles . . . 6
1.3 Background . . . 9
1.3.1 A Brief History of Fuel Cell Vehicles . . . 9
1.3.2 Current Challenges for Fuel Cell Vehicles . . . 11
1.4 Test Vehicles - Microcab H4 and Microcab H2EV . . . 15
1.5 Energy Management Strategy (EMS) . . . 16
1.6 Research Aims and Objectives . . . 17
1.7 Contributions . . . 18
1.8 Thesis Format . . . 19
1.9 Publications . . . 20

2 Literature Review **21**
2.1 System Design . . . 22
2.1.1 Fuel Cells . . . 22
2.1.2 Batteries . . . 22
2.1.3 Capacitors . . . 24
2.1.4 DC/DC Converters . . . 24
2.1.5 Component Sizing . . . 25
2.1.6 Summary . . . 27
2.2 EMS Requirements . . . 28
2.2.1 Fuel Economy . . . 28
2.2.1.1 EMS Strategy Examples . . . 30
2.2.1.2 Summary . . . 30

2.2.2 Fuel Cell Degradation . . . 32
2.2.2.1 Catalyst Layer . . . 32
2.2.2.2 Membrane Layer . . . 33
2.2.2.3 Gas Diffusion Layer (GDL) . . . 34
2.2.2.4 Low-Level Controller . . . 35
2.2.2.5 EMS Strategy Examples . . . 35
2.2.2.6 Summary . . . 36
2.2.3 Battery Degradation . . . 38
2.2.3.1 Lead Acid Batteries . . . 38
2.2.3.2 Lithium-ion Batteries . . . 40
2.2.3.3 EMS Strategy Examples . . . 41
2.2.3.4 Summary . . . 41
2.2.4 Drive-ability . . . 44
2.2.4.1 Gear Shifts . . . 44
2.2.4.2 Power Availability . . . 45
2.2.4.3 Summary . . . 46
2.2.5 Conclusions . . . 47
2.3 EMS Techniques . . . 50
2.3.1 Heuristic Controllers . . . 51
2.3.1.1 "Rule-Based" Controllers . . . 51
2.3.1.2 State Based Controllers . . . 52
2.3.1.3 Equivalent Consumption Minimization Strategy (ECMS) 53
2.3.1.4 Summary . . . 55
2.3.2 Machine Learning Techniques . . . 56
2.3.2.1 Neural Networks . . . 57
2.3.2.2 Deterministic Dynamic Programming (DDP) . . . 57
2.3.3 Stochastic Dynamic Programming (SDP) . . . 61
2.3.3.1 Infinite Horizon Markov Decision Process (MDP) . . . 62
2.3.3.2 Finite Horizon MDP using Commuting Time Estimation 62
2.3.3.3 Terminal State MDP . . . 63
2.3.3.4 SDP Summary . . . 64
2.3.4 Game Theory (GT) . . . 64
2.3.5 Model Predictive Control (MPC) . . . 64
2.3.6 Summary . . . 65
2.4 Conclusions . . . 67
2.4.1 Research Questions . . . 69

3 Vehicle Model 71
3.1 Model Based Design (MBD) . . . 72
3.2 Test Vehicles . . . 73
3.2.1 Microcab H4 . . . 73
3.2.2 Microcab H2EV . . . 76
3.3 Model Architecture . . . 77
3.3.1 Reduced Model . . . 78
3.4 Simulation Plant Model . . . 80
3.4.1 Vehicle Model . . . 80

3.4.1.1 Reduced Model . . . 81
3.4.1.2 Characterisation . . . 81
3.4.2 Motor & Driveline . . . 83
3.4.2.1 Reduced Model . . . 84
3.4.2.2 Characterisation . . . 85
3.4.3 Battery Pack . . . 87
3.4.3.1 Characterisation . . . 88
3.4.4 DC/DC Converter . . . 91
3.4.4.1 Reduced Model . . . 91
3.4.4.2 Characterisation . . . 92
3.4.5 Fuel Cell . . . 94
3.4.5.1 Reduced Model . . . 95
3.4.5.2 Model Validation . . . 95
3.5 Control System Models . . . 99
3.5.1 Drive-cycle Reference . . . 99
3.5.2 "Driver" Model . . . 99
3.5.3 EMS Supervisory Controller . . . 100
3.5.3.1 "Thermostatic" Controller . . . 100
3.5.3.2 Battery Voltage Controller . . . 100
3.5.3.3 Stochastic Dynamic Programming (SDP) Controller . . . 101
3.6 Summary . . . 101

4 Markov Chain Modelling of Duty Cycle 103
4.1 Introduction . . . 104
4.1.1 Other Practical Uses of the Markov Model . . . 105
4.2 Data Logging . . . 106
4.3 Data Processing . . . 107
4.3.1 Initial Processing . . . 107
4.3.2 Identify and Extract Individual Trips . . . 108
4.3.3 Post Processing . . . 110
4.3.3.1 SAFD Analysis . . . 111
4.3.4 Analysis of Identified Trips . . . 112
4.3.4.1 SAFD Comparison . . . 114
4.3.4.2 Summary . . . 116
4.4 Probability Matrix Generation . . . 117
4.4.1 Discretizing the Data . . . 117
4.4.2 Results . . . 121
4.4.3 Terminal State . . . 123
4.5 Validation . . . 124
4.5.1 SAFD Analysis . . . 128
4.6 Conclusions . . . 129
4.6.1 Suitability for EMS Development . . . 130
4.6.2 Suitability for Other Practical Uses . . . 131

5 Controller Development **133**
5.1 Introduction . . . 134
5.2 MDP Problem Definition . . . 136
5.2.1 Input Grid Resolution . . . 137
5.2.2 Cost Function . . . 138
5.2.2.1 Fuel Consumption . . . 139
5.2.2.2 Fuel Cell Degradation . . . 139
5.2.2.3 Battery State of Charge (SoC) Maintenance . . . 140
5.2.2.4 Final Cost Function . . . 141
5.2.3 Probability & Cost Matrix Generation . . . 142
5.2.3.1 Battery SoC Estimation . . . 143
5.2.3.2 Cost Calculation . . . 143
5.2.3.3 Simulation Output . . . 143
5.2.3.4 Computational Efficiency . . . 144
5.3 SDP Solution . . . 145
5.3.1 Mathematical Description . . . 146
5.3.1.1 Infinite Horizon . . . 146
5.3.1.2 Terminal State . . . 147
5.4 SDP Parameter Selection . . . 148
5.4.1 Discount Factor Selection . . . 148
5.4.2 Number of Policy Evaluations . . . 149
5.4.3 Convergence Criteria . . . 149
5.4.4 Summary . . . 149
5.5 Example Policy . . . 150

6 Strategy Simulation & Analysis **153**
6.1 Testing Procedure . . . 154
6.1.1 Weighting Factors - Hydrogen and Fuel Cell Stack Cost . . . 154
6.1.2 Controller Design . . . 155
6.1.2.1 Baseline Controller - Current Microcab Strategy . . . 155
6.1.2.2 Minimal Fuel Consumption (MFC) Controller . . . 155
6.2 1.2kW Fuel Cell . . . 156
6.2.1 Baseline Strategy . . . 157
6.2.2 MFC Strategy . . . 159
6.2.3 Degradation Inclusive (DI) Strategy . . . 162
6.2.4 Comparison and Summary . . . 164
6.3 4.8kW Fuel Cell . . . 168
6.3.1 Baseline Strategy . . . 168
6.3.2 MFC Strategy . . . 171
6.3.3 DI Strategy . . . 173
6.3.4 Comparison & Summary . . . 176

7 Optimisation of Hybrid Component Sizes **183**
7.1 Introduction . . . 184
7.2 Sweep of Fuel Cell Maximum Power . . . 185
7.2.1 SoC Sustenance . . . 186
7.2.2 Fuel Consumption . . . 189

7.2.3 Fuel Cell Lifetime . . . 191
7.2.3.1 Transient Degradation . . . 192
7.2.3.2 Operating Point Degradation . . . 192
7.2.3.3 Cycling Degradation . . . 193
7.2.4 Running Cost . . . 194
7.2.4.1 Sensitivity to Fuel Cell Cost . . . 196
7.2.5 Summary . . . 198
7.3 Effect of Battery Capacity . . . 199
7.3.1 SoC Sustenance . . . 200
7.3.2 Fuel Consumption . . . 202
7.3.3 Fuel Cell Lifetime . . . 204
7.3.3.1 Transient Degradation . . . 205
7.3.3.2 Operating Point Degradation . . . 206
7.3.3.3 Cycling Degradation . . . 206
7.3.4 Running Cost . . . 207
7.3.5 Summary . . . 208
7.4 Conclusions . . . 210

8 Conclusions and Further Work 213
8.1 Summary . . . 214
8.2 Optimal Control of the Microcab H4 . . . 215
8.2.1 1.2kW Fuel Cell . . . 216
8.2.2 4.8kW Fuel Cell . . . 217
8.2.3 Key Findings . . . 218
8.3 System Design Using Optimal Control . . . 219
8.3.1 Key Findings . . . 220
8.4 Research Questions . . . 222
8.5 Conclusions . . . 226
8.6 Recommendations for Further Work . . . 228
8.6.1 Development of the Strategy . . . 228
8.6.2 Applications of the Strategy . . . 229

References 239

Appendix A Drive-cycle Trip Analysis Plots 241

List of Figures

1.1 Vehicle curb weight sensitivity to the Battery Electric Vehicle (BEV) range depending on various driving cycles, considering a compact car (C segment vehicle) - *Eberle et al.* [1] . . . 3
1.2 Hydrogen Tank Packaging in GM HydroGen4 - *Eberle et al.* [1] . . . 4
1.3 Estimated Oil Production - "Best Guess" Scenario - *Mohr et al.* [2] . . . 6
1.4 1966 General Motors (GM) Electrovan Fuel Cell System Layout - *Qin et al.* [3] 9
1.5 2015 Toyota Mirai - *Vehicle Sales Brochure* . . . 11
1.6 The Microcab H4 FCHEVs at the University of Birmingham - *Kendall et al.* [4] 15

2.1 Fuel cell efficiency vs. load - *Rousseau et al.* [5] . . . 28
2.2 Sankey diagram showing the average efficiency of the Microcab powertrain - *Iain Staffell* [6] . . . 29
2.3 Major Causes of Electro-Chemical Active Surface Area ("ECASA") Reduction 33
2.4 Major Causes of Membrane Degradation . . . 34
2.5 End of Life Lead Acid Battery Grid - *Ruetschi* [7] . . . 38
2.6 Drive-ability Metrics, Pisu *et al.* [8] . . . 44
2.7 Strategy Flowchart - *Xiong et al.* [9] . . . 53

3.1 Microcab Electrical Powertrain Schematic . . . 73
3.2 Microcab Mechanical Powertrain Schematic . . . 74
3.3 Detailed Model Outline . . . 77
3.4 Reduced Model Outline . . . 78
3.5 Forward Facing Vehicle Model . . . 80
3.6 Backwards Facing Vehicle Model . . . 81
3.7 Coast-down Test . . . 82
3.8 Motor & Driveline Model . . . 83
3.9 Reduced Motor & Driveline Model . . . 84
3.10 Motor & Driveline Efficiency Map . . . 85
3.11 Motor Model Validation . . . 86
3.12 Battery Model . . . 87
3.13 Battery Voltage Estimation . . . 89
3.14 Battery Test Data . . . 90
3.15 DC/DC Converter Model . . . 91
3.16 DC/DC Converter Model . . . 92
3.17 DC/DC Converter Test Data . . . 93
3.18 DC/DC Converter Output Power vs. Input Power . . . 93
3.19 Fuel Cell Model . . . 94

3.20 Fuel Cell Model . . . 95
3.21 Fuel Cell Test Data . . . 95
3.22 Fuel Cell Polarisation Curve . . . 96
3.23 Fuel Cell Test Data . . . 97
3.24 Fuel Cell Polarisation Curve . . . 98
3.25 "Driver" Model . . . 99
3.26 "Thermostatic" EMS Controller . . . 100
3.27 Voltage EMS Controller . . . 100
3.28 SDP EMS Controller . . . 101

4.1 Forward facing simulation of the Microcab H4 over the New European Driving Cycle (NEDC) . . . 104
4.2 Grounds and Gardens Raw Collected Data . . . 107
4.3 Grounds and Gardens Processed Data . . . 109
4.4 Grounds and Gardens False Positive . . . 110
4.5 Microcab Mail Room Trip Analysis . . . 112
4.6 Loughborough Grounds & Gardens Trip Analysis . . . 113
4.7 Loughborough Mail Room Vehicle Refuelling . . . 114
4.8 Loughborough Mail Room Data with Refuelling Journeys Removed . . . 114
4.9 Example Markov Chain Drive-cycle Model . . . 117
4.10 Discretization at Initial Speed = 5ms^{-1} and Initial Acceleration = 0ms^{-2} . . . 118
4.11 Discretization at Initial Speed = 12ms^{-1} and Initial Acceleration = -1ms^{-2} . . . 120
4.12 State Transition Probability Matrix - Loughborough Mail Room Cycle (5ms^{-1}) 121
4.13 State Transition Probability Matrix - Loughborough Mail Room Cycle (12ms^{-1}) 122
4.14 Terminal State Transition Probability - Loughborough Mail Room Cycle . . . 123
4.15 Randomly Generated Drive-cycle Comparison . . . 124
4.16 Statistical Comparison for Loughborough Mail Room Cycle using Rounding Discretization Method . . . 125
4.17 Statistical Comparison for Loughborough Mail Room Cycle using Interpolation Discretization Method . . . 126
4.18 Statistical Comparison for Loughborough Mail Room Cycle using Gaussian Discretization Method . . . 127

5.1 Flowchart of the procedure used to generate the real-time controller . . . 135
5.2 EMS Controller Structure - Simulink Model . . . 135
5.3 Probability & Cost Simulation Steps . . . 142
5.4 Policy Example . . . 150

6.1 Test Journey . . . 156
6.2 Accumulated Running Cost for the Current Microcab Controller (1200W) . . . 157
6.3 Transient loading due to reactive fuel cell load (1200W) . . . 157
6.4 Accumulated Running Cost for the Fuel Only Optimised Controller (1200W) 159
6.5 Detailed Comparison of baseline and MFC Strategies . . . 160
6.6 Accumulated Running Cost for the Degradation Inclusive Optimised Controller (1200W) . . . 162
6.7 Cost Comparison (1200W), Left Bar = Baseline, Middle = MFC, Right = DI . . . 164
6.8 Range Comparison (1200W) . . . 165

6.9 Fuel Consumption Comparison (1200W) . . . 166
6.10 Estimated Lifetime Comparison (1200W) . . . 166
6.11 Accumulated Running Cost for the Current Microcab Controller (4800W) . 168
6.12 Baseline Controller Energy Management (4800W) . . . 169
6.13 Accumulated Running Cost for the Fuel Only Optimised Controller (4800W) 171
6.14 Accumulated Running Cost for the Degradation Inclusive Optimised Controller (4800W) . . . 173
6.15 Detailed Comparison of MFC and DI Strategies . . . 174
6.16 Fuel Consumption Comparison (4800W) . . . 176
6.17 Range Comparison (4800W) . . . 177
6.18 Cost Comparison (4800W), Left Bar = MFC, Right = DI . . . 178
6.19 Estimated Lifetime Comparison (4800W) . . . 179

7.1 SoC Sustenance vs. Fuel Cell Size . . . 186
7.2 Minimum, Maximum and Initial SoC vs. Fuel Cell Size . . . 188
7.3 Fuel Consumption vs. Fuel Cell Size . . . 189
7.4 Fuel Cell Degradation vs. Fuel Cell Size . . . 191
7.5 Running Cost vs. Fuel Cell Size . . . 195
7.6 Running Cost vs. Fuel Cell Size (assuming lower rate of cycling degradation) 197
7.7 SoC Sustenance vs. Battery Capacity . . . 200
7.8 Fuel Consumption vs. Battery Capacity . . . 202
7.9 Fuel Cell Degradation vs. Battery Capacity . . . 204
7.10 Running Cost vs. Fuel Cell Size . . . 207

A.1 Loughborough Electrical Trip Analysis . . . 241
A.2 Loughborough Mail Room Trip Analysis . . . 242
A.3 Loughborough Security Trip Analysis . . . 242
A.4 Loughborough Teaching Support Trip Analysis . . . 243
A.5 Microcab Teaching Support Trip Analysis . . . 243
A.6 Microcab Testing Trip Analysis . . . 244

List of Tables

2.1 EMS Strategy Concerns for Limiting Fuel Cell Degradation 37
2.2 EMS Strategy Concerns for Limiting Battery Degradation 43
2.3 EMS Strategy Concerns for Drive-ability 46
2.4 Primary EMS Strategy Objectives 49

3.1 Vehicle Specification 81
3.2 Motor and Driveline Specification 85
3.3 Battery Pack Specification 89
3.4 Battery Pack Model Coefficients 89
3.5 DC/DC Converter Specification 92

4.1 Summary Logged Campus Vehicle Data 106
4.2 SAFD Agreement Between Duty Cycle Types (%) 115
4.3 SAFD Agreement Between Duty Cycle Types with Limited Speed (%) . . . 115
4.4 SAFD Agreement for Each Discretization Method (%) 128

5.1 Controller State Definition 137
5.2 PEM Fuel Cell Degradation Rates (per cell) 140

6.1 Performance Summary for the Current Microcab Controller (1200W) . . . 158
6.2 Performance Summary for the Fuel Only Optimised Controller (1200W) . . 161
6.3 Performance Summary for the Degradation Inclusive Optimised Controller (1200W) 163
6.4 Performance Summary for the Current Microcab Controller (4800W) . . . 170
6.5 Performance Summary for the Fuel Only Optimised Controller (4800W) . . 172
6.6 Performance Summary for the Degradation Inclusive Optimised Controller (4800W) 175

7.1 Controller State Definition 184
7.2 Fuel Cell Sweep Values 185
7.3 Battery Capacity Sweep Values 199

Nomenclature

α	Battery Voltage Penalty [-]
β	Road Gradient [rad]
γ_f	Monetary Value of Fuel [$/kg]
γ_{FC}	Monetary Value of Fuel Cell [$]
Γ	Instantaneous Cost [$]
Γ_f	Fuel Cost [$]
Γ_{FC}	Fuel Cell Cost [$]
Γ_t	Total Cost [$]
Γ_V	Battery Voltage Penalty [$]
ζ	Equivalence Factor [-]
η_b	Battery Efficiency [%]
η_{DC}	DC/DC Converter Efficiency [-]
η_E	Engine Efficiency [%]
η_m	Motor Efficiency [%]
λ	Discount Factor [-]
$\pi(S_t)$	Control Action in State, S [-]
π^*	Optimal Control Action [-]
ρ	Air Density [kgm^{-3}]
ω	Rotational Speed [rads^{-1}]
ω_E	Engine Speed [rads^{-1}]
ω_m	Motor Speed [rads^{-1}]
ω_w	Wheel Speed [rads^{-1}]
A	Set of Possible Actions [-]
a	Action Index [-]
A_d	Coefficient of Rolling Resistance [-]
A_f	Frontal Area of Vehicle [m^2]
B_d	Coefficient of Rolling Resistance [-]
c	Capacitance [F]
C_d	Aerodynamic Drag Coefficient [-]
C_n	Normalised Battery Capacity [Ah]
C_p	Peukert Capacity [-]
$D_{FC,c}$	Cycling Degradation [μV]
$D_{FC,l}$	Transient Load Degradation [μV]
$D_{FC,p}$	Operating Point Degradation [μV]
D_{max}	Degradation Limit [μV]
E	Expected Cost [$]
F	Absolute Depth of Discharge [Ah]
f	Relative Depth of Discharge [%]
F_A	Aerodynamic Drag Force [N]
F_B	Braking Force [N]
F_a	Inertial Drag Force [N]
F_d	Total Drag Force [N]
F_w	Tractive Force [N]
F_I	Incline Drag Force [N]
F_R	Rolling Resistance Force [N]
G	Gear Shift Indicator [-]
g	Gravitational Acceleration [9.81ms^{-2}]
H	Battery State of Charge [-]
H_K	Final Battery State of Charge [-]
H_T	Target Battery State of Charge [-]
I_{bat}	Battery Current [A]
$I_{DC,in}$	DC/DC Conv. Input Current [A]
$I_{DC,out}$	DC/DC Conv. Output Current [A]
I_{FC}	Fuel Cell Current [A]
I_m	Motor Current [A]
J	Cost [-]
J_π	Cost Given Control Policy, π [-]
J_t	Instantaneous Cost [-]
K	Final Time Step Index [-]
k	Time Step Index [-]
k_f	SoC Voltage Coefficient [-]
k_s	Shepherd Coefficient [-]
m	Vehicle Mass [kg]
m_e	Equivalent Vehicle Mass [kg]

m_f	Fuel Mass [kg]
$\dot{m}_f$	Mass Flow Rate of Fuel [kgs^{-1}]
N	Design Constant [-]
N_ω	Number of Wheel Speed Indices [-]
N_{cyc}	Max. Number of Cycles [-]
NOx	NOx Emissions [%]
N_P	Number of Power Indices [-]
n_p	Peukert's Exponent [-]
P_b	Battery Power [W]
P_{dem}	Demanded Power by Driver [W]
P_E	Engine Power [W]
P_{EMS}	EMS Power Demand [W]
P_{FC}	Fuel Cell Net Power [A]
PM	Particulate Matter [ppm]
P_m	Motor Power [W]
r_g	Gear Ratio [-]
R_i	Internal Resistance [Ω]
r_r	Rolling Radius of Wheel [m]
S	Set of Vehicle States [-]
S_0	Initial State [-]
S_k	State at time step, k [-]
T	Set of Decision Epochs [-]
t	Time [s]
T_b	Braking Torque [Nm]
T_{dem}	Driver's Torque Demand [Nm]
T_E	Engine Torque [Nm]
T_m	Motor Torque [Nm]
u	Optimal Control Policy [-]
V	Voltage [V]
v	Vehicle Speed [ms^{-1}]
V_{bat}	Battery Voltage [V]
$V_{bat,0}$	Battery Voltage at Open-Circuit [V]
$V_{DC,in}$	DC/DC Conv. Input Voltage [V]
$V_{DC,out}$	DC/DC Conv. Output Voltage [V]
V_{FC}	Fuel Cell Voltage [V]
V_m	Motor Voltage [V]
V_{max}	Upper voltage limit [V]
V_{min}	Lower voltage limit [V]
W	Weighting Factor [-]
W_G	Gearshift Weighting Factor [-]
W_H	SoC Weighting Factor [-]
W_{NOx}	NOx Weighting Factor [-]
W_{PM}	PM Weighting Factor [-]

Acronyms

A-ECMS Adaptive Equivalent Consumption Minimization Strategy 215
BEV Battery Electric Vehicle 74
CMAC Cerebellar Model Arithmetic Computer 57
CD Charge-Depleting 148
CS Charge-Sustaining 148
DDP Deterministic Dynamic Programming 104
DI Degradation Inclusive 216
DoD Depth of Discharge 87
DoE Department of Energy 194
DTC Doctoral Training Centre i
DPF Diesel Particulate Filter 7
ECASA Electro-Chemical Active Surface Area 214
ECMS Equivalent Consumption Minimization Strategy 215
ECU Electronic Control Unit 45
EMS Energy Management Strategy 214
FCHEV Fuel Cell Hybrid Electric Vehicle 214
FMEA Failure Mode and Effects Analysis 32
GDL Gas Diffusion Layer 32
GFRP Glass-Fibre Reinforced Plastic 75
GM General Motors 214
GPS Global Positioning System 103
GT Game Theory 226
HEV Hybrid Electric Vehicle 21
HIL Hardware-in-the-Loop 229
ICCT International Council on Clean Transportation 12
ICE Internal Combustion Engine 216
ITS Intelligent Transport System 229
MBD Model Based Design 72
MDP Markov Decision Process 133
MEA Membrane Electrode Assembly 32
MFC Minimal Fuel Consumption 216
MIRA Motor Industry Research Association 81
MPC Model Predictive Control 226
MTTF Mean Time To Failure 48

NASA The National Aeronautics and Space Administration 9
NEDC New European Driving Cycle 230
NiMH Nickel Metal-Hydride 23
NYCC New York City Cycle 104
NN Neural Network 69
PI Proportional Integral 77
PID Proportional Integral Differential 57
PEM Proton Exchange Membrane 76
PM Particulate Matter 7
RECMS Rule-Based Equivalent Consumption Minimization Strategy 54
RHE Reversible Hydrogen Electrode 33
SAFD Speed-Acceleration Frequency Distribution 226
SDP Stochastic Dynamic Programming 215
SEI Solid Electrolyte Interface 40
SLI Starter Lighter Ignition 23
SOFC Solid Oxide Fuel Cell 76
SoC State of Charge 215
SP-SDP Shortest Path Stochastic Dynamic Programming 145
SUV Sport Utility Vehicle 62
UAV Unmanned Aerial Vehicle 21

Chapter 1

Introduction

This chapter presents an overview of the subject area of fuel cell hybrid electric vehicles and the motivation for research in this field. The benefits of this type of powertrain over conventional vehicle powertrains are described, and the areas for further development are highlighted. At the end of the chapter, the scope of the project is defined and an outline of the report is given along with a list of the specific contributions made.

1.1 Overview

The prime motivation for the development of Fuel Cell Hybrid Electric Vehicles (FCHEVs) is a reduction of the transport industry's current reliance on limited fossil fuel resources. Until recently, almost every vehicle on the road relied exclusively on an Internal Combustion Engine (ICE) converting the chemical energy contained within a fossil fuel into kinetic energy. Not only are fossil fuels a limited resource, but on combustion they produce harmful emissions such as carbon monoxide (CO), carbon dioxide (CO_2) and oxides of nitrogen (NO_x). These gases have been shown to have a harmful effect on the environment on a global scale. To compound the issue, demand for personal transportation has increased dramatically over the past 20 years due to world population increase and the trend is set to continue as developing countries such as China, India and Mexico continue to expand [10]. Fuel cells offer the benefit that they are able to use a renewable energy source, and produce no harmful emissions from the vehicle, whilst still being able to compete with conventional powertrains in terms of performance, range and ease-of-use.

Through consumer awareness and taxation incentives, the automotive industry is experiencing ever-increasing pressure to produce more energy efficient and less polluting vehicles in order to combat these issues. Over the past two decades, increasingly stringent legislation and rising fossil fuel prices have driven the industry to significantly improve the thermal efficiency and dramatically reduce the emissions of ICEs; however, these engines will always be limited by the Carnot efficiency. This represents the maximum possible thermodynamic efficiency as defined by the temperature rise of the combustion gases. As a result, these efficiency gains are quickly becoming less substantial, more complicated and more expensive to develop and therefore the industry has begun to explore alternative powertrain arrangements.

Over the past few years almost every major vehicle manufacturer has introduced at least one Hybrid Electric Vehicle (HEV) or Battery Electric Vehicle (BEV) into their range. This represents a major step in the implementation of low carbon transport and a radical departure from the ICE which has been the sole power source of almost every mainstream vehicle for over a century. BEVs have a lot to offer in terms of efficiency and emissions, especially for urban driving, but they are subject to a major drawback in terms of range and recharging time. A high performing BEV, available today, the Tesla Model S, has a range of up to approximately 300 miles and requires an hour to charge in ideal circumstances, whereas an ICE vehicle will travel a much larger distance before refuelling and even then be refuelled in a matter of minutes. Barring a technological breakthrough, there is very little that can be achieved to improve these figures drastically. The battery pack already represents a significant proportion of the mass of these vehicles and increasing its size will only serve to further increase this; meaning more energy is required to propel the vehicle and therefore diminishing returns are seen in terms of additional range (Figure 1.1). This makes BEVs ideal for city driving, but unsuitable for consumers wishing to travel large distances and has led to design of the hybrid vehicle, defined by the use of multiple energy storage devices on board the vehicle.

A typical hybrid vehicle on sale today uses the ICE in combination with a battery with the aim to maximise the benefits of each. A hybrid powertrain has a number of advantages over a conventional powertrain with regards to both efficiency and emissions. Firstly, for the majority of designs, it is possible to operate the vehicle at low speeds purely on electrical

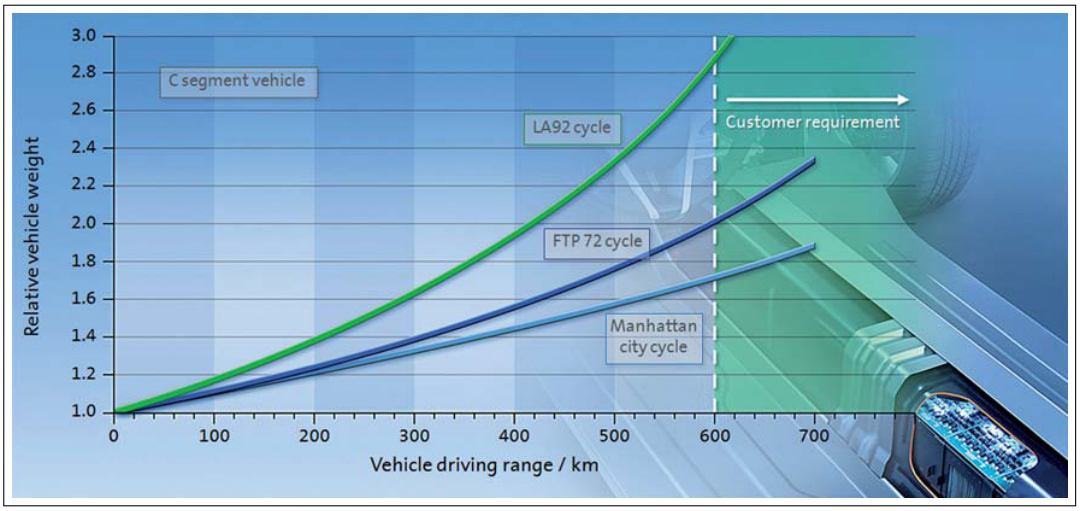

Figure 1.1: Vehicle curb weight sensitivity to the BEV range depending on various driving cycles, considering a compact car (C segment vehicle) - *Eberle et al.* [1]

power. This allows the vehicle to operate as a battery electric vehicle for short journeys (where the engine would not have time to warm up and reach maximum efficiency), or in low emission zones (which are becoming increasingly common in major cities where localised pollution can be a problem). A second major benefit is that the kinetic energy of the vehicle can be recovered by regenerative braking. This energy would normally be lost as heat in the brakes of the vehicle and can represent a significant efficiency gain for certain types of journey. Finally, the effective efficiency of the ICE can be improved upon by operating it more frequently at its most efficient operating points. This is achieved by using the electric motors to make up the difference in load in order to meet the driver's demand. Due to these benefits, ICE HEVs are highly likely to dominate the automotive market for the next few decades, however, using an ICE on board the vehicle means that they still rely on diminishing fossil fuel supplies and still produce harmful emissions.

In the long-term, hydrogen offers many benefits over fossil fuels. It is a renewable resource and can be produced by the electrolysis of water almost anywhere in the world. This means that not only is there almost unlimited availability, but also alleviates many energy security issues and reliance on politically unstable oil-rich countries. In addition to this, it can be produced locally by remote communities and therefore is not subject to the high transportation costs of fossil fuels. Finally, hydrogen does not produce any harmful emissions when oxidised and therefore no emissions are produced by the vehicle. This is particularly beneficial in urban environments where localised pollution can be a severe problem. Although hydrogen can be combusted in an ICE, the benefits are maximised if it is used in a fuel cell which is able to operate at a much higher overall efficiency.

When compared to a pure BEV, a FCHEV has the potential to provide a competitive range at a lower mass and packaging volume cost, whilst still maintaining all of the advantages of a full electric powertrain. This is because a fuel cell system has a much higher energy density by mass. This allows for more chemical energy to be stored without increasing the mass of the vehicle significantly. The main reason for this is that hydrogen has a very high energy density and that the energy storage and the conversion elements of the fuel cell system are completely decoupled. As a result, the tanks can be sized to meet the

storage requirements while the stack itself can be sized to meet the power requirements. Another advantage of storing energy separately is that the tanks can be re-filled in a comparable manner to fossil fuels, unlike a battery which must be recharged electrically and hence is limited by the rate at which the electrical energy can be safely supplied and converted into chemical energy by the battery. Fuel cells are generally considered to be a strong candidate for the transportation market in the long-term, but in the short to middle term there are a number of technological challenges to overcome. These include the cost and lifetime of the stack, and the production, transportation and storage of hydrogen as a fuel. In its gaseous form, hydrogen is extremely energy dense by mass, but exhibits very low volumetric density and therefore it can be hard to package on board a vehicle, see Figure 1.2.

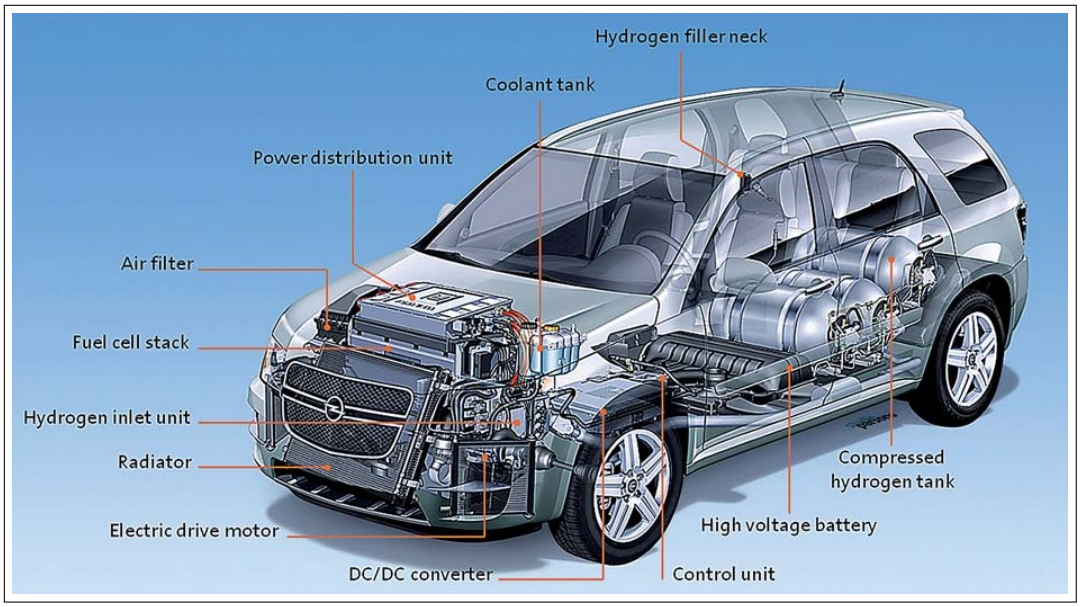

Figure 1.2: Hydrogen Tank Packaging in GM HydroGen4 - *Eberle et al.* [1]

This means that it is generally highly compressed (350-700 bar) or cryogenically liquefied when stored on board a vehicle. These techniques have various drawbacks, such as safety concerns due to the high pressure of the tank in the case of gaseous storage, or the requirement for high performance insulation and gas venting due to "boil-off" in the case of liquid storage. A third alternative is chemical storage using compounds such as metal-hydrides, hydrazine, ammonia, or organic compounds. This can overcome issues with the energy density by volume and improve packaging concerns. However, metal-hydrides tend to have a very low gravimetric density (up to around 9% in the case of lithium, boron and aluminium based compounds), organic compounds can introduce impurities into the hydrogen to which may degrade Proton Exchange Membrane (PEM) fuel cells very quickly, and for most compounds the chemical reaction required to release the hydrogen often requires an input of energy and may be subject to slow rates of reaction, limiting the rate of release of the fuel.

With regards to cost, current fuel cell stack technology is estimated as costing as little as $59/kW (2015) under mass production [11], however this is still almost double the US Department of Energy (DoE) target of $35/kW [12]. This issue is aggravated by the relatively short lifetime of the fuel cell stack, estimated at less than 3000 hours by Chen

et al. [13], well short of the DoE target of 5000 hours. These issues combine to make the purchasing and maintenance of prohibitively expensive for consumers when compared to conventional technology. Economically, the issues of high cost and the short lifetime of fuel cells are interdependent. The cost of the fuel cell can be reduced, for example, by reducing the platinum loading on the catalyst layer, however this will tend to affect the long-term performance of the cell and therefore reduce its usable lifetime. The cost of the system could also be reduced by using a smaller stack and running it at a higher relative power, however this will also tend to reduce the operating efficiency and is likely to increase the rates of degradation, reducing the lifetime of the system. This means that it is hard to gauge whether the initial cost saving of using a lower platinum loading or a smaller stack will be outweighed by the increased maintenance cost due to reduced reliability.

The final problem preventing mass production of fuel cell vehicles is that of infrastructure. Whereas fossil fuels are widely available around the world, there are still only a few hydrogen re-fuelling stations which are open to the public. This presents a typical "chicken and egg" scenario due to the fact that consumers are unlikely to purchase a vehicle they are unable to re-fuel and re-fuelling stations are unlikely to supply hydrogen until there is demand from consumers.

Despite these drawbacks, there is considerable interest from industry with a number of major automotive manufacturers beginning to produce hydrogen fuel cell vehicles for consumer market in limited numbers. These vehicles include the Honda FCX-Clarity (2007), Hyundai ix35 FCEV (2014), and the Toyota Mirai (2015). In addition to these vehicles, Daimler AG, Nissan, Renault and Ford have announced a strategic agreement develop a common fuel cell system for mass market vehicles for as early as 2017 and Alfa Romeo, Audi, BMW, Chang'an, FAW, Fiat, General Motors (GM), Lotus, Kia, Mazda, Peugeot, SAIC, Subaru, Suzuki and Volkswagen have all released concept FCHEVs in the past 10 years.

1.2 The Requirement for Low Carbon Vehicles

The number of cars worldwide passed the 1 billion mark around 2010 [14] and it is predicted that there could be 1.5 billion vehicles by 2020 [1], 2 billion by 2035, and 2.5 billion by 2050 [15]. The main reason for this growth is due to dramatic worldwide population increase from 7 billion today to an estimated 9 billion by 2050 [14], and the on-going growth of developing nations such as China, India and Mexico. Currently, more than 95% [1] of the fuel used for propulsion purposes comes from fossil sources. The combustion of limited fossil fuel reserves on this immense scale causes a number of significant issues in our society including depletion of crude oil reserves, risks to energy security, greenhouse gas emissions and air pollution. Each of these is covered in more detail below;

Oil Depletion Fossil fuels are formed from the remains of decaying organic matter which has been exposed to heat and pressure over millions of years. As a result, they are a limited resource and over time will become increasingly complicated and expensive to extract and refine. A recent model [2] suggests that we may have already hit a peak of oil production which could be expected to plateau (with gradual decline) for another 50-100 years before beginning to decline more sharply (Figure 1.3[1]). This plateau is explained by the extraction of unconventional sources partially offsetting declines in conventional oil. Given the estimated increase in the number of vehicles worldwide it is therefore imperative that this fuel is used as efficiently as possible.

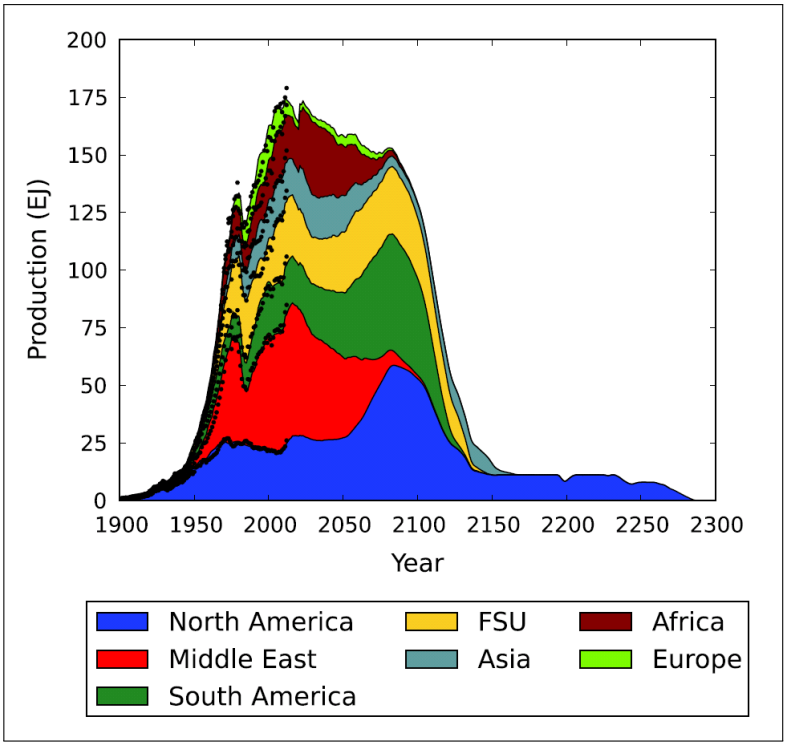

Figure 1.3: Estimated Oil Production - "Best Guess" Scenario - *Mohr et al.* [2]

[1]FSU - Former Soviet Union

Energy Security The global scale of this problem has a number of societal and political implications worldwide. One of the most worrying issues is energy security. Oil is not uniformly distributed around the world and some of the largest conventional reserves are concentrated in politically unstable regions. Europe has very little of its own reserves and hence relies heavily on foreign oil for more than 80% of its supply [14]. Unless demand reduces in line with the anticipated reduction in supply, political tensions around this issue are set to become more volatile.

Greenhouse Gas Emissions The greenhouse effect is the process by which the atmosphere reduces the loss of heat from the planet and therefore maintains a surface temperature higher than it would be otherwise. Earth's natural greenhouse effect is critical to supporting life; however, the emission of greenhouse gases, primarily due to the burning of fossil fuels, can increase its effect and hence artificially increase global temperatures ("Global Warming"). Carbon dioxide is by far the leading greenhouse gas emitted by road vehicles; however, there are a number of other greenhouse gases that are also emitted by vehicle exhaust pipes including methane (CH_4) and oxides of nitrogen (NO_x). In the United Kingdom, the transportation sector contributes 21% of total greenhouse gas emissions, of which 92% is due to road transportation alone [16]. Worldwide, approximately 3 billion tonnes of CO_2 are produced each year due to road vehicles [14].

Air Pollution The combustion of fossil fuel produces a number of chemicals harmful to health and to the environment. There are a number of compounds emitted from the exhaust pipe of the vehicles which are of concern;

1. **Carbon dioxide (CO_2)** is a direct product of complete combustion (along with water) and is therefore produced under ideal combustion conditions. As well as being a greenhouse gas, it dissolves in water to form carbonic acid which contributes to acid rain and oceanic acidification. In ideal combustion circumstances, CO_2 emissions are directly proportional to the fuel consumption; therefore, CO_2 emissions can be reduced by improving the efficiency of the engine.
2. **Carbon monoxide (CO)** is the result of incomplete combustion of fuel. It combines with haemoglobin to produce carboxyhaemoglobin, which reduces the bloods ability to carry oxygen. In high enough doses, it is fatal, and in smaller doses causes dizziness, headache, nausea and fatigue. Under normal operating conditions, very little carbon monoxide should be emitted from the vehicle due to reaction with oxygen in the catalytic converter to form carbon dioxide.
3. **Particulate Matter (PM)** is another, more extreme, result of incomplete combustion, most often seen as soot from the exhaust. PM is made up of microscopic solid and liquid matter suspended in the exhaust gas, and can cause a number of health problems including respiratory disease and cancer. They are more likely to be produced by diesel vehicles, and therefore modern diesels are often fitted with a Diesel Particulate Filter (DPF) which can reduce PM emissions by up to 80%.
4. **Hydrocarbon** emissions are generally the result of unburned fuel or oil. This covers a wide range of compounds found in petrol/diesel which can cause asthma, liver disease, lung disease and cancer.

5. **Oxides of nitrogen (NO_x)** is the generic term for nitric oxide (NO) and nitrogen dioxide (NO_2) which are formed from air due to extremely high temperatures and as a result are actually produced when the engine is running most efficiently. This means that the objective to reduce NO_x often competes with the objective to minimise fuel consumption, and hence CO_2 emissions. NO_x can cause or worsen respiratory diseases such as bronchitis or emphysema.

Over the next 50-100 years, as the world population grows and developing nations emerge, the global demand for personal mobility is certain to increase. Even the most advanced conventional powertrain options cannot prevent this leading to a higher crude oil demand by the transportation sector. Unless the transportation industry becomes less reliant on fossil fuels, this is likely to cause increased levels of air pollution, greenhouse gases and rising transport costs due to dwindling fossil fuel supplies. Fortunately, there are a number of ways this can be achieved including BEVs and hybridisation in the short term and exploring alternative, clean, renewable fuels, such as hydrogen, in the long-term.

1.3 Background

1.3.1 A Brief History of Fuel Cell Vehicles

The invention of fuel cells is usually credited to Sir William Grove in 1839. Although it was initially only considered a curiosity due to immaturity of electrical technology, it was an idea far ahead of its time. Almost 100 years later, in 1932, Francis Thomas Bacon developed the first practical hydrogen-oxygen fuel cell, and in the 1960s The National Aeronautics and Space Administration (NASA) began using fuel cells on the Apollo space program. Fuel cells were chosen due to their small size and weight compared to batteries and solar, relative safety compared to nuclear power, and an abundance of hydrogen fuel already on board the spacecraft. Alkaline fuel cells continued to be used throughout the Apollo and Space Shuttle missions.

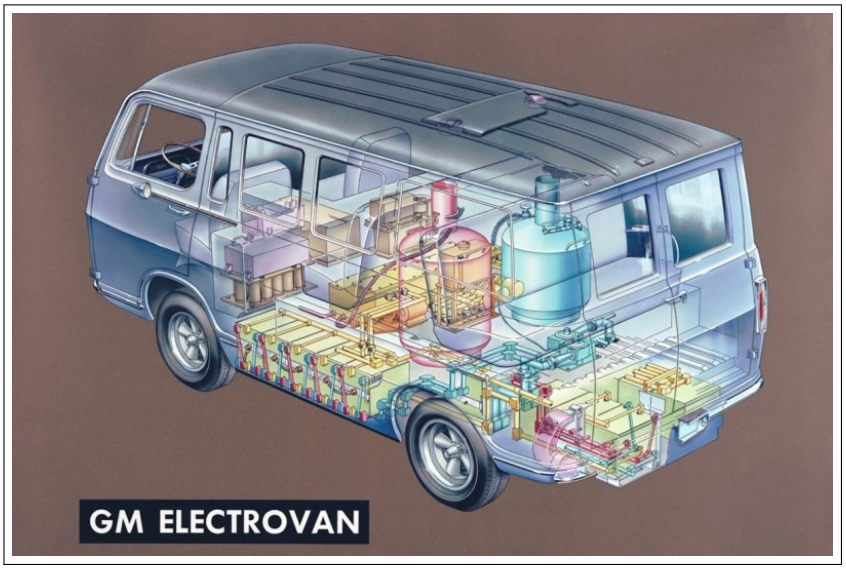

Figure 1.4: 1966 GM Electrovan Fuel Cell System Layout - *Qin et al.* [3]

In the automotive industry, the world's first Fuel Cell Hybrid Electric Vehicle (FCHEV) was the "Electrovan" (Figure 1.4) developed by GM in 1966 which also used an alkaline fuel cell and cryogenic liquid hydrogen (and oxygen) storage [1]. It had only two seats due to the 1800kg fuel cell system and storage tanks taking up most the rear of an originally 6 seater Handivan and weighed 3220kg [17]. The 160kW (peak) Union Carbide fuel cell stack was rated for 1000 hours of use and propelled the van to top speeds of 70mph with a range of 100-150 miles [17]. It was only used on company property due to safety reasons, and the technology was deemed too expensive for commercial exploitation and so the project was discontinued. Marks *et al.* [17] summarised the problems relating to the fuel cell as;

1. Heavy weight and large volume
2. Short lifetime
3. Complicated and lengthy start-up and shut-down procedures.
4. Removal and disposal of exhaust products such as by-product water, gas bleeds, and gas leaks.
5. Sensitivity to contamination, both in the gases and the electrolyte.

6. Complexity of the three separate fluid systems of hydrogen, oxygen, and electrolyte.
7. Difficult temperature control requirements.
8. New safety problems such as high voltages, electrolyte leaks, hydrogen leaks, possible collision hazards.
9. Critical gas-electrolyte pressure balance during transient conditions and on grades or curves.

The Proton Exchange Membrane (PEM) fuel cell was invented during the 1960s by Willard Thomas Grubb and Leonard Niedrach of General Electric. This invention alleviated many of the above concerns which were due to the use of liquid potassium hydroxide (KOH) electrolyte in the Electrovan, however a new problem was introduced: The Nafion ionomer electrolyte used in PEM fuel cells is very sensitive to temperature and therefore high quantities of platinum catalyst are required in order to make reaction rates feasible for energy generation. These issues prevented further development of fuel cell vehicles for another 30 years until developments in compressed hydrogen storage, computer based controllers and low platinum loading catalysts drove down the cost and complexity of fuel cell stacks, making the development of the FCHEV feasible again.

These developments coincided with the closure of the Apollo program which saw many NASA experts move to private companies and therefore a new era of development in FCHEVs was stimulated. In 1994, Daimler-Benz AG introduced the NeCar I, the world's first PEM FCHEV powered by a 50kW fuel cell stack developed and supplied by Ballard Power Systems [18]. The vehicle was based on a MB-180 van and used compressed hydrogen stored at 300 bar. This was followed by the NeCar II, a passenger minivan in May 1996, the NeCar III, based on Mercedes's B-Class passenger car, and the NeBus, a fully functioning city transit bus in 1997. The latest generation, the NeCar IV was introduced in 1999, with a 70kW Ballard fuel cell, a top speed of 90mph and a range of 280 miles bringing fuel cell vehicles much closer to modern production vehicles in terms of usability and performance. During the same period, Toyota, GM, Mazda, Ford, Honda, Nissan and Volkswagen also began development on their own fuel cell powered vehicles with fuel cells stacks ranging in power from 10 to 75kW and demonstrated ranges of up to 310 miles [3].

The performance of this generation of FCHEVs was a lot closer to that of their ICE counterparts; however, a number of problems still presented themselves. Ferdinand Panik [18] states that the gravimetric and volumetric densities of the system still required compromise in terms of passenger and luggage space with the NeCar III, and lists this as a priority target for the NeCar IV, based on the Mercedes Benz A-Class. Panik also mentioned the high cost of the system to be a major disadvantage compared to conventional technology.

The GM HydroGen project was started in the late 1990s. Early versions used an Opel Zafira MPV body style with liquid hydrogen storage, but GM later moved to 700 bar compressed hydrogen storage with the HydroGen4 (introduced 2007) which was fitted to a Chevrolet Equinox crossover with a number of structural modifications to the chassis for packaging safety reasons [19]. This gave the vehicle 4.2kg of Hydrogen and a range of approximately 250 miles. By 2012, 119 HydroGen4 vehicles had been driven by over 10,000 customers, accumulating over 4 million kilometres. From this testing, GM highlighted that the reliability of the system required further work, stating that 10% of the fuel cell stacks would fail before 650h usage and 50% before 1450 hours. Analysis into failure methods highlighted membrane degradation due to humidity changes, Ostwald ripening of the platinum catalyst and carbon corrosion of the catalyst [1]. Eberle *et al.* state that many of these

failure methods can be tackled by the control strategy due to the fact that under ideal operating conditions in a laboratory, fuel cell stacks can operate for several thousand hours. As a result, they demonstrated a number of simple modifications which could improve the 50% failure time to 3500 hours.

The new millennium has seen a big push by major automotive manufacturers to mature hydrogen and fuel cell technology with the introduction of the HydroGen project by GM and the first limited leasing of Toyota's FCHV in 2002 to the recent introduction of the first commercially available fuel cell vehicles, the Hyundai ix35 Fuel Cell, and the Toyota Mirai (Figure 1.5) in 2015. In addition to these, GM, Honda, Daimler AG, Nissan, Renault and Ford are all also planning to release FCHEVs over the next 5 years. However, there are still a number of technical issues that must be overcome before FCHEVs will be truly competitive with conventional technology.

1.3.2 Current Challenges for Fuel Cell Vehicles

Despite the recent releases of the Honda FCX-Clarity, Hyundai ix35 FCEV, and the Toyota Mirai, there are a number of problems preventing FCHEVs from being competitive with ICE vehicles. These are the cost and reliability of the fuel cell stack itself, and the supply, storage and transportation of the hydrogen fuel. These have been previously mentioned in the overview section; however, they are covered in more detail below.

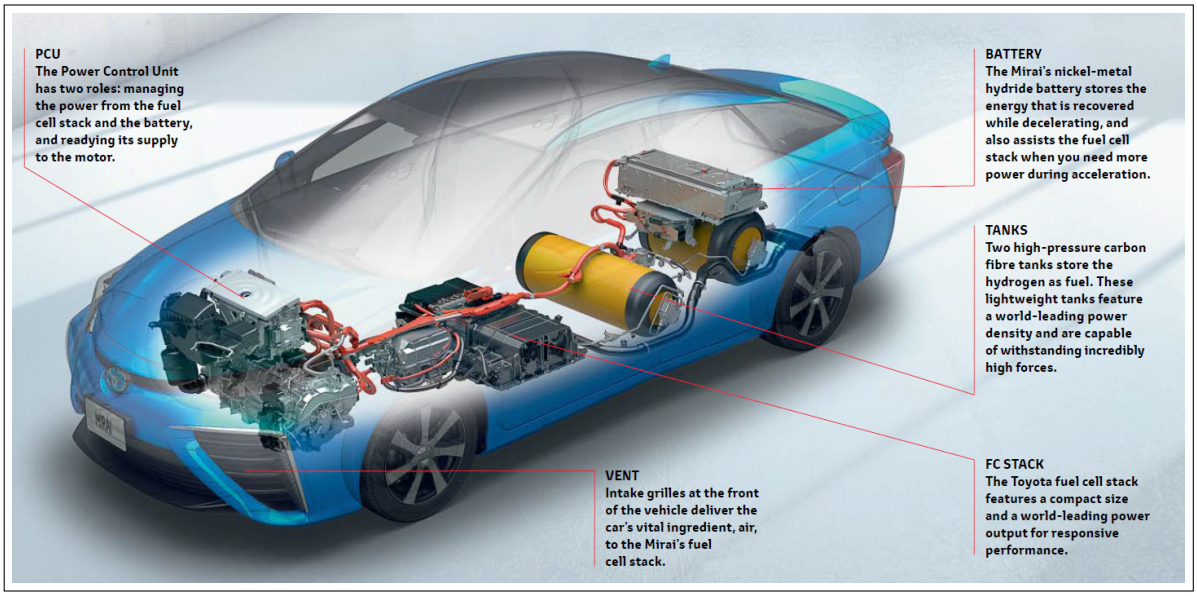

Figure 1.5: 2015 Toyota Mirai - *Vehicle Sales Brochure*

1. **Cost** Fuel cells are expensive compared to conventional technology. As of 2016, the Toyota Mirai is available to buy in the US for $57,500. This can be compared to Toyota Camry Hybrid which is priced at $27,625. This price is slightly higher than a 2011 estimate by the International Council on Clean Transportation (ICCT) [20] putting the estimated cost of a fuel cell vehicle at $50,000 in 2015. The reason for their high cost is due to a number of reasons including the immaturity of the technology and manufacturing processes, the low production volumes, but also due to the materials involved [14]. The cost of fuel cell vehicles is therefore expected to be reduced over the next decade, as manufacturing technology matures and production volumes increase, many sources estimate than the price of a FCHEV could be around $27,000 - $30,000 by 2026 [20].

   A major material cost of a fuel cell is the platinum required for catalysis. Catalysts currently require high quantities of platinum which significantly inflate the cost of the system and therefore there is a lot of research into how to reduce the amount of platinum on the catalyst. GM estimate approximately 80g of platinum was required per vehicle in 2012, but estimate that this could be reduced down to 30g by 2015, and just 5-10g by 2020-2025 by using platinum-alloy shell on a more affordable core [1], this represents a reduction from approximately $3000 per vehicle to just $200-$400 and corresponds to the amount used in catalytic converters for ICE engines.

2. **Durability** Fuel cells tend to degrade gradually in a similar way to batteries and therefore they are generally assessed by the number of hours of usage until a certain level of performance has been lost. The US DoE [12] has set a target of 5000 hours for vehicular applications based on a 250,000km lifetime at an average speed of 50km/h. A lot has been achieved in this area over the past decade; in 2003, 50% of the HydroGen3 project vehicles had failed before 250 hours of usage, however by 2012 their average lifetime had increased by a factor of almost 6 to 1450 hours. GM believe to be able to increase this further to 3500 hours using demonstration level technology [1] and anticipate that production vehicles released around 2017 could last 7500 hours on average with only 10% failing before 5500 hours.

   A major area of focus for durability is the proper management of the fuel cell. Fuel cells for static applications can have lifetimes in the 10,000's of hours due to much more predictable and stable loading, as well as significantly fewer start-stop cycles. When used for transport, fuel cells are subject to a much harder life including significantly more start-stop cycling, transient loading and operation under conditions known to cause accelerated ageing such as idling and high power usage. By controlling these conditions, and advanced start-up and shut-down control, the lifetime of the fuel cell can be significantly increased.

3. **Hydrogen Storage** It is nearly impossible to compete with the high energy density of liquid fossil fuels of approximately 12kWh/kg. Although hydrogen has a high energy density by mass (33kWh/kg), it has a very low density by volume and therefore needs to be compressed for storage on board a vehicle [14]. This typically reduces its effective energy density to just 10% of an equivalent tank of fossil fuel. There are a number of storage methods that have been used including high pressure compression at 350-700 bar, liquefaction, and chemical storage. Each of these will be discussed individually;

(a) **Compression** - The most popular method in use today is simply to compress hydrogen at 350-700 bar for storage in pressure vessels. The advantages of this method are that it is relatively mature technology and compression of the fuel is relatively efficient at 80-91% [21]. Pressure vessels exhibit very little permeation, and do not introduce impurities into the fuel. However, there are a number of targets yet to be met, including the cost of the system and the volumetric and gravimetric densities. The latest "Type IV" carbon fibre over-wrapped pressure vessels are a relatively mature and robust solution, but at $17/kWh, still cost more than double the US DoE's 2017 target [22]. "Type IV" tanks can achieve approximately 5.2wt.% at 700 bar [14].

(b) **Liquefaction** - Liquefaction of hydrogen involves cooling it to approximately -253°C (20K) where it becomes a liquid and therefore the pressure is no longer an issue. The major advantage of this method is that high gravimetric densities of approximately 5wt.% [23] can be achieved without the safety concerns associated with a high pressure vessel. The downside is that liquefaction of hydrogen requires the input of a lot of energy, equivalent to approximately 30% of the fuel, and that the tank on board requires significant insulation to maintain the fuel at this temperature. Despite this, there is still "boil-off" of hydrogen which needs to be vented and results in a loss of approximately 0.3% per day [21].

(c) **Chemical Storage** - There are a number of chemical options for binding with hydrogen including metal-hydrides, amine borane complexes, hydrazine, ammonia, and organic compounds such as carbohydrates, hydrocarbons and cycloalkanes. These chemicals work by binding with the hydrogen and storing it as in liquid or solid state as part of a compound and as such allow much higher volumetric energy densities. The best compounds are able to store up to approximately 10.9wt.% in theory [21] ($NaAlH_4$); however, figures closer to 6wt.% are achievable in reality [14]. The main downsides to chemical storage are the energy required to release the hydrogen, the rate of release of hydrogen, potential contamination of the fuel, and potential toxicity of the compounds used.

(d) **Hybrid Storage** - A relatively new field of storage involves the combination of more than one type from the three aforementioned categories. Cryo-compressed hydrogen uses a solution similar to liquid hydrogen storage, but the liquid hydrogen is contained within a pressure vessel meaning that "boil-off" gas does not need to be vented until pressures reach 100's of bar. In most cases, the hydrogen will be used by the vehicle before this will occur meaning that this energy is not lost. Toyota are also targeting 8wt.% by combining metal-hydride storage with compressed gas [14].

The reason hydrogen storage density is an issue is due to range requirements and so it is closely related to the tank-to-wheel efficiency. Obviously if the fuel cell was more efficient, less fuel would be required to achieve the same range and therefore the requirement on the storage system is reduced. For example, the Honda FCX Clarity has 4.1kg of hydrogen storage capacity, equating to 490MJ of chemical energy and a range of 240 miles. In comparison, the modern petrol engine in the VW

Golf VI has 40Kg of petrol storage capacity, equating to 1800MJ and a range of 552 miles. This means the Golf has 3.6 times the energy storage capacity, but only 2.3 times the range due to the much lower tank-to-wheel efficiency of the ICE.

4. **Hydrogen Infrastructure** The problem with infrastructure is a classic chicken and egg scenario. Without existing refuelling stations, consumers will be reluctant to purchase a FCHEV, but without an existing customer base, refuelling stations are reluctant to provide hydrogen. This is compounded by the immaturity of the technology especially that regarding storage due to variations in the requirements for the refueller in terms of coupling standards, supply pressure, safety standards, and even the supply of gaseous or liquid hydrogen as required by different vehicles.

   The industry has responded to this situation with a number of joint initiatives between various interested parties, including collaboration projects between vehicle manufacturers to introduce a standardised fuel cell vehicle architecture such as that between Daimler AG, Nissan, Renault and Ford. There have also been projects to create "hydrogen highways" in California, Europe and Japan where chains of hydrogen equipped refuelling stations allow customers to use FCHEVs locally.

   The Toyota Mirai is currently only available in limited locations where there is a 700 bar hydrogen supply including South East London and Swindon in the UK, and in California in the US. This allows people to use the vehicles locally, but would mean that another vehicle would usually be required for distance driving. To account for this, Toyota provides free rental vehicle service when additional range is required. As more vehicles are sold, the expectation is that it will become economical to open more hydrogen refuelling stations and therefore more locations will become available.

In summary, fuel cell vehicles are just beginning to appear on the market; however, they are not yet truly competitive with conventional technology and are only available in limited locations due to high cost, low reliability, poor range, and limited infrastructure. As a result, they are a niche product aimed at the luxury market as a second car similar to early BEVs. Over the next decade, through incremental improvements in the technology and the natural cost reduction in cost due to maturity of the technology and higher production volumes, many of the technical targets are expected to be met and FCHEVs will begin to become more competitive with current ICE powertrains.

1.4 Test Vehicles - Microcab H4 and Microcab H2EV

The Microcab H4 was developed by Microcab, a spin-out company from Coventry University, and 5 examples were delivered to the University of Birmingham campus in early 2008, see Figure 1.6. The H4 is designed to replace diesel vans and cars which were formally used for mail delivery, food distribution and estate services [24]. For campus operation, the diesel vehicles were found to be extremely polluting and inefficient due to the low speed, intermittent usage patterns, each emitting approximately 4 te of CO_2 per year.

Figure 1.6: The Microcab H4 FCHEVs at the University of Birmingham - *Kendall et al.* [4]

The Microcab H4 has been designed specifically for this type of duty cycle at minimal cost and therefore has a very low top speed of approximately 30mph and a peak acceleration of just $3ms^{-2}$. The Microcabs cost just £50,000 each to manufacture including the mould for the composite bodywork. They are fitted with a 1.2kW nominal Ballard Nexa PEM fuel cell stack in combination with 4 deep-discharge AGM lead acid batteries giving a total battery capacity of 2.1kWh at a nominal 48V. This is used to supply electricity to the brushed DC motor supplied by GE. The motor has a nominal peak power of 10kW [24], rising to 20kW in short peaks. Finally, the vehicle is also fitted with a small 12V auxiliary battery which is used to supply power to ancillaries and lighting and also for fuel cell start-up.

The vehicles were used at the University of Birmingham for approximately 2 years accumulating over 4000km of usage as urban taxis and for mail delivery. During this period, it was found that the tank-to-wheel efficiency of the vehicle was below expectations at just 18%. Staffell [6] reports that this could be improved by examining the vehicle from a system level in order to match the efficient operating regions of various components, and the implementation of more advanced control strategy to optimise the operating state of the powertrain in a holistic sense.

Two of the vehicles used at the University of Birmingham have been made available at Loughborough for examination and development purposes. In addition to this, there is the possibility of limited access to the new Microcab H2EV through MIRA, a project sponsor. The Microcab H2EV is an evolution of the H4, which features a redesigned chassis, a 5kW Horizon fuel cell stack, 4.3kWh lithium-ion battery pack and two 20kW peak DC motors. This gives the vehicle an increased top speed of 55mph although it is still in active development by Microcab and specification is liable to change. In addition to this, there is limited availability for testing for the Microcab H2EV. More details on both test vehicles are given in Chapter 3 - Vehicle Modelling.

1.5 Energy Management Strategy (EMS)

The control requirements of any hybrid powertrain are not necessarily trivial. On a traditional vehicle with no hybridisation, the driver controls the engine using the accelerator pedal. The movement of the pedal directly determines the operating state of the ICE in order to produce the mechanical power required to drive the vehicle. However, on a hybrid vehicle, having an additional energy conversion device means that there is now an extra degree of freedom for control purposes. There is still only one control input, the driver demand; however, this demand can be satisfied by either the ICE, the electric motors, or by some combination of each. Using the ICE will directly result in some fuel consumption; however, using the electric motor will deplete the battery. Therefore some fuel can be saved in the short term by using the electric motor in order to reduce the load on the ICE; however, the battery State of Charge (SoC) must later be replenished usually at the cost of additional load on the ICE. The overall operating efficiency of the system is highly dependent on how the load is applied to the ICE over time. In order to make this decision, many hybrid vehicles use a supervisory controller, which is generally known as the Energy Management Strategy (EMS).

Put simply, the role of the EMS is essentially to control the energy stored in the batteries. There are two main strategy types; Charge-Depleting (CD) and Charge-Sustaining (CS). A CD strategy will allow the battery SoC to gradually fall over time with the assumption that the vehicle will be recharged when it is stopped. A CS strategy on the other hand, will attempt to maintain a relatively constant SoC in the batteries during usage because the battery is not intended to be recharged during times when the vehicle is inactive. It is possible to achieve these targets with relatively simple strategies; one example is the "thermostatic" strategy. This strategy works in an analogous way to a thermostat (hence its name). The battery is initially allowed to discharge until it drops below a fixed threshold, at which point it is charged. Once the SoC reaches a second, higher, threshold, the charging is stopped, and the battery is allowed to discharge again. The actual operating points of the components during discharge and charge conditions will vary depending on the design of the vehicle. For example, the ICE may be off during discharge and run at its most efficient operating point during charge, or the ICE may be run at maximum efficiency during discharge and at maximum power during charge.

The decisions made by the EMS determine the operating points of various powertrain components, and therefore will have a large effect on the overall operating efficiency of the vehicle. A well designed EMS has been shown to improve fuel economy in the order of 10% - 20% [25–27]. However, the fuel consumption is not the only concern of the EMS. A strategy optimised solely on the fuel consumption may exhibit a number of negative aspects. For example, in an ICE hybrid equipped with an automatic gearbox, the EMS is usually responsible for choosing the active gear. If no consideration to the number of shifts, the optimal strategy will likely change gear frequently to ensure the vehicle is always in its most efficient state, however this behaviour may be unpleasant to the driver. Equally, for a FCHEV, the strategy may cause highly transient loading on the fuel cell in order to avoid cycling losses in the battery, however this will tend shorten the life of the fuel cell.

There is a great quantity of research in the literature with regards to optimisation of the EMS. The vast majority of this work focuses on ICE based hybrid vehicles, and much of this work is equally valid for fuel cell vehicles. However, there are a number of issues

that are specific to fuel cells, especially those linked to the challenges mentioned previously. Although the EMS cannot affect the cost of the stack directly, it is possible that by improving its operating efficiency the fuel cell stack could be downsized, leading to a reduction in cost indirectly. In addition to this, increased efficiency will also reduce hydrogen storage requirements. Finally, the reliability of a fuel cell will depend on how it is used. For example, vehicular applications are generally quite harsh on the fuel cell due to a high degree of transient loading. If the EMS is designed to take account of common degradation methods, then the reliability of the stack could be improved.

1.6 Research Aims and Objectives

The overall goal of this work is to identify the best methods in which to optimise the holistic design of a FCHEV using pre-existing or already available components. Research will focus on two inter-related areas; the Energy Management Strategy (EMS) and the electrical system design. It has been chosen to investigate both areas concurrently, rather than to simply focus on one in order to highlight the interactivity of these two design choices. The EMS will have a significant effect on the optimal system design, however the system design will also affect the decisions made by the EMS. Therefore, it is important to consider them concurrently in order to arrive the at the optimal final design.

Specific objectives for the research are;

- To identify the specific design requirements for an EMS on board a FCHEV based on a thorough review of engineering literature.
- Identification of the latest methods for the optimisation of FCHEV electrical powertrain system design.
- Application of state-of-the-art EMS techniques to the Microcab H4 and/or Microcab H2EV (depending on availability).
- Evaluation of the potential scope for improvement with regards to the challenges faced for FCHEVs (covered in Section 1.3.2).

1.7 Contributions

The specific contributions made in this thesis are as follows:

- A comprehensive review of the major requirements for the EMS of a FCHEV, inclusive of fuel efficiency, fuel cell degradation, battery degradation, and drive-ability (Chapter 2).
- Quantification of fuel cell degradation modes under control of the EMS suitable for use in the cost function for optimisation of the EMS (Chapter 3).
- Development of a validated reduced order model of a FCHEV, specifically the Microcab H4 (Chapter 3).
- Development of a process for stochastic drive-cycle modelling based on real-world logged data (Chapter 4).
- A novel application of Stochastic Dynamic Programming (SDP) which is inclusive of fuel cell degradation in addition to fuel consumption. Each of these costs has been weighted by their monetary values in order to estimate the total running cost of the vehicle. This is compared to the state-of-the-art optimal techniques based solely on fuel consumption (Chapters 5 and 6).
- A component sizing exercise for a fuel cell vehicle using the optimal control strategy for each system design examining the running cost of each design, and the effect of battery and fuel cell stack size on the operating efficiency, operating range and stack lifetime (Chapter 7).

1.8 Thesis Format

This thesis details the development and testing of an EMS for a low speed FCHEV. The contents of each chapter are;

Chapter 2 - Literature Review

The second chapter is the literature review. The literature review begins with a brief explanation of the various components which may be used in the system design of a FCHEV, and how these components are sized in order to optimise the performance of the vehicle as a whole. Following on from this, the requirements of the EMS are investigated. A variety of work including EMS development, accelerated ageing techniques and Failure Mode and Effects Analysis (FMEA) are examined in order to identify the criteria for optimisation of the EMS. Finally, a number of techniques for optimising the EMS itself are outlined and compared. The chapter concludes with a summary of potential areas for further work.

Chapter 3 - Vehicle Model

The third chapter defines the vehicle model used for development of the EMS. Two models have been created; a detailed forward-facing model has been used for testing and a reduced order model which has been developed for EMS optimisation. SDP optimisation is a highly computationally expensive technique which requires computationally efficient calculations in order to estimate the probability and cost of transitioning between each state. Both models are validated against test data obtained from the Microcab H4 available at Loughborough University.

Chapter 4 - Markov Chain Modelling of Duty Cycle

The development of an EMS using SDP requires a stochastic model of the anticipated duty cycle. In order to produce this model, test data of the Microcabs logged at the University of Birmingham have been used in conjunction with logged data of a variety of campus vehicles used at Loughborough University. These datasets have been used to develop a Markov chain which represents the probability of the vehicle's subsequent acceleration, given its current velocity and acceleration.

Chapter 5 - Controller Development

Chapter five describes the main focus of the work, the development of the SDP optimised control strategy. The problem is explicitly defined at the beginning of the chapter, and following this the method used for calculating the required probability and cost matrices is described. A cost function is derived which estimates the anticipated fuel consumption and stack degradation and weights these by their respective monetary values. Finally, the parameters of the optimisation are chosen and an example of an optimised strategy is shown.

Chapter 6 - Strategy Simulation & Analysis

Chapter six describes the effect of the novel control algorithm on both the fuel consumption and the fuel cell degradation of the Microcab H4. The results of the control strategy are compared to that of the current strategy employed on the Microcab, and a fuel consumption only optimisation representative of recent work in the literature. It is found that for the current design, the 1.2kW fuel cell is insufficient to maintain the battery SoC under normal usage even when the optimal control strategy is applied. Therefore, the results are recalculated for a 4.8kw stack representative of that in the newer Microcab H2EV. It is found that the current control strategy is no longer appropriate for the system design and that the degradation inclusive controller reduces the estimated degradation by approximately 15% for only a 4% increase in fuel consumption when compared to the strategy optimised purely on the fuel consumption. This gives an overall running cost saving of around 9%.

Chapter 7 - Optimisation of Hybrid Component Sizes

Chapter seven presents a component sizing exercise using the results of the SDP optimised controller. A number of system designs with a variety of fuel cell stack sizes and battery capacities are proposed. The optimal control strategy for each design is calculated using SDP and the simulated results of each system design are compared. It is found that the running cost of the vehicle is minimised by using the smallest possible fuel cell stack that will satisfy the average power demand of the duty cycle and that increased battery size up to double the current capacity results in reduced fuel consumption and degradation.

Chapter 8 - Conclusions and Further Work

The closing chapter draws conclusions from the results obtained and presents recommendations for further research.

1.9 Publications

Sections of this work have previously been published as the following;

- Tom Fletcher, Rob H Thring, Martin Watkinson, and Iain Staffell. *Comparison of fuel consumption and fuel cell degradation using an optimised controller.* ECS Transactions, 71(1):85-97, 2016. DOI: 10.1149/07101.0085ecst
- Tom Fletcher, Rob Thring, and Martin Watkinson. *An Energy Management Strategy to concurrently optimise fuel consumption & PEM fuel cell lifetime in a hybrid vehicle.* International Journal of Hydrogen Energy, 0360-3199, 2016. DOI: 10.1016/j.ijhydene.2016.08.157

Chapter 2

Literature Review

There is a great quantity of research into Energy Management Strategy (EMS) in the literature, although the volume of work into the optimisation of Fuel Cell Hybrid Electric Vehicles (FCHEVs) is relatively limited [4–6, 19, 24, 28–40]. The vast majority of research has investigated the effect of new energy management algorithms with respect to Internal Combustion Engine (ICE) hybrid vehicles [8, 9, 25–27, 41–67]. This work has been included in the literature review because many of the same techniques can be used in order to optimise FCHEV energy management. The results are likely to differ however because FCHEVs tend to have significantly different constraints on the optimisation in terms of fuel economy (see Figure 2.1) and component lifetime. In addition to ICE hybrid research, a few niche applications of EMSs, such as Unmanned Aerial Vehicles (UAVs) [68], have also been included where they are appropriate to the discussion.

Different techniques used to optimise the EMS on board Hybrid Electric Vehicles (HEVs) are compared. The literature review is broken down into three sections. The first section focusses on the system design and component sizing. Each of the major components are described and different approaches to the sizing of components for a FCHEV are examined. In the second section, the requirements of the energy management are examined. The vast majority of research focuses solely on fuel economy, however the EMS can affect other areas of performance and therefore examination of the literature in these fields is also important. In the concluding section, the algorithms used to optimise the fuel economy will be broken down into progressively complex methods, with the latest techniques at the end of the literature review. The literature review concludes with suggested areas for further research and development.

2.1 System Design

"We strongly feel that the "optimization" of a fuel cell vehicle must encompass all these aspects jointly, i.e., storage capacity, supervisory control policy, low-level FC controller and the interplay between them." Guezennec *et al.* [28]

System design, especially component sizing, is very closely related to the EMS strategy and they should be considered concurrently. This is because the strategy decisions made by the EMS will have significant effect on the size of the fuel cell and batteries required. Conversely, the optimal strategy will depend on the size of the components available. As an example, the size of the battery pack required to balance transient loads will depend on the EMS strategy decisions as to how much energy buffer is required. If EMS only uses 5% of the capacity of the battery, the battery pack specified may be too large. On the other hand, if the battery pack is downsized, the resulting penalty on using a larger State of Charge (SoC) range will cause the EMS to behave differently. Considering both aspects simultaneously will result in the best overall system design.

2.1.1 Fuel Cells

A fuel cell is an incredibly efficient method of extracting the energy from hydrogen fuel. Proton Exchange Membrane (PEM) (also known as Polymer Electrolyte Membrane (PEM)) fuel cells operate at a relatively low temperature, which means they have fast start-up and shut-down times, and a low system packaging volume and mass. These advantages over other technologies make them ideal for transportation use. Unfortunately, the low temperature operation also means that they require expensive Nobel metal catalysts in order to work and are sensitive to poisoning from impurities in the hydrogen supply.

Fuel cells running on pure hydrogen produce no emissions other than water and are much more efficient at extracting the chemical energy and converting it into electrical energy than an ICE and generator. In addition to this, they have a much simpler design with fewer moving components. This makes a fuel cell the ideal choice for a zero-carbon vehicle. Unfortunately, fuel cells are sensitive to transient loads which can cause increased rates of degradation. They can also be aged by running them at power levels above/below their optimal range. For this reason, fuel cells are often combined with a short-term energy buffer such as batteries and/or supercapacitors to absorb the transient loads experienced in transportation duty cycles.

2.1.2 Batteries

Modern battery technology, especially the development of lithium-based batteries, has meant that in recent years their use in personal transportation has almost become competitive with ICEs. Using lithium-ion batteries, the Nissan Leaf is a competitive family car which offers a range of up to 120 miles on the New European Driving Cycle (NEDC) operating on battery power alone. This range makes the Leaf suitable for everyday driving for most people; however, it is considerably less than an equivalent ICE vehicle. The battery pack on the Leaf also increases the price of the vehicle, making it significantly more expensive than its ICE counterparts.

There are three main battery chemistries used in transportation; lead acid, Nickel Metal-Hydride (NiMH), and lithium-ion. The lead acid battery has been used as a Starter Lighter Ignition (SLI) battery for many years. Lead acid batteries are maintained best by keeping them at full charge, which means they are particularly suited to this use, where they are constantly charged by the alternator on the engine. Lead acid batteries are relatively cheap and when used as SLI batteries, they are well understood and tend to be reliable. Unfortunately, they degrade relatively quickly when more deeply discharged, especially if they are not recharged fully. Compared to other types of re-chargeable battery chemistry they have a relatively low energy and power density. Lead acid batteries have been also used in electric vehicles such as the General Motors (GM) EV1 and the Reva G-Wiz.

NiMH batteries are best known in transportation as the battery type used on the Toyota Prius, although they were also used as the battery for the second generation of the GM EV1. They have higher specific energy and power than lead acid, but not as high at lithium-ion. They are generally used for high power applications due to their low internal resistance, but suffer from high rates of self-discharge so are equally unsuitable for low power applications. Unfortunately, NiMH batteries exhibit poor cycle efficiency. In transportation, NiMH batteries represent the "middle-ground" between lead acid and lithium-ion in terms of both cost and energy density.

Finally, lithium-based battery chemistry has the most promising future in transportation. Lithium-ion battery technology has improved significantly in recent years due to its use in consumer electronics such as laptops and mobile phones. Lithium-ion batteries have high energy and power densities compared to other battery chemistries, meaning that Battery Electric Vehicles (BEVs) based on lithium-ion batteries are beginning to be competitive with conventional vehicles for short-range journeys, especially city driving. They also have a high cycling efficiency improving the fuel economy of hybrid vehicles, and the charging cost of BEVs. Unfortunately, they are very expensive and the battery pack on a modern BEV represents a significant proportion of the cost of the vehicle (even leading some manufacturers to offer the battery on lease separately to the purchase of the vehicle). Despite this, the energy density of lithium-ion batteries is relatively poor compared to gasoline, so although modern BEVs such as the Nissan Leaf are able to compete on everyday driving cycles, they must be recharged on longer distance journeys. Many consumers aren't willing to accept this, especially when even a "fast charge" may take around 45 minutes and would have to be performed at least twice just to meet the range of a conventional vehicle.

Even the gravimetric energy density of lithium-ion batteries is too low for current BEV to be truly competitive with conventional vehicles in terms of cost and range. However, they offer a number of advantages when combined with an ICE or a fuel cell to create a hybrid vehicle. The battery can be used to alter the operating point of the fuel cell in order to optimise the fuel economy, or to balance the load and reduce transient loading in order to protect the stack. Another advantage of using a battery pack with a fuel cell is to absorb regenerative braking energy; however, this will tend to degrade the battery. This is due to the high charge current which may over-charge the battery, or produce excess heat due to the internal resistance of the battery. In general, batteries are aged by overcharging them, deeply discharging them, by extremes of temperature and by excessive cycling. Batteries tend to cope with transient loads better than fuel cells mostly due to the lack of an external reactant supply; however, they will still exhibit some degradation.

2.1.3 Capacitors

Capacitors offer an alternative to batteries in hybrid vehicles, and are occasionally used in addition to a battery pack. Capacitors have a much higher power density, but a lower energy density. They are also very resilient to transient loading and cycling. This means they can be charged at very high rates of current such as those available when regeneratively braking. Another advantage of capacitors is that they require very little maintenance. Unfortunately, their low energy density means that they are only suitable for very short-term energy storage.

Supercapacitors work well to reduce the damage to the batteries and fuel cell. Work by Sun and Kolmanovsky [69], suggests that the use of a supercapacitor alongside a high pressure fuel cell helps alleviate some of the most damaging transients caused by compressor spooling. This is because when a sudden current demand occurs, the cathode pressure decreases as the oxygen is reacted more quickly. This means the compressor is required to increase its power in order to maintain the pressure, and this increase in compressor load adds to the already increased current draw, exacerbating the problem. Adding a supercapacitor to the fuel cell output helps dampen this transient load, decreasing the degradation on the fuel cell. Thounthong *et al.* [70] have performed a demonstration of a fuel cell/battery/supercapacitor hybrid power source. Detailed examination of the current drawn from each of the power sources showed that the supercapacitors absorbed many of the transients, alleviating the potential damage to both the batteries and fuel cell.

2.1.4 DC/DC Converters

A common component in many FCHEVs is the DC/DC converter. DC/DC converters are primarily used to step the voltage of different components up or down to meet the voltages of other components. The Microcab H4 has 3 DC/DC converters due to three different operating voltages used on-board. The main converter is used to step the fuel cell voltage up from a nominal 24V to the nominal 48V of the battery pack and motor. The other two are used to step the 24V of the fuel cell down to the nominal 12V of the auxiliary components such as the lights, and to step the 12V auxiliary system back up to the 24V of the fuel cell in order to provide power to start the fuel cell.

It is not necessary to include a DC/DC converter in a hybrid vehicle if the fuel cell, battery and capacitor voltages are correctly matched. However, there are a number of advantages to doing so. Firstly, the inclusion of a controllable DC/DC converter is a straightfoward way for the EMS to manipulate the load on the fuel cell. Secondly, the capability to step up or down the voltage between the battery pack gives more freedom to the design of the fuel cell stack and/or battery pack. For example, traction batteries tend to operate at high voltages in order to minimise ohmic losses, which will be proportional to the current. This can be achieved by running individual cells in series rather than in parallel, however it is not as easy to design a high voltage fuel cell stack, which may require re-design of reactant gas channels, cooling, and product removal methods. Some energy will be lost; however, DC/DC converter efficiency is generally quite high. Therefore, a higher overall efficiency may be possible by using a DC/DC converter than by running the battery pack at a lower voltage.

2.1.5 Component Sizing

Given the advantages of a hybrid system, the question arises of the best way to combine the multiple power sources in order to create an optimal design. Component sizing has been heavily researched, and a multitude of distinct designs have come forward. Available on the automotive market today are a variety of varying degrees of hybridisation, generally classified into three categories; "Stop-Start Technology", "Mild Hybrids" and "Full Hybrids". Stop-start technology represents the mildest degree of hybridisation where a conventional vehicle is capable of rapidly stopping and starting the engine, quickly enough to reasonably allow the engine to be stopped when the vehicle is stopped, but still allow the engine to be restarted without driver intervention. Some stop-start vehicles, such as the 2013 BMW 1-Series are even capable of low levels of regenerative braking by using the existing alternator. Mild hybrids are generally defined by the replacement of the starter-alternator system with an electric traction motor allowing higher levels of regenerative braking in addition to stop-start technology. Mild hybrids have less of a cost and weight penalty when compared to full hybrids, but still offer many of the advantages of a hybrid system. Finally, full hybrids are generally defined by the ability to operate in electric only mode for a limited range. Full hybrids generally offer all of the advantages of a hybrid system, albeit at an increased weight and cost compared to a conventional vehicle.

Most FCHEVs (including the Microcab H4 and H2EV) fall into the full hybrid category because they are generally able to run on battery power alone (although some fuel cell vehicles do not incorporate a significant battery pack and so would fall into the mild hybrid category). The comparative size of each of the components needs to be optimised in order to maximise the benefits of the hybridisation. A lot of research has been performed in this area for both ICE based HEVs as well as FCHEVs. This work generally consist of a parameter sweep simulations of differently sized engines, fuel cells, batteries and capacitors over a single or multiple drive-cycles. Inputs to the parameter sweep are generally the capacity, cost and weight of the components and outputs are the performance, cost and weight of the system. These simulations are heavily affected by the control algorithms used to perform the EMS. Power management and component sizing are the biggest factors that affect the fuel efficiency of FCHEV and Kim and Peng [71] suggest that they should be considered concurrently.

Basic component sizing techniques involve manual calculation of the required component sizes based on simple rule-based controllers. For example, Wu and Gao [72] describe a method used to size the components of a fuel cell/supercapacitor HEV. Calculations are performed to determine the power required to meet performance targets such as top speed and grade-ability. It is assumed that the cost of the fuel cell and supercapacitor banks are a function of the number of units. The cost, weight and volume of the system are then optimised and the results are subsequently simulated.

A better method for sizing components involves a parameter sweep of component sizes in order to find the best overall system. Schaltz *et al.* [36] present the results of a parameter sweep simulation investigating the influence of battery and ultracapacitor sizing on a FCHEV. The energy management for this investigation is rule-based and is used to ensure that the fuel cell can be run continuously at a fixed power, whilst the supercapacitors and battery pack absorb any short and long-term transients respectively. Schaltz *et al.* [36] concentrate on the trade-off between the size, mass and cost of the system and the battery lifetime and concludes that over-sizing the battery pack and ultracapacitors will decrease

the battery degradation significantly for an increase in system cost, but without affecting vehicle performance.

Bauman and Kazerani [73], perform a comparative study in order to assess the effects of using each technology on component lifetime and system cost. The MATLAB simulation uses a rule-based controller in order to manage the SoC of the capacitors and batteries and to limit transient loads on the fuel cell. They conclude that overall, the best designs minimise the cost by sizing the fuel cell to cope with power demand at the highest cruising speed of the vehicle. According to Bauman and Kazerani, the most desirable designs require a battery pack due to the low energy density of using ultracapacitors on their own. The usage of ultracapacitors is marginal, increasing the cost of the system, but improving the fuel economy and lifetime of the battery pack.

Rousseau *et al.* [5] use simulation to assess the required degree of hybridisation for a fuel cell vehicle. In the simulation, a heuristic energy management strategy is used, specifying a minimum power to turn the fuel cell on and battery SoC targets based on vehicle speed. It is decided that the vehicle requires a peak power of 160kW, and various combinations of battery and fuel cell power are used to meet this goal. It is found that as the battery size increases, more regenerative braking energy can be recovered. Conversely, as the battery size increases, and the fuel cell size is decreased and more energy is re-cycled through the battery. This gives an optimum degree of hybridisation for fuel economy. It is also found by Rousseau *et al.* [5] that modifications to the parameters used in the rule-based controller can have significant effect on the results. It is therefore imperative that the control algorithm used accurately represents that of the final vehicle.

Under certain conditions, the control algorithm used for component sizing exercises may give an unfair representation of the results. For example, a heuristic algorithm which prioritises regenerative braking over fuel cell operating efficiency could be designed by aggressively targeting a relatively low SoC in the battery. This may result in a high battery capacity appearing relatively unattractive because the controller ensures that capacity is available at all times. Conversely, if the algorithm prioritises the fuel cell operating efficiency, perhaps by allowing the battery SoC to vary over a larger range, a higher battery capacity will appear more attractive. Therefore, using an identical control algorithm for each design doesn't necessarily give an objective comparison. In order to isolate the advantages of each design, the control strategy should be optimised individually.

In order to eliminate effects caused by variations in the controller, it is possible to use dynamic programming to calculate the optimal EMS for each design. Dynamic programming techniques allow optimal control, effectively allowing each design to perform to its maximum performance potential. This gives the system designer the best possible result for each configuration. Sinoquet *et al.* [74] present a parametric study focussed on variations in size of powertrain components for a hybrid vehicle with respect to fuel consumption. Results are obtained using a Deterministic Dynamic Programming (DDP) controller which shows that a 1.04kWh battery pack gives the best fuel consumption. Lower battery capacity results in a loss of recovered braking energy, but higher capacity increases the mass of the system, resulting in an overall increase in fuel consumption. Kim and Peng [71] present a combined optimisation problem using Stochastic Dynamic Programming (SDP) to be used to choose both the component sizing and the power management strategy in order to maximise fuel efficiency.

2.1.6 Summary

In summary, the electrical system of a FCHEV is usually made up of a fuel cell, batteries and an electric motor. The fuel cell is used as the primary power source, with the battery pack included to absorb transient loads in order to protect the fuel cell; however, this will tend to age the battery pack. Supercapacitors are sometimes used either instead of the battery pack or in addition to it. As they a very resilient to transient loading and high currents, they are often used to protect the battery (or fuel cell directly) from transient loads and the high currents associated with regenerative braking at the expense of addition cost and complexity to the system. There have been a number of works examining the optimal sizing of components, mostly using "rule-based" controllers (see Section 2.3.1). These controllers may favour particular system designs due to heuristic assumptions and therefore this bias is eliminated by using optimal control methods. Techniques such as DDP and SDP will exploit the advantages of each individual design allowing for a fairer comparison.

2.2 EMS Requirements

"In a fuel-cell-battery vehicle, the battery stores regenerative braking energy, provides extra power during accelerations, and propels the vehicle at low speeds to avoid operating the fuel cell at low power (in its low-efficiency region)." Bauman and Kazerani [73]

The key role of the EMS is to manage multiple energy storage devices in order to meet the driver's requirements. In order to understand how to control the EMS, the system design of a FCHEV must be understood. Fuel cells are hybridised with a battery for two main reasons. Firstly batteries (and/or capacitors) are able to absorb regenerative braking energy and secondly the battery can be used to balance the load on the fuel cell in order to operate it for efficiently and reliably. Sekine and Kojima [38] mention that degradation and cost are two major areas for improvement in FCHEVs. Using the battery to balance transient loads and operate the fuel cell within its optimum region will limit the degradation of the fuel cell [73]. Using the battery to provide additional power also allows the fuel cell to be downsized, potentially reducing the cost [36]. In addition to improving its lifetime, operating the fuel cell within its optimum region will also improve its efficiency.

2.2.1 Fuel Economy

The vast majority of research into the EMS focuses solely on improving the fuel economy of the vehicle [5, 9, 29–31, 44–47, 51, 52, 56, 63, 71, 73, 74]. This is important for FCHEVs not only to reduce running costs, but also to improve the range without increasing energy storage requirements. The efficiency of the fuel cell depends on its load. At low loads, the ancillaries such as the compressor, fans and humidifier use a significant proportion of the current compared to the useful output, causing a reduced overall efficiency. As the load is increased, this ancillary draw becomes less significant, but ohmic losses increase. At very high loads, the mass transport of chemical species across the fuel cell becomes the limiting factor and the voltage begins to drop significantly. Rousseau *et al.* [5] compares the typical operating efficiency for a fuel cell system and an ICE in Figure 2.1.

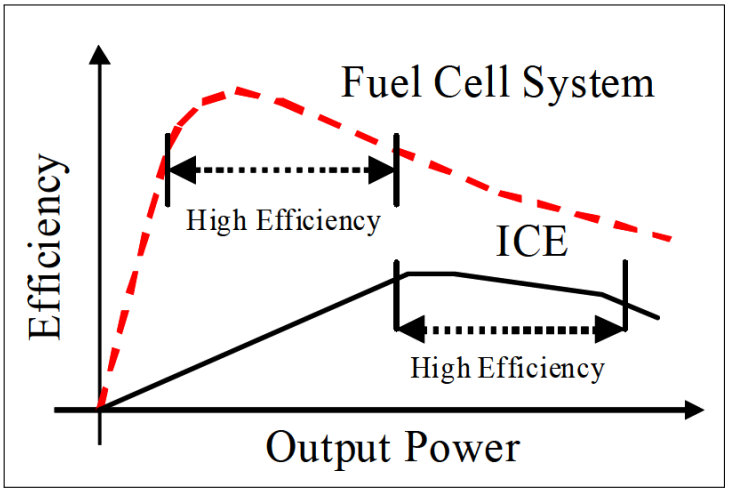

Figure 2.1: Fuel cell efficiency vs. load - *Rousseau et al.* [5]

In addition to the operating point of the fuel cell, the efficiency of other components in the system must be considered. The efficiency of energy recovery from braking will depend on the SoC of the battery at the time of braking events. If the battery is fully charged, or the braking power is higher than the battery can accept, then the energy will be lost [29]. It is therefore important to maximise the power that the battery can accept before any braking procedure in order to maximise the energy recovered. Bauman and Kazerani [73] achieve this in a fuel cell-ultracapacitor hybrid vehicle by ensuring that the energy stored in the capacitor is inversely proportional to the kinetic energy of the vehicle.

As part of the system design there may also be power electronics present, such as DC/DC converters and inverters. For example, in the Microcab H4 test vehicle there are a total of three DC/DC converters used. The efficiency of these devices will have an effect on the overall fuel economy [6, 73]. The main DC/DC converter is used to step the fuel cell output voltage (24V nominal) up to the battery voltage (48V nominal). As the efficiency of this converter will likely vary with the load, it must be taken into account when considering the optimal operating point for the fuel cell. Additional efficiency losses may include the traction motor, auxiliary loads and battery cycling. Staffell [6] has produced a Sankey diagram showing the energy losses obtained from 4000km of mileage accumulation of the Microcab H4 on the University of Birmingham campus, see Figure 2.2.

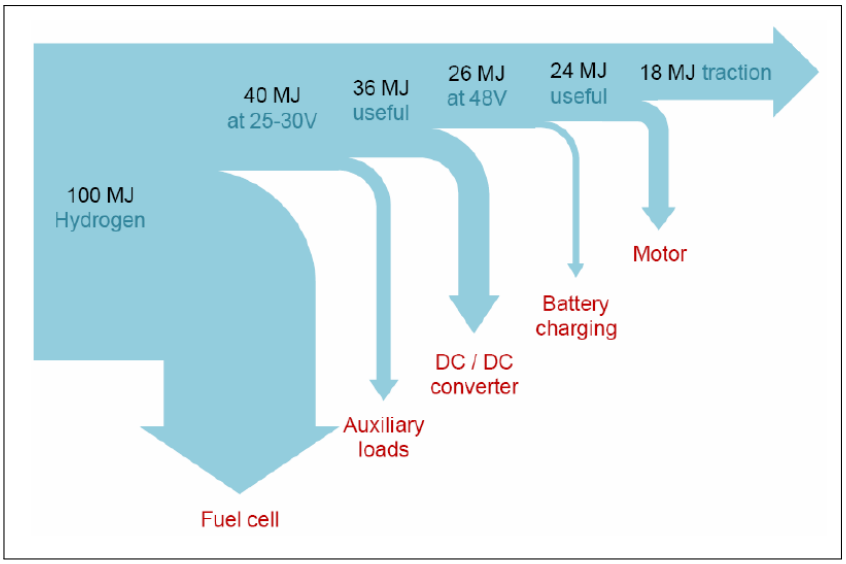

Figure 2.2: Sankey diagram showing the average efficiency of the Microcab powertrain - *Iain Staffell* [6]

The Sankey diagram shows that the overall efficiency of the Microcab H4 powertrain is approximately 18%, but Staffell [6] states that 30% to 50% [19, 35] efficiency has been reported in other FCHEVs, which could be achieved by system level optimisation of the Microcab powertrain. This can be attained by improved component selection including more advanced DC/DC converters in combination with a more effective EMS [6]. It can also be seen from the Sankey diagram, that the efficiency of the brushed DC motor is particularly low (75%). This puts a significant additional load on the rest of the system which could be reduced by using a more efficient motor.

"The optimal running points of individual components do not necessarily coincide with one another, meaning that a global compromise is required to avoid undesired operating points within the system" Iain Staffell [6]

Staffell also points out that some of the different components may have competing objectives in order to maximise their individual efficiencies. For example, is it more efficient to run the fuel cell at its most efficient operating point even if this causes the batteries to be cycled more than necessary (with the associated efficiency loss)? It is the role of the EMS to make decisions in order to answer this question. Overall, the EMS must be able to identify the global optimal operating points for the full powertrain, taking into account all significant efficiency losses in the system, in order to optimise the fuel economy of the vehicle as a whole.

2.2.1.1 EMS Strategy Examples

The optimisation of vehicle fuel economy is the main focus of almost all research into EMS strategy. This is because the EMS has a direct influence on the fuel economy of any HEV and gains of around 30% [48] can be achieved with sophisticated control strategies.

Lin *et al.* [45] look solely at improving the fuel economy of an ICE powered FedEx delivery truck using hybridisation. It is found that with simple "rule-based" control, the fuel economy is improved by 31% over the FTP cycle, which is further improved on by an additional 14% due to optimisation of the rule-based controller using DDP. Guezennec *et al.* [28] examine the potential to increase the system efficiency of a FCHEV using mild hybridisation. The introduction of hybridisation using an Equivalent Consumption Minimization Strategy (ECMS) strategy resulted in a 48% improvement in the fuel economy. This improvement is achieved by running the fuel cell in its optimal efficiency operating region for a higher proportion of the drive-cycle tested and a reduction in the time the fuel cell spends idling. It is also found that the peak power demand from the fuel cell is dramatically reduced. This results in an efficiency increase due to the reduction in ohmic losses which are proportional to the fuel cell power.

Schiffer *et al.* [29] explore the potential to optimise the fuel economy of a FCHEV using supercapacitors for regenerative braking. A number of potential state based strategies are examined and it is found that the best fuel saving can be achieved by maximising the supercapacitors capability for powering acceleration and absorbing regenerative braking energy over a strategy. This strategy shows a 25% reduction in fuel consumption when compared to a strategy which purely aims to run the fuel cell in its most efficient operating region.

2.2.1.2 Summary

In summary, there are various ways that the EMS can optimise the fuel economy of a FCHEV. Firstly, the fuel cell should be run in its optimal operating region for as much time as possible. The efficiency of the fuel cell varies significantly with its load. At idle or low loading, current is still required to run ancillary devices meaning that poor efficiency is achieved. At high power, ohmic losses and mass transport limitations significantly affect the output voltage leading to a drop in efficiency (see Figure 2.1). Therefore, it is best to run the fuel cell at part load, with approximately 30% of the maximum rated power being optimal. Secondly, the advantages of being able to store recovered braking energy should

be maximised. This often means that the battery SoC should be kept well below 100%, and its temperature should be kept low, in order to maintain its capability to absorb this energy. Finally, the operating efficiency of all other components in the powertrain should also be considered. This is because the efficiency of some devices such as DC/DC converters varies with load and this efficiency loss can significantly affect the efficiency of the system as a whole.

When compared to an ICE hybrid, the optimisation of fuel consumption on a FCHEV is generally quite simple. This is because the operating state of the fuel cell can be defined by a single parameter, its total power output, rather than the combination of speed and torque output. FCHEVs are set up in a series configuration and therefore the efficiency is totally decoupled from the vehicles velocity.

Overall, the system should be considered in a holistic sense. The various targets mentioned above may compete with each other under certain circumstances and therefore potential savings due to various strategies should be compared in order to obtain the lowest fuel economy possible. For example, although it is beneficial to keep the fuel cell running around 30% power, if this means that the batteries will become highly charged and therefore unable to recapture kinetic energy from braking, this may be detrimental to the overall fuel economy. Equally, the DC/DC converters may be very inefficient at 30% power, and it may be more beneficial to target a slightly higher or lower operating region after they are taken into account. Depending on the design of the system, each of these targets may have varying effect on the overall system efficiency and the optimal strategy for one design may not coincide with the optimal design for another.

2.2.2 Fuel Cell Degradation

"Component decay or failure is affected by many internal and external factors, including material properties, fuel cell operating conditions (such as humidification, temperature, cell voltage, etc.), impurities or contaminants in the feeds, environmental conditions (e.g., subfreezing or cold start), operation modes (such as start-up, shut-down, potential cycling, etc.), and the design of the components and the stack."
Yuan *et al.* [75]

There is a large volume of research into fuel cell degradation ranging from detailed electrochemical modelling [76] to empirical work on accelerated ageing testing [75, 77] to Failure Mode and Effects Analysis (FMEA) [78]. Therefore, the literature shown in this report [12, 32, 69, 75–85]only represents a fraction of the work being performed . However, the main targets for the reduction of fuel cell degradation have been examined in order to identify achievable targets for a supervisory controller to work with. The US Department of Energy [12] sets a target of 5000 hours lifetime for vehicle based fuel cells in order to compete with conventional technology. A typical figure representative of current PEM fuel cells is approximately 3500 hours [1]. The EMS is not directly responsible for managing the fuel cell; however, the decisions it makes can significantly affect the conditions in the stack [80]. An effective EMS has the potential to not only increase the useful lifetime of the fuel cell, but also to reduce the required number of hours of operation to be competitive with conventional ICEs by running the fuel cell for less time relative to the vehicle's operational time.

Fuel cell component failure and decay can occur due to a variety of reasons including material properties, operating conditions, impurities in the reactants and environmental conditions [75]. The EMS will have no control over some of these degradation methods, such as impurities in the fuel, but can have a significant effect on degradation due to operating conditions. External influences such as environmental conditions can also be managed by the EMS by varying the operational mode in order to minimise their effect. This section will review the most well-known causes of Membrane Electrode Assembly (MEA) performance degradation, which can be split into three categories; catalyst layer, membrane layer, and Gas Diffusion Layer (GDL). The main targets for the EMS are summarised in a table at the end.

2.2.2.1 Catalyst Layer

The catalyst layer of a PEM fuel cell is generally made up of a porous carbon support to which platinum catalyst particles are attached. In order to maximise the effectiveness of the catalyst and minimise the material cost of the fuel cell, platinum particles of nanometre scale are distributed as evenly as possible across the support (see Figure 2.3). Catalyst layer degradation is largely due to two main causes; the agglomeration and sintering of the platinum particles and the corrosion of the carbon support. Both of these have the effect of reducing the Electro-Chemical Active Surface Area (ECASA) and hence reducing reaction rates and therefore cell voltage. These processes generally occur naturally within the cell and over time the cell voltage will decrease, however certain operating conditions can increase the rate of degradation significantly and therefore these should be avoided.

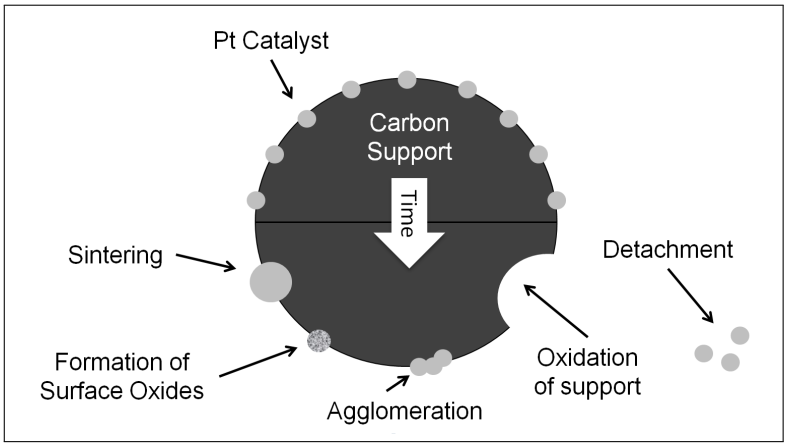

Figure 2.3: Major Causes of Electro-Chemical Active Surface Area ("ECASA") Reduction

Carbon corrosion is one of the major causes of catalyst layer degradation, and occurs due to the electrochemical oxidation of carbon catalyst support. As the support degrades, the catalyst particles become detached and either fall to the bottom of the cell or are carried away in the waste products. The effect is minimal at low potentials due to the slow kinetics of the reaction [75]. Despite the presence of the platinum catalyst in a PEM fuel cell, potentials below 0.55V vs. Reversible Hydrogen Electrode (RHE) [75] pose negligible risk of carbon corrosion. Carbon corrosion happens fastest as high cell potentials, or low current loading, and is especially accelerated at open-circuit. During start-up and shut-down, and in situations of fuel starvation, the non-uniform distribution of fuel on the anode can also increase the rate of carbon corrosion. These circumstances must be avoided when at all possible in order to limit the degradation of the catalyst layer.

The agglomeration and sintering of catalyst particles can occur due to migration as the carbon support is degraded and the particles become mobile. This leads to an ECASA reduction and hence a reduction in cell performance. High cathode potentials may also cause the formation of oxides on the surface of the catalyst which can lead to a loss of activity. Although the oxide layer tends to be temporary, the particles may agglomerate as the platinum is reduced leading to a permanent loss of activity.

2.2.2.2 Membrane Layer

The membrane layer of a PEM fuel cell is generally made of Nafion ionomer which is chosen due to its excellent proton permeability and relative thermal and mechanical stability. It forms a barrier preventing the electron conduction whilst allowing protons to pass through. Damage may occur to the membrane due to a variety of inter-related reasons (see Figure 2.4) each of which may exacerbate the others.

Membrane degradation can be split into mechanical, chemical and thermal damage [75]. Mechanical damage may occur due to defects during the MEA fabrication; however, it can also occur due to thermal stress and drying of the membrane. Thermal stress will cause the membrane to dehydrate which leads to a loss of proton conductivity [75]. Decreased proton conductivity causes an effective increase in the internal resistance of the cell which itself can lead to further heating. Chemical damage is caused by cationic contaminants which can penetrate the membrane and lead to reduced protonic conductivity.

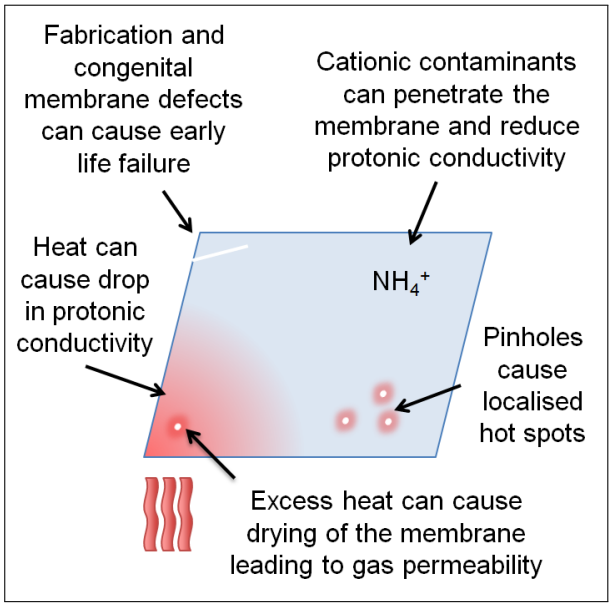

Figure 2.4: Major Causes of Membrane Degradation

The EMS can do very little about congenital defects or mechanical damage introduced during fabrication of the MEA. Equally contaminants in the reactant supply are out of the scope of the EMS; however, the EMS can have a large effect on the thermal homoeostasis of the membrane. The controller may be able to take action in order to prevent over-heating and subsequent dehydration of the membrane by monitoring the temperature and humidity of the fuel cell. Nafion-112 swells to 167% of its dry volume when it is fully saturated with water [1] which can put significant mechanical stress on the membrane. Liu and Case [80] show that cyclic loading of the MEA in a PEM fuel cell increases the membrane degradation when compared to constant current. This is attributed to hydrothermal-mechanical stress resulting from wet-dry cycling which may cause microscopic and macroscopic holes in the membrane.

Zhang *et al.* [77] explain that open-circuit voltage without electrical loading enhances MEA degradation in addition to carbon corrosion of the catalyst support. This is due to the formation of peroxide radicals generated by incomplete reduction of oxygen at the cathode, and by the significant gas crossover which occurs at the anode/membrane interface under open circuit voltage [77]. Conversely, if the reactant gases are over saturated with water due to high current loading, the electrodes and gas diffusion layer can become flooded, causing blockages and hence localised reactant starvation and thermal gradients across the membrane [77].

2.2.2.3 Gas Diffusion Layer (GDL)

The gas diffusion layer and bipolar plates are generally the most stable components of the fuel cell, but may suffer from carbon corrosion in a comparable manner to the catalyst [75]. However, due to the absence of platinum, the reaction kinetics are even slower than the catalyst layer. From an EMS standpoint, the catalyst layer represents a tighter constraint. Similarly, the bipolar plates may suffer from thermal distortion, but are not damaged by excessive heat as quickly as the membrane and therefore thermal protection of the membrane should also prevent damage to the bipolar plates.

2.2.2.4 Low-Level Controller

Depending on the complexity of fuel cell system, there may be a low-level controller responsible for controlling the auxiliary components such as a fan, compressor, and/or humidifier. It is therefore useful to consider the low-level control of the fuel cell as separate to the supervisory control performed by the EMS. The fuel cell controller is responsible, for example, for controlling the fan in order to manage the fuel cell temperature. The EMS, on the other hand, is responsible for supervisory control, e.g., managing power in the battery and providing the power demand to the fuel cell controller. Guezennec *et al.* [28] mention that they should be considered simultaneously. This is because in order to provide an optimal system, the EMS must be aware of the constraints on the low-level controller. The fuel cell system on the Microcab H4 is provided with a built-in controller that will manage temperature, humidity and reactant supply. The EMS is therefore only responsible for choosing the operating point of the fuel cell with regards to load. Depending on the control authority of the low-level control, sudden changes in this load may cause the fuel cell to operate outside optimal conditions. The EMS must therefore take these constraints into account in its design in order to minimise fuel cell degradation.

2.2.2.5 EMS Strategy Examples

A number of authors have proposed EMSs that combat fuel cell degradation, mainly focussed on two major causes; the reduction of transient loading, and prevention of reactant starvation. Thounthong *et al.* [70, 86] and more recently Aouzellag *et al.* [87] target the reduction of transient loading with a "rule-based" approach using rate of load change limits on the fuel cell and the battery pack. Pukrushpan *et al.* [88], Vahidi *et al.* [32] and Lin *et al.* [31] focus on the control of oxygen flow in order to prevent reactant starvation. More recently, Xu *et al.* [89] has developed a multi-mode strategy that includes limitations on the upper and lower fuel cell power as well as the reduction of transient loads by using penalty functions on a DDP optimisation.

Vahidi *et al.* [32] mention data shown in a patent by Ballard [90] where the fuel cell voltage is reversed during oxygen starvation. They also mention that low concentrations of oxygen may also cause a significant rise in temperature within the fuel cell. In high pressure fuel cells, the oxygen is supplied using a compressor which may account for up to 30% of the fuel cell power during a rapid increase in air flow. This means that the compressor adds to the power demand on the fuel cell making the problem worse. The EMS can alleviate this problem by avoiding the sudden demand of high current and instead ramping up the load on the fuel cell slowly, allowing the fuel cell controller to maintain the reactant supply reliably.

Thounthong *et al.* [86] develop a hybrid EMS for a fuel cell/battery/supercapacitor power supply where the rate of fuel cell demand power is limited in order to reduce the transient loading on the fuel cell. This also has the advantage of limiting high power usage potentially allowing the fuel cell to be downsized. A similar method is used by Guezennec *et al.* [28] for an ECMS and by Di Cairano *et al.* [66], who use Model Predictive Control (MPC) to predict the anticipated power demand over a short horizon in order to smooth the engine power of an ICE in a hybrid vehicle. Although not applied to a fuel cell vehicle, it is mentioned that this approach could be used to extend the lifetime of a fuel cell on board a FCHEV.

It must be mentioned that these limits represent hard constraints on the controller and are heuristic in nature. This means that although they seem to be beneficial in simulation testing, no quantifiable advantage is given other than a pure reduction in the transient loading and the implied advantages of this. Aside from the work in this thesis, no research has been found that quantitatively relates the degradation methods mentioned above to the optimisation of the EMS.

2.2.2.6 Summary

In conclusion, the most important degradation methods from an EMS standpoint are carbon corrosion of the catalyst layer and dehydration damage to the membrane due to wet-dry cycling and overheating. Carbon corrosion occurs at high cell potentials, during start-up and shut-down and due to fuel starvation. This can be limited by avoiding low power operation and refraining from start-stop cycling of the fuel cell where possible. Thermal degradation can lead to damage to the membrane and bipolar plates. Although the low-level controller is primarily responsible for managing the temperature of the fuel cell, the EMS can assist by avoiding higher power demand for extended periods of time. Finally, reactant starvation and sudden humidity changes can be avoided by limiting the rate of load changes and avoiding transient loads on the fuel cell [28].

Although the EMS can do little to prevent a number of significant degradation methods, there is a lot that the EMS can do to limit degradation due to the operating condition of the fuel cell. Overall targets for the EMS are to limit start-stop cycling and minimise transient loading in order to prevent localised fuel starvation and humidity changes to the membrane. The EMS should also avoid running the fuel cell at extreme loading conditions including both high and low power demand. Low power demand causes a high potential, leading to corrosion of the catalyst support, oxidation of the catalyst and the production of peroxide radicals. On the other hand, high current demand can cause increased cell internal resistance leading to overheating and dehydration of the membrane as well as fuel starvation due to potential supply limitations. A concise list of the main EMS strategy concerns for limiting degradation of PEM fuel cells has been summarised in Table 2.1.

Method	Mechanism	EMS Action
Carbon Corrosion of Catalyst Support	The carbon catalyst support is electrochemically oxidised more rapidly at high cell potentials, leading to ECASA reduction [75]	Ensure fuel cell is electrically loaded when running
	Fuel starvation due to current demand exceeding supply limit leads to oxidation of the carbon support [75]	Ensure current demand does not exceed reactant supply limitations
	Non-uniform distribution of fuel on the anode during start-up and shut-down leads to localised reactant starvation and hence oxidation of the carbon support [75]	Limit start-up/shut-down cycling where possible
	Non-uniform distribution of fuel on the anode during transient loading leads to localised reactant starvation and hence oxidation of the carbon support [75]	Limit sudden transient loading
	Cell "flooding" can cause localised fuel starvation and hence oxidation of the carbon support [75, 77]	Ensure current demand does not exceed product removal limitations
Formation of Oxides on Surface of Catalyst	Oxidation/Reduction cycling of the catalyst surface causes the particles to agglomerate and hence ECASA reduction [75]	Ensure fuel cell is electrically loaded when running
Membrane Chemical Attack	Open-circuit voltage causes formation of peroxide radicals and high gas crossover at the anode/membrane interface [75, 77]	Ensure fuel cell is electrically loaded when running
Membrane Hydrothermal-Mechanic Stress	Load cycling can cause the membrane to swell and contract as the humidity changes leading to mechanical stress on the membrane and the formation of holes [1, 80]	Limit sudden transient loading
Membrane Thermal Degradation	Thermal stress due to high current demand causes membrane dehydration and decreased proton conductivity leading to further heating and possible membrane damage [75]	Ensure current demand does not exceed heat removal limitations
	Oxygen starvation can cause rapid temperature rises [32, 69, 75, 79]	Ensure current demand does not exceed reactant supply limitations
	Cell "flooding" can cause localised oxygen starvation [75, 77]	Ensure current demand does not exceed product removal limitations

Table 2.1: EMS Strategy Concerns for Limiting Fuel Cell Degradation

2.2.3 Battery Degradation

"Particularly high temperatures, high currents, and high energy throughput are the main factors that force the deterioration of batteries' electric characteristics." Roscher *et al.* [91]

The EMS is directly responsible for the SoC and current loading of the battery at any point in time. This means that it will have a significant effect on how quickly the battery degrades. Batteries degrade for a number of reasons depending on the chemistry, but the most significant methods of degradation are caused by operating them outside of their temperature and voltage limits [7, 36, 91] or by over-cycling them [7, 91]. Generally, a battery should never exceed its maximum voltage [7, 91]. This can be caused by either attempting to charge a fully charged battery or exceeding the current that the battery can safely absorb. For traction batteries, this is most likely to occur during regenerative braking. Equally the battery should not be allowed to drop significantly below its minimum voltage ("deep-discharge") [36]. This may occur by either attempting to draw current from an empty battery or exceeding the current that the battery can readily supply, and is most likely to happen during traction. Finally, charge-discharge cycles will cause incremental damage to the battery and therefore the EMS should avoid cycling the battery more than necessary. Manufacturers will usually provide a battery lifetime estimate which is given as a number of cycles before the battery is reduced to 80% of its original capacity.

2.2.3.1 Lead Acid Batteries

Lead acid batteries are currently used as the battery in the Microcab H4 which is available for testing at Loughborough University and therefore an understanding of lead acid battery degradation causes is important for the design of an EMS suitable for this vehicle. Ruetschi [7] and Nakamura *et al.* [92] have written comprehensive articles analysing lead acid battery degradation mechanisms. The ageing mechanisms depend on the use of the battery and are often interdependent, i.e., degradation due to one mechanism may increase the rate of another. The most common ageing mechanisms are listed below;

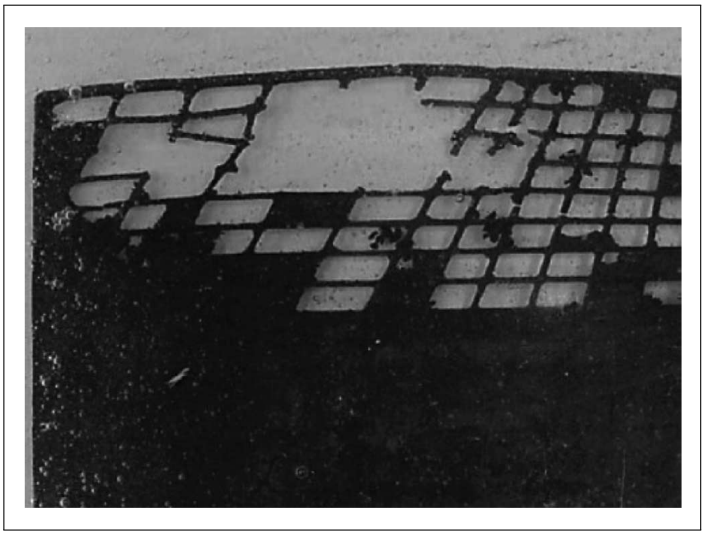

Figure 2.5: End of Life Lead Acid Battery Grid - *Ruetschi* [7]

1. **Anodic corrosion (of grids, plate-lugs, straps or posts, see Figure 2.5)** Anodic corrosion is considered by Ruetschi [7] to be the "natural" ageing mechanism in lead acid SLI batteries. Anodic corrosion is caused by the inherent electrochemical instability of metallic lead in the positive plate meaning that it is practically unavoidable, however the kinetics of the corrosion are so slow (due to a formed corrosion film) that satisfactory service life is possible. In order to achieve the best service life, Ruetschi [7] recommends that over-charging should be avoided and end of charge voltage should be appropriately limited.

2. **Positive active mass degradation and loss of adherence to the grid (shedding, sludging)** As the battery is recharged after being discharged, lead oxide may be re-deposited in slightly different morphology than existed before. With repeated cycling, the active anode mass gradually changes shape, losing mechanical strength and electrical conductivity. Charging at high current has a favourable effect on the positive active mass, possibly due to the higher temperature associated. In fact, up to 60°C [7] has shown to be optimal, above which grid corrosion may become the life-limiting factor. With appropriate design for deep-discharge, batteries may reach 1500 cycles to a Depth of Discharge (DoD) of 80%, but standard SLI batteries would not cope with 100 such cycles [7].

3. **Negative active mass degradation and loss of adherence to the grid** It has been found that the high current charging in electric vehicles as a result of regenerative braking has a tendency to degrade lead acid batteries. Nakamura *et al.* [92] suggest that the elevated temperature caused by high current charging causes additives in the cathode active material to decompose. In order to confirm this, a number of tests were performed where the temperature of the battery was carefully managed. It was seen that the capacity of the battery dropped significantly when charged at temperatures above 50°C.

4. **Irreversible formation of lead sulphate in the active mass (crystallization, sulphation)** "Sulphation" is a major cause of lead acid battery failures and results from the irreversible formation of crystalline lead sulphate. Lead sulphate can only be partially reconverted back into an electrochemically active form, leading to a reduction in the capacity of the battery. It is most likely to occur when the batteries remain in a partially discharged form for prolonged periods of time. This has been shown by Nakamura *et al.* [92] to be a major cause of traction battery failure in electric vehicles due to irregular charging patterns and continued usage after a partial re-charge, such as from regenerative braking.

5. **Short-circuits** Short-circuits are almost always the result of deep-discharge [7]. This is caused by lead sulphate precipitation in the dilute acid. On recharge, this lead sulphate is converted to metallic lead potentially shorting the separator medium. Short-circuits can also occur from loose, partly sulphated, lead oxide particles which have broken off the anode corrosion layer. Suspended in the electrolyte, they can be transported to the edges of the plates or the bottom of the cell, potentially causing a short-circuit.

6. **Loss of water** Although many modern lead acid batteries are considered maintenance free, suffering from very little (if any) water loss, there are certain situations which can cause significant evaporation or electrolysis of the water. Overcharging leads to rapid loss of water through electrolysis and should be limited to a maximum of 4% [7] in order to prevent this. Self-discharge electrolysis can also take place if the batteries are left at open-circuit voltage for extended periods of time.

2.2.3.2 Lithium-ion Batteries

Lithium-ion batteries are quickly becoming the default design choice for any high power, high capacity energy storage application, especially where the weight is important due to their high energy and power densities. The new Microcab H2EV uses lithium-ion batteries for energy storage, and therefore an understanding of degradation causes is important for the design of an EMS for this vehicle. The degradation of lithium-ion batteries is also the result of complex interactions between different processes occurring within the cells [93]. A summary of the processes associated with lithium-ion battery degradation can be found below [93–95].

1. **Electrolyte decomposition** [93, 95] As with lead acid batteries, the lithium-ion battery anodes operate at potentials outside of the electrochemical stability of the electrolyte components. This causes an irreversible decomposition of lithium-ions at the electrode/electrolyte interface, which builds up a protective layer known as the Solid Electrolyte Interface (SEI). The SEI protects the electrolyte from reduction, and simultaneously defends the charged electrode from corrosion. Unfortunately, the SEI does not provide complete protection and this reaction continues to occur (albeit at lower rates) throughout the batteries life. As time passes, the SEI will eventually penetrate into pores in the electrodes (and the separator) causing an effective decrease in the active surface area of the anode, increasing the impedance of the cell. Excessive heat will increase the kinetics of this reaction, and temperatures above 80°C [93] have been known to cause exothermic side reactions in the SEI which can lead to "thermal runaway".

2. **Solvent co-intercalation** [93] Solvent co-intercalation is caused by overcharging the battery and causes a loss of active material on the anode, as well as a permanent loss of active lithium.

3. **Current collector corrosion** [93] Current collector corrosion is caused by over-discharging the battery ("deep-discharge") and causes over-potentials at the anode which lead to impedance rises and inhomogeneous distribution of current and potential.

4. **Lithium metal plating** [93] Lithium metal plating occurs mainly at low temperatures, high cycling rates, and inhomogeneous current and potential distributions. This causes lithium metal to react directly with the electrolyte, contributing to loss of the electrolyte.

5. **Structural changes in the active material** [93] Only minor changes are expected to occur within the active material (typically less than 10% [93]) during the uptake and removal of lithium-ions from the electrode under normal use. Structural

changes, however, can cause mechanical stress which might result in cracking or related damage.

Work by Peterson *et al.* [94] and Zhang *et al.* [95] suggest that for modern lithium-ion cells used in electric vehicles, the most common degradation mode is decay of the SEI layer and associated capacity loss. The SoC range used by Zhang *et al.* [95] was between 30% and 80% DoD. In conclusion, the decay of the SEI due to high temperatures (above approximately 60°C) is by far the most common cause of lithium-ion battery degradation seen in automotive use, even for batteries with a large SoC duty range. Elevated temperatures are most likely to be caused by excessive power draw. In contrast to lead acid batteries, lithium-ion batteries do not exhibit significant degradation caused by partial charging (e.g., "Sulphation") or self-discharge and therefore are more suitable for battery vehicle duty cycles where they will be required to absorb regenerative braking energy and not necessarily maintained at full charge.

2.2.3.3 EMS Strategy Examples

Vagg *et al.* [96] develop a control strategy for a retrofit hybridised vehicle using the square of the current to estimate the stress on the electrical powertrain. Although this does not directly relate to any physical ageing mechanism, the square of the current is proportional to the ohmic losses and therefore heat generation in the battery and motor. By minimising the heat generation, the thermal stress on the battery should be minimised. This is incorporated into the cost function in order to allow trade-off against the fuel consumption by changing the weighting value. It is found that it is possible to reduce the mean square battery current by approximately 13% without compromise to the fuel economy.

Moura *et al.* [64] use two different models to predict the ageing of a lithium-ion battery. The first is a detailed electrochemical model to predict the growth of the SEI film depending on the current and SoC of the battery. Using a weighting parameter, the SEI film growth is incorporated into the cost function for a Charge-Depleting (CD) strategy. The results show that the controller tends to deplete the battery quickly initially in order to avoid the elevated level of growth which occurs at high SoC. The SoC begins to stabilise around 50-60% slowly depleting to around 25% until near the end where the strategy becomes charge-sustaining.

The second method employed by Moura *et al.* [64] is simply to penalise the energy throughput of the battery and hence attempt to limit excessive charge/discharge cycling. It is found that by minimising the energy throughput of the battery, the fuel consumption of the vehicle is dramatically increased due to the engine spending a much higher proportion of the journey at undesirable operating points. Specifically, for a 57% reduction in energy throughput, the fuel consumption is increased by 82%. This demonstrates the fundamental trade-off that exists between these two targets.

2.2.3.4 Summary

In summary, lithium-ion batteries are much more suited to be traction batteries when compared to lead acid. This is not only due to their higher gravimetric energy density, but also because they do not exhibit degradation caused by partial charging such as that caused by regenerative braking events. In contrast lead acid batteries should be maintained at 100% charge whenever possible. This may mean that the capacity of lead acid batteries to

absorb regenerative braking energy may be reduced when compared to lithium-ion. Ideally, lithium-ion batteries should be maintained at approximately 80% charge allowing for a higher reserve capacity for regenerative braking events and a lower risk of overcharging, although work by Moura *et al.* suggests that even lower SoC is desirable when considering SEI growth.

Lead acid batteries are fairly resilient to charging and discharging at temperatures up to 50°C, however the temperature of lithium-ion batteries should be controlled very carefully. This is because the major causes of degradation, such as SEI decay, occur at much higher rates at elevated temperatures. In addition to this, exothermic reactions which can lead to catastrophic failure of the battery may occur at temperatures above 80°C. The temperature of the battery can be managed by the EMS by avoiding high currents which may lead to heating due to the internal resistance of the cell.

Both chemistries are degraded by overcharging and "deep-discharge". For lead acid batteries, this competes with the objective to maintain a high SoC, whereas this is easily managed for lithium-ion batteries by targeting a lower SoC. Equally, for both chemistries, excessive cycling should be avoided. This can lead to active mass redistribution leading to a reduced active surface area and hence lower cell performance in both chemistries, and to lithium metal plating in lithium-ion batteries. A concise list of the main EMS strategy concerns for limiting degradation of lead acid and lithium batteries has been summarised in Table 2.2.

Method	Chemistry	Method	EMS Action
Negative Active Mass Degradation	Lead Acid	High currents and associated temperatures caused by regenerative braking charging events cause the cathode to degrade [92]	Reduce Regenerative Braking if Battery Temperature Increases
Formation of Lead Sulphate ("Sulphation")	Lead Acid	Partial charging caused by regenerative braking events as well as never completely charging the cell can cause gradual formation of lead sulphate [7, 92]	Try to maintain battery at full charge where possible
Short-circuits	Lead Acid	Deep-discharge events cause precipitation of lead sulphate in the dilute acid, subsequent charging converts this to metallic lead potentially shorting the separator [7]	Avoid deep-discharge
Water Loss	Lead Acid	Water loss is most often caused by overcharging the battery [7]	Avoid over-charging
Positive Active Mass Degradation	Lead Acid Mainly	As the battery is cycled the active mass is gradually redistributed on the anode causing a reduction in mechanical stability and electric conductivity [7]	Avoid cycling battery
Anodic Corrosion	Both	Anodic corrosion occurs constantly in both chemistries. Although the kinetics of the reaction are slow, it occurs at higher rates when the temperature is increased. In lead acid, it can be accelerated significantly by over-charging [7]	Avoid over-charging and manage temperature
SEI Decomposition	Lithium-ion	SEI Decomposition occurs constantly in lithium-ion batteries, but reaction kinetics are increased by increased temperatures [93, 95]	Manage temperature at all times
Solvent Co-intercalation	Lithium-ion	Solvent co-intercalation is caused by overcharging the battery [93]	Avoid over-charging
Current Collector Corrosion	Lithium-ion	Current collector corrosion is caused by over-discharging the battery ("deep-discharge") [93]	Avoid deep-discharge
Lithium Metal Plating	Lithium-ion	Lithium metal plating occurs mainly at low temperatures, high cycling rates, and inhomogeneous current and potential distributions [93]	Limit cycling where possible, avoid deep-discharge and manage temperatures

Table 2.2: EMS Strategy Concerns for Limiting Battery Degradation

2.2.4 Drive-ability

"Drivability is a rather vague term that covers many aspects of vehicle performance including acceleration, engine noise, braking, shifting activity, shift quality, and other behaviours." Opila et al. [53]

The term "drive-ability" covers a wide range of parameters perceived by the driver of the vehicle. This includes pedal response, noise and vibration [8, 53]. The vehicle should be able respond to the driver's input in a predictable and consistent manner. For example, this means that the vehicle should not be slower to accelerate when the battery SoC is low. Drive-ability may also take into account the behaviour of the system in the event of a component failure [56]. Drive-ability concerns are often taken into account after optimisation of the fuel economy of the vehicle, leading to a non-optimal overall solution [62]. By including drive-ability concerns in the optimisation routine of the EMS, a globally optimal solution can be found.

2.2.4.1 Gear Shifts

The majority of the work in the literature with concern to drive-ability is focussed on HEVs with automatic transmissions. In situation, the EMS is usually responsible for choosing the optimal gear in order to control the operating point of the engine. Obviously for a FCHEV with a single fixed gear such as the Microcab, gear shift vibration is not a concern; however, some of the lessons learnt in the development of these controllers are still relevant for many FCHEVs, and potentially for the new Microcab H2EV. Work by Pisu *et al.* [8, 50] seeks to minimise driveline vibration and achieve smooth gear changes by modelling the stiffness' of the driveshafts (see Figure 2.6) and incorporating the resulting vibration into the optimisation of their controllers.

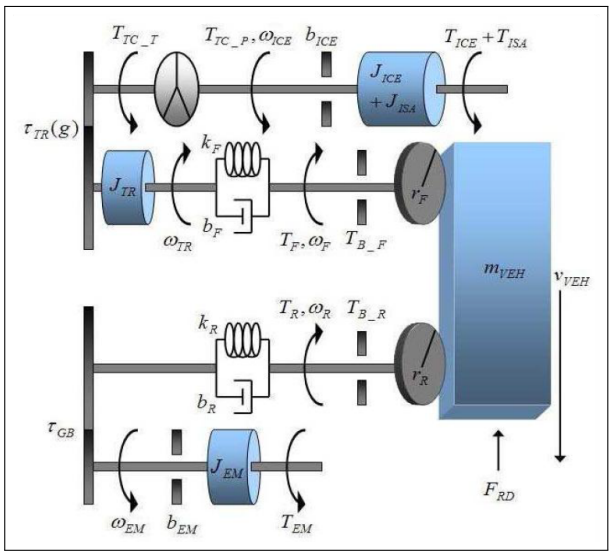

Figure 2.6: Drive-ability Metrics, Pisu *et al.* [8]

Opila *et al.* [26, 53] attempt to combat a number of other issues after discussion with drive-ability experts at Ford Motor Company. A primary concern for Ford is the driver's perception of what the engine and transmission are doing. The driver is often aware of changes in engine noise, and of gear shifts. The main problems are high frequency of engine stop-start events, high frequency of gear shifts, including "hunting" and unexpected gear shifts [53]. Opila *et al.* [26, 53] break these issues down to two baseline metrics, the number of engine stop-start events and the number of gear shifts. By incorporating a penalty into their optimisation function, they are able to reduce the number of engine stop-start events and the number of shifts, with the secondary effect of reducing gear shift "hunting". By tuning the penalty weighting factors for fuel economy, engine stop-start events and gear shift events, they are able to trade the drive-ability of the vehicle against the fuel economy. In their 2012 work [26], it is shown that they are able to maintain the drive-ability of Ford's baseline controller whilst improving fuel economy by 11% by using their optimised controller. Vidal-Naquet and Zito [62] show that without drive-ability included in the optimisation, there are over 300 gear shifts with approximately 30% of these taking place within 2 seconds of one another. By including the drive-ability metrics and tuning the weighting parameters, a final result of just 107 shifts is achieved with only 2% increase in fuel consumption.

2.2.4.2 Power Availability

Vidal-Naquet and Zito [62] treat the instantaneous potential acceleration available as a drive-ability metric in addition to the frequency of gear shift events. The instantaneous acceleration metric improves the "feel" of the vehicle, because more power is available in reserve if the driver chooses to accelerate. Generally, for a HEV fitted with an automated transmission, the optimal fuel economy will be achieved by shifting gear as soon as possible to ensure the engine speed is low. The acceleration potential metric will tend to delay the shifts so that more power reserve is available, however this will be directly at the expense of the fuel economy [62]. Vidal-Naquet and Zito [62] note that the weighting parameters can be tuned to achieve manufacturers desired drive-ability/fuel consumption balance for different vehicle driving modes such as "Sport", "Normal" and "Economy". FCHEV transmissions are often single speed, and therefore this drive-ability metric is not affected by the transmission. However, Schiffer *et al.* [29] use a benchmark termed "Power Constraint" in their optimisation. This metric penalises times when the fuel cell and supercapacitors in their vehicle are unable to cope with driver demand, effectively a negative instantaneous potential acceleration. This drop in power will affect the driver's perception of the vehicle, however Schiffer *et al.*'s method does not measure acceleration potential above of the normal driver demand. Overall, a combination of both metrics would be ideal, the instantaneous available power should be maximised, but additional penalty should be added if it becomes negative.

Traditionally, the throttle pedal of an ICE vehicle is used to directly control the engine throttle valve, but increasingly the pedal position is electronically sent to the engine Electronic Control Unit (ECU) as a measure of the driver's torque demand. For non-hybrid vehicles, this is simply done so that the ECU can over-ride the drivers demand in situations such as cruise control or traction control action is in effect. Under normal circumstances, the position is passed straight through to mimic a cable controlled throttle. In HEVs however, the question arises of what the driver expects when the pedal is depressed. There are

multiple sources of mechanical torque on parallel and combined HEVs so should the pedal mimic a cable throttle, directly control engine torque, or overall wheel torque including actions of the gearbox and traction motors? Boris *et al.* [97] have found that the driver is not significantly affected by a throttle pedal which mimics a cable throttle or by a pedal which directly controls engine torque. However, the driver is often unable to compensate for pedals which directly control the wheel torque including the actions of an automatic transmission.

2.2.4.3 Summary

The test vehicle available for this project is the Microcab H4 which has a single fixed gear ratio, meaning that no optimisation is required for gear change events. However, the fuel cell can be compared to the ICE in a fossil fuel HEV, and the frequency of fuel cell start-stop events will contribute to the driver's perception of the vehicle. In addition to this, the power reserve available for acceleration may be related to the fuel cell power because of the limited power capability of the batteries, especially on the H4, and therefore this could be included in the optimisation of the EMS strategy. The motor is the sole source of mechanical torque and so the pedal should directly control the produced motor torque. Similar brake pedal control concerns exist for regenerative braking, especially when combining with the mechanical brakes, however on the Microcab H4, regenerative braking has been disabled [4]. Finally, the fuel cell system may generate some additional noise at high power due to the fans running at a higher speed. This may be of concern to the driver under certain conditions. A summary of the drive-ability concerns has been provided in Table 2.3, the main concerns for a FCHEV highlighted in bold text.

Drive-ability Issue	**EMS Strategy Concerns**
Driveline Vibrations	Minimise torque oscillations
Engine/Fuel Cell Stop-Start	**Penalise Engine/Fuel Cell On-Off Cycling**
Engine/Fuel Cell Noise	**Penalise High Power Engine/Fuel Cell Usage at Low Speed**
Excessive Gear Changes	Penalise Gear Change Events
Gear Change "Hunting"	Penalise Gear Change Events
Power Availability	**Penalise Lack of Power Availability**
Accelerator Pedal Control	**Pedal Controls Motor Torque**
Braking Pedal Control	**Pedal Controls Total Braking Torque**

Table 2.3: EMS Strategy Concerns for Drive-ability

2.2.5 Conclusions

Tate *et al.* [52] list the main objectives for conventional vehicle powertrain optimisation as *"fuel economy, emissions, torque deviations and component protection"*. Hybrid vehicle vehicles also require additional objectives: *"In addition to certification requirements, a manufacturer may have other control objectives including battery life management, system thermal management to prevent component overheating, and minimization of the customer's perceptions of 'odd' behaviour."*

It can be seen that there are various requirements for the EMS, some of which may have competing objectives. Work in the literature shows a number of different approaches to this problem. A sizeable proportion of research papers simply compare the fuel economy of different EMS methods. This simplifies the results and makes them easier to compare directly. This is particularly useful when performing sizing exercises or comparing different algorithms for suitability purposes. However, these results may not be useful under real-world conditions due to an undesired amount of component degradation and/or poor drive-ability. When used on board vehicles, these algorithms are often modified to improve durability and/or drive-ability aspects, inevitably leading to a reduction in overall performance.

Fuel cell and/or battery degradation and the associated replacement costs can represent a significant running cost of a HEV and therefore should be considered concurrently with fuel running cost. Much of the work in the literature tends to include simple constraints used in order to manage the degradation of the battery, but these are often quite simplified and are implemented arbitrarily. One example of this is Sinoquet *et al.* [74] who set hard constraints on the battery SoC, at a minimum of 50% and maximum of 70% SoC. These numbers seem to be set arbitrarily and significantly reduce the usable capacity of the battery pack. By incorporating realistic battery degradation metrics into the EMS strategy, additional battery degradation could be traded off against fuel economy for optimisation of overall long-term running cost. In addition to this, the usable capacity of the battery pack can be maximised, leading to a reduction in the required battery size for similar levels of performance.

For real-world vehicles, drive-ability constraints are often added to the EMS strategy after optimisation [62]. This means that the EMS strategy is optimised based on fuel economy and/or a cost function and then additional algorithms are subsequently added to over-ride the optimised strategy when it would detriment drive-ability aspects of the vehicle. This is a consequence of the product design cycle where the EMS strategy has caused poor drive-ability, which has only become apparent during testing. This leads to an EMS strategy which may suffer from significantly degraded performance when compared to the optimised strategy. A lot of work has been done by manufacturers to identify what drivers perceive to be poor drive-ability. By incorporating these metrics into the optimisation, the fuel economy may be improved significantly while still maintaining good "feel" to the driver. As an example of this Opila *et al.* [26] show that they are able to maintain the drive-ability of Ford's baseline controller whilst improving fuel economy by 11% when using their optimised EMS strategy.

Many research papers propose cost functions based on a number of factors including fuel economy, emissions, component degradation and drive-ability. Fuel economy is generally treated as the overall target for optimisation. Generally, component (especially battery) degradation is accounted for by the use of constraints. For example, SoC limits for the bat-

tery [74] or load change rate limits for the fuel cell [28]. There is potential for improvement by including the component degradation as part of the cost function optimisation. Component degradation could potentially be appropriately weighted by Mean Time To Failure (MTTF) and replacement cost to optimise long-term running cost rather than simply the fuel cost. Drive-ability is very difficult to quantify and requirements may change depending on the type of vehicle and its use. Vidal-Naquet and Zito [62] recommend the use of a variable weighting depending on the manufacturer's requirements.

In conclusion, this section has identified a large number of objectives for the EMS strategy and how they can be combined using a cost function. Some of these objectives are mutually beneficial, for example avoiding cycling of the battery will increase its operating efficiency and protect it from degradation, however others are competitive, avoiding transient loads on the fuel cell may protect the fuel cell, but will tend degrade the battery. By incorporating multiple objectives into the cost function and weighting them representatively, the overall optimal strategy can be calculated. The primary objectives for the EMS have been summarised in Table 2.4.

EMS Concern	Reason	Potential Action
Optimise Fuel Economy	Minimise Running Costs	Penalise fuel usage over drive-cycle
Attempt to Maintain Battery at Full Charge	Lead Acid Only - Prevent "Sulphation"	Penalise deviation from full charge
Avoid Cycling Battery	Prevent Positive Mass Degradation of Battery	Penalise Battery Charge/Discharge
Avoid Overcharging Battery	Prevent Anodic Corrosion of Battery	Penalise high SoC
Avoid Deep Discharging Battery	Prevent Solvent Co-intercalation in Lithium-Ion Batteries and Potential Short-circuits in Lead Acid	Penalise low SoC
Manage Battery Temperature	Prevent a Number of Battery Degradation Causes	Penalise High/Low Battery Temperature
Avoid Low Current Demand on Fuel Cell	Prevent ECASA Reduction	Penalise low fuel cell current loading
Avoid High Current Demand on Fuel Cell	Prevent Reactant Supply, and Product and Heat Rejection Limits Being Exceeded	Penalise high fuel cell current loading
Limit Fuel Cell Start-Stop Cycling	Prevent ECASA Reduction and Membrane Degradation	Penalise number of fuel cell stop/start events
Avoid Transient Fuel Cell Loading	Prevent Hydrothermal-Mechanical Stress of Membrane and Localised Fuel Starvation	Penalise high rates of fuel cell load change
Limit Fuel Cell Start-Stop Cycling	Improve Drive-ability	Penalise number of fuel cell stop/start events
Maximise Power Availability	Improve Drive-ability	Penalise low power availability

Table 2.4: Primary EMS Strategy Objectives

2.3 EMS Techniques

A very good overview of optimal energy management strategies can be found in the April 2007 IEEE Control Systems Magazine by Sciarretta and Guzzella [48]. This work concentrates on ICE HEVs, but much of the work is appropriate to FCHEVs also. According to Sciarretta and Guzzella, achievable improvements in fuel consumption can be as high as 30% over conventional vehicles, but improvements of this magnitude can only be realised with sophisticated control systems.

The simplest strategies are those used in practical situations, especially industrial applications [30, 73], where the emphasis is to get a vehicle up and running as quickly as possible. Generally, under these circumstances, the EMS strategy is based on a number of hard coded heuristic rules, for example increase the engine/fuel cell power when the battery SoC is low. Heuristic controllers vary greatly in complexity [9, 73] and performance, but are generally very robust and quick to implement in real-time [36]. Unfortunately, they often require manual tuning and therefore can be very time-consuming to optimise.

Following on from heuristic controllers, there are a number of works utilising machine learning techniques in order to optimise the EMS such as neural networks [68], game theory [67], and dynamic programming [45, 46, 98]. These techniques generally use a model of the vehicle in order to optimise the control strategy using a cost function. As a result, they generally produce better results than heuristic controllers. They also have the advantage that they are much quicker and easier to adapt the control strategy to different vehicles and/or duty cycles simply by re-running the optimisation using different input data.

In order to maximise the performance of HEVs there has been considerable effort into implementing optimal control using Deterministic Dynamic Programming (DDP). DDP guarantees the optimal strategy for a specific drive-cycle [45], but these strategies are time variant and therefore the solution requires ideal prior knowledge of the drive-cycle and is impossible to implement directly on board a vehicle [63]. However, DDP is often used in order to analyse the ideal solution for comparison purposes, or for the design of "rule-based" strategies [46]. By analysing the decisions made by the DDP solution, the logic of a "rule-based" controller can be optimised to maximise its performance. In addition to this, because DDP provides the optimal solution to the problem, it makes a consistent baseline for comparison purposes to other techniques, therefore it is common to researchers to report the performance of their controller compared to the DDP solution.

In order to overcome the limitations of DDP, Stochastic Dynamic Programming (SDP) is used to generate strategies that are based on the state of the vehicle. By modelling the driver's demand as a Markov Decision Process (MDP), SDP techniques can be used to find the optimal control action to perform in each possible vehicle state. SDP solutions yield causal state feedback controllers and are entirely time-invariant [47]. This means that they can be implemented directly on board the vehicle. The performance of the SDP generated strategy is generally very near optimal [51], but will heavily depend on the quality of training data used.

SDP has become the most popular technique for EMS in recent years [16, 26, 30, 31, 44, 47, 53, 63, 64, 71, 96]. There is a lot of research going into refinement of the technique by using different algorithms, such as *Shortest Path* SDP. Other authors are investigating refinement of the cost function to include additional requirements such as drive-ability [53], battery degradation [64, 96] and emissions [63].

2.3.1 Heuristic Controllers

"Early energy-management controllers were based on heuristic considerations inspired by the expected behaviour of the propulsion system. For instance, the maximum torque of an ICE is low at low speeds, while electric motors can usually produce high low-speed torques. Thus, a common control strategy is to run the powertrain in a purely electrical mode from standstill to a chosen vehicle speed." Sciarretta and Guzzella [48]

2.3.1.1 "Rule-Based" Controllers

The simplest form of energy management control, and hence the basis for early EMS strategies, is the "rule-based" controller. Rule-based controllers use a set of predetermined "rules" to determine the operating state of the system. One of the simplest methods is to "thermostatically" control the battery SoC. In these controllers, the engine or fuel cell is switched on (or increased in power) when the battery goes below a pre-designated "low" level and switched off (or reduced in power) when the battery SoC goes above a prescribed high level. The "thermostatic" controller is often used as a reference baseline [30] or to form the backbone of more complicated strategies. Bauman and Kazerani [73] describe a rule-based strategy for a FCHEV where the battery is only charged by the fuel cell when the SoC is lower than 50%. This is to minimise the losses associated with DC/DC converters, resistance in the wiring, and cycling efficiency of the battery. A number of other rules are also specified in order to maximise the efficiency. These include a minimum fuel cell current of 7.55% of the maximum in order to avoid the poor efficiency operating region, and a rate limit on the fuel cell power in order to stay within manufacturer guidelines.

Another rule-based strategy is described by Bauman and Kazerani [73] for a FCHEV using ultracapacitors. It is decided that the ultracapacitors are to be used solely for acceleration and regenerative braking, as opposed to a battery which would also be used for low speed operation. This means that the energy stored in the ultracapacitors and the vehicles kinetic energy should sum to a constant at all times, see Equation 2.3.1 where W represents a weighting factor and N represents a design constant.

$$W\frac{1}{2}mv^2 + \frac{1}{2}cV^2 = N \tag{2.3.1}$$

This strategy is very effective assuming that there is no benefit in using the ultracapacitors for any other reason. This is not always true. For example, this equation does not consider changes in the gravitational potential energy of the vehicle (although this would only require a simple modification). It also runs the fuel cell reactively in order to meet this requirement, not necessarily running it at its optimal efficiency and meaning that the efficiency of the complete system may not be as high as possible.

A similar approach is used by Schaltz *et al.* [36] and by Thounthong *et al.* [86], however in these papers, the fuel cell is designated as the primary energy source for the vehicle. Rather than controlling the fuel cell based on the battery SoC, it is controlled based on the power load of the vehicle. Transient loads are avoided by the use of a low pass filter on the control, meaning that the battery is required to balance the difference. This strategy should have the same overall effect as managing the fuel cell loads based on a filtered battery SoC, however in this case the fuel cell is being managed directly and therefore low efficiency operating states can be avoided more easily.

An alternative approach, performed by Rousseau *et al.* [5], is to examine the limitations of the components, and set rules in order to ensure proper behaviour of each component. The EMS controls the set-points of the fuel cell and motor torque, and turns the fuel cell on or off. The strategy proposed by Rousseau *et al.* is to set a number of rules to ensure that the motor does not exceed its maximum speed and torque limits, the battery SoC stays within a predefined operating range, and the fuel cell does not exceed its rate of load change limits. On top of these rules, an algorithm is used to ensure that the battery SoC deviation is minimalised. This technique for developing a strategy tends to give better component degradation protection at the expense of fuel economy.

Thounthong *et al.* [70] also propose an EMS strategy based on the limits of the components. Using a fuel cell/battery/supercapacitor hybrid power source on a test bench, the voltage of a DC bus is controlled. This DC voltage is the supply to a motor which is ramped up with constant acceleration. Each of the components is connected to the DC bus using a DC/DC converter and each is actively controlled. Because the supercapacitors have the quickest response, feedback control is used to run the supercapacitors in such a way as to regulate the voltage on the bus. The batteries are then controlled based on the SoC of the supercapacitors, but limited to a maximum current slope. Finally, the fuel cell is controlled based on the SoC of battery, limited by a (smaller) maximum current slope. These parameters are chosen in order to limit the degradation to the batteries and fuel cell. It is shown that the strategy manages the three sources very well during ramp up of an electric motor, and that the fuel cell and batteries are not subjected to harsh transients. However, because the voltage of the batteries and supercapacitors are controlled to constant set-points rather than based on variables such as the kinetic energy of the vehicle, it is anticipated that the efficiency of regenerative braking may be poor unless the supercapacitors and/or batteries are heavily over-sized. In addition to this, there is no guarantee on the efficiency of the system, because the feedback controllers run the fuel cell reactively to the battery voltage and therefore the actual operating point of the fuel cell is not managed.

2.3.1.2 State Based Controllers

More complex rule-based strategies are generally state-based. Schiffer *et al.* [29] describe a control strategy represented by four vehicle states; standstill, acceleration, constant speed and braking. In each of the inertial states, different control options are described. For example, during the standstill state, Schiffer *et al.* suggest that the battery could be charged at constant power, at fuel cell maximum power, at the fuel cell maximum efficiency or the maximum power within the acceptable efficiency region of the fuel cell. By combining the options in each state, three strategies are proposed and these are each simulated over a number of drive-cycles.

In order to compare the results, Schiffer *et al.* [29] use three benchmarks; the fuel consumption, energy lost in the brakes and "power constraints" (when the fuel cell and capacitors cannot supply the demanded power). It is decided from the results that the best overall strategy is to use the supercapacitors as much as possible during braking and acceleration. At constant speed and standstill it is best to charge or discharge them at the highest rate within acceptable efficiency of the fuel cell in order to reach an optimal voltage based on the vehicle speed. This strategy gives the best overall fuel consumption and power availability; however, more energy is lost to the brakes than one of the alternative strategies proposed. It is concluded that the best fuel economy is achieved because the best strategy prioritises

the efficiency of the fuel cell over the efficiency of the regenerative braking.

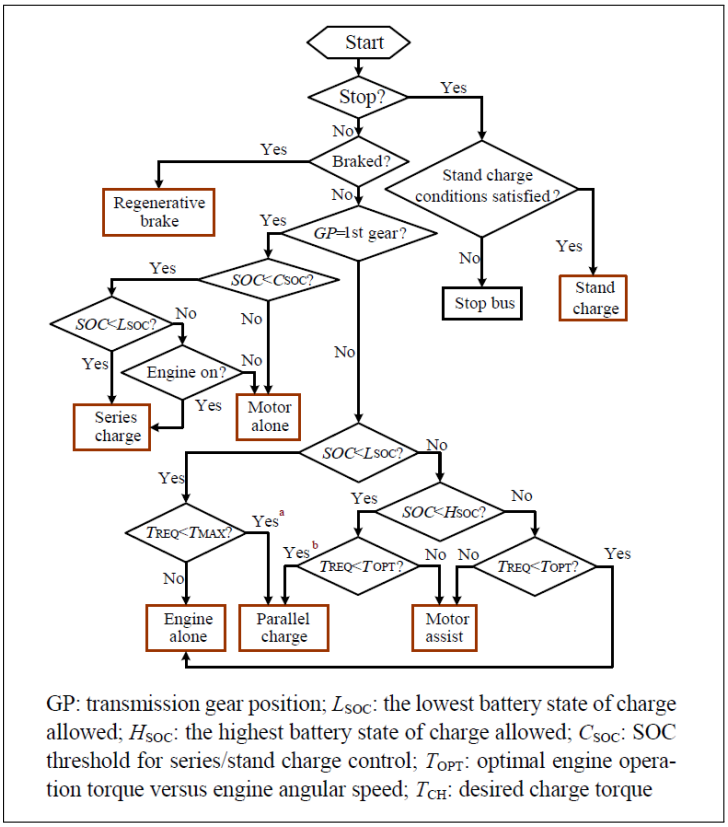

Figure 2.7: Strategy Flowchart - *Xiong et al.* [9]

Xiong *et al.* [9] propose another state-based controller. In the strategy proposed by Xiong *et al.*, the states are based on the component operating modes, rather than the vehicle states. The modes consist of; 1) Motor only, 2) Engine only, 3) Series Charge, 4) Parallel Charge, 5) Motor Assist, 6) Standing Charge and 7) Regenerative Braking. The driver has some degree of control over the operating mode of the vehicle because the vehicle is fitted with a manual transmission with 1st gear removed. When the driver selects first gear, the vehicle operates as a series hybrid, while all other gears operate the vehicle as a parallel hybrid. The EMS strategy then picks the operating mode of the vehicle based on the battery SoC and the torque requested by the driver. The decisions are made according to the flowchart shown in Figure 2.7. It can be seen that despite the fairly complex implementation and the ability to cope with driver selected operating modes, the overall function of the strategy is to "thermostatically" control the battery SoC while simultaneously meeting the drivers torque demands.

2.3.1.3 Equivalent Consumption Minimization Strategy (ECMS)

Equivalent Consumption Minimization Strategy (ECMS) involves calculating the equivalent fuel consumption related to the SoC variation of the battery. The instantaneous cost function is the sum of the actual fuel consumption and of the equivalent fuel consumption relating to the use of the battery. See Equation 2.3.2, where $\dot{m}_f(P_E(t))$ represents the fuel consumption and $\zeta(P_b(t))$ represents the fuel equivalent of electrical energy. The assump-

tion behind this method is that the variation in the SoC will be compensated at some point in the future by a change in the fuel consumption. The electrical energy and fuel energy are not directly comparable; therefore, the challenge with this method is to calculate the equivalence between the two as accurately as possible.

$$J_t = \dot{m}_f(P_E(t)) + \zeta(P_b(t)) \tag{2.3.2}$$

The advantage of ECMS over other heuristic strategies is that the controller can be optimised for fuel economy using this cost function whilst still maintaining the battery SoC. "Rule-based" controllers tend to either control the SoC, but not necessarily run the fuel cell (or ICE) as efficiently as possible, or optimise the fuel economy over the short-term, but may be subject to gradual SoC drift over time depending on the duty cycle. This means that separate charge or discharge modes are often required in case the battery is under/over-charged which can lead to long-term efficiency loss [42]. ECMS, on the other hand, uses an estimate of the future anticipated cost of using battery SoC in order to optimise the long-term fuel economy whilst still maintaining a Charge-Sustaining (CS) strategy.

ECMS is a relatively popular technique in the literature due to its relatively simple implementation for real-time control, but also the ability to optimise for a wide range of targets including emissions [42, 99] and drive-ability [28, 56, 62]. There are also a number of techniques for the calculation of the equivalence factors using theoretical data [42], empirical data [99], and even online adaptation based on the current driving conditions [100].

Johnson *et al.* [42] use theoretical derived graphs to map the fuel consumption to battery SoC change. This is then adjusted using a regulation factor based on engineering judgement to ensure battery SoC sustenance. This factor is included for a number of reasons. Primarily it corrects for inaccuracies in the equivalence calculations, but it also helps to constrain the battery SoC range and long-term target. Finally, it corrects for any additional goals in the cost function such as emissions regulation that aren't accounted for in the equivalence factor.

In order to account for component failure and inaccuracies in the equivalence factor, Zhang [56] suggests the inclusion of some rule-based strategy and introduces Rule-Based Equivalent Consumption Minimization Strategy (RECMS). The controller works by using an ECMS based strategy under normal conditions, when the battery SoC is between 40% and 70%. If the SoC deviates from this range, the rule-based strategy is used instead. This strategy is shown to be more fault tolerant than pure ECMS.

The performance of ECMS is highly dependent on the equivalence factors used. Musardo *et al.* [100] show that if the equivalence factor is optimised based on the expected duty cycle of the vehicle, the performance of ECMS is only slightly sub-optimal compared to the DDP solution. In this case, no SoC regulation factor is required. Unfortunately, this is only possible if the duty cycle is known in advance, which is not the case for real-world driving. If the duty cycle varies in any way, the SoC is liable to deviate, leading to worse overall performance. Rather than using a regulation factor, Musardo *et al.* propose Adaptive Equivalent Consumption Minimization Strategy (A-ECMS), which involves the real-time adjustment of the equivalence factor parameters, based on recent driving history. This method is shown to reliably regulate the battery SoC over a wide range of drive-cycles and improve fuel economy by 20% compared to a baseline "thermostatic" strategy.

2.3.1.4 Summary

"Rule-based" strategies are fairly simple for the user to understand, and are usually simple and robust enough to implement on a real-time controller. Even the simplest strategies exploit many of the advantages of a hybrid electric powertrain and often show significant fuel economy gains over conventional ICE vehicles of up to 30% [45]. However, further gains can be achieved using more complex controllers, or by using a different sets of rules based on the state of the vehicle. The best heuristic strategies use ECMS to optimise the fuel economy (and other targets) using predictions as to how SoC deviations will affect future fuel consumption. Under ideal conditions, ECMS controllers are able to achieve near-optimal results [100].

For each of these controllers, the decisions made by the EMS adhere to reasonably theories, but may neglect some opportunity to further improve their effectiveness. Very often it would be trivial to implement minor changes in order to improve the strategy. For example, by adding an additional rule to prevent running the fuel cell at low load, or reducing the battery current when it is hot. However, "rule-based" controllers can quickly get very complicated. As additional rules are added, new parameters are created which must be tuned for each vehicle and its likely usage pattern.

Heuristic strategies tend to be very dependent on the exact configuration of the test and the components used on the vehicle. For example, if the fuel cell has a larger efficient operating region or the drive-cycle includes more frequent braking events, the alternative strategy proposed by Schiffer *et al.* [29] prioritising regenerative braking efficiency may have been more efficient overall. The design of a rule or state based strategy that is able to cope with a large number of real-world circumstances, may become quickly become very complex in order to be sure that the strategy is safe for both the driver and for the components [9]. Even for ECMS, the performance of the strategy is highly dependent on the optimisation of the equivalence factor. This means that a heuristic strategy which works well for one design may not necessarily translate very well to a different design. In fact, Bauman and Kazerani [73] used three different strategies for three different vehicle architectures during their simulated comparisons.

Of the heuristic strategies that have been proposed, A-ECMS seems to be by far the most effective. This is because it overcomes the major downside to many heuristic strategies in that it adjusts the equivalence factor on board the vehicle based on recent driving history. However, A-ECMS has only been shown to work at optimising the fuel consumption. It has been found by Johnson *et al.* [42] that the equivalence factor can be affected by additional targets such as emissions, and further work could be performed to investigate whether A-ECMS could account for this disturbance.

2.3.2 Machine Learning Techniques

Machine learning has a distinct advantage over heuristic controllers in that the control output can be optimised automatically, which tends to give much better performance without the complexity of a large number of "rules". Another significant advantage is that the controller can be re-optimised for different vehicle architectures with minimal effort when compared to heuristic controllers. In the majority of circumstances, machine learning is performed offline and the subsequent result applied to the test vehicle, although some less computationally expensive algorithms can be performed on board the vehicle for continuous optimisation [68].

Machine learning techniques work by using a model of the vehicle, including all components relevant to the EMS. The performance of the vehicle under a wide range of operating conditions and control actions can then be assessed with regards to the objectives set out in Section 2.2. These results can then be used to optimise the control actions of the EMS in order to minimise a cost function. This results in a strategy which tends to give much better performance than a heuristic controller of similar complexity due to the fact that the optimisation can take into account the relative performance and interaction of every component in the powertrain and optimise the system as a whole.

There are various downsides to machine learning techniques, however. Firstly, a model of the vehicle which is capable of reproducing the vehicles behaviour and the interaction between various components is required. This must accurately simulate the vehicle over a wide range of operating conditions, often inclusive of conditions that may be undesirable in reality, such as at the extremes of battery SoC. This is because the model must appropriately penalise these conditions. In actuality, this is only a minor downside because these models are often required for optimisation of heuristic controllers anyway.

More importantly, machine learning algorithms are often very computationally expensive, requiring high performance computer hardware and significant amounts of time to produce an adequate solution. As a result, the model of the vehicle is often simplified, and the number of states are minimised in order to run the algorithm efficiently. This may affect the performance of the strategy when it comes to full-scale testing.

Finally, the optimisation is subject to the "Garbage-in. Garbage-out." principle, and therefore not only must the model be accurate, but also the cost function must be sufficient to assess the vehicles performance. If the vehicle model is inaccurate or the cost function is not sufficient, often the resultant strategy requires subsequent heuristic modification before implementation on board a real vehicle. This will often detriment its performance. Examples include considerations as to the drive-ability of the vehicle [53] and the capabilities of the real-time hardware [16]. It is important to include as many as these considerations into the optimisation as possible, however this often competes with the requirement for computational efficiency.

Overall, due to their increased performance, and the continual improvements in computer technology, machine learning techniques are becoming more popular in both academia and industry for optimisation of the EMS on board HEVs. A number of machine learning techniques and closely related algorithms have been used in the literature, ranging from artificial neural networks [68], to the application of game theory [67], and dynamic programming [45, 46, 98].

2.3.2.1 Neural Networks

Harmon [68] describes the energy management strategy used on board a hybrid electric UAV using a Cerebellar Model Arithmetic Computer (CMAC) neural network. As a baseline, Harmon uses a rule-based controller based on the ideal operating line of the ICE. This runs the ICE up to its most efficient operating point and uses battery power to supplement this when required. This is a Charge-Depleting (CD) controller, which may not always be sufficient and so an alternative Proportional Integral Differential (PID) Charge-Sustaining (CS) controller based on battery SoC is also used when necessary. When compared to optimal control and other approaches mentioned in the literature, Harmon states that the CMAC controller (along with fuzzy logic) tends to be much less computationally complex and therefore more efficient when used on board the vehicle. Harmon performs the learning offline, but notes that the algorithm could be implemented on board the vehicle due to its computational efficiency.

2.3.2.2 Deterministic Dynamic Programming (DDP)

Although DDP is not technically covered by machine learning, many machine learning techniques rely on the same principles and so it makes sense to cover DDP as part of this section. Deterministic Dynamic Programming (DDP) is a method for solving complex problems by breaking them down into smaller sub-problems. By solving the simpler sub-problems, a combination of the solutions can then be used in order to reach the optimal overall solution. The advantage of DDP over brute-force methods is that the solutions to the sub-problems are stored or "memo-ized"; this means that identical sub-problems only need to be solved once, dramatically reducing computational time when there is a large degree of overlap. Because DDP examines every possible solution before picking the best one, it is guaranteed to produce the optimal solution to the problem and is not subject to the issue of local minima. The downside of DDP is that it requires perfect prior knowledge of the problem, and that it still has a large computational burden for complex problems involving many states.

The energy management problem in a hybrid vehicle is highly suitable for the application of DDP. This is because it exhibits the properties of "overlapping sub-problems" and "optimal substructure". A problem is said to have "overlapping sub-problems" if it can be broken down into a number of sub-problems for which the solution can be reused multiple times. That is to say that in an attempt to find the optimal solution to the energy management problem, if the vehicle is at the same point in the drive-cycle, with the same battery SoC as in a previous attempt, then the previous solution can be reused rather than attempting to solve the same problem again. This gives DDP its advantage over more naive techniques that do not reuse previous solutions. A problem is said to have "optimal substructure" if the overall solution can be efficiently constructed from the optimal solutions to its sub-problems. This means that if the optimal solution for the entire drive-cycle requires that the vehicle is at a specific battery SoC at a particular time, then the optimal solution to reach this point combined with the optimal solution to get from this point to the end will be identical to the solution to the complete drive-cycle.

One of the first research papers to apply DDP techniques to EMS strategy is by Brahma *et al.* [98]. The authors explain that many rule-based strategies rely on the assumption that the globally optimal solution results from the instantaneously optimal control decisions

and that in reality, this is not the case because the control choices at one instant may affect future decisions. This is particularly true for CS techniques where the final SoC is desired to be the same as the initial value. In this case, there may be an advantage in allowing the battery SoC to fluctuate during the cycle whilst still meeting the final constraint. This can introduce significant complexity for rule-based controllers. Brahma *et al.* produce a highly simplistic model of a series hybrid vehicle represented by the Equation 2.3.3 [98].

$$P_m = P_b\eta_b + P_E\eta_E \tag{2.3.3}$$

P_m represents the motor power, P_b represents the battery power and P_E represents the engine power. The efficiencies defined above, η_b and η_E, represent the full efficiency of each branch of the powertrain, not just the efficiency of the corresponding component. Brahma *et al.* set the vehicle's power demand, P_m, and a battery SoC deviation as constraints. The objective function to be minimised is the chemical energy consumed over the drive-cycle, and in addition to this, SoC deviation is also penalised using a weighting factor. The power split is controlled using the sole unconstrained degree of freedom (given the motor power constraint) which is the engine power, P_E. Although DDP is more computationally efficient than brute-force methods, it can still take a significant amount of time to find the solution. In order to minimise the time that their algorithm takes, the simulation is discretized into one second time-steps and 5kW engine power increments. It is found that the time for the simulation and the accuracy must be balanced, but increasing the fidelity of the simulation past a certain level does not noticeably improve the results.

Lin *et al.* [45] present a more complex DDP optimisation of an EMS strategy. In their work, the vehicle is a parallel hybrid and includes an automated transmission. This means that the EMS is responsible for controlling the motor power and gear selection in addition to the engine power. The motor power becomes a dependent variable due to a constraint that the total power produced by the engine and the motor must meet the demand power; however, the gear selection adds an additional dimension of complexity to the optimisation. The optimisation also includes a number of additional constraints in order to improve the durability of the components and the drive-ability of the vehicle. These are represented by limits on the engine speed, engine torque, motor torque, battery SoC and transmission input shaft speeds. These prevent the components from exceeding the manufacturers recommended limits, but are also included to ensure that the system operates smoothly from the driver's perception. Finally, the cost function is mainly based on the fuel consumption, but is augmented in order to penalise battery SoC deviation, and frequent gear shifts. This results in the final cost function shown in Equation 2.3.4 [45].

$$\min J = \min_{\{T_{E,k},\text{shift}_k\},k=0,1,\ldots K-1} \left\{ \sum_{k=0}^{K-1} \Big[m_f(k) + W_G G(k) \Big] + W_H H_K \right\} \tag{2.3.4}$$

Where $m_f(k)$ represents the fuel consumption at each time step, $W_G G(k)$ represents the gear shift penalisation factor (weighted) and $W_H H_K$ represents the final battery SoC deviation penalisation factor (weighted). Note that in contrast to the work by Brahma *et al.* [98], only the final battery SoC deviation is penalised, rather than the SoC deviation at each time step. This is beneficial because it does not encourage additional cycling of the battery in order to keep the battery SoC near to the initial value throughout the drive-cycle. The cost function can be designed to include any number of parameters. In a separate paper Lin *et al.* [46] present an alternative cost function that includes the emissions of the vehicle rather than the number of gearshifts. See Equation 2.3.5 where W_{NOx}, W_{PM} and W_H represent different weighting parameters for NOx, particulate matter and SoC deviation respectively.

$$J = \sum_{k=0}^{K-1} \Big[m_f(k) + W_{\text{NOx}}\text{NOx}(k) + W_{\text{PM}}\text{PM}(k) \Big] + W_H (H_K - H_T)^2 \tag{2.3.5}$$

Lin *et al.* [46] remark that complex models are of no use for dynamic optimisation due to their high number of states. This means that they take unnecessarily long to perform the calculation. Therefore, in order to perform the optimisation, Lin *et al.* develop a simplified vehicle model to run at 1Hz. It is decided that the dynamics faster than this can safely be ignored from an EMS standpoint. This is achieved by the use of quasi-steady state sub-models which can be quickly simulated. The final optimised solution can then be simulated on a highly detailed model to ensure the results from the simplified model are reliable and accurate.

Ansarey *et al.* [40] remark that DDP has a very high computational cost, and that multi-dimensional problems such as the work by Lin *et al.* [45, 46] where more than one control output is optimised, can potentially take a prohibitive amount of time. This is known colloquially as the "curse of dimensionality", because each additional state significantly increases the amount of time required to run the optimisation. This problem has so far precluded many DDP strategies from being useful on real-time controllers used on board vehicles; however, it is still useful for offline optimisation of a strategy as long as the number of states is kept low.

Perhaps a more significant problem with DDP is the requirement to know the drive-cycle of the vehicle in advance so that the entire trip can be simulated. DDP works by calculating the optimal control action to perform at each instant in the drive-cycle, and the solution will be a time dependent set of control actions. This also means that the DDP solution is only optimal for the exact drive-cycle simulated (and if changes were to occur, the result would need to be recalculated). Therefore, DDP cannot be used directly on board a vehicle without an accurate prediction of the future power demands. Dextreit [67] notes that DDP optimisation techniques are typically used for "1) assessing the best achievable performance of a given powertrain over a given drive-cycle and 2) calibrating parameters of a conventional rule-based (RB) control policy to replicate the optimal state and control trajectories generated by the DDP policy".

Lin *et al.* [45, 46] examine the results of their DDP optimisation in order to produce a "rule-based" controller that will perform with similar performance on board a vehicle. By detailed examination of patterns in the DDP solution, a number of "rules" are devised. In particular, the gear shift logic obtained from the DDP solution was found to have a dramatic effect on the fuel economy when compared to a baseline "rule-based" controller. It was found through independent dynamometer testing that hybridisation of a delivery truck using the baseline controller improved the fuel economy by 31%, and the optimised "rule-based" controller improved the fuel economy by a further 14% [45].

One final problem with DDP based algorithms is that they are generally based on the optimisation over a single drive-cycle, which may or may not be representative of real-world driving. Because of this, DDP strategies tend to exhibit "cycle-beating" [47] traits. They usually exhibit features that, to some degree, give very good performance over the drive-cycle that they have been optimised for, but do not translate well on other drive-cycles, or for real-world driving. This can lead to inferior performance during real-world use. Therefore, care must be taken to ensure that more than one drive-cycle solution is examined and that all drive-cycles used for development are representative of real-world use.

An alternative use for DDP optimisation is as a reference baseline for different EMS strategies [28, 53]. It is known that DDP will give the optimal solution, and therefore it provides a fair baseline for comparison. DDP has been used in this way for a large number of strategies such as SDP [31,47], ECMS [61], Game Theory (GT) [67], Neural Networks [27] and MPC [54]. Finally, DDP makes an excellent controller for sizing and parameterisation studies [53, 74]. DDP gives the best possible solution for any given powertrain design so results are directly comparable, and will not be affected by the "priorities" of a rule-based controller. Sinoquet *et al.* [74] present a parametric study focussed on variations in the size of powertrain components for a hybrid vehicle with respect to fuel consumption. Results are obtained using a DDP controller and are used to find the optimum size of key powertrain components for a given drive-cycle. The advantage of using DDP is that it finds the optimal strategy for any combination of components. This avoids the risk that the control policy affects the results. For example, a "rule-based" control policy that "prioritises" regenerative braking over efficient engine operating points may skew the results towards a larger battery than would be optimal. Sinoquet *et al.* [74] conclude that these figures are very sensitive to inaccuracies in the initialisation variables and parameters used in the cost function and therefore care must be taken when choosing these values.

In conclusion, DDP is useful technique because it is able to find the optimal solution to a particular problem. However, a high computational burden, the requirement for perfect prior knowledge of the drive-cycle, and "cycle-beating" traits mean that it is generally not suitable for direct implementation in real-time controllers. Generally, DDP is most often used for development of rule-based controllers, which attempt to mimic the behaviour of the DDP solution in order to provide a very well performing sub-optimal solution. These controllers, however, can still exhibit "cycle-beating" traits and therefore, care must be taken during examination of DDP solutions, and preferably, the solution to multiple different drive-cycles should be examined. However, DDP is still an extremely useful technique for generating a baseline in order to compare alternative strategies, or for comparison between different system design options. This is because the DDP solution is the optimal solution to the specific problem, of which there is only one.

2.3.3 Stochastic Dynamic Programming (SDP)

Although DDP produces the optimal solution to a specific problem known *a priori*, there are a number of limitations when it comes to using it on board a vehicle for real-time control. In order to overcome these issues, Lin *et al.* [47] propose the use of Stochastic Dynamic Programming (SDP). SDP is a similar technique to DDP, but rather than examining a single drive-cycle in the time domain, SDP works by finding the optimal solution based on the state of the vehicle, and the probability of transitioning to another state. Using SDP allows multiple drive-cycles, or even real-world data, to be examined concurrently by combining the data using a Markov Chain. SDP produces a causal solution which is entirely time-invariant and therefore suitable for direct implementation on board a vehicle. It must be noted, however, that SDP is often even more computationally expensive than DDP, and for an individual drive-cycle, the solution will almost certainly be less effective than the (optimal) DDP solution.

Lin *et al.* [47] propose that the driver power demand can be modelled as a finite sequence of discrete-time values, see Equation 2.3.6 [47].

$$P_{dem} \in \{P_{dem}^1, P_{dem}^2, ..., P_{dem}^K\} \tag{2.3.6}$$

It is then assumed that the driver power demand in the next time step, P_{dem}^{k+1} can be predicted using a two-dimensional Markov Chain depending on both the wheel speed, ω_w^k, and the driver power demand, P_{dem}^k, in the current time step. See Equation 2.3.7 [47]. This allows the driver power demand to be modelled using a number of transitional probabilities. These are obtained by Lin *et al.* by analysis of standard drive cycles; however, other authors such as Moura *et al.* [64] and Zhang *et al.* [63] have used real-world logged data such as that obtained from the National Household Travel Survey [101].

$$\begin{aligned} p_{il,j} &= \mathbb{P}\left(P_{dem}^{k+1} = P_{dem}^j | P_{dem}^k = P_{dem}^i, \omega_w^k = \omega_w^l\right) \\ i, j &= 1, 2, ..., N_P, l = 1, 2, ..., N_\omega \end{aligned} \tag{2.3.7}$$

This stochastic model of the drive-cycle allows the generation of a state transition matrix, which represents the probability of the vehicle transitioning to each future state based on its current state. The following states can then be calculated from the probabilities for that state and so on. The cost of each of these transitions can also be calculated, and dynamic programming is then used to find the optimal control action to perform in each state in order to minimise the cost function considering the likelihood of all future vehicle state transitions and their associated costs. In order to produce a meaningful result, the solution must converge. This can be achieved by;

1. Discounting each future state in an infinite horizon problem [30, 31, 47, 51, 96].
2. Considering only a finite number of states by estimating the typical journey length [63].
3. Including an absorbing terminal state with no on-going cost accumulation [26, 52, 53, 64]

2.3.3.1 Infinite Horizon Markov Decision Process (MDP)

The earliest and by far the most common technique [30, 31, 47, 51, 96] to employ SDP is by defining an infinite horizon problem. The objective is to find the optimal control policy, $u = \pi^*(S)$, so as to minimise the total expected cost, $J_\pi(S_0)$, over an infinite horizon, see Equation 2.3.8 [47].

$$J_\pi(S_0) = \lim_{K\to\infty} E\left\{\sum_{k=0}^{K-1} \lambda^{k-1}\Gamma\left(S_k, \pi(S_k)\right)\right\} \tag{2.3.8}$$

In this equation, Γ is the instantaneous cost incurred and λ is a discount factor between 0 and 1 that allows for the infinite horizon problem to converge as the time step, t, increases. It can be seen in the equation that the cost, $J_\pi(S_0)$, and hence the resultant control policy, $\pi(S_0)$, is purely related to the initial state of the vehicle, S_0, and is completely independent of any other variables including time. This means the solution is causal and time-invariant and therefore it is trivial to implement the solution on board the vehicle.

Lin *et al.* [47] test their SDP derived EMS over a number of standard and random drive-cycles and find that this approach offers a more robust power management strategy that outperforms previous work [45, 46] using an optimised rule-based strategy based on the DDP solution.

This technique is also used by Schell *et al.* [30] who describe the design of the Daimler-Chrysler Town and Country "Natrium" FCHEV and the development of its control strategy. A traditional rule-based strategy using battery SoC management is used as a baseline for the SDP algorithm. Simulation results show a possible 15km (2-3%) increase in range using the SDP controller. In 2006, Lin *et al.* [31] describe the use of their SDP algorithm in order to optimise the fuel consumption of a FCHEV. Following on from the work in [30, 47], the SDP algorithm is show to improve the fuel consumption of a medium sized Sport Utility Vehicle (SUV) on a range of different drive-cycles. This SDP result is also shown to reduce fuel cell voltage fluctuation which may increase the reliability of the fuel cell stack.

2.3.3.2 Finite Horizon MDP using Commuting Time Estimation

One of the downsides to the infinite horizon algorithm is choosing an effective discount factor which is representative of real-world driving. A small discount factor tends to optimise more effectively for shorter journeys than for longer ones and will tend to over penalise SoC deviation mid-cycle if the solution is required to be charge-sustaining [52]. In order to overcome this issue, Zhang *et al.* [63] suggest including a "Commuting Time Distribution" in the calculation. Using historic data concerning the drivers previous total journey times, the problem can be solved as a finite horizon MDP, negating the requirement for a discount factor. Zhang [63] uses simulation to show that this technique is able to produce an 11.6% improvement in fuel economy over the rule-based controller used on board the Toyota Prius.

$$J_\pi(S_0) = \lim_{K\to k_{max}} E\left\{\sum_{k=0}^{K-1} \Gamma\left(S_k, \pi(S_k)\right)\right\} \tag{2.3.9}$$

This technique effectively sets the drive-cycle length to optimise over, but the solution can be subject to a similar downfall to an infinite horizon solution with too small a discount factor. This is because it may not consider what would be the optimal solution if the drive-cycle were to carry for longer than expected. Using a finite horizon solver may also tend to promote Charge-Depleting (CD) behaviour if the horizon is not long enough, which is undesirable if a Charge-Sustaining (CS) strategy is required.

2.3.3.3 Terminal State MDP

A more advanced method to eliminate the discount factor is to include an absorbing "terminal state" with no on-going cost. Given an infinite horizon, the probability of being "absorbed" at some point by the terminal state becomes 1. Because the terminal state has no on-going cost, the solution will converge as this happens. This technique has been used by a number of authors, such as Tate *et al.* [52], Opila *et al.* [26, 53] and Moura *et al.* [64]. Moura *et al.* mention that this terminal state allows for more accurate representation of drive-cycle length, when compared to an infinite horizon, which is critically important for plug-in HEVs with a CD strategy.

The definition of the Markov chain is slightly complicated by the addition of the terminal state, S_e, see Equations 2.3.10 to 2.3.13 [64].

$$p_{il,j} = \mathbb{P}\left(P_{dem}^{k+1} = P_{dem}^{j} | P_{dem}^{k} = P_{dem}^{i}, \omega_w = \omega_w^l\right) \tag{2.3.10}$$

$$p_{il,e} = \mathbb{P}\left(P_{dem}^{k+1} = P_{dem}^{e} | P_{dem}^{k} = P_{dem}^{i}, \omega_w = 0\right) \tag{2.3.11}$$

$$1 = \mathbb{P}\left(P_{dem}^{k+1} = P_{dem}^{e} | P_{dem}^{k} = P_{dem}^{e}, \omega_w = 0\right) \tag{2.3.12}$$

$$i, j = 1, 2, ..., N_P, l = 1, 2, ..., N_\omega \tag{2.3.13}$$

It can be seen that simultaneous with the probabilities of transitions between states (Equation 2.3.10), there is also the chance of transitioning to a terminal state when the vehicle's speed is 0 (Equation 2.3.11). The vehicle will then remain in this state indefinitely (Equation 2.3.12). The probability of a transition to the terminal state allows for the cost function to converge as K goes to infinity. This means that a discount factor is no longer required when calculating the infinite horizon cost, $J_\pi(S_0)$, see Equation 2.3.14.

$$J_\pi(S_0) = \lim_{K\to\infty} E\left\{\sum_{k=0}^{K-1} \Gamma\left(S_k, \pi(S_k)\right)\right\} \tag{2.3.14}$$

As well as more accurately representing drive-cycle length, the terminal state SDP technique allows for costs based on the final state of the vehicle. For example, the cost function could be designed to be CS by allow penalising a difference between the initial and final states only. This means that the SoC may be allowed to fluctuate throughout the cycle in a comparable manner to an energy balance "rule-based" controller (see Equation 2.3.1).

2.3.3.4 SDP Summary

In conclusion, SDP overcomes the main disadvantages of DDP and produces a solution which can be directly used on board the vehicle. This is because the solution to the SDP problem is entirely causal, and time-invariant. It is also guaranteed to be the optimal solution to the given problem and can account for a large quantity of training data without much increase in computational effort. However, SDP is very dependent of the quality of the training data and its accuracy with regard to the future use of the vehicle. It is highly computationally intensive and therefore optimisation is required to be performed offline, with only the solution, $\pi^*(S_0)$, stored in the real-time controller. This means that it won't take into account changes in the duty cycle of the vehicle. There is also limited research available as to the real-world implementation and effectiveness of SDP controllers outside of simulation. This is of concern because often the simulation models of SDP based solutions are often heavily simplified in order to reduce the computational burden.

2.3.4 Game Theory (GT)

Dextreit [67] presents the experimental implementation of a Game Theory (GT) controller on board the Freelander2 HEV at Jaguar Land-Rover. The controller penalises the fuel consumption, NOx emissions, vehicle operating condition deviation and battery SoC deviation in a non-cooperative game between the driver and the powertrain. The controller is drive-cycle and time independent and is shown to outperform the baseline controller over real-world driving cycles. The baseline controller is a rule-based controller based on the DDP solution optimised on the NEDC. Dextreit [67] states that HEV controller optimisation techniques in the literature typically penalise fuel consumption and battery SoC deviation only. In the game theory solution, the driver is the first "player" who selects the drive-train operating conditions, wheel speed and torque request. In response to this, the powertrain controller is the second "player" who then selects the powertrain control variables. This represents a non-cooperative game based on the assumption that the driver does not think about or try to optimise the fuel economy or emissions whilst driving. Using simulation, the GT controller is shown to outperform a SDP controller despite providing an optimised solution almost 200 times faster. The GT controller also outperforms the baseline controller significantly on the NEDC in simulation, and in multiple drive-cycles on chassis dynamometer testing.

2.3.5 Model Predictive Control (MPC)

Johannesson [51] compares the potential improvement in fuel economy depending on the amount of prior information that the controller has available. A baseline controller assumes perfect access to the complete future power demand and therefore DDP is used to calculate the optimal control. Three strategies are developed and tested for fuel efficiency over the same route. The first strategy is a SDP solution based on city driving usage patterns. Johannesson also develops a single step MPC controller capable of using location and traffic data obtained from the Global Positioning System (GPS) on-board and in real-time. These controllers are compared to the DDP optimal solution. It is shown that the controller with the lowest amount of information can achieve a fuel economy 1-3% from the optimum, and the controller with traffic information can achieve within 0.3% of the optimal control strat-

egy. Johannesson concludes that the performance of the position dependent and optimal controllers is almost identical. The position independent controller is capable of very good performance as long it is well tuned to the drive cycles it is tested on. As the simulation is limited to repetitions of the same route, Johannesson suggests further work could be done to test the robustness of the algorithms on different routes and varying types of driving. Johannesson also mentions that relying on previously measured data is often impracticable and investigation into a controller that uses information stored in a digital map would be worthwhile.

2.3.6 Summary

Machine learning techniques offer a significant benefit over heuristic controllers in that they are able to optimise the strategy in a holistic sense much more easily. The performance of heuristic controllers is generally very dependent on the specific vehicle configuration and usage pattern and as a result a strategy that performs well in one instance may be inadequate in another. There is a great variety of examples of many different machine learning techniques in the literature, although by far dynamic programming and SDP are the most common. DDP can provide the optimal solution to a specific duty cycle and is therefore very useful as a baseline for comparison or for tuning "rule-based" strategies for real-time implementation. Unfortunately, the solution provided by DDP is time dependent and requires perfect knowledge of the exact duty cycle *a priori*.

In order to overcome this issue, SDP instead finds the optimal solution to a statistical model of typical usage patterns. This produces a time-invariant policy which is based on the state of the vehicle. As a result, it can be directly implemented on board the vehicle. There are a number of variants in the application of SDP to the EMS problem. Firstly, the inclusion of additional inputs to define the vehicle state allows the transitional probabilities to be more accurate and the cost function to be made more complex, however this can significantly increase the computational time required to solve the optimisation. Another area of refinement is the exact method used. Finite horizon solvers assume a fixed number of steps which can be chosen based on historical data [63]. Infinite horizon solvers, however, continue to refine the strategy until it converges. In order to do this, they require a discount factor which exponentially reduces the weight on future steps. Finally, Shortest Path Stochastic Dynamic Programming (SP-SDP) solutions include an absorbing terminal state which does not accumulate cost. As a result, they are able to converge without the use of a discount factor. The choice of method is largely determined by the type of strategy required, with infinite horizon solutions tending to produce the most effective controllers for CS strategies and terminal state solutions proving most effective for CD strategies.

Alongside SDP, there are a number of other techniques which have been experimented with in the literature. Harmon [68] used a neural network to generate the EMS for an UAV, showing improvement when compared to "rule-based" algorithms, although no quantifiable comparison to SDP is given. Harmon did remark however, that the technique is much more computational efficient and as a result could be performed in real-time on board the vehicle. Dextreit [67] used GT in order to develop an EMS based on a non-cooperative game between the driver and the powertrain. It is noted that the EMS based on GT outperformed the SDP solution despite being much more computationally efficient, however the exact implementation of neither controller is given, which may have some bearing on the results.

Finally, Johannesson [51] investigated the potential benefit of providing real-time information of the vehicles location to the EMS. MPC was used to provide an estimation of a single step using location data obtained using GPS. The results showed that performance within 0.3% of the optimal solution was achievable; however, this was only marginally better than the solution provided by SDP based on offline learning. As a result, the additional complexity of the technique may not be justified purely on a raw performance basis. One potential advantage of this technique however, is that it may be more robust than the SDP for real-world scenarios where the vehicles usage patterns may not be accurately represented by the offline learning, or may change over time.

2.4 Conclusions

Due to the relatively immaturity of hybrid vehicles, there is a large variety of different approaches to the problem of energy management and the optimisation of the powertrain. At one end of the scale there are a number of papers describing heuristic controllers which have been developed and implemented on board test vehicles. These range in complexity from simple "thermostatic" battery SoC management, to complex state machines which vary their behaviour depending on the operating conditions of the vehicle and the actions of the driver. At the other end of the scale, there are theoretical results for advanced optimisation techniques such as dynamic programming and even predictive control based on real-time location data.

In consideration of the techniques presented in the literature there are a number of areas with scope for further research. Firstly, limited work has been found to apply GT, although Dextreit [67] suggests that it can outperform SDP, which is by far the most popular technique in recent years. Because SDP calculates the statistically optimal solution, this is a surprising result, and warrants further investigation. One plausible reason for this is that SDP requires discretization of the vehicles state space. Due to the computational burden of the optimisation process, and despite modern processing speeds, this discretization is usually quite coarse in order to produce results in a reasonable amount of time. Dextreit mentions that the GT controller is optimised approximately 200 times quicker than the SDP strategy and therefore it is possible that finer control is achievable using GT. Conversely, other authors have mentioned that diminishing returns are seen when increasing the fidelity of the SDP optimisation and therefore it is equally possible that given a finer discretization, the SDP may still be more effective.

Another possible area with scope for further research is MPC, and the potential for improving the performance of the EMS using real-time information about location, route and road conditions. Many modern vehicles are factory fitted with GPS navigation and internet connectivity. As a result, the assumption that the duty cycle of the vehicle cannot be known in advance is no longer necessarily valid. It may soon be possible to implement DDP on board the vehicle, calculating the optimal EMS for any journey. There are two major challenges with this however. Even with advanced technology, such as real-time road condition information provided for by systems such as Intelligent Transport Systems (ITSs), it is impossible to have perfect knowledge of the future loading conditions on the EMS. Therefore, it would be interesting to investigate the robustness of such controllers given imperfect information. Secondly, DDP is computationally expensive and it may be difficult to perform the optimisation in real-time. However, one way to get around this problem would be to perform the optimisation off-board and transmit the solution to the vehicle using wireless networking.

In addition to the method used for the optimisation, the variables to be optimised must also be taken into consideration. A significant proportion of the work in the literature focuses solely on the optimisation of the fuel consumption. Although this makes a good baseline for the comparison of different techniques, it has been found when performing vehicle testing that other concerns such as component reliability and the driver's perception are equally important. Strategies optimised purely on the fuel consumption tend to require subsequent modification to ensure that they are suitable for real-world use, which inevitably results in a loss of performance. Optimisation of a cost function which takes

into account these additional considerations often results in a strategy which is suitable for real-world testing with only a minor increase in fuel consumption.

A relatively broad literature review has been undertaken which has considered not only FCHEVs, but also other types of hybrid vehicle including gasoline hybrid passenger vehicles, commercial vehicles and even UAVs. At this point, it is therefore important to bring the focus back to FCHEVs in particular and how these innovations identified from surrounding research areas can be applied in the context of this project.

In contrast to their ICE hybrid counterparts, the vast majority of research into the design of the EMS specifically for FCHEVs is relatively sparse. There are a number of papers in which the ICE emissions are optimised alongside the fuel consumption, or the number of gear shifts is minimised to improve the drive-ability of a parallel hybrid fitted with an automatic gearbox. The main area of focus specific to fuel cells is generally focussed on the reduction of transient loading using heuristic techniques, however, and very little work has been found to minimise this using computational optimisation techniques. No work has been found that is intended to specifically reduce the effect of other degradation methods such as those caused by open-circuit conditions or excessive temperature.

As was mentioned in Chapter 1, the reliability of the fuel cell stack is one of the principal areas which requires further development for transport applications. The EMS can have a significant effect on the degradation due to the fact that it is directly responsible for controlling the operating point of the fuel cell at any time. Therefore, the management of fuel cell lifetime using the EMS will form the main focus of this work. This will differ from previous work in the literature in that a quantitative model of the fuel cell degradation suitable for SDP optimisation will be developed. This model will include a number of degradation causes, not just transient loading, and will allow estimation of the fuel cell lifetime to be predicted. The resulting controller can be compared to other controllers in the literature in order to assess its benefit and also be used for component sizing exercises for investigation and optimisation of the hybrid powertrain design.

2.4.1 Research Questions

The following specific research questions have been identified from the literature, with the questions that will be tackled in this thesis highlighted in bold;

1. Many of the real-time EMS techniques use stochastic methods for predicting the future demand on the powertrain either inherently, such as SDP or through online "learning" algorithms, such as A-ECMS and GT. Modern vehicles are often equipped with a range of information technology such as GPS and wireless networking capable of providing more accurate predictions of future demand. What impact would this additional information have on the operating efficiency of the vehicle compared to current methods?

2. There is relatively little research into techniques such as GT, Neural Networks (NNs) and MPC, but what research there is shows promising results. Further research could be done using these techniques, especially in comparison to popular techniques such as ECMS and SDP.

3. The major causes of fuel cell degradation are relatively well understood under controlled conditions, however there is room for improving the estimation of the relative contributions of each cause under automotive applications. **Under real-life driving scenarios, which degradation methods are the most significant?**

4. The EMS may have a significant effect on fuel cell ageing by avoiding situations known to cause excessive degradation of the fuel cell. **To what extent can the fuel cell ageing be reduced by optimising the EMS with regard to known fuel cell degradation causes?**

5. Popular techniques for optimisation of the EMS such as ECMS and SDP involve the use of a cost function. A number of fuel cell degradation methods have also been identified. **How can these degradation methods be quantified so as to be used in a degradation inclusive cost function?**

6. The weighting parameters used in multi-objective optimisation can have significant effect on the results. **How should the degradation of the fuel cell be weighted fairly against more traditional optimisation metrics such as the fuel consumption?**

7. Popular heuristic methods for choosing a fuel cell size are to either; a) Choose a fuel cell with a maximum power equivalent to an ICE. b) Choose a fuel cell with a maximum power slightly higher than the power required to cruise at maximum cruising speed. or c) Choose a fuel cell with peak efficiency at the average power demand. **What effect does each of these choices have on the performance and reliability of the vehicle as a whole?**

8. The interactivity between system design and EMS is often mentioned, however there are only a handful of papers which use optimal control methods for system design exercises, thereby maximising the benefits of each individual design option. **What effect would different system designs have on the control decisions made by an EMS designed using optimal control?**

Chapter 3

Vehicle Model

This chapter describes the design of the vehicle model environment used for the control development and validation testing. Two bespoke models have been created in the MATLAB®/Simulink®environment in order to characterise the test vehicle. The first is a detailed forward-facing model which accurately represents the test vehicle in as much detail as possible. The second model is a backward-facing model which has been reduced in order to perform optimisation techniques much more quickly. The results of the reduced model are shown to accurately reproduce the detailed model under normal conditions.

A modular approach has been taken with focus on keeping the vehicle model as high a level as possible. The optimisation of the Energy Management Strategy (EMS) using Stochastic Dynamic Programming (SDP) requires the model to be simulated for every possible action from every possible initial state. This requires a huge number of simulations, and therefore it is imperative that the model is kept as simple as possible in order to minimise the computational effort. This has been achieved by using steady state and quasi-steady state models where possible, and the use of empirical data to describe multiple components in order to maximise model reduction.

This chapter begins with a description of the overall modelling philosophy taken for this project. The overall outline of each of the two models is described, and the steps taken to reduce the detailed model are given. Following this, each of the component models are described in turn, accompanied by the parameters used for the Microcab H4, and validation at the component scale. At the end of the chapter, the control models are described, ready for optimisation using SDP.

3.1 Model Based Design (MBD)

Simulation forms a significant part of the design process in the development of any modern control algorithm. This is due to the fact that simulation offers a number of advantages when compared to full-scale testing;

Safety - Most importantly, testing the controller in a fully simulated environment on a desktop computer involves no risk of damaging the equipment and no risk of harming personnel. Not only does this allow the safety of the algorithms to be checked before any equipment or personnel are put at risk, but it also allows examination of situations that may be too dangerous or expensive to test in full scale.

Speed - It possible to get immediate feedback on any design changes with minimal organisational overhead. This allows testing to be performed much more frequently, with the added benefit of significantly reducing the debugging time of the controller code. This also allows parameter sweeps to be undertaken in a very short time compared to full-scale testing and with excellent repeatability.

Detail - Simulation models usually include variables which would be difficult or impossible to measure on a vehicle. This allows the effect of the controller to be examined in more detail than would be possible during full-scale testing (assuming the model is accurate).

Repeatability - Finally, simulation does not require the use of experimental hardware which may be prone to malfunction or poor calibration. This also means that the results are extremely repeatable.

Simulation models can be used for a number of reasons and their design often depends on the level of detail required from the results. Firstly, simple models are useful for early design when details of the system have not been set. Simple models are quick to produce and run very quickly. This makes them especially useful for parameter sweeps and component sizing because many potential configurations can be tested in a relatively short amount of time. Complex optimisation algorithms also require the model to be relatively simple due to the large number of simulation runs. If the model is too complex, the optimisation can take a prohibitive amount of time to be feasible. However, adding additional detail to the simulation model allows more representative results to be obtained. For the Microcab H4, the design has been finalised and therefore it is possible to generate detailed models of the vehicles, using experimental data in order to validate the model. The higher level of accuracy to the actual system means that these models represent the vehicles more closely and therefore there are likely to be fewer differences between the simulation result and experimental testing. In much of the literature, optimisation of the EMS is performed using a reduced model and the solutions are subsequently tested using a more detailed model to ensure the validity of the results.

For this project, a simple model of the vehicle must be constructed that is capable of being used for EMS strategy optimisation and a more detailed model that can be used for validity testing of the solution. For the best results, both models should be able to reproduce experimental results to a relatively high degree of accuracy. Although simple models are generally quick to implement, it is often unknown what assumptions can be safely made about the vehicle in advance. Therefore, common practice is to produce a relatively detailed model that represents the vehicle as accurately as possible. The results of this model can be

directly compared to experimental data to ensure that the system is well understood, and the important characteristics are accurately represented. This detailed model can then be successively simplified while comparing the results in order to produce the reduced model that still represents the important characteristics of the system.

3.2 Test Vehicles

3.2.1 Microcab H4

Loughborough University currently has access to two hydrogen fuel cell vehicles previously used on the University of Birmingham's campus as fleet vehicles. These were designed in Coventry by Microcab and are each fitted with a 1.2kW fuel cell operating at a nominal voltage of 24V. These are connected to a 2.1kWh lead acid battery pack operating at 48V through a DC/DC converter. A 0.6kg hydrogen tank allows a range of up to 80km [4]. Peak acceleration is approximately $3ms^{-2}$ and the top speed is approximately 30mph [4]. These vehicles are very low power, but are highly suited to the campus drive-cycle they were designed for. A schematic of the electrical powertrain is shown in Figure 3.1.

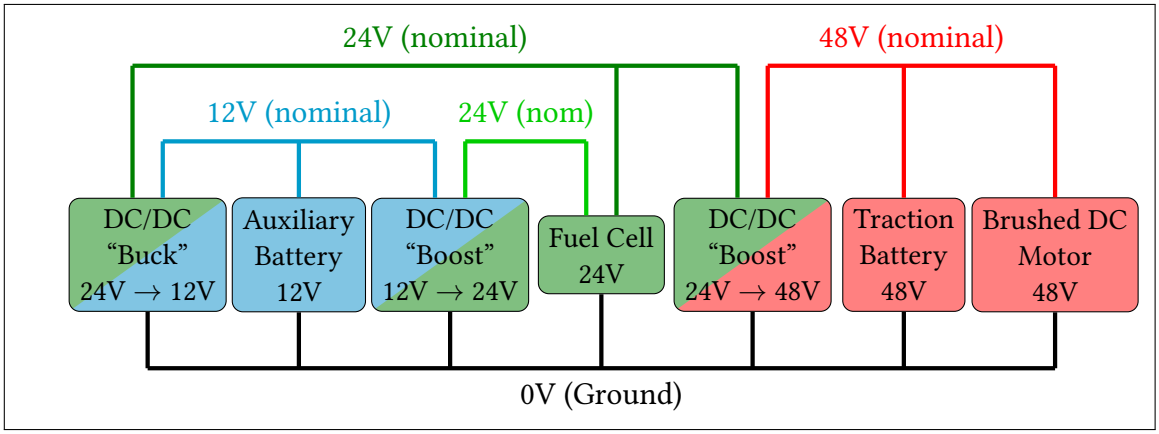

Figure 3.1: Microcab Electrical Powertrain Schematic

The Microcab H4 has four separate power supply voltages. The first of these is the nominal 12V system for running auxiliary components such as the lights, heaters and dashboard electrics. This has been chosen to allow the use of standard automotive parts in order to minimise the cost of the vehicle. The 12V system uses a 16Ah lead acid battery. The 12V system is also stepped up to a nominal 24V using a "boost" type DC/DC converter to supply power to the fuel cell accessories. This allows the fuel cell to be started and run using the 12V system. Once the fuel cell is running, it outputs power to a second 24V nominal system, which in turn is dropped back down to a nominal 12V using a "buck" type DC/DC converter in order to charge the auxiliary battery. This 24V (nominal) system will vary much more than the first depending on the total output power of the fuel cell and in reality, can range between approximately 27V at full load and 42V at idle. Tractive electrical power to the motors is primarily supplied by the traction batteries which run in parallel with a third DC/DC converter on a nominal 48V system. This "boost" converter is also supplied by the fuel cell.

The mechanical design of the powertrain is comparatively simple. The motor controller draws electrical power from the 48V system as required and supplies it to the DC brushed motor. The motor controller controls the separately excited DC motor by varying the voltage to the motor armature whilst maintaining a fixed field. For negative torque, or to drive the vehicle backwards, a negative armature voltage is supplied. The brushed DC motor drives the rear wheels of the vehicle through a fixed gear ratio differential mounted to the rear axle. A schematic of the mechanical powertrain layout is shown in Figure 3.2.

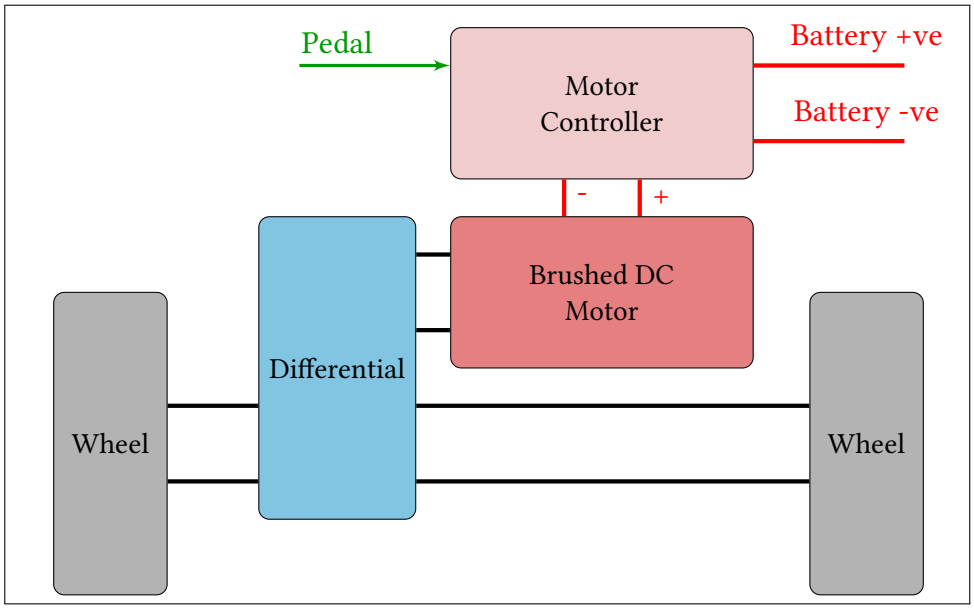

Figure 3.2: Microcab Mechanical Powertrain Schematic

During operation over a small area, such as a university campus, fleet vehicles such as small diesel vans obtain a very poor fuel economy and contribute significantly to the university's emissions, emitting 400 tons of carbon dioxide into the atmosphere [4]. This has led the University of Birmingham to trial a number of Battery Electric Vehicles (BEVs) on campus, but these have a poor range and the batteries suffer from a short lifetime due to deep discharging. Kendall *et al.* [4] suggest that the use of Fuel Cell Hybrid Electric Vehicles (FCHEVs) will avoid these problems allowing faster refuelling and increasing the lifetime of the batteries. Kendall *et al.* [4] present the design of these vehicles and the initial results of approximately 2000km of usage at the University of Birmingham. The vehicles were shown to operate successfully with a number of advantages over BEVs such as the refuelling time and battery life improvement. The vehicles had acceptable performance for the campus drive-cycles that they were subjected to, but upgrading of the fuel cell, battery and motor would be required to meet the ECE15 urban drive-cycle. Kendall *et al.* [4] also mention that the introduction of regenerative braking and increased complexity of the control systems on board in order to optimise the efficiency of the system is also required.

Five prototype Microcab H4 FCHEVs were used on the University of Birmingham campus for 21 months as urban taxis and light goods transport accumulating over 4000km utilising approximately 68kg of hydrogen. Staffell [6] presents the results of this mileage accumulation study and discusses potential areas of improvement that will have the great-

est effect on the performance of the vehicle. The Microcab H4 was designed in order to produce a cost effective sustainable transport solution. Each of the vehicles cost approximately £50,000 to manufacture including the cost of the master mould for the Glass-Fibre Reinforced Plastic (GFRP) body panels. The vehicle was designed from scratch in order to minimise vehicle weight and hence the requirements for the fuel cell, battery and motor. The target weight of 500kg was not achieved, however, which Staffell [6] cites as the result of using production parts from existing vehicles for items such as the windscreen and seats, as well as a switch from aluminium to steel for the chassis. Both of these choices were made to minimise the cost of design. The inclusion of the battery pack allowed the fuel cell to be downsized, and it was normally operated at full power until the battery State of Charge (SoC) reached 100%. The results of the study showed that the vehicles averaged 18% tank-to-wheel efficiency, with a peak efficiency of approximately 27%. Staffell [6] concludes that the efficiency could be improved by examining the vehicle from a systems level and matching the efficient operating points of the various components more effectively. This would also require a more advanced control algorithm to maintain the vehicles powertrain state in this efficient region.

The current control strategy for managing the battery SoC is to simply run the fuel cell at maximum power until the battery reaches 100% state of charge [4]. This is achieved by the DC/DC converter which is programmed to output its maximum voltage of 57.8V unless limited by the maximum input current of 50A. The DC brushed motor on board the Microcab H4 is capable of drawing up to 15kW of power from the battery, but the maximum power from the fuel cell through the DC/DC converter is only approximately 1.3kW. This means that even over a low speed drive-cycle, such as the campus drive-cycle used by the University of Birmingham or the New European Driving Cycle (NEDC) urban drive-cycle, the batteries will tend to be discharged. The fuel cell is programmed to stay on after key-off in order to recharge the batteries. During a typical journey on the University of Birmingham campus, Kendall *et al.* [4] reports that the batteries were depleted by approximately 25% and required on average 7 minutes of additional charging time to recover.

Even a highly optimised EMS may not have significant effect on the performance of the Microcab H4 due to the size of the fuel cell. The fuel cell is not capable of meeting the average power demands over even a low speed drive-cycle. This would mean that the present EMS strategy of running the fuel cell at maximum power as much as possible may be the only realistic option. In terms of fuel cell degradation, the fuel cell is run at constant power so does not suffer from transient loading, but it is generally run above its optimal operating point. Drive-ability of the vehicle is generally quite good because the fuel cell is running in parallel with the batteries, but as the battery pack is discharged, the throttle pedal response of the vehicle deteriorates. Again, without upgrading the fuel cell, there is little that can be done about this.

It must also be noted that the battery pack in the Microcab has no cell balancing mechanism and over a number of cycles, significant voltage difference between individual 12V batteries has been noted. This means that some batteries are being significantly overcharged by the fuel cell, whereas others are being undercharged and hence more deeply discharged when the vehicle is used. This has lead to the battery pack being replaced twice since the vehicles have been at Loughborough University.

3.2.2 Microcab H2EV

Another vehicle available to the project is the Microcab H2EV. This vehicle is the latest iteration of the Microcab and features a 5kW fuel cell, 4.3kWh lithium-ion battery pack, and two 20kW peak power DC motors. The hydrogen tank has been upgraded to 1.8kg to achieve an estimated range of 180 miles. The maximum speed of the vehicle has also been improved to 55mph. The Microcab H2EV is available to the project through MIRA Ltd., an industrial sponsor to this project. Unlike the H4, the H2EV is still in active use, however, so the potential for modification is much lower. A report by Fisher *et al.* [39] discusses the changes made to the Microcab for the CABLED project in 2011 & 2012.

The Microcab H2EV was used in the CABLED project which involved the H2EV, along with a number of electric vehicles, being made available to a number of people from diverse backgrounds. Data were collected concerning the range, performance, driver behaviour and battery charging infrastructure. Fisher *et al.* [39] state that the H2EV was the only vehicle in the project to have a hydrogen fuel cell. This meant that the recharging time involved refilling the 1.8kg hydrogen tank which took only 5 minutes compared to a 6-8 hour [39] charging time for the other electric vehicles. Fisher *et al.* [39] also mention a number of problems that have been noted in previous works involving an earlier version of the vehicle which included the size of the fuel cell, and purity requirements of the fuel. In order to meet the requirements of the ECE15 drive-cycle, the fuel cell has been upgraded to a 3.2kW high temperature Proton Exchange Membrane (PEM) fuel cell. Fisher *et al.* [39] state that commercial off-the-shelf Solid Oxide Fuel Cells (SOFCs) were not considered due to long start-up times. The battery pack has also been upgraded from approximately 1.9kWh lead acid pack to a 4.8kWh lithium-ion pack with a higher cyclic efficiency (74% to 83%). In order to meet performance objectives, the previous 2.25kWe separately excited DC motor has been replaced with two 12.56kWe permanent magnet AC motors, one driving each front wheel. According to Fisher *et al.* [39], the fuel cell is now able to keep up with average urban usage and the battery pack is sized to allow sufficient time for the fuel cell to warm up or drive for approximately 15 miles without hydrogen. A number of issues were encountered during the integration of the new components and a lot of work was performed to ensure the safety of the vehicle under a range of failure modes. This means that the development of the energy management system is limited and there is further work possible in this area.

The Microcab H2EV is currently in constant development and since the CABLED project the high temperature 3.2kW PEM fuel cell has been replaced by a 5kW Horizon fuel cell. The H2EV is road legal, and the new components mean that it is able to cope with a number of low speed drive-cycles. Unfortunately, because it is still in active development by Microcab, this project will have limited access to it for testing purposes.

3.3 Model Architecture

A simulation environment has been created for this project using MATLAB®/Simulink®. The main plant model is a forward-facing simulation model controlled using a Proportional Integral (PI) "driver" to control the vehicle speed, see Figure 3.3. The model can be split into two main components; the controller and the plant model. The plant model (red) can be broken down into the vehicle, motor/driveline, DC/DC converter, traction battery and fuel cell sub-models. The controller (blue) can be split into two main components; the "driver" which controls the speed of the vehicle and the EMS which is responsible for controlling the output power of the fuel cell.

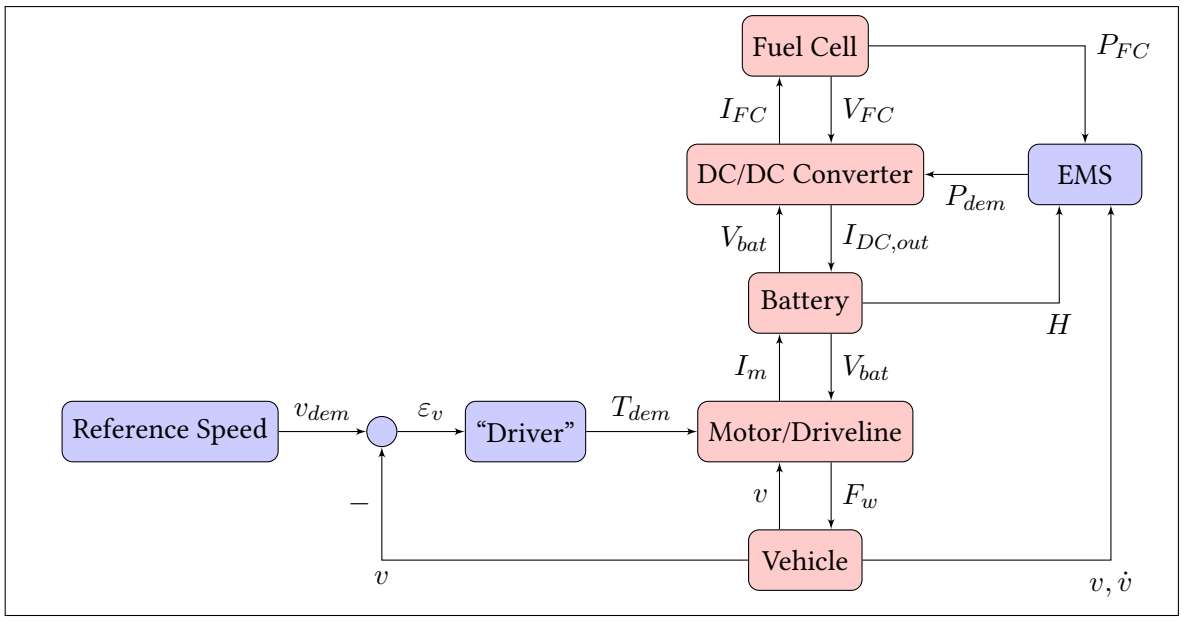

Figure 3.3: Detailed Model Outline

The plant model follows the vehicle's powertrain architecture using a modular approach. The fuel cell is connected to the battery pack using a DC/DC converter. The battery pack is connected directly to the motor and the motor power is dependent on the driver's demand. Each of these components is connected using the voltage and current signals in a feedback loop. The motor is controlled by the "driver" PI controller which is based on the difference between the drive-cycle demand speed and the speed of the vehicle as calculated by the vehicle model. The EMS controls the DC/DC converter output power based on the speed and acceleration of the vehicle, the current battery SoC and the current fuel cell demanded power.

The forward-facing approach accurately represents the chain of causality observed in the real world. The "driver" will attempt to follow the demanded speed reference, based on the response of the vehicle. In contrast, in a backward-facing model, the speed of the vehicle is assumed to perfectly follow the reference signal. For this reason, forward-facing models are generally considered to be the more thorough approach, more accurately representing the likely behaviour of the vehicle in all conditions. The inclusion of comprehensive "driver" models may also allow study into the interaction between the driver and the vehicle in terms of drive-ability.

A more significant advantage of a forward-facing model, especially in regard to the Microcab, is that the behaviour of the vehicle is more accurately represented outside of its normal performance limits. If the vehicle is unable to achieve a speed or acceleration represented in the drive-cycle, the vehicle will accelerate at its maximum rate. In comparison, a backward-facing model may attempt to simulate speeds or accelerations that the vehicle is physical incapable of achieving. In this case, the model may fail, or produce erroneous results. As the Microcab is relatively low powered and operates close to its performance limits, a forward-facing approach has been chosen for the validation model.

3.3.1 Reduced Model

For optimisation using SDP, it is imperative that the model is as simple as possible due to the large number of iterations required (10,000+). As a result, a reduced model has been created which dramatically reduces the computational effort required for the optimisation process. The overall architecture is very similar to the detailed model and the reduced model reuses a number of sub-models created for the detailed model, however two major changes have been made to improve the speed of the calculations, see Figure 3.4. Firstly, the reduced model is backward-facing in order to remove the feedback loop associated with the "driver" controller. Secondly, the reduced model is based on the flow of power between components rather than the coupling of a flow and an effort (e.g., voltage and current, speed and force etc.). This eliminates a number of algebraic loops within the sub-models, dramatically improving the computational efficiency.

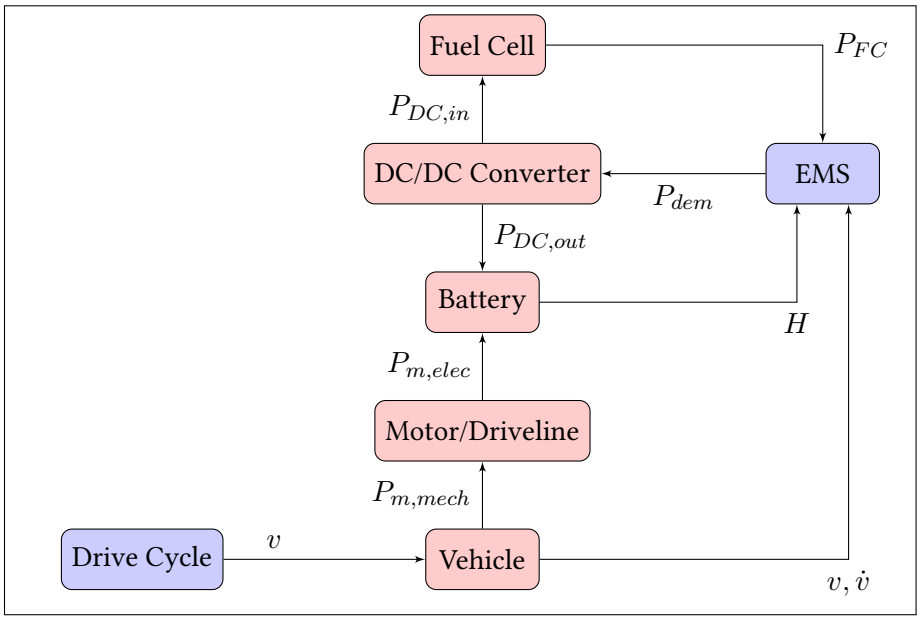

Figure 3.4: Reduced Model Outline

Although the forward-facing model gives a more accurate representation of the vehicle outside of its performance limits, this is not necessarily required for SDP optimisation. The optimisation process uses logged data for reference and as a result does not contain demands that exceed the performance limits of the vehicle. In addition to this, the logged data represents the actual speed of the vehicle inclusive of any interaction between the driver and the road conditions. In this case, a backward-facing approach is more appropriate, as

long as the assumption that the reference data does not exceed the performance limitations of the vehicle holds valid. Therefore, the use of a backward-facing model should not affect the accuracy of the results in any way.

Feedback loops can considerably increase the time required for the simulation to complete. This is because these loops are iteratively solved at each time step until the result converges within a set tolerance. The variable step solver may need to reduce the time step in order to achieve this, which leads to an even higher number of calculations and hence a slower simulation. By basing the model on the power flow between electrical components, rather than the voltage and current, these feedback loops are eliminated, resulting in a much more efficient model. The removal of these loops may affect the results due to the assumption that the performance of the electrical components are unaffected by their supply voltage. Although it is expected that this effect will be small, the detailed model can be used for validation of the optimised controller.

3.4 Simulation Plant Model

3.4.1 Vehicle Model

The forward-facing vehicle model calculates the speed of the vehicle based on the tractive effort and the drag forces on the vehicle, see Figure 3.5.

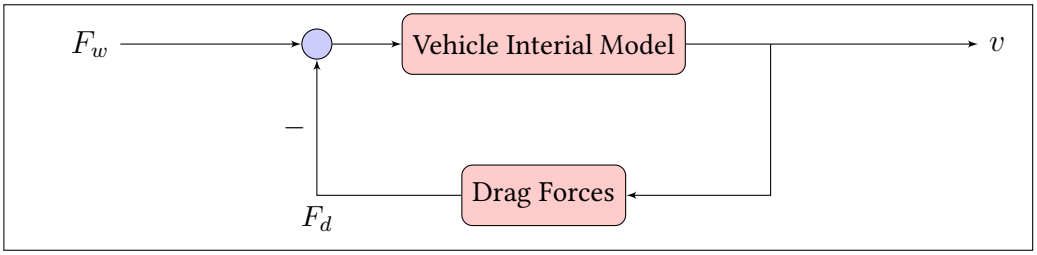

Figure 3.5: Forward Facing Vehicle Model

To calculate the drag forces, the vehicle model uses the standard straight-line performance equation, where the total force due to drag, F_d, is made of components from the rolling resistance F_R, the aerodynamic drag F_A, the incline of the road, F_I, and the braking force F_B, see Equation 3.4.1.

$$\begin{aligned} F_d &= F_A + F_R + F_I + F_B \\ &= \frac{1}{2}\rho C_d A_f v^2 + mg(A_d + B_d v) + mg\sin(\beta) + T_b/r_r \end{aligned} \tag{3.4.1}$$

The acceleration of the vehicle is then calculated based on the difference between the tractive effort supplied by the motor, F_w, and the drag force, divided by the effective mass of the vehicle, m_e, (inclusive of rotational inertia of the driveline). The vehicle speed, v, is the integral of the acceleration (Equations 3.4.2 & 3.4.3).

$$\dot{v} = \frac{F_w - F_d}{m_e} \tag{3.4.2}$$

$$v = \int \left(\frac{F_w - F_d}{m_e}\right) dt \tag{3.4.3}$$

3.4.1.1 Reduced Model

The reduced model uses a backward-facing approach and therefore the same equations are used in the reverse order. The model calculates the required tractive effort based on the vehicle speed, see Figure 3.6. It can be seen in Figure 3.6 that the flow of information is now unidirectional, which results in a significant reduction of the computational burden.

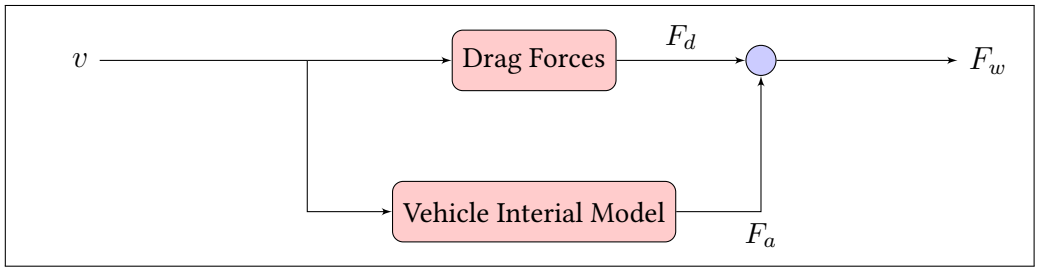

Figure 3.6: Backwards Facing Vehicle Model

3.4.1.2 Characterisation

The Microcab H4 was subjected to a coast-down test at the Motor Industry Research Association (MIRA) proving grounds as part of a final year project by Jonathon Mansell [102]. The vehicle motor was disconnected and the vehicle was towed up to 60km/h, the tow bar was released and the vehicle was allowed to coast to a stop. Further information about the test procedure can be found in the project report [102], available from the Department of Aeronautical and Automotive Engineering, Loughborough University. The time to decelerate was recorded in 5km/h steps. These data have been used to estimate the parameters used in the vehicle model as shown in Table 3.1.

Parameter	Value
Gross Mass, m	940 kg
Frontal Area, A_f	1.43 m^2
Coefficient of Rolling Resistance, A_d	0.017
Coefficient of Rolling Resistance, B_d	0.00065
Coefficient of Aerodynamic Drag, C_d	0.482

Table 3.1: Vehicle Specification

The test data and the model results are shown in Figure 3.7. It can be seen that the selection of these parameters accurately match the deceleration seen during testing. Compared to a typical car, the coefficients are relatively high; a modern vehicle would be aiming to achieve approximately 0.01 for A_d and 0.3 for C_d. This is likely due to the "box" shape of the vehicle and drag in the drive-train, however especially for the aerodynamic drag, it is relatively unimportant due to the design for low speed.

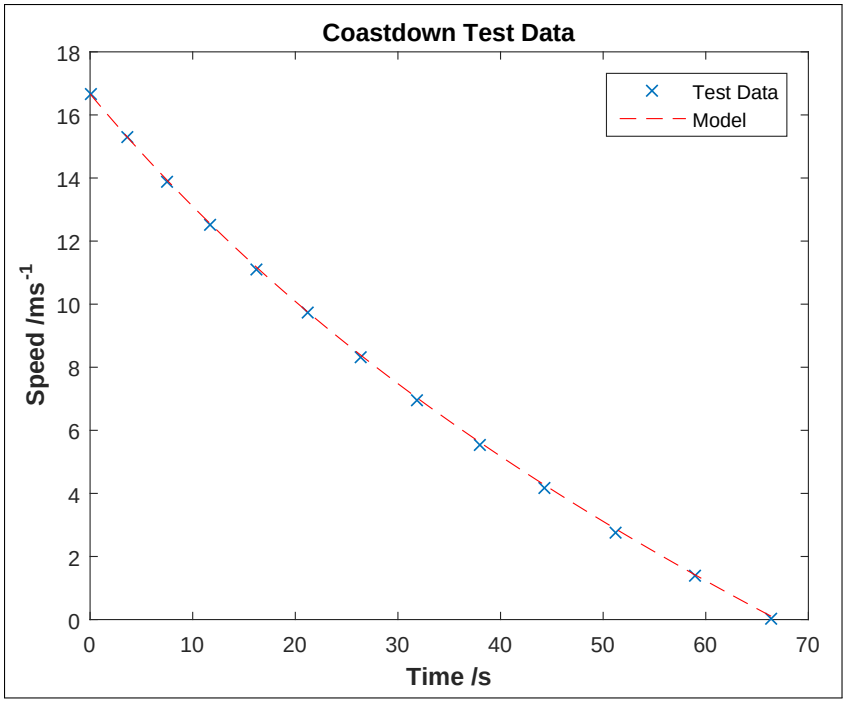

Figure 3.7: Coast-down Test

3.4.2 Motor & Driveline

The motor and driveline model provides two main functions. Firstly, the model calculates the torque based on the driver's demand and subsequently the tractive force. Secondly, it uses the mechanical load on the vehicle to calculate the electrical load on the battery and fuel cell, see Figure 3.8. An empirical model has been created of the motor and driveline efficiency which calculates the current drawn by the motor based on the vehicle's speed, the driver's torque demand and the battery voltage. This model encompasses the entire mechanical driveline, the electric motor and its power electronics. Although a physical model would give better insight into what is happening within this system, this information is of little use for development of the control system due to the fact that the EMS has no control over the efficiency losses within this system.

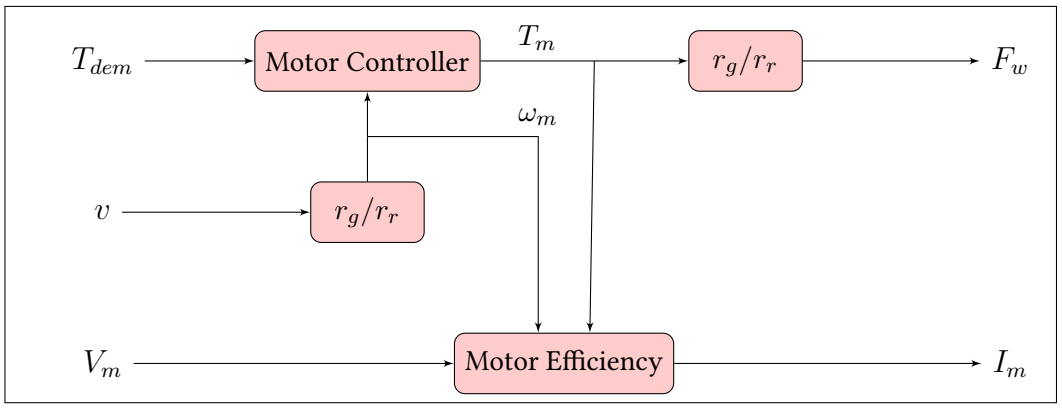

Figure 3.8: Motor & Driveline Model

The Microcab motor directly drives the wheels through a differential with a fixed ratio. There is only a single gear, and therefore the operating conditions of the motor and driveline are directly proportional to the speed and acceleration of the vehicle. As these are the only degrees of freedom, the model of the motor and driveline can be very simple. The motor speed, ω_m, is calculated using the vehicle speed, v, the final drive ratio, r_g, and the rolling radius of the wheel, r_r, see Equation 3.4.4. The motor torque, T_m, is calculated as a function of the driver demand, T_{dem}, and the motor speed (Equation 3.4.5). The tractive effort is calculated using the motor torque, the final drive ratio, and the rolling radius of the wheel 3.4.6

$$\omega_m = v\frac{r_g}{r_r} \tag{3.4.4}$$

$$T_m = f(T_{dem}, \omega_m) \tag{3.4.5}$$

$$F_w = T_m\frac{r_g}{r_r} \tag{3.4.6}$$

The efficiency of the motor and mechanical driveline has been mapped against motor speed and torque using chassis dynamometer testing. This efficiency map is included in the model as a lookup table (Equation 3.4.7). The current drawn by the motor, I_m can be calculated as the mechanical power of the motor, P_m, divided by the driveline efficiency, η_m and the motor supply voltage, V_m (Equation 3.4.8).

$$\eta_m = f(T_m, \omega_m) \tag{3.4.7}$$

$$I_m = \frac{\omega_m T_m}{\eta_m V_m} \tag{3.4.8}$$

3.4.2.1 Reduced Model

The reduced model uses the same empirical data to calculate the electrical power requirements of the motor; however, there is no longer the requirement to calculate the motor torque from the driver demand. Both the speed and the tractive force are obtained from the vehicle model. The motor speed and torque are calculated using the rolling radius and final drive ratio and multiplied to calculate the total ideal mechanical power. This is divided by the total driveline efficiency obtained from the empirical data to calculate the total electrical power drawn by the motor, see Figure 3.9.

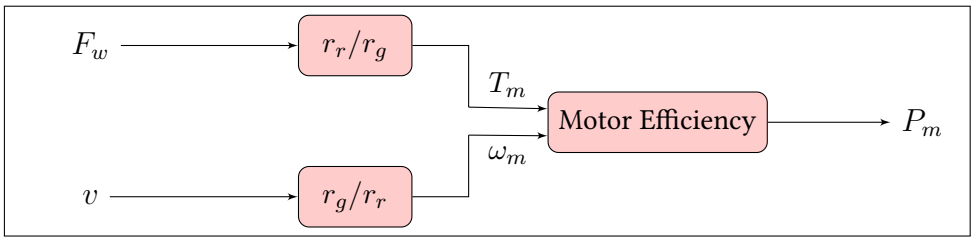

Figure 3.9: Reduced Motor & Driveline Model

3.4.2.2 Characterisation

The specification of the motor and driveline can be found in Table 3.2. As the motor is able to run at its peak rating for up to one hour, the peak power and peak torque have been used as limits on the model. This is because the motor is unlikely to ever exceed this time rating for campus driving cycles.

Parameter	Value
Maximum Torque, $T_{m,max}$	46 Nm
Maximum Speed, $\omega_{m,max}$	3650 rpm
Peak Power, $P_{m,max}$	12 kW
Continuous Power, $P_{m,cont}$	2.24 kW
Rated Torque, $T_{m,rated}$	5.86 Nm
Peak Time Rating, $t_{m,rated}$	60 minutes
Gear Ratio, r_g	8.47
Rolling Radius, r_r	0.276 m

Table 3.2: Motor and Driveline Specification

The efficiency of the motor and driveline as a whole has been empirically derived using chassis dynamometer testing at Loughborough University. The objective of these tests was to calculate the electrical power draw of the motor at a range of speeds and tractive effort forces. The vehicle was driven onto the chassis dynamometer, which was operated at constant force. The vehicle speed was controlled by the driver using the accelerator pedal. At each mapping point, the motor supply voltage and current draw were measured using sensors installed on the vehicle and logged alongside the dynamometer sensors using National Instruments hardware. The efficiency was calculated as the total mechanical power generated at the wheels as measured by the dynamometer, divided by the total electrical power supplied to the motor. This efficiency will therefore take into account all losses which occur between these points in the vehicle including; ohmic losses in the motor and motor controller, eddy currents in the motor, windage and friction in the motor and driveline. The motor torque curve and final efficiency map are shown in Figure 3.10.

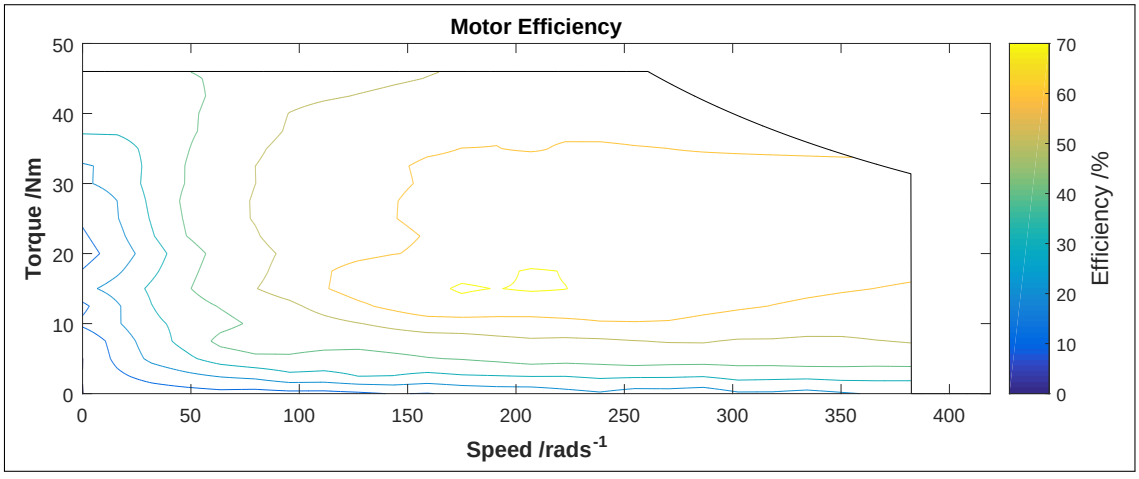

Figure 3.10: Motor & Driveline Efficiency Map

It can be seen that the peak operating efficiency of the motor and driveline is slightly above 70% at approximately 200 $rads^{-1}$ and 16Nm. However, much of the main operating region is between 40% and 70%. This is fairly typical for a brushed DC motor as used in the Microcab, but significantly lower than brushless DC motors as used in many other electric vehicles such as the Microcab H2EV. Although the motor is capable of regenerative braking, this functionality has been disabled in the Microcab due to component failures (for more information see "Hydrogen Hybrid Vehicles for University of Birmingham Campus" [24]), and therefore it has not been possible to determine the efficiency map of the motor operating at negative torque values.

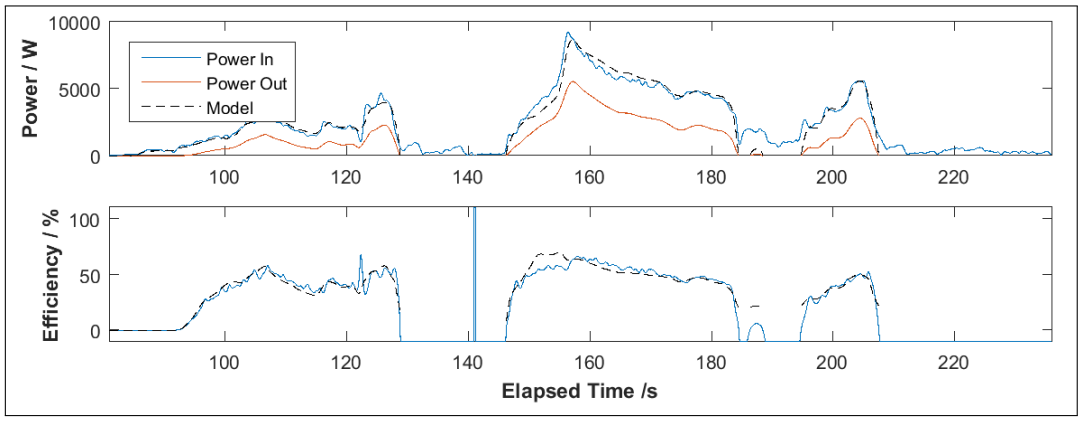

Figure 3.11: Motor Model Validation

Figure 3.11 shows a sample of test data also gathered during dynamometer testing of a logged duty cycle (see Chapter 4). The top graph shows the electrical power drawn by the motor in blue, and the tractive power measured by the dynamometer in red. The dashed black line shows the model estimation of electrical power based on the measured tractive power. The lower graph directly compares the efficiency calculated from the test data and from the model. It can be seen that, despite its simplicity, the model accurately represents the complete motor and driveline efficiency under the majority of circumstances, although the fit could be refined further with additional testing.

3.4.3 Battery Pack

The battery model is a quasi-steady state semi-empirical model used to calculate the SoC and voltage of the battery based on the net current flow. The battery current is positive for current flowing into the battery, calculated by subtracting the current drawn by the motor from that supplied by the DC/DC Converter. The SoC estimation is a simple a charge accumulation model based on the nominal capacity of the battery. The voltage estimation uses a combination of the Shepherd equation and Peukert's Law, see Figure 3.12.

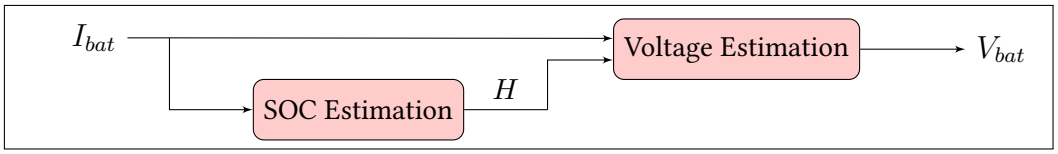

Figure 3.12: Battery Model

The Shepherd equation (Equation 3.4.9) is a semi-empirical model used to predict the voltage of the battery, V_{bat}, dependent on the current, I_{bat}, and the SoC, H. The first term, V_0, represents the open-circuit voltage, the second, $k_f(1-H)$, represents the voltage drop due to the battery SoC, the third due to the internal resistance, R_i, and the final term empirically represents the sudden voltage drop at low SoC using an experimentally determined over-voltage coefficient, k_s, also known as the Shepherd coefficient.

$$V_{bat} = V_{bat,0} - k_f(1-H) - R_i I_{bat} - k_s \frac{1}{H} \tag{3.4.9}$$

For lead acid batteries, the over-voltage coefficient is highly dependent on the current. At low current draws, the voltage will not begin to suddenly drop until a very low SoC is reached, whereas at high loading, the effect of this parameter will occur much sooner. This can be accounted for by using Peukert's Law (Equation 3.4.10). Peukert's law describes how the capacity of the battery is affected by the current loading. This uses the Peukert exponent, n_p, to calculate the Peukert capacity, C_p, which is constant for all current loadings.

$$k_p = I_{bat}^{n_p} t \tag{3.4.10}$$

Peukert's law can be rearranged to solve for the time to depletion, t, and multiplied by the current in order to calculate the normalised capacity of the battery, see Equation 3.4.11.

$$C_n = C_p I_{bat}^{1-n_p} \tag{3.4.11}$$

Combining this with the Shepherd equation gives Equations 3.4.12 and 3.4.13, where F represents the absolute Depth of Discharge (DoD) (measured in Ah) and $f(I)$ represents the relative DoD at that current (expressed as a ratio between 0 and 1). These equations differ slightly depending on whether the cell is charging or discharging, and the empirically derived parameters C_p, k_s, n_p, V_0, k_f, and R_i are subscripted to differentiate between charging, c, and discharging, d.

$$f(I) = \begin{cases} \dfrac{F}{C_{p,d} I^{1-n_{p,d}}}, & \text{if } I_{bat} \leq 0 \\ 1 - \dfrac{F - C_{p,c}(1 - |I|^{1-n_{p,c}})}{C_{nom}}, & \text{otherwise} \end{cases} \tag{3.4.12}$$

$$V_{bat} = \begin{cases} V_{bat,0,d} - k_{f,d}\dfrac{F}{C_{nom}} - R_{i,d} I - k_{s,d}\dfrac{1}{f-1}, & \text{if } I \leq 0 \\ V_{bat,0,c} - k_{f,c}\dfrac{F}{C_{nom}} - R_{i,c} I - k_{s,c}\dfrac{1}{1-f}, & \text{otherwise} \end{cases} \tag{3.4.13}$$

This model does not include dynamic effects due to internal resistance or mass transport within the cell, and also does not include the effects of temperature. In order to prevent algebraic loops in the model, a low pass filter has been used to simulate some delay in the reaction of the output voltage. This filter roughly replicates the response of the battery during testing, however, it is anticipated that the dynamic effects of the battery should not significantly affect the results due to the fact that the dynamics of the battery are much faster than that of the EMS as a whole.

Temperature, however, may have significant effect on the performance of the battery, but has been neglected in this model because **a)** it is not the focus of the investigation, **b)** inclusion would significantly increase testing and validation requirements, and **c)** the extra state would increase the computational effort required for optimisation. The major advantage of this model is that it is relatively simple, but detailed enough to include the main effects of current and SoC over a wide range of values, and that can easily be parameterised using experimental results, and as a result, the reduced model uses an identical battery sub-model.

3.4.3.1 Characterisation

The traction battery pack in the Microcab is made up of four AGM lead acid batteries connected in series, giving a total nominal voltage of 48V and a total nominal capacity of 44Ah (2.1 kWh). AGM lead acid batteries were chosen due to their deep discharge capacity and low cost. The specification of the battery pack is shown in Table 3.3.

The battery pack has been characterised using the battery testing rig available at Loughborough University. A single battery was charged and discharged at various levels of current and the voltage was measured as the state of charge decreased. The resulting data were compiled and used to optimise the coefficients used in the combined Shepherd-Peukert model. The final optimised coefficients are shown in Table 3.4, and the resultant map of battery voltage against current and state as charge is shown in Figure 3.13. It has been assumed that all four batteries will behave identically and therefore the output voltage of the single battery can simply be multiplied by a factor of 4. Although in reality this is a simplification, it represents the ideal case. This model represents a battery pack maintained by a battery management system, although technically the Microcab H4 is not fitted with one. Battery balancing may have an effect on the results, however, it is difficult to accurately represent typical deviations between batteries and still generate reproducible results.

Quantity	Value
Battery Model	Enersys PC1200
Chemistry	Lead Acid
Battery Type	AGM
Nominal Voltage, $V_{bat,nom}$	12 V
Maximum Voltage, $V_{bat,max}$	12.84 V
Minimum Voltage, $V_{bat,min}$	11.7 V
Nominal Capacity, C_{nom}	44 Ah
Short-circuit Current, $I_{bat,max}$	2600 A
Batteries in Series, N_s	4
Batteries in Parallel, N_p	1
Internal Resistance, R_i	4.5 mΩ

Table 3.3: Battery Pack Specification

Parameter	Value
Open-Circuit Voltage, V_0	12.84 V
SoC Voltage Drop Coefficient, k_f	1.14 V
Shepherd Discharge Coefficient, $k_{s,d}$	0.2
Shepherd Charge Coefficient, $k_{s,c}$	0.1
Nominal Capacity, C_{nom}	44 Ah
Peukert Exponent (Discharge), $n_{p,d}$	1.28
Peukert Exponent (Charge), $n_{p,c}$	1.013
Peukert Capacity (Discharge), $C_{p,d}$	100 Ah
Peukert Capacity (Charge), $C_{p,c}$	100 Ah
Internal Resistance (Discharge), $R_{i,d}$	4.5 mΩ
Internal Resistance (Charge), $R_{i,c}$	10 mΩ

Table 3.4: Battery Pack Model Coefficients

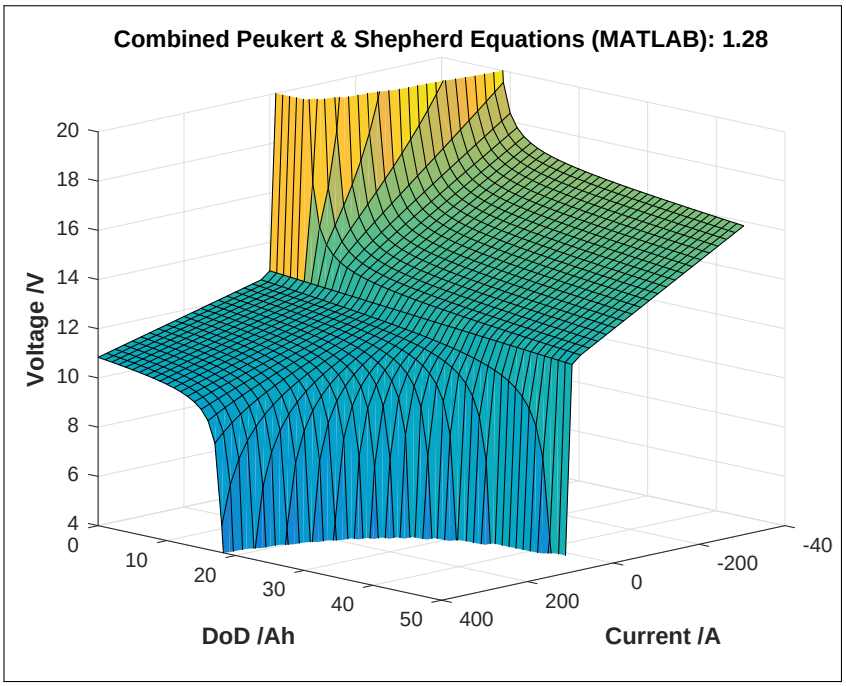

Figure 3.13: Battery Voltage Estimation

The results of the battery model have been compared to test data logged on the vehicle during dynamometer testing. Figure 3.14 shows the comparison between the test data in blue, and the model estimation of battery voltage and power based on the input current and depth of discharge (calculated by coulomb counting). The model estimation is shown as a dashed black line. It can be seen that the model accurately represents the test data during both charging and discharging.

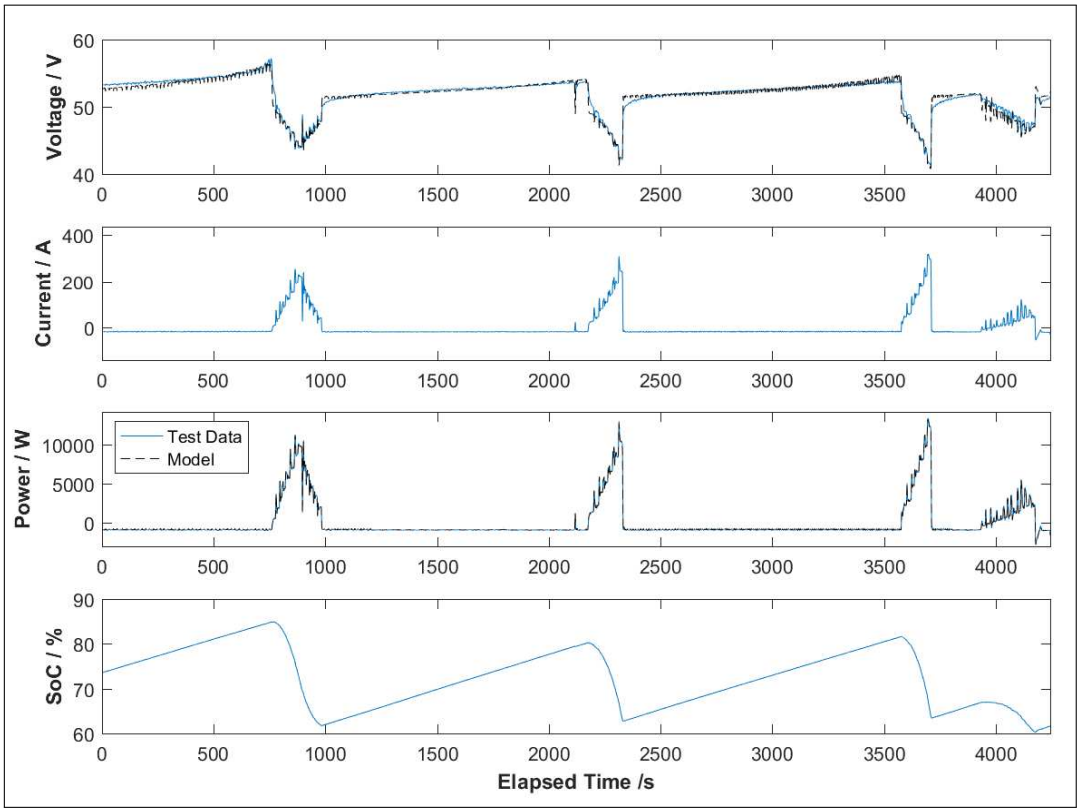

Figure 3.14: Battery Test Data

3.4.4 DC/DC Converter

The role of the main DC/DC converter is to step up the voltage generated by the fuel cell (nominally 24V) to the traction battery pack voltage (48V nominal). The model assumes that the DC/DC converter output power perfectly follows the demand from the EMS controller and any dynamic effects can be safely ignored. As a result, the model DC/DC converter can be extremely simple, see Figure 3.15.

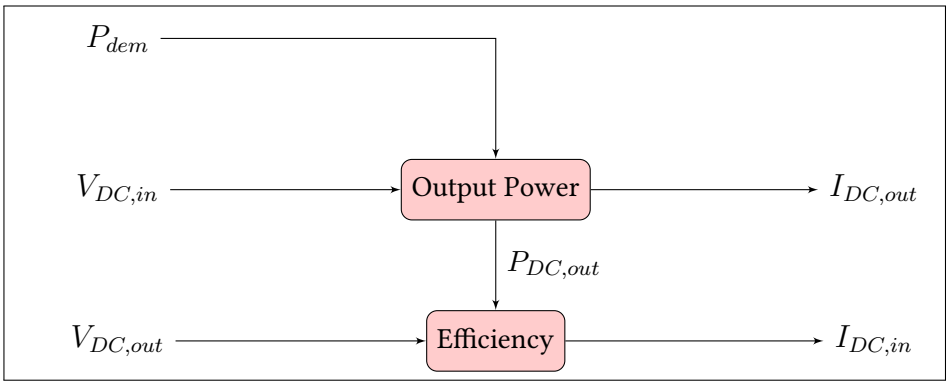

Figure 3.15: DC/DC Converter Model

The output current, $I_{DC,out}$, is calculated as the EMS demand, P_{dem}, divided by the output voltage, $V_{DC,out}$, see Equation 3.4.14.

$$I_{DC,out} = \frac{P_{dem}}{V_{DC,out}} \tag{3.4.14}$$

An empirically derived linear equation is used to calculate the power drawn at the input. The input current, $I_{DC,in}$, is simply calculated by dividing the input power by the input voltage, $V_{DC,in}$, see Equation 3.4.15.

$$I_{DC,in} = \frac{1}{\eta_{DC}(P_{DC,out})} \frac{P_{DC,out}}{V_{DC,in}} \tag{3.4.15}$$

3.4.4.1 Reduced Model

The reduced model of the DC/DC converter neglects the coupling of voltage and current and is based solely on the flow of power through the DC/DC converter. As a result, there is no feedback between the fuel cell and DC/DC converter, nor between the battery and DC/DC converter and the model is entirely unidirectional in order to maximise the computational efficiency of the model, see Figure 3.16.

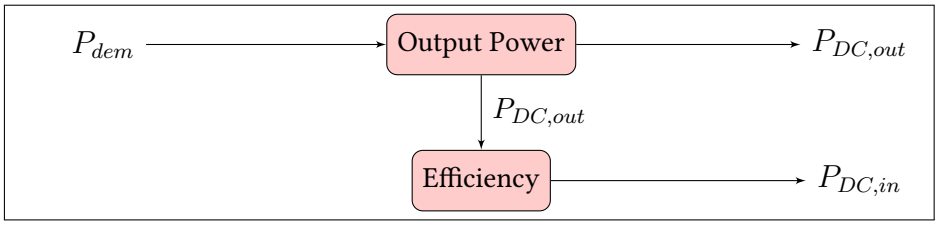

Figure 3.16: DC/DC Converter Model

3.4.4.2 Characterisation

The specification of the DC/DC converter is shown in Table 3.5. The DC/DC converter is rated to a maximum power of 1.7kW, however, the fuel cell is only rated at 1.2kW and therefore the true output power of the DC/DC converter is actually limited by the supply voltage from the fuel cell. The maximum efficiency of the fuel cell is given as 81% which correlates well with the test data.

Parameter	Value
Model	Zahn DC6350F-SU
Maximum Power, $P_{DC,max}$	1.7 kW
Input Voltage Range, $V_{DC,in}$	24-63 V
Output Voltage Range, $V_{DC,out}$	24-63 V
Maximum Input Current, $I_{DC,in,max}$	50 A
Maximum Output Current, $I_{DC,out,max}$	46 A
Switching Frequency	125 kHz
Maximum Efficiency, $\eta_{DCDC,max}$	81 %

Table 3.5: DC/DC Converter Specification

Analysis of around 110 hours of data collected at the University of Birmingham by Iain Staffell shows that the DC/DC converter efficiency can be approximated using a linear relationship between output power and input power. In reality, the relationship is likely to be more complicated than this, and the efficiency is likely to vary depending on the input and output voltages as well as the loading. However, the DC/DC converter on the Microcab is used under a relatively limited range of operating points, each of which can be fully described using only a single variable, either the input power or output power. As a result, it is possible to simplify the model significantly with minimal loss of fidelity.

Figure 3.17 shows a selection of the data logged during the Microcab's usage on the University of Birmingham campus. The linear relationship is used to predict the output power of the DC/DC converter based on its input power. It can be seen that the linear relationship accurately represents the vast majority of the test data. Figure 3.18 shows the relationship of output power to input power for the same test data. The linear relationship is very clear in this plot. There is a very high amount of noise in these data, which is most apparent around 1000W output power. This is because the DC/DC converter spends a substantial proportion of its time in this region.

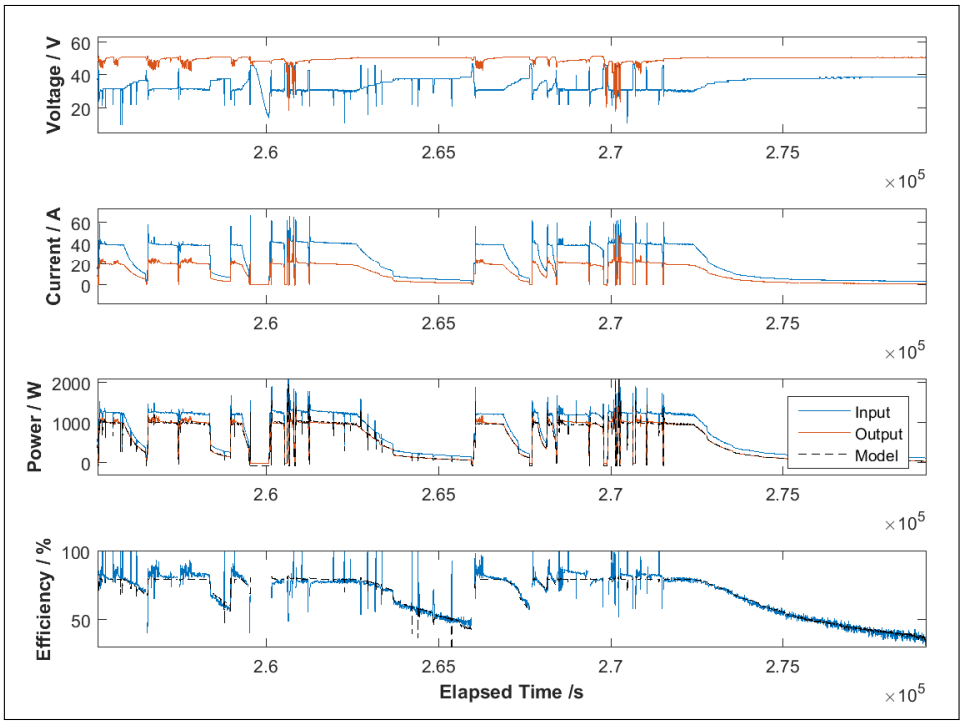

Figure 3.17: DC/DC Converter Test Data

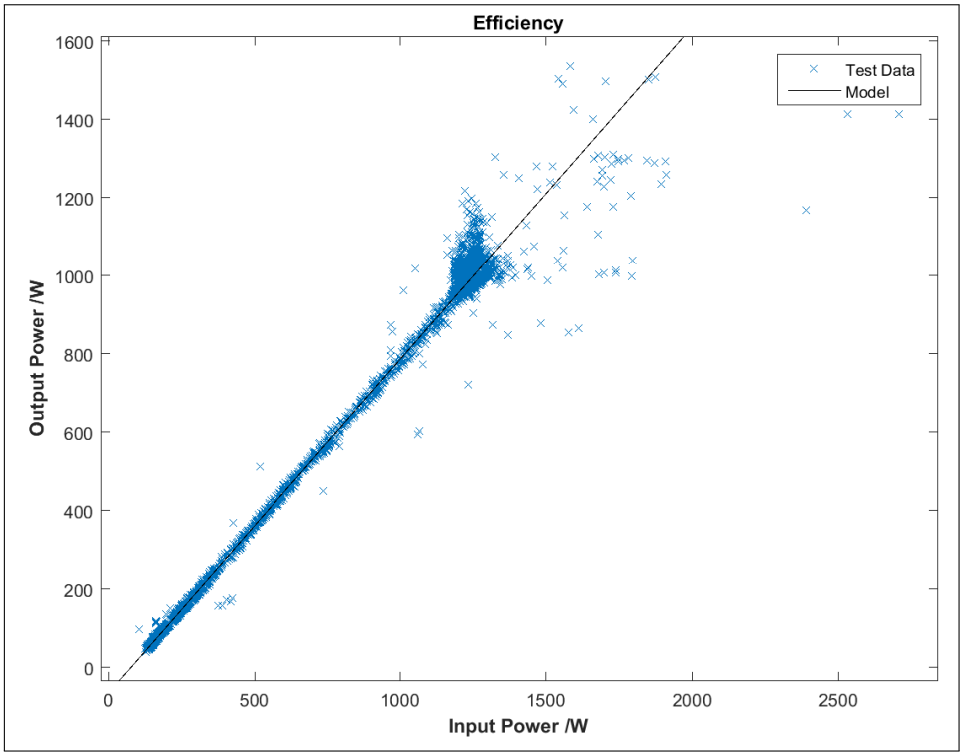

Figure 3.18: DC/DC Converter Output Power vs. Input Power

3.4.5 Fuel Cell

The fuel cell model calculates the voltage of the fuel cell stack dependent on the current drawn by the DC/DC converter. The model also calculates the fuel consumption, and the degradation of the stack. Like many of the other sub-models, the fuel cell model is a steady state model based on empirical data in order to maintain simplicity. The fuel cell stack on the Microcab includes an integrated controller which is responsible for managing the internal operating state of the stack. It has been assumed that this controller is able to manage the stack conditions at a much faster rate than the EMS is likely to change the load and therefore any dynamic effects can be neglected. This assumption may not be valid, especially for rapid changes in load, such as instantaneously moving from idle to full load, however the EMS will be designed to avoid such dynamic effects and therefore this assumption should have negligible effect on the final results.

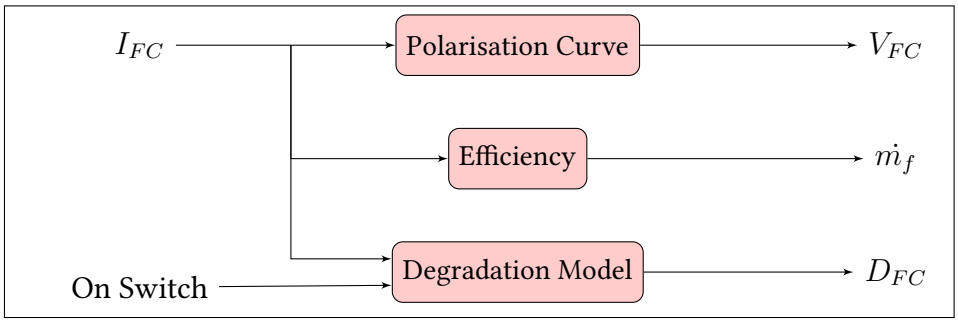

Figure 3.19: Fuel Cell Model

The fuel cell polarisation curve from the equipment datasheet is used to calculate the operating voltage from the current drawn by the DC/DC converter, see Equation 3.4.16. The fuel consumption, $\dot{m}_f$, and degradation voltages due to the operating point, $D_{FC,p}$, and transient loading, $D_{FC,l}$, are also calculated in a similar fashion (Equations 3.4.17, 3.4.18 & 3.4.19). Finally, the degradation due to cycling, $D_{FC,c}$, is accounted for each time the fuel cell is switched from off to on, see Equation 3.4.20, where a negative fuel cell power denotes that the fuel cell is switched off.

$$V_{FC} = f(I_{FC}) \tag{3.4.16}$$

$$\dot{m}_f = \int f(I_{FC})dt \tag{3.4.17}$$

$$D_{FC,p} = \int f(I_{FC})dt \tag{3.4.18}$$

$$D_{FC,l} = \int f\left(|\frac{dP_{FC}}{dt}|\right)dt \tag{3.4.19}$$

$$D_{FC,c} = \begin{cases} \sum \frac{1}{N_{cyc}}, & \text{if } P_{FC,t} \geq 0 \wedge P_{FC,t-1} < 0 \\ 0, & \text{otherwise} \end{cases} \tag{3.4.20}$$

3.4.5.1 Reduced Model

The reduced model is almost identical except that the separation of voltage and current is no longer required and therefore the polarisation curve is not included. This also means that the empirical relationships are based on the net power rather than based on the fuel cell current loading.

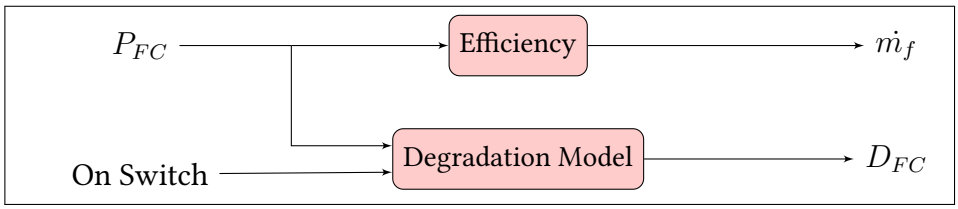

Figure 3.20: Fuel Cell Model

3.4.5.2 Model Validation

The fuel cell has been tested in-situ, logging data using a serial interface to the built-in controller. An example set of results is shown in Figures 3.22-3.24. It can be seen that the model based on the datasheet shows a good correlation with the test data despite the age of the fuel cell system.

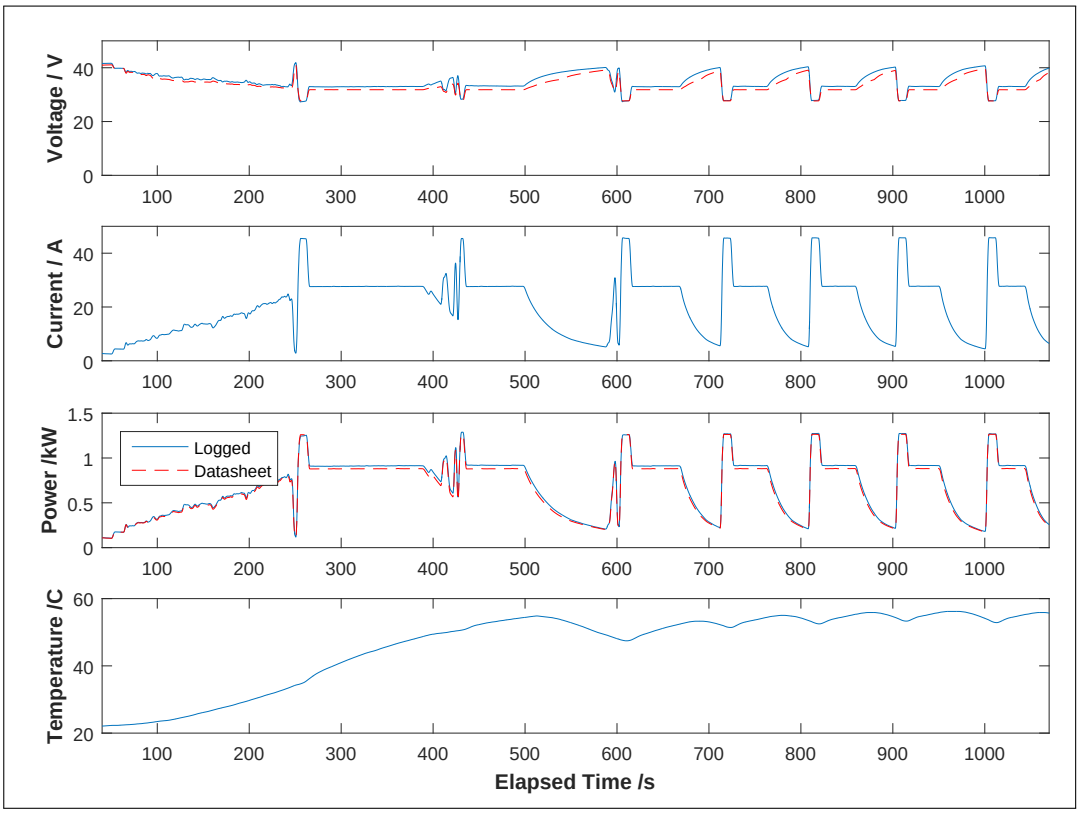

Figure 3.21: Fuel Cell Test Data

Figure 3.21 shows the raw measured voltage, net current, power and temperature of the fuel cell against time. The model estimation of voltage and power based on the datasheet are calculated from the measured current. It can be seen that the model shows a very good correlation in general, but tends to underestimate the voltage slightly in the mid-range around approximately 20A. This also leads to a slight underestimation of the net power in the same range.

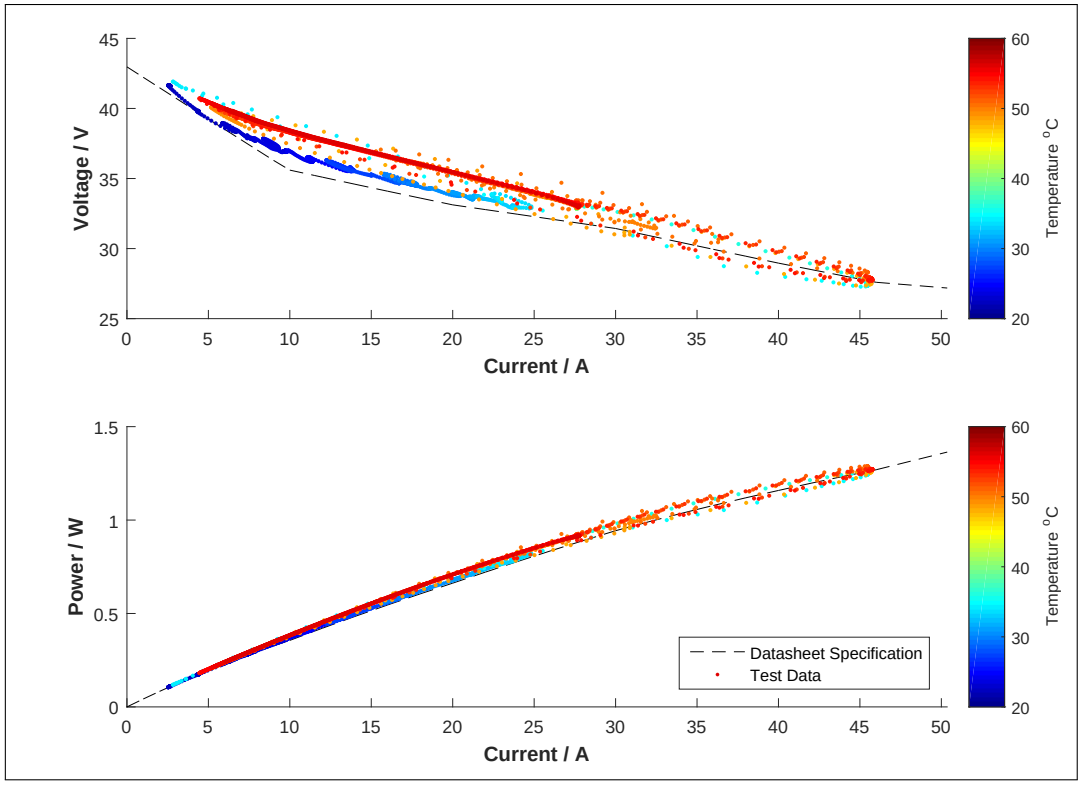

Figure 3.22: Fuel Cell Polarisation Curve

Figure 3.22 shows the same data using the net current as the independent axis. The temperature is represented by the colour of each data point. It can be seen that the measured fuel cell voltage is consistently higher than that predicted by the datasheet, and as a result the net power is also slightly underestimated by the model. There also seems to be a slight variation in the voltage due to temperature. It can be seen that the voltage at the beginning of the test where the fuel cell was between 20°C and 40°C is closer to the model prediction that that later in the test where the fuel cell is running between approximately 40°C and 60°C. This can be explained by higher reaction rates at elevated temperatures, although this could also be due to other factors than the lower temperature at the beginning of the test, such as recharging of the auxiliary battery. Finally, it can be seen in Figure 3.22 that the data are very consistent. The fuel cell was cycled between 200W and 1200W five times at the end of the test while the fuel cell was at normal operating temperature. The measured data for each of these cycles overlays almost perfectly. This suggests that the model is competent at describing the fuel cell accurately under normal operating conditions despite its simplicity. This is likely due to the effective management of the fuel cell by its integrated controller.

Figures 3.23 and 3.24 show the measured hydrogen usage and calculated efficiency for the same test. It can be clearly seen that the estimation of fuel consumption based on the datasheet is very accurate under all conditions. As a result, the operating efficiency is also accurately represented by the model. Detailed examination shows that the efficiency calculated by the model is very slightly lower than the measured data at medium load at normal operating temperature. This is likely due to the underestimation of the voltage, and hence underestimated net power output. Therefore, this can be easily remedied by adjusting the polarisation curve to fit the data.

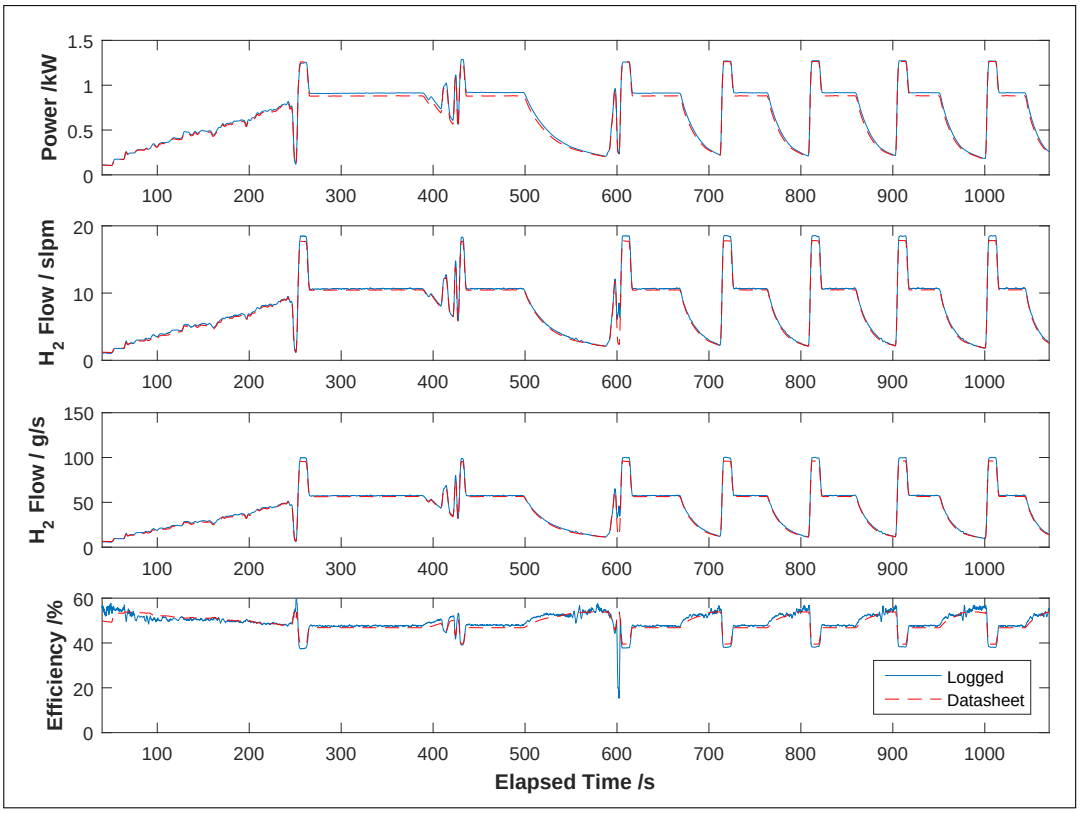

Figure 3.23: Fuel Cell Test Data

It can be seen in Figure 3.24 that the efficiency of the fuel cell correlates well with theory. The efficiency is very low at idle and low loads due to the current drawn by the ancillaries. Although this current draw is very small, the net power output is also small and therefore it is significant in terms of energy usage. The efficiency quickly rises to a maximum of around 55% at around 200W, and then gradually declines to around 40% at 1200W net power output. The linear drop in efficiency is largely due to increased ohmic losses as a result of the increase in current. Above approximately 1000W, the hydrogen consumption increases slightly more quickly than in the range below. This is likely due to mass transport restrictions as the fuel cell stack gets close to its maximum load. This increase in consumption can be clearly seen in the efficiency data as a steeper decline between 1000W and 1200W.

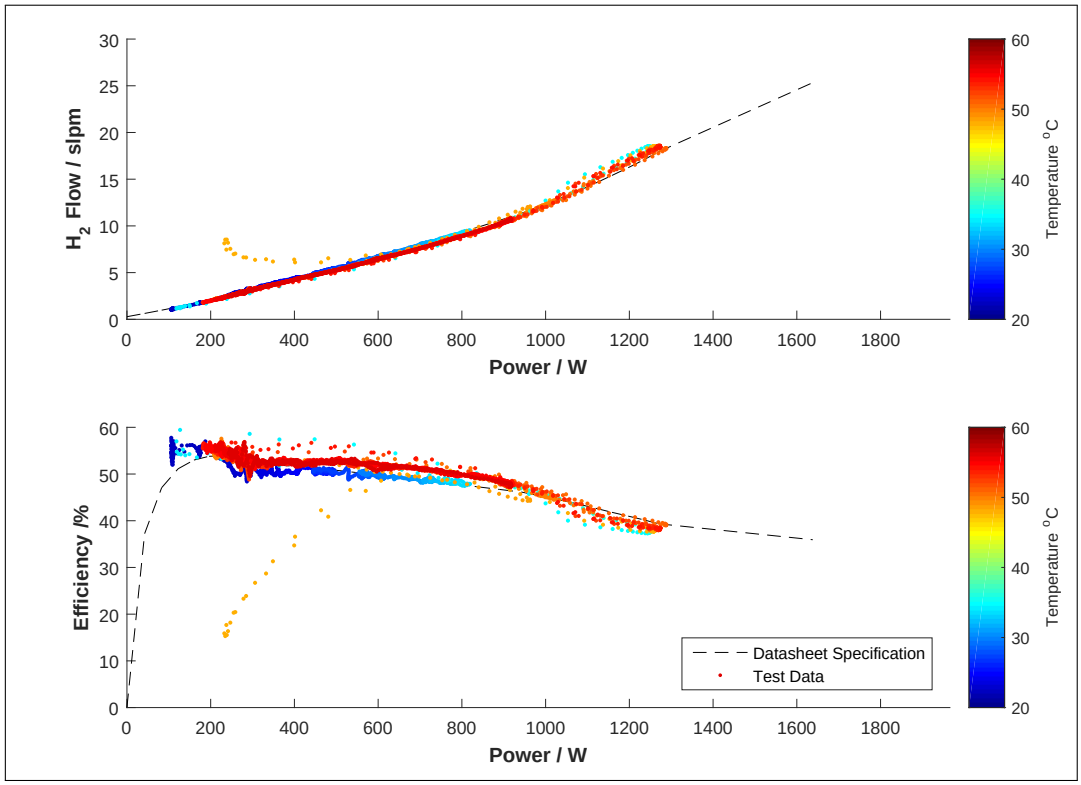

Figure 3.24: Fuel Cell Polarisation Curve

Overall, despite its simplicity, the model describes the test data very well. Some variation in stack voltage due to temperature is seen in the test data, however in the range of normal operating conditions, this was negligible and therefore it can be safely ignored in the model. It can be seen in Figure 3.21 that once the fuel cell has warmed up its temperature is regulated by the fuel cell controller to within approximately 5°C of 55°C. Within this range, the efficiency of the fuel cell varies by less than the noise in the logged data as can be seen in Figure 3.24. The efficiency of the fuel cell, however, is slightly lower during the initial warm-up, until the temperature reaches approximately 40°C, which corresponds to approximately 5 minutes of running. The inclusion of temperature could, therefore, improve the results, however this would significantly increase the time required to accurately parameterise the model, and would also introduce an additional state into the controller optimisation. This would, in turn, dramatically increase the computational requirements of the optimisation and therefore it has been neglected, however it could be included with further work. In addition to this, the estimation of stack voltage is slightly too low in the mid-range of current loading. This can be easily remedied by adjusting the lookup table in order to fit the test data rather than using the datasheet information directly.

3.5 Control System Models

The control systems models used for both the detailed and reduced models are almost identical, aside from the fact that the detailed model includes an extra sub-model for controlling the vehicle speed based on feedback from the vehicle. The reduced model is backward-facing and as a result, it is assumed that the vehicle perfectly follows the drive-cycle demand and hence does not require the "driver" model. As previously mentioned, this means that the reduced model is able to simulate much faster for SDP optimisation, but may produce erroneous results if the vehicle is unable to achieve the reference speed or acceleration demands.

The control system is broken down into three main components; the drive-cycle reference demand, the "driver", and the EMS supervisory controller. The reference demand and the "driver" are responsible for controlling the speed of the vehicle, whereas the EMS control system is responsible for managing the operating point of the fuel cell and hence the SoC of the battery pack.

3.5.1 Drive-cycle Reference

The role of the drive-cycle reference block is to provide the duty cycle that the model is going to simulate. This block forms the main input to the simulation. The drive-cycle block is a simple lookup table based on time. This block outputs the demanded vehicle speed and any gradient that has been predefined in the drive-cycle. Using this block, it is possible to simulate any legislative or academic drive-cycle, but also logged data and steady state conditions, such as fixed speeds or accelerations and gradients.

3.5.2 "Driver" Model

The role of the "driver" model is to control the vehicle speed based on the drive-cycle reference demand and feedback from the plant model. The interaction of the driver and vehicle for drive-ability study is not of concern for this project and therefore the "driver" model has been designed to follow the reference speed as closely as possible rather than accurately model real driver behaviour.

The model works using a Proportional Integral (PI) controller based on the error between the feedback from the model and the reference demand. The Microcab H4 does not have regenerative braking capability and therefore positive torque requests are sent to the vehicle as throttle demands to the motor and negative demands are transmitted as braking torque requests to the vehicle model, see Figure 3.25.

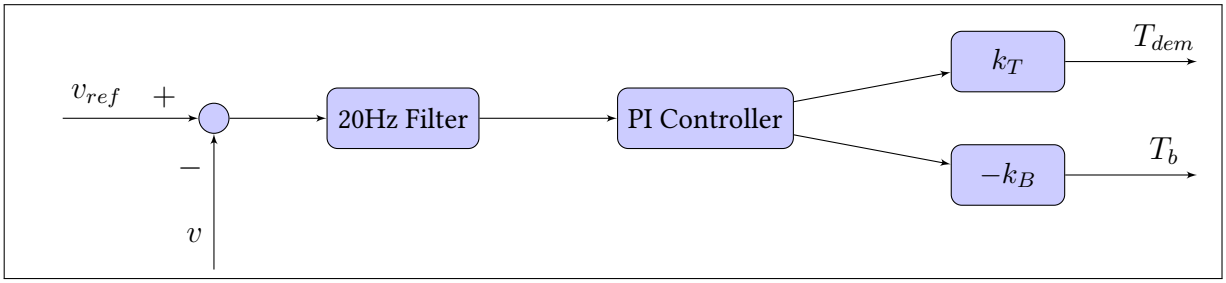

Figure 3.25: "Driver" Model

3.5.3 EMS Supervisory Controller

The EMS is responsible for managing the SoC of the battery pack by controlling the output power of the DC/DC converter. This block is the focus of the project and three different controllers have been developed for this purpose.

3.5.3.1 "Thermostatic" Controller

The first is a binary "thermostatic" controller. This model was initially created as a placeholder for testing the plant model and works by turning the fuel cell on at full power when the battery SoC drops below a set level. The fuel cell is turned off again when the SoC reaches a higher level. This model is often used as a baseline in the literature due to its simplicity, see Figure 3.26.

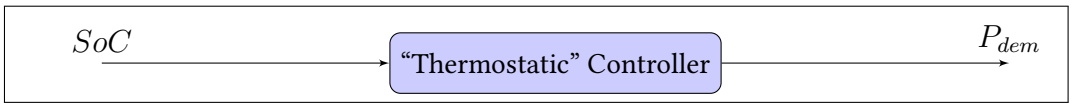

Figure 3.26: "Thermostatic" EMS Controller

3.5.3.2 Battery Voltage Controller

The second option is a battery voltage controller. The model mimics the current behaviour of the test vehicle and works by producing a power demand that is designed to control the battery voltage to a set level. This differs from managing the SoC directly because the output power of the DC/DC converter will be ramped up when the battery is under high load as well as when the SoC is low. This is because both of these conditions will cause the operating voltage of the battery to drop. The Microcab H4 does not have an explicit EMS, but the DC/DC converter is set to produce a constant output voltage of 57.6V when not restricted by maximum power limitations. As a result, the fuel cell is run reactively to battery voltage drops. The model replicates this by using a PID controller with the output limited between zero and the maximum output power of the DC/DC converter, see Figure 3.27.

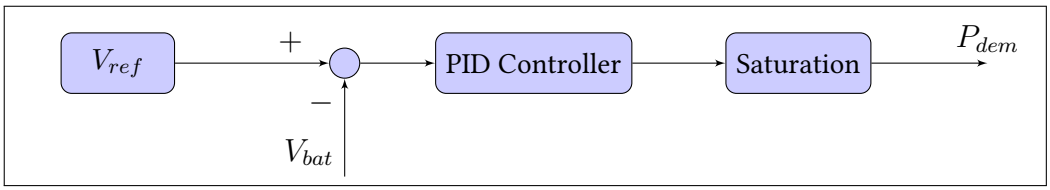

Figure 3.27: Voltage EMS Controller

3.5.3.3 Stochastic Dynamic Programming (SDP) Controller

The final option is the strategy optimised using SDP. SDP produces a causal policy based on the inputs provided to the algorithm. The algorithm chooses the optimal action to take in each possible vehicle state in order to minimise the cost function over a finite or infinite horizon. As a result, the output can be represented by a lookup table which can be directly implemented in simulation or on board the vehicle.

The SDP controller, therefore, can be very simply represented by a single four-dimensional lookup table of power demand based on the vehicle speed, acceleration, battery SoC and the previous output power, see Figure 3.28. Contrary to the rest of the simulation this sub-model is iterated at a fixed time-step of 1 second.

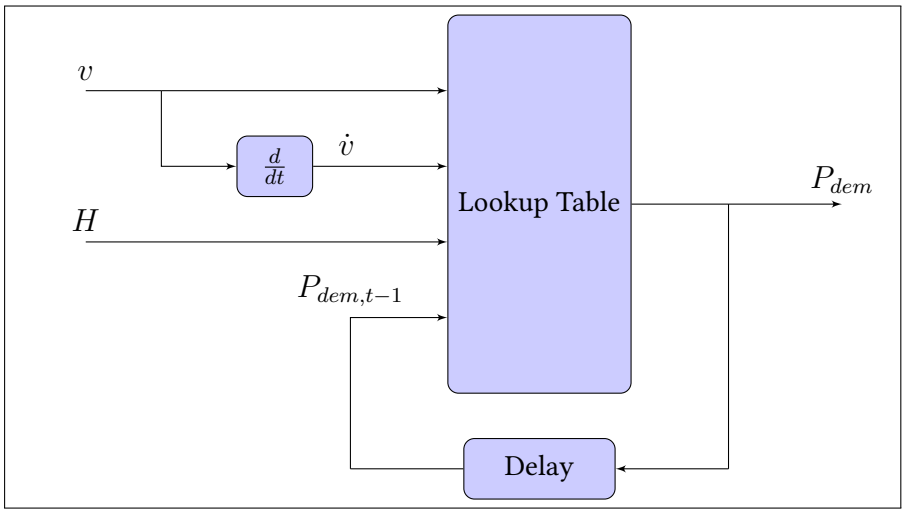

Figure 3.28: SDP EMS Controller

3.6 Summary

Two vehicle models have been created for this project. The first is a detailed forward-facing model which accurately represents the causality of the vehicle in the real world. This model is used for testing the controller and examination of its behaviour under a range of conditions. The second model is a reduced order model which has been simplified in order to dramatically reduce its computational burden. This model is used for the SDP optimisation process which requires the model to be simulated at least tens of thousands of times and possibly hundreds of thousands of times for high resolution results. As a result, it is required to be very quick to simulate.

Both models used a modular substructure allowing individual components to be tested in isolation. The model is parameterised based on the Microcab H4, but as few parameters as possible have been used in order to allow the model to be easily changed should more test data about the Microcab H2EV become available. Experimental data has been used to create empirical and semi-empirical models of each component to ensure that the behaviour is representative of the test vehicle. Where possible, independent validation data has been used to check the accuracy of the model, which has been included in the report.

Chapter 4

Markov Chain Modelling of Duty Cycle

This chapter describes the development of the Markov Chain model which is used to describe the usage patterns of the Microcab for mail delivery and passenger transport on a university campus. Logged data has been obtained from the Microcab's usage at the University of Birmingham and also for a variety of duty cycles at Loughborough University. Global Positioning System (GPS) data of the vehicles usage was collected by Matt Lintern at Loughborough University, and by Iain Staffell at the University of Birmingham. These data have been processed and used to generate a Markov Chain model which can be used for development of the Stochastic Dynamic Programming (SDP) control strategy.

The first two sections describe the methods used to collect and process the data and identify all individual journeys that were made by the vehicles. It was found that only 11 trips were made by the Microcabs themselves in the data available and therefore the duty cycles logged at Loughborough have been compared to the Microcab data to identify a suitable substitute should these data be insufficient.

Section 4.4 describes the development of three different methods used to generate the probability matrix that defines the Markov chain. The advantages of each of the methods are compared and a sample of the results is presented.

Finally, Section 4.5 presents a validation of the results and a comparison of each of the methods described in Section 4.4 to the original data. The Markov model is used to generate a number of random drive-cycles using the Monte-Carlo method. These drive-cycles are then compared to the original data using Speed-Acceleration Frequency Distribution (SAFD) analysis in order to assess the validity of the Markov model. Results show a high degree of fidelity of above 97% for almost all of the duty cycles.

4.1 Introduction

The development of a SDP control strategy requires a model of the vehicles usage pattern as an input. In comparison to Deterministic Dynamic Programming (DDP), where it is assumed that the vehicle speed profile is known "a priori" to calculating the control strategy, SDP instead uses stochastic model of the duty cycle that the vehicle is likely to face. This means that it is not required for the exact profile of each journey to be known in advance. Typically, a Markov Chain model is used for this purpose; this type of model contains the probabilities of transitioning between vehicle states based on the current and past states of the vehicle. The production of the Markov model of the duty cycle alongside a cost associated of transitioning between states, allows the Energy Management Strategy (EMS) optimisation process to be formulated as a Markov Decision Process (MDP) problem.

The probabilities of the Markov model can be populated using existing data. It is common in the literature for this probability matrix to be generated either from a number of standard drive-cycles such as the New York City Cycle (NYCC) and the New European Driving Cycle (NEDC), however a number of authors have instead used logged data to generate this information [64]. There are advantages to both methods; the use of standard drive-cycles allows the results to be easily replicated by others and results can be easily compared, however the use of logged data is usually a more accurate representation of real-world driving patterns and the controller is therefore unlikely to exhibit "cycle-beating" traits.

The Microcab H4 is a relatively low powered vehicle designed for use in and around a university campus. In order to keep the cost as low as possible, the vehicle is equipped with a DC drive motor, similar to that used in forklift vehicles. As a result, it has a maximum speed of around 12.5ms^{-1} or 45km/h [6]. This means that it is unable to complete the vast majority of standard drive-cycles satisfactorily, see Figure 4.1.

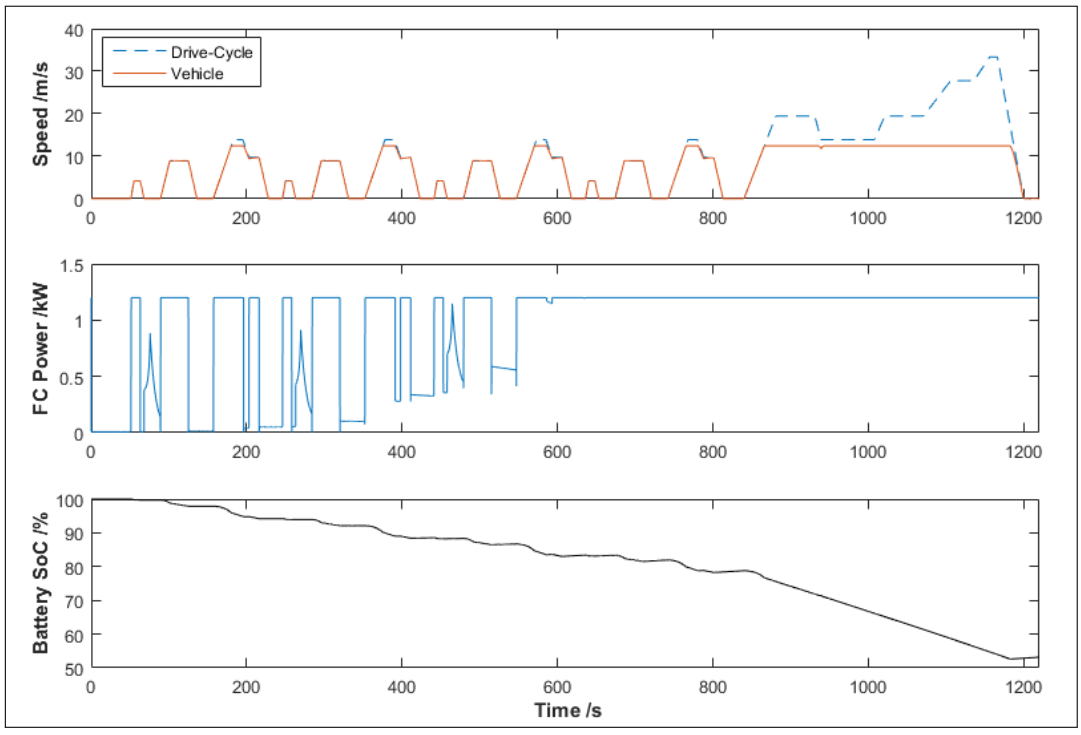

Figure 4.1: Forward facing simulation of the Microcab H4 over the NEDC

It would be, therefore, unsuitable to use standard drive-cycles as a basis for the Markov model. However, a large amount of logged data which describes campus drive-cycles is available to the project. This has been obtained from a variety of campus vehicles used at Loughborough University and also from data recorded during the Microcabs usage at the University of Birmingham. This data is also much more representative of the type of journey that the vehicle is designed for and is therefore much more likely to increase the vehicles performance in the real world. The generation of the probability matrices used to describe the Markov model can be split into four steps;

1. Data Logging (Section 4.2)
2. Data Processing (Section 4.3)
3. Probability Matrix Generation (Section 4.4)
4. Validation (Section 4.5)

Each of these steps is described in the following sections, along with justifications of the decisions made in order to produce the best results. There are a number of ways in which this method could be improved in the future which were not feasible for this project and so suggestions have been included which could further improve the accuracy of the results.

4.1.1 Other Practical Uses of the Markov Model

In addition to development of the control strategy, stochastic modelling of a vehicle's intended duty cycle has a number of other potential uses. In fact, the stochastic model could in theory replace standardised drive-cycles in a number of areas for both the design of the vehicle, as well as for legislative testing. Because the stochastic model is able to capture a much wider variety of circumstance, it has the potential to represent real-life driving conditions in a much more realistic manner. It is well known that the real-world performance of many, if not all, vehicles does not often match the figures quoted by the manufacturers for both fuel consumption and emissions. This problem emerges because the vehicle's design and optimisation often exhibits "cycle-beating" traits.

These design features may in some cases may be unintended, however very often they are purposely designed in order to obtain optimal performance in legislative testing, at the expense of the performance of the vehicle in other real-world circumstances. Whether these features are intended or not by the manufacturers, they are in fierce competition with each other in order to present vehicles with the highest possible performance, and these metrics are often used by consumers when choosing their next vehicle. The discrepancy is most apparent in simplified drive cycles such as the NEDC, however it is still present in vehicles designed against more realistic drive-cycles such as the FTP-75, and Artemis cycles. In order to overcome this problem, Markov models of real-world driving conditions could be used to produce the next generation of legislative tests using the techniques described in this chapter.

Designing the vehicle based on a Markov model of the intended duty cycle rather than specific drive-cycles will allow manufacturers to produce vehicles which do not exhibit these "cycle beating" traits and therefore the vehicle's performance in the real-world is likely to be much more similar to the manufacturers "estimated" figures. By incorporating the process into legislative testing would also serve to encourage manufacturers to do this, and allow consumers a fairer comparison of how the vehicles are likely to perform in the real-world.

4.2 Data Logging

The raw data used for this work were obtained from two previous projects; one at Loughborough University and another at the University of Birmingham. At Loughborough University, the collection of data was performed by Matt Lintern for a final year project focussed on the definition a standardised Loughborough University campus drive-cycle. GPS data loggers were attached to a variety of campus vehicles and data were logged at 1Hz over a period of approximately 3 months whilst the vehicles were used normally. Over this period, a total of 840 hours of data representing almost 3000km of usage was collected.

At the University of Birmingham, the data was collected by Iain Staffell as part of a PhD project analysing the operation of five Microcab H4 test vehicles. These vehicles were used for passenger transport, mail delivery and experimental testing around the campus over a period of two years, travelling a total distance of more than 4000km [6]. The main focus of this project was on the operating efficiency of the fuel cell and electrical powertrain components, however approximately 9 hours of up to 10Hz GPS data, representing 80km, has been made available for statistical analysis of normal usage duty cycle on campus. A summary of the raw data available can be found in Table 4.1.

Location	**Duty Cycle**	**Logged Frequency** /Hz	**Total Time** /hours	**Total Distance** /km	**Max Speed** ms^{-1}	**Peak Accel** ms^{-2}
Loughborough	Electrical	1	117	325	19	5.0
	Grounds & Gardens	1	157	387	10	2.9
	Mail Room	1	181	431	21	3.7
	Security	1	281	1511	25	4.4
	Teaching Support	1	103	187	14	3.5
Birmingham	Mail Room	3	2	12	11	2.0
	Teaching Support	3	1	8	10	1.7
	Testing	10	6	60	15	2.6

Table 4.1: Summary Logged Campus Vehicle Data

On first impression, the data collected from the Microcab vehicles themselves during their usage on Birmingham campus is the ideal candidate for optimisation of the SDP controller. However, there is very little data available, of which only approximately 3 hours is representative of typical usage patterns, the rest was collected for analysis of the vehicles themselves. The SDP optimisation process is highly sensitive the quality of the input data, and the generation of the Markov chain will produce a more reliable estimate if given large volumes of data.

In total, almost 3000km of data have been collected at Loughborough. However, some of this is not representative of the type of journeys that the Microcabs have been designed for. From examination of the table, it can be seen that the Microcab logged data matches best with the Grounds and Gardens style duty cycle collected at Loughborough. This is because these vehicles did not significantly exceed the maximum speed or peak acceleration of the Microcabs when used at the University of Birmingham.

4.3 Data Processing

For the purposes of this work, the main logged signal that is of interest is the vehicle's speed. This is generated by a GPS data logger using on the current location of the vehicle and its previous location. The vehicle speed is also used to calculate the acceleration of the vehicle. The GPS data also contains an estimate of the vehicles altitude, which could be used to include the road gradient in the analysis, however the data available is not accurate enough for this purpose and therefore has been neglected. The raw data requires some processing before it can be used to analyse the usage pattern of the vehicle for SDP optimisation.

4.3.1 Initial Processing

Firstly, the individual logs must be accumulated, and any overlap between logs must be removed. The logging stops after a fixed interval of 8 hours, therefore may stop in the middle of a trip. Any incomplete trips must be removed. The raw GPS data are subject to an accuracy of approximately $\pm$2m which can lead to false readings in the speed trace. Fortunately, these errors can be effectively removed by filtering the data with only a minor loss of fidelity. The vehicle is assumed to be stopped during any gaps in the data. This means that these gaps will not affect the analysis as only times when the vehicle is moving are of interest. Overall, the initial processing gives a single continuous speed trace of the vehicle over the entire logged period encompassing all completed journeys that occurred. It can be seen in Figure 4.2 that the logging for the Ground and Gardens vehicles began on a Wednesday and continued for approximately 4 weeks. Logging took place during working hours with only one missed day (Tuesday) during the final week.

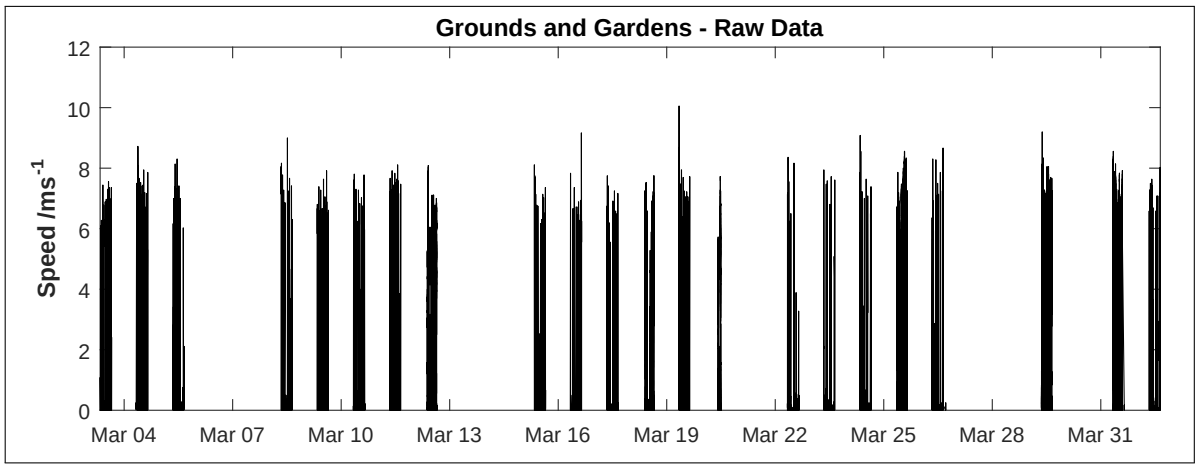

Figure 4.2: Grounds and Gardens Raw Collected Data

4.3.2 Identify and Extract Individual Trips

The Markov model is required to describe the usage of the vehicle only whilst the vehicle is active. Ideally, this would be related to the state of the ignition switch of the vehicle, but these data are not available. Therefore, a number of assumptions have been made to estimate when the vehicle is likely to be active.

1. The vehicle is moving when its speed is greater than 1.2ms^{-1} for a period of 60s or more. This is to avoid noise in the data when the vehicle is static.
2. The vehicle becomes active 10 seconds before it starts moving and remains active for 10 seconds after it stops. This is to ensure the entire journey is captured including some stationary time either side of the journey.
3. If the vehicle is stationary for less than 10 minutes between periods where it is moving, it assumed that this is part of a single journey. This accounts for times when an Internal Combustion Engine (ICE) vehicle may be stationary, but with the engine running, such as waiting for passengers, or delivering mail. It also ensures that the journey is not broken by shorter stops such as at traffic lights.

This process splits the single continuous speed trace into a number of discrete trips. Figure 4.3 shows an example trip. The top graph shows the raw unprocessed data. In the second graph, the red solid line denotes the trip, and the dashed black line shows regions in the processed data which have been removed. The lowest graph shows the speed of the vehicle in relation to its location on a map. This journey appears to begin at the maintenance building and drive around campus stopping at the Stuart Miller building, the multi-storey car park and the library before finishing at the Edward Herbert building. Overall, the journey takes approximately 16 minutes, of which approximately 11 minutes is spent moving. The maximum speed was approximately 8ms^{-1} (18mph), slightly above the campus speed limit of 15mph.

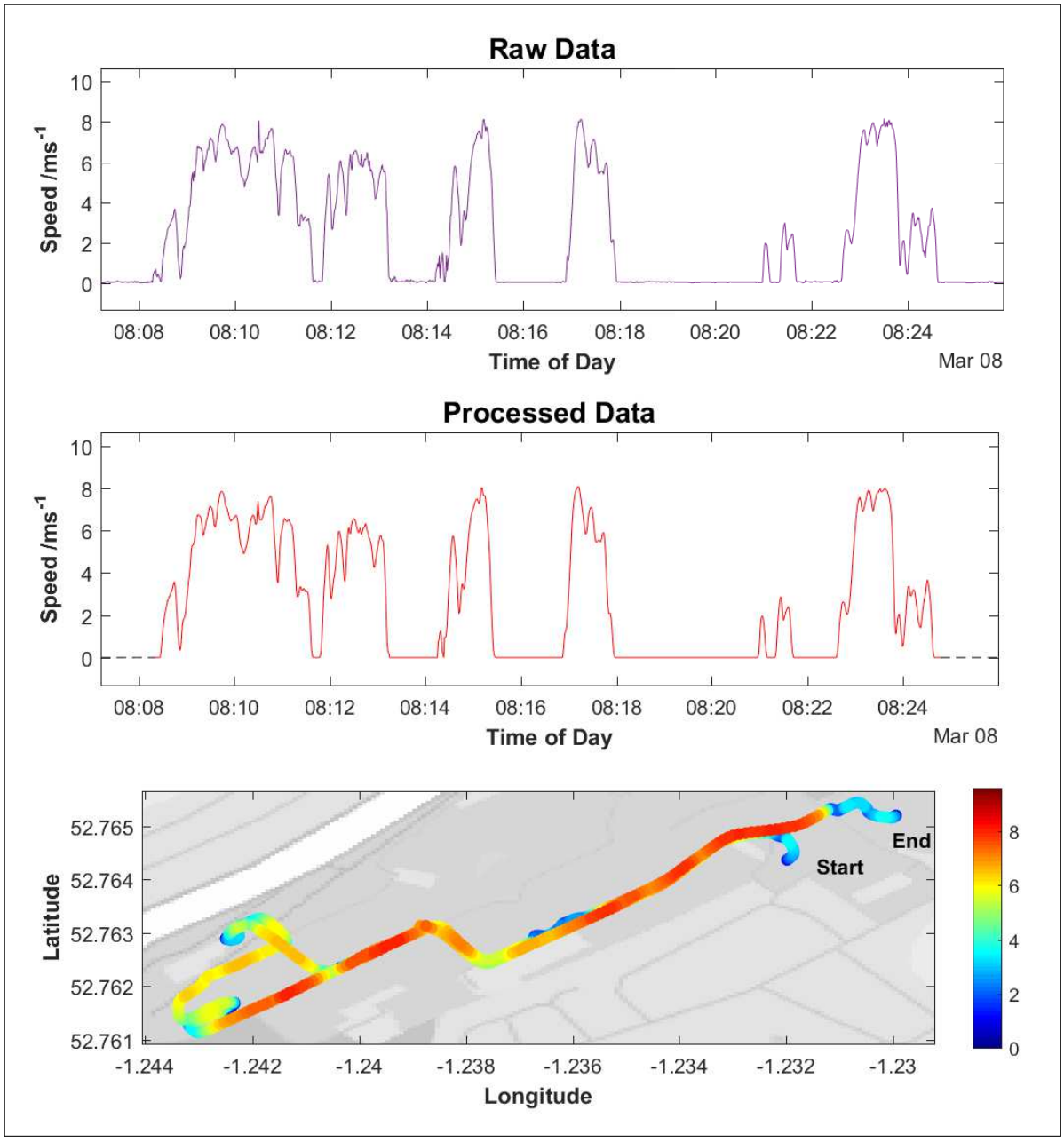

Figure 4.3: Grounds and Gardens Processed Data

4.3.3 Post Processing

For the Grounds & Gardens vehicles, a total of 193 trips are identified using this method. However there are a number of "false positives" where the vehicle is identified as moving for a period of greater than 60 seconds, but the vehicle does not appear to be active when the GPS data are examined in detail. This is likely due to errors in the GPS data which are not effectively removed by the 1.2ms^{-1} stationary speed limit. Increasing the stationary speed limit will reduce the number of true trips that are captured and therefore SAFD analysis (see Section 4.3.3.1) is used to identify any trips which do not correlate with the rest. An example is shown in Figure 4.4.

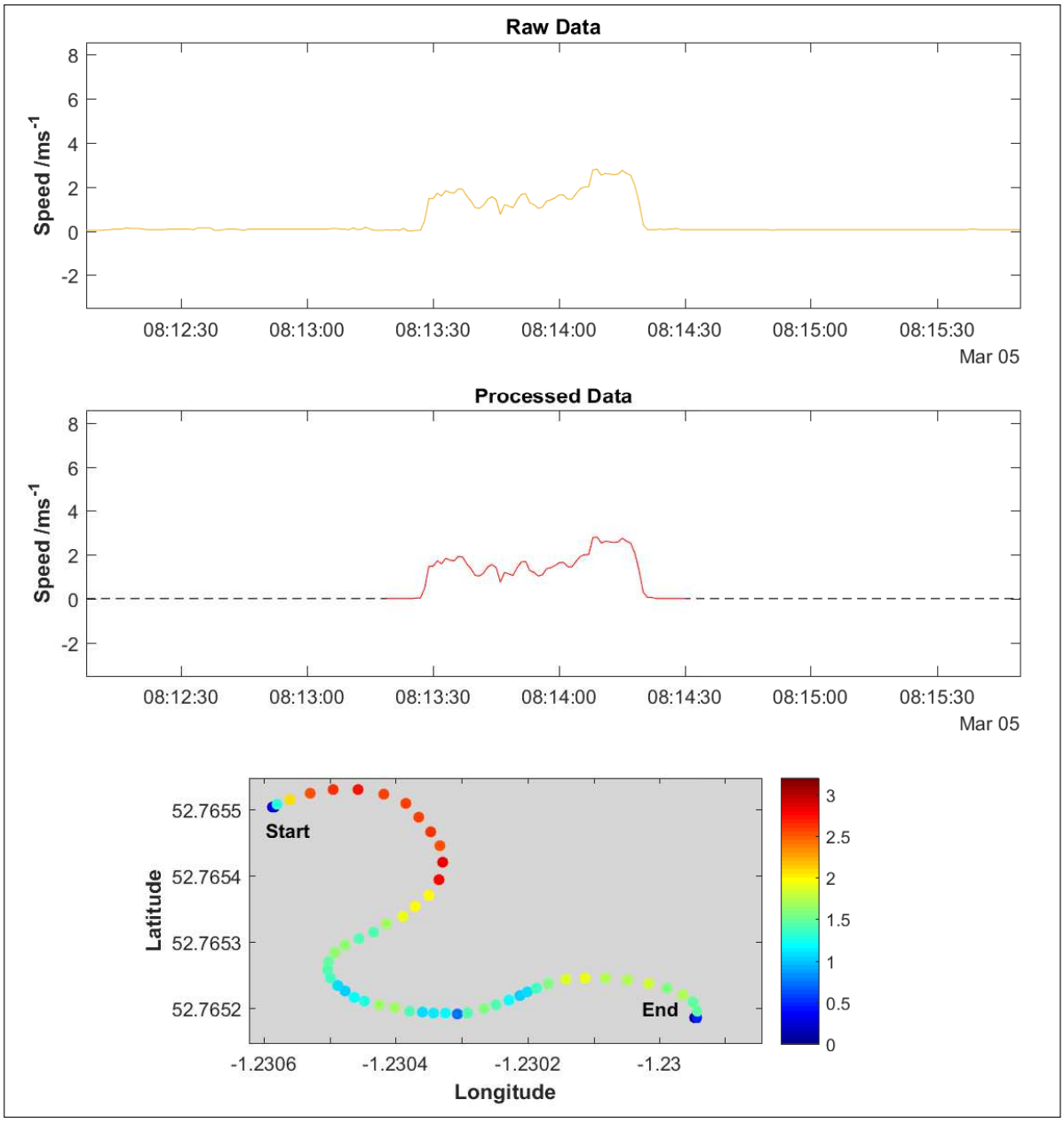

Figure 4.4: Grounds and Gardens False Positive

It can be seen in Figure 4.4 that the trip only lasts for approximately 70 seconds reaching a maximum speed of approximately 3mph. From the bottom plot, it can also be seen that the vehicle does not move appreciably during this time and follows a strange path not related to any roads on the map. Although, it is possible that this is genuine data, it is much more likely that this speed trace is due to drift in the GPS data, possibly due to poor satellite visibility. By analysing the frequency of speed and acceleration in the journeys, any outliers can be easily identified and removed. This technique is known as Speed-Acceleration Frequency Distribution (SAFD) analysis.

4.3.3.1 SAFD Analysis

Analysis of driving patterns can be a very complex subject, due to the fact that there a large number of parameters that can be used to characterise a particular journey. For optimisation of the EMS, the characteristics that most appropriately describe a journey are those associated with the power usage. This includes terms such as the speed and acceleration of the vehicle and the incline of the road.

The most basic approaches simply examine the averages or maxima of specific parameters such as the average speed or peak acceleration. This technique is very good for examining the requirements of the vehicle design and for analysis into whether the vehicle is likely to be able to complete the cycle. Although this will give a quick initial idea of how two drive-cycles compare, there are circumstances where this kind of analysis is too simple. For example, a drive-cycle which contains a lot of stop-start driving may exhibit the same maximum speed and acceleration as one that doesn't, but will more than likely require a much higher average power requirement. Looking at the power requirement directly would introduce a lot more complexity into the situation because this would be dependent on the specification of the vehicle used. Vehicle parameters such as mass and aerodynamics would be introduced into the equation which would make comparisons between drive-cycles logged using different vehicles difficult.

More complicated techniques examine the cumulative frequency distributions [103] of these parameters, which can give a much wider insight into the energy requirements of the duty cycle. Two cycles can be compared with the aim to match the frequency distributions of speed, acceleration and gradient, however considering these variables in isolation can give the wrong impression. For example, an acceleration at high speed or travelling up a hill will require more power than the equivalent acceleration at low speed or on flat ground.

SAFD analysis decouples the speed and acceleration using a two-dimensional discrete state space. Each sample point in the drive-cycle can then be placed in the appropriate bin and the frequency distribution of each speed-acceleration pair can be calculated. This gives a three-dimensional histogram where the sum of all bins is equal to one. The shape of the histogram gives a detailed insight into the driving patterns and the anticipated power requirements without the additional complexity of including vehicle parameters. The technique could also be extended to include other parameters such as the road gradient with little additional complexity although there would be a requirement for additional data to ensure reliability of the distributions.

SAFD analysis can also be used to numerically compare the percentage agreement between two trips using Equation 4.3.1. Note that the divisor of two is required because two SAFD matrices with no overlap would have a total difference of two.

$$\text{Agreement} = 1 - \frac{\Sigma|\text{SAFD}_1 - \text{SAFD}_2|}{2} \tag{4.3.1}$$

Although not commonly used, this technique has been known about for a long time [104] and has been more recently used for analysis of driver behaviour [16] and the development of the ARTEMIS European driving cycle [105]. Using SAFD analysis, any individual journeys which show particularly poor correlation to the total distribution, such as that shown in Figure 4.4 can be identified and removed. However, care must be taken to avoid losing genuine data, and therefore the threshold is set deliberately low. For the purposes of this work, any journeys which show less than 30% agreement have been removed.

4.3.4 Analysis of Identified Trips

The logged data can now be analysed with regard to input into the Markov model generation. It is important that the Markov model accurately represents the typical usage pattern for the Microcab with regards to the expected load on the powertrain. Analysis of the trips identified for the Microcab Mail Delivery route and the Loughborough Grounds & Gardens route are shown in Figure 4.5 and Figure 4.6 respectively. The results for the other duty cycles are shown in Appendix A. The left-hand side of each figure shows histograms of important aspects of the drive-cycles, the right-hand side shows the SAFD analysis of the complete dataset.

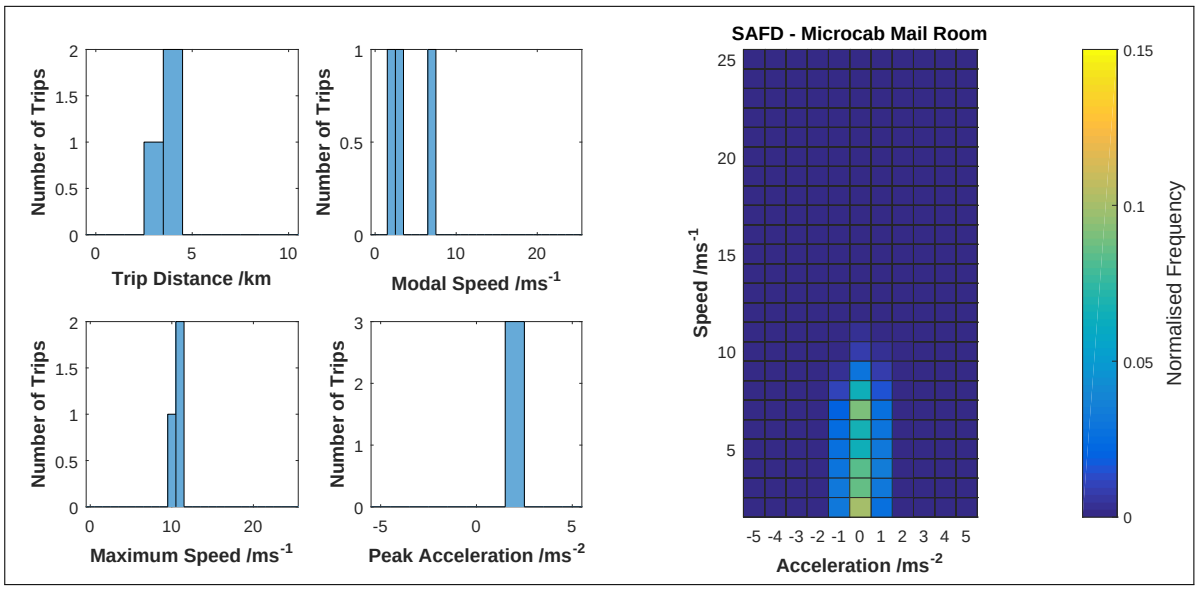

Figure 4.5: Microcab Mail Room Trip Analysis

Unfortunately, due to the fact that limited data are available for the Microcab, only 3 trips were identified for mail delivery, 2 for teaching support and 6 for testing. For the mail delivery and teaching support, the trips varied between 3.5km and 3.9km. The testing data had trips up to 20km although this is not likely representative of normal usage. As a result, the data are not sufficient to describe every circumstance that the vehicle is likely to encounter and therefore not ideal for SDP optimisation.

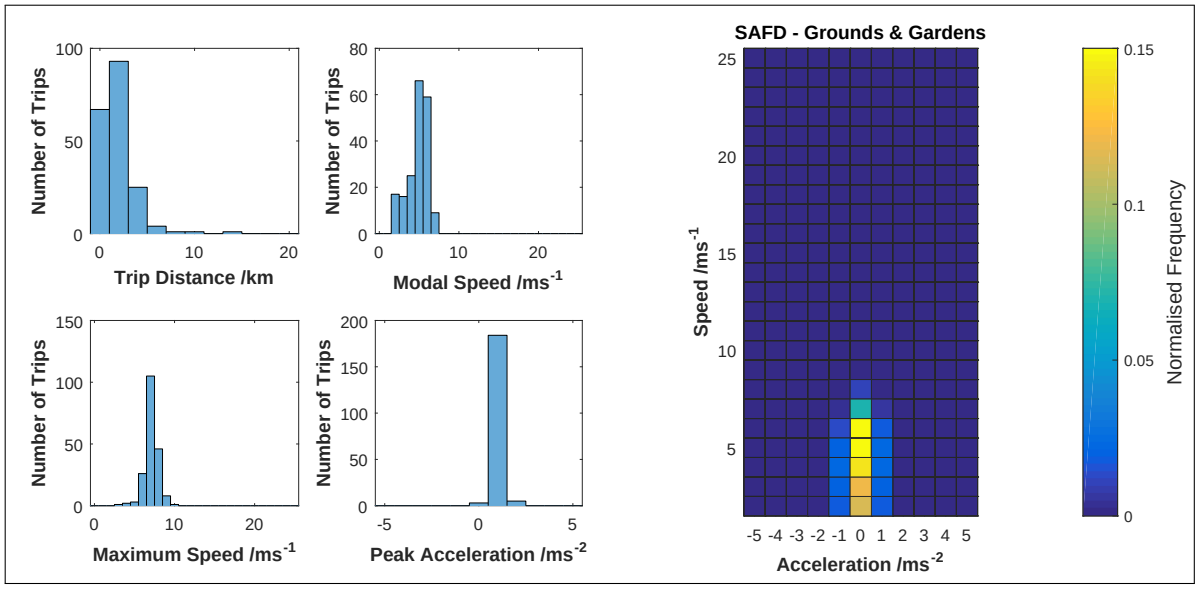

Figure 4.6: Loughborough Grounds & Gardens Trip Analysis

An alternative is to use some of the data collected at Loughborough. Initial inspection identified that the Grounds and Gardens data are the most likely to represent the usage that the Microcab is likely to encounter. It can be seen in the analysis of the trips identified in Figure 4.6 that the trips varied in distance from 1km up to approximately 13km, although the vast majority were below 5km, the modal speeds for these trips varied from 2km/h to 7km/h, the same range as the Microcab, suggesting that similar speed limits were observed by the drivers. It is very important that the Microcab is able to complete the trips in regard to speed and acceleration limits. If the vehicle is unable to achieve the maximum speed or peak acceleration, this will severely affect the optimisation results. The Microcab saw a maximum speed of 11ms^{-1} in normal usage and 15ms^{-1} during testing, a peak acceleration of 2ms^{-2} was reached although 1ms^{-2} peak was more common for the teaching and testing trips. The grounds and gardens vehicles saw a maximum speed of 10ms^{-1} in one trip, however maximum speeds of around 7.5ms^{-1} were more common, and a peak acceleration of 2ms^{-2}, but again 1ms^{-2} was the modal peak acceleration across all trips.

Of the other duty cycles logged at Loughborough, the electrical (Figure A.1) and security (Figure A.3) vehicle trips were least appropriate due to much higher maximum speeds and peak accelerations of more than 3ms^{-2}, which the Microcab would be unable to achieve. Typical trip lengths for the security vehicles were also much too long. This is largely due to the fact that these vehicles often leave campus and drive on local roads, and that security vehicles are occasionally used to patrol the area for extended periods rather than for point to point journeys. The mail room (Figure A.2) and teaching support (Figure A.4) vehicles showed a fairly good correlation with the Microcab data, however maximum speeds of higher than 15ms^{-1} were observed occasionally. Detailed examination of these trips shows that they are most likely due to re-fuelling at a nearby service station which requires driving down a 40mph dual carriageway (Figure 4.7). As the Microcab would be refuelled on campus, this type journey is not required. Therefore, by removing any trips which exceed the 15ms^{-1}, the correlation to the Microcab data can be improved, see Figure 4.8.

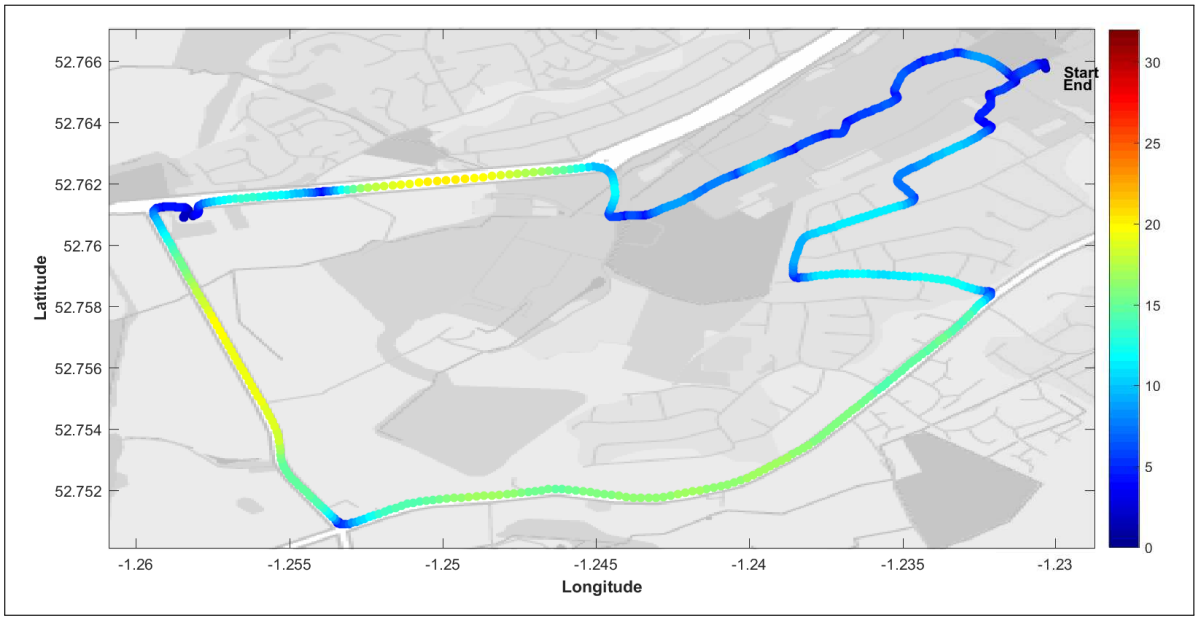

Figure 4.7: Loughborough Mail Room Vehicle Refuelling

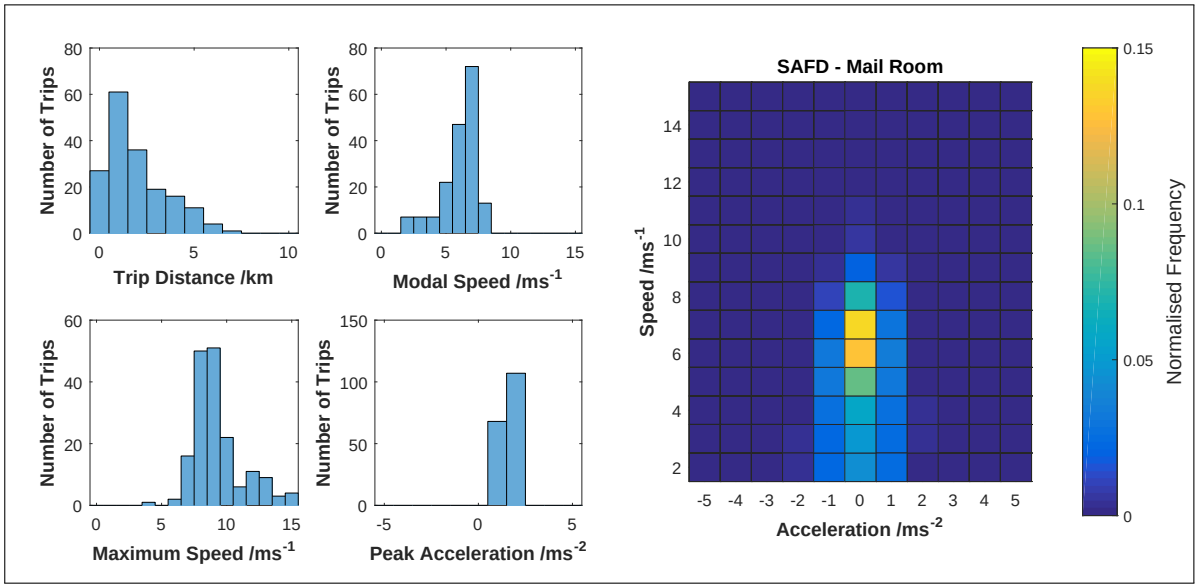

Figure 4.8: Loughborough Mail Room Data with Refuelling Journeys Removed

4.3.4.1 SAFD Comparison

SAFD analysis can be used to compare the agreement of the various usage patterns numerically. The comparisons between each type of driving are shown in Table 4.2. It can be seen that the Loughborough University mail room vehicles most accurately match the real-world Microcab data. As was mentioned in the previous section, these cycles included re-fuelling journeys which exceeded the Microcab's maximum speed. The Grounds and Gardens trips were all achievable by the Microcab, but showed comparatively poor agreement. Therefore, the SAFD agreement has been recalculated without journeys that exceed 15ms^{-1}, the results of which are shown in Table 4.3.

	Electrical	Grounds & Gardens	Mail Room	Security	Teaching Support	Microcab Mail Room	Microcab Teaching Support	Microcab Testing
Electrical	100	47.5	77.1	71.4	86.6	67.8	70.3	81.8
Grounds & Gardens	47.5	100	64.4	72.6	60.3	68.9	56.3	61.1
Mail Room	77.1	64.4	100	78.5	88.2	83	77.7	77.1
Security	71.4	72.6	78.5	100	81.3	77.5	63.3	76.8
Teaching Support	86.6	60.3	88.2	81.3	100	78	74.4	85.8
Microcab Mail Room	67.8	68.9	83	77.5	78	100	66.1	77.5
Microcab Teaching	70.3	56.3	77.7	63.3	74.4	66.1	100	64.8
Microcab Testing	81.8	61.1	77.1	76.8	85.8	77.5	64.8	100

Table 4.2: SAFD Agreement Between Duty Cycle Types (%)

	Electrical	Grounds & Gardens	Mail Room	Security	Teaching Support	Microcab Mail Room	Microcab Teaching Support	Microcab Testing
Electrical	100	48.1	77.1	71	87.3	68	71.2	82
Grounds & Gardens	48.1	100	65.2	76.5	60.3	68.9	56.3	61.1
Mail Room	77.1	65.2	100	80.6	87.7	82.8	78.9	76.5
Security	71	76.5	80.6	100	82.7	79.1	66.9	78
Teaching Support	87.3	60.3	87.7	82.7	100	78	74.4	85.8
Microcab Mail Room	68	68.9	82.8	79.1	78	100	66.1	77.5
Microcab Teaching	71.2	56.3	78.9	66.9	74.4	66.1	100	64.8
Microcab Testing	82	61.1	76.5	78	85.8	77.5	64.8	100

Table 4.3: SAFD Agreement Between Duty Cycle Types with Limited Speed (%)

Removing any trips that exceed $15ms^{-1}$ only affects the journeys made outside campus which, aside from the security data, were mainly for re-fuelling the vehicles. Therefore, this should not affect the validity of the remaining data. Firstly, it can be seen that the grounds and gardens and teaching support agreement is unchanged. This is to be expected as none of the trips exceeded $15ms^{-1}$. The electrical, mail room and security SAFD agreements have changed slightly, but more importantly all included trips now remain below the Microcab's maximum speed. The electrical and security vehicles did still exceed the maximum acceleration limit of the Microcab. Although these journeys could theoretically be filtered out in an equivalent way, there is no real-world justification for this. Therefore, the validity of the data would be compromised and the SAFD would no longer be representative of real-world driving patterns.

4.3.4.2 Summary

The data obtained from the Microcab's usage in Birmingham are the most accurate representation of the duty cycle that the vehicle is likely to see. This is because it represents the actual usage of the vehicles whilst they were used for teaching support and mail delivery on the University of Birmingham campus. Because this is logged data from the actual vehicles, it is unlikely to show any speeds or accelerations that the vehicle is unable to achieve, however it must be noted that the gradient data have been neglected and therefore it is possible that the vehicles could have exceeded their maximum acceleration or speed if assisted by gravity during testing. Unfortunately, only limited data from actual use are available and therefore it may be preferable to use alternative data available from the vehicles logged on Loughborough University campus.

Initial analysis of the data from Loughborough highlighted the Grounds and Gardens vehicles as the most likely candidate for an alternative. This is because these vehicles are similar in performance to the Microcab and rarely leave campus. As a result, the maximum speeds and acceleration seen in the data do not exceed the capability of the Microcab. However, after some simple data processing, SAFD analysis shows a better correlation between the mail room cycle and the Microcab data. Unfortunately, the mail room vehicles occasionally exceeded the capability of the Microcab. On closer inspection of the data, it has been observed that these trips were made in order to re-fuel the vehicle at a nearby service station. This would not be required for the Microcab as hydrogen would be available on campus, and therefore they can be removed without affecting the validity of the recorded data.

4.4 Probability Matrix Generation

The Markov chain calculates the probability distribution of the subsequent acceleration over the next time-step given the current speed and acceleration of the vehicle. An example is shown in Figure 4.9. A discrete-time, discrete-state method will be used with a fixed time-step of 1 second. This is likely to account for the transient dynamics of the system for the purposes of the EMS and has been used by a number of previous authors [31, 64]. The number of states is determined based on the quantity of the data available, but also on the computational time of the SDP algorithm. For the purposes of this work, an acceleration step of 1ms^{-2} has been chosen. This also determines that the speed step size should be 1ms^{-1}. Increasing the number of vehicle states or reducing the time-step would improve the accuracy of the model, however this would significantly increase the computational time required to solve the SDP algorithm. An additional state is added to the Markov Chain to describe the termination of the drive-cycle for shortest-path SDP, see Section 2.3.3.3.

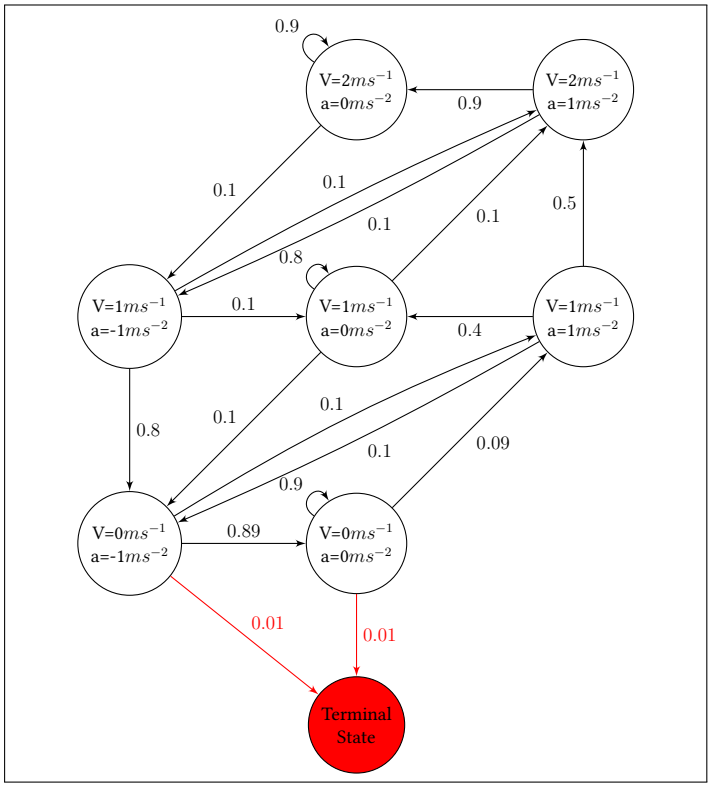

Figure 4.9: Example Markov Chain Drive-cycle Model

4.4.1 Discretizing the Data

There are a number of potential methods for discretizing data for generation of the Markov chain probability matrix. The simplest method is to round the input data to the nearest state. This is the quickest method and generates satisfactory results; however, it does involve the loss of some information. An alternative method is to interpolate the input data between each state and applying a weighting to the states either side of the input data. For example, whereas 2.5ms^{-1} would round to 3ms^{-1}, the interpolation method would apply a

weighting of 0.5 to both 2ms^{-1} and 3ms^{-1}. As a result, more information contained within the input data is retained and the resulting probability matrix should be more accurate. This method is more computationally intensive however. A third alternative is to assume a probability distribution function for the subsequent acceleration. This gives a continuous function allowing for the generation of more states given a limited dataset and may be more accurate in some cases. However, this method requires the accurate prediction of the correct probability distribution for the problem, and still requires sufficient data in order to fit this distribution accurately. A comparison of the methods is shown in Figures 4.10 and 4.11.

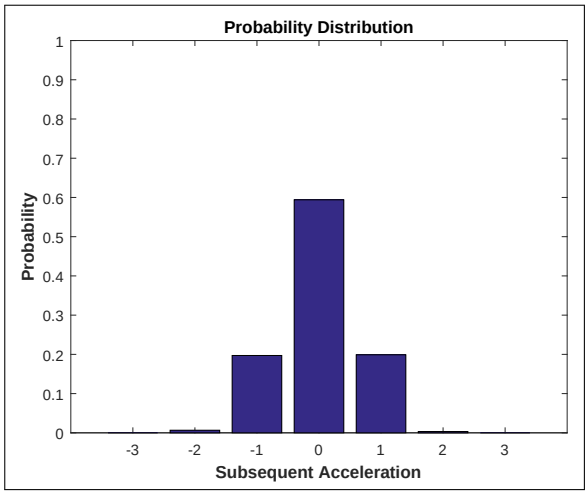

(a) Rounding Method

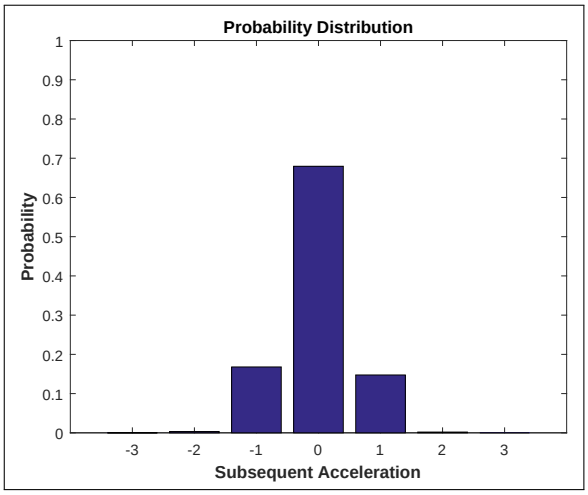

(b) Interpolation Method

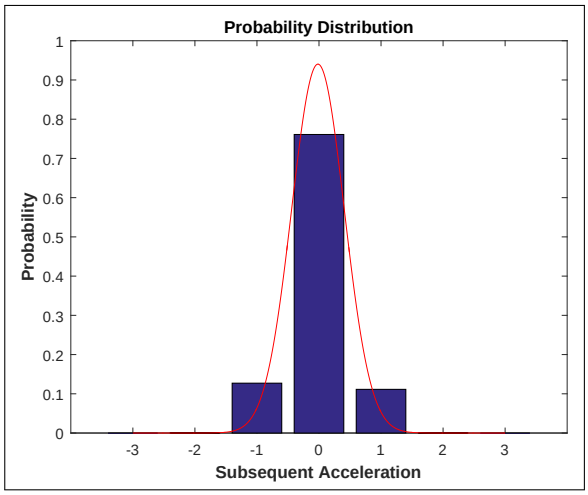

(c) Gaussian Method ($\mu = 0.02, \sigma = 0.42$)

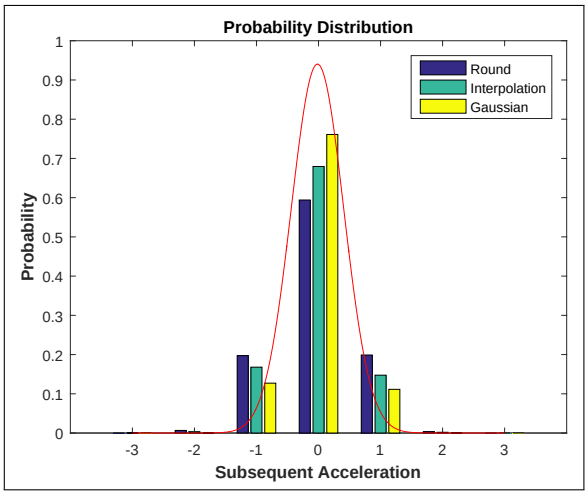

(d) Comparison

Figure 4.10: Discretization at Initial Speed = 5ms^{-1} and Initial Acceleration = 0ms^{-2}

In the mail room data, there are a large number of sample points available at an initial speed of 5ms^{-1} and initial acceleration of 0ms^{-2} and therefore all methods should perform well. It can be seen in Figure 4.10, that the data show a symmetrical distribution of accelerations around a modal value of approximately 0ms^{-2}. The result of the rounding method has the greatest standard deviation, with only 60% of the subsequent accelerations being equal to 0ms^{-2}. It also shows a higher number of accelerations at -2ms^{-2} and 2ms^{-2} compared

to the other two methods. The accuracy of the interpolation method should in theory be higher. This is because no information is lost due to the rounding of the data. The fitted Gaussian distribution for this dataset has a mean of -0.02 and a standard deviation of 0.42. This gives a distribution of subsequent accelerations where almost 80% are equal to 0ms^{-2}. Because of the quantity of data available, the difference to the interpolated method suggests that the Gaussian distribution is not ideal for the fit because otherwise there would be a close correlation between the two.

Considering real-world driving scenarios, this is likely to be true. Under most circumstances, there are a number of discrete decisions that the driver could make. For example, consider a vehicle travelling at a constant speed. The driver may make one of three possible actions; accelerate up to a higher speed, maintain the same speed, or decelerate to a lower speed. Each of these decisions would result in different discrete value of subsequent acceleration, and may each have their own distribution due to continuous variables such as the gradient of the road and the weight of the vehicle. There may even be more than three actions; acceleration due to an increase in speed limit may be quite gentle, but an acceleration due to an overtaking manoeuvre could be much more aggressive.

An alternative dataset is shown in Figure 4.11. In this situation the vehicle is decelerating from a relatively high initial speed. It can be seen that the rounding method shows a very different distribution in this situation compared to the interpolation method and Gaussian methods. This is because many of the values round to either 0ms^{-2} or -2ms^{-2}, even though the weighted values give a much higher probability of a continuation of the -1ms^{-2} deceleration. This shows that the loss of information inherent in rounding the data can have a significant effect on the outcome of the algorithm. It can also be seen that there is a much better correlation between the interpolation method and the Gaussian prediction. This correlates with the previous suggestion because when the vehicle is decelerating, the discrete set of control actions is reduced. In this situation, it is unlikely for the driver to accelerate, leaving only the continuation of the deceleration, or cessation to maintain constant speed. The fact that the rounded values show a lower chance of a -1ms^{-2} deceleration may also confirm this theory.

A final consideration for the Gaussian distribution method is that the distribution probability reduces exponentially at the extremes, but does not reach zero, unlike the rounding and interpolation methods. This is of importance due to how the SDP optimisation accounts for constraints. The SDP cost function applies a very large penalty at the limits of the battery voltage in order to ensure that the optimised result does not exceed them. If there is even a very small probability that these limits will be reached, then this could significantly affect the optimised results.

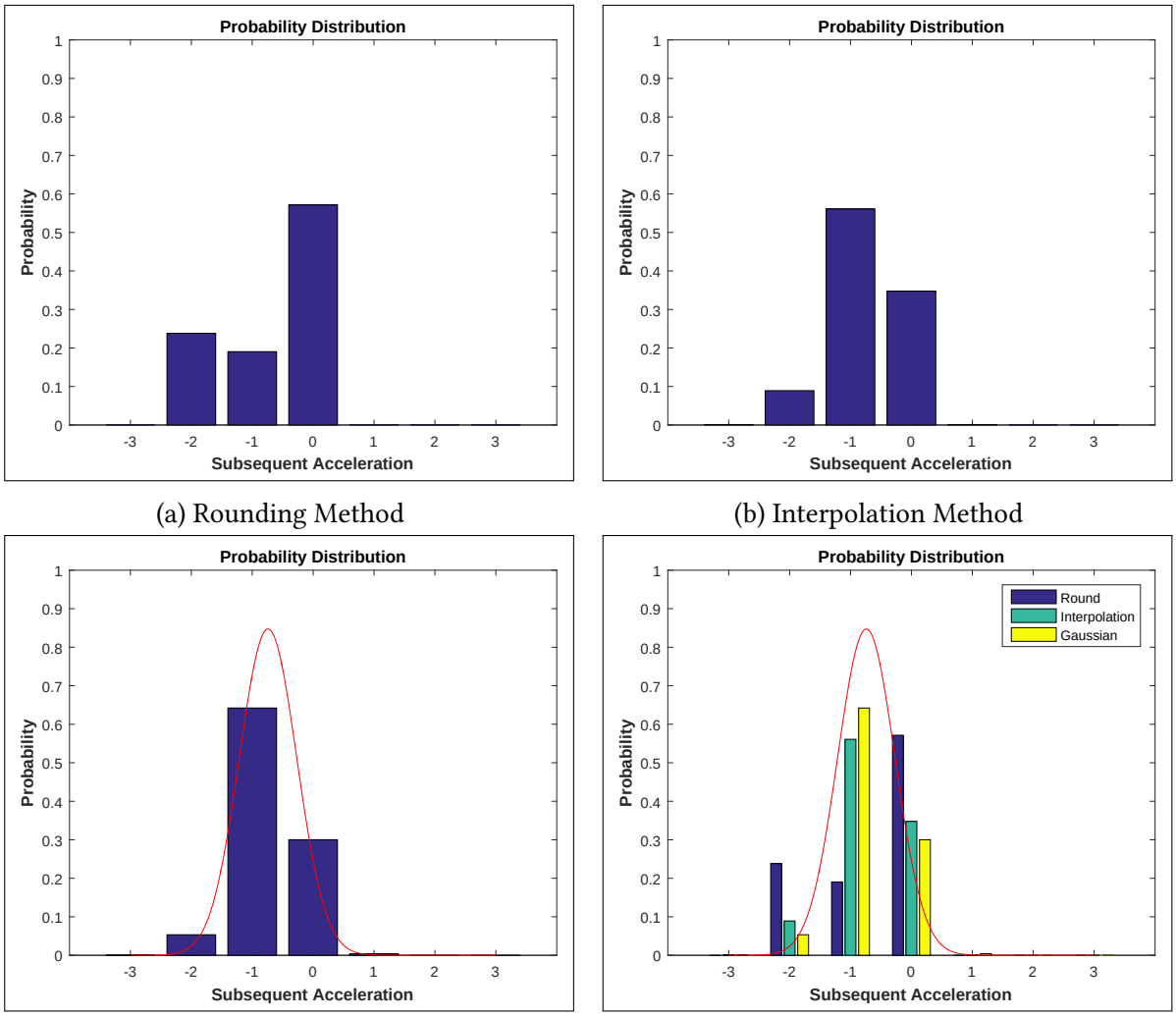

(a) Rounding Method

(b) Interpolation Method

(c) Gaussian Method

(d) Comparison

Figure 4.11: Discretization at Initial Speed = 12ms^{-1} and Initial Acceleration = -1ms^{-2}

4.4.2 Results

Once the data has been discretized, the algorithm loops through each possible state and calculates the probability of each subsequent acceleration using one of the algorithms above. A sample of the transitional probability matrix is shown in Figure 4.12. Each column of the grid shown should always sum to 100%. It can be seen that, in general, at $5ms^{-1}$ the vehicle is most likely to continue on its previous trajectory. If the previous acceleration was $0ms^{-2}$, it is most likely to continue to be $0ms^{-2}$. Gentle acceleration and all deceleration follow this trend, however high acceleration shows a tendency to begin to reduce. If the previous acceleration was $2ms^{-2}$, it is most likely to continue at $1ms^{-2}$ for example.

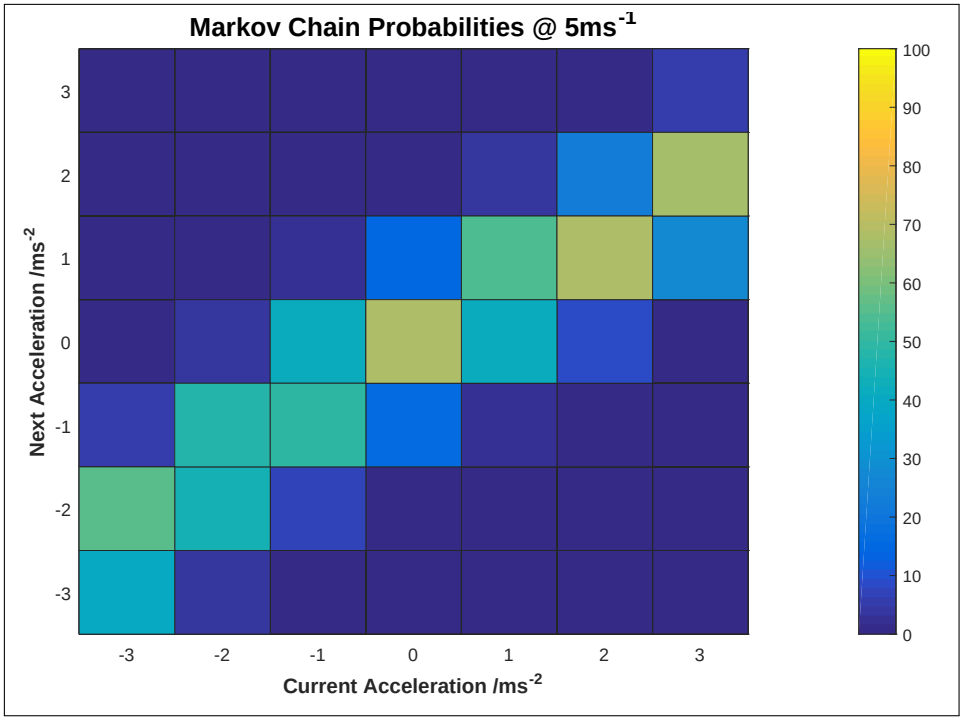

Figure 4.12: State Transition Probability Matrix - Loughborough Mail Room Cycle ($5ms^{-1}$)

There are states where there was no data available. This is because the vehicle did not enter the state at any point in the logged data. This does not pose a problem for the rounding method because if the state was not entered in the data, then the transitional probability of transitioning to it will be zero. As a result, it will not affect the optimisation in any way. For the interpolation and Gaussian discretization methods, however, this can cause issues. It may be possible for the transitional probability of entering a state that was not reached in the data to be greater than zero, although it will most likely be a very small probability. For the Gaussian distribution model, this is due to the fact that the probability reduces away from the mean value, but never reaches 0. For the interpolation method, this could occur under certain circumstances, such as a previous speed of $2.4ms^{-1}$ and an acceleration of $1.3ms^{-2}$. In this situation, there is a potential initial speed of either $2ms^{-1}$ or $3ms^{-1}$, and a potential acceleration of either $1ms^{-2}$ or $2ms^{-2}$. Therefore, for an initial speed of $3ms^{-1}$, there will be a small probability of acceleration of $2ms^{-2}$ (up to $5ms^{-1}$) even if $5ms^{-1}$ was never reached in the data. Modifying the algorithm to be based around the subsequent speed rather than acceleration is possible; however, this results in a similar issue with the subsequent acceleration.

This situation can pose a significant problem for EMS optimisation when using the interpolation or Gaussian methods. If there is a probability of transitioning into a state where no data is available, then the probability of transitioning out of this subsequent state will be undefined. This means that it is not possible to continue the stochastic model after this point and the optimisation will fail. Therefore, it is necessary to estimate what will happen in this situation.

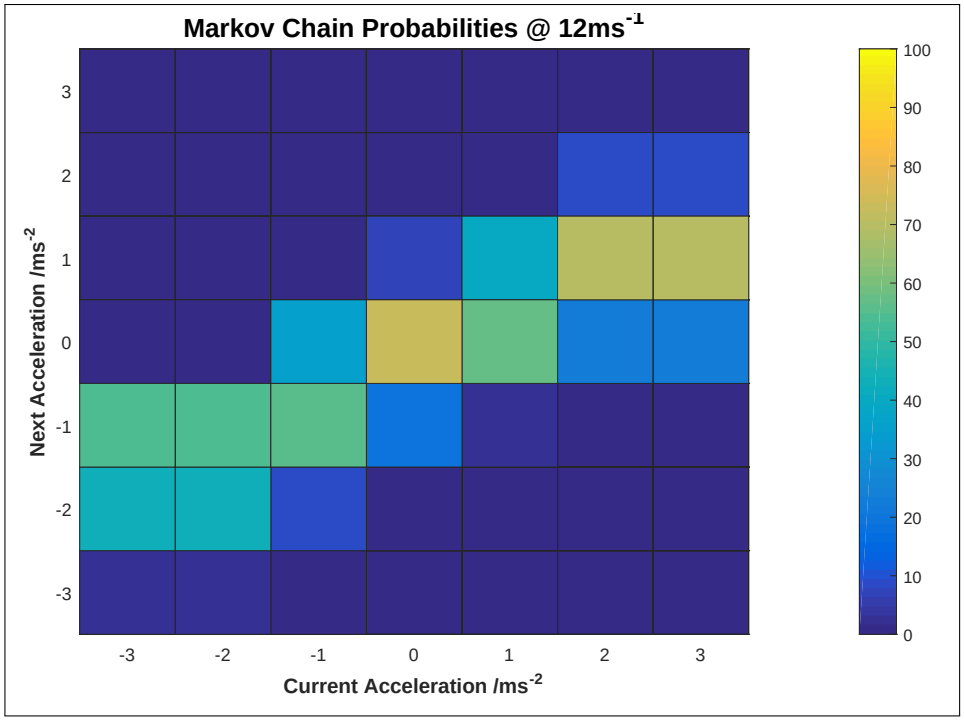

Figure 4.13: State Transition Probability Matrix - Loughborough Mail Room Cycle ($12ms^{-1}$)

In order to alleviate this problem, the transitional probabilities for states which were not reached can be extrapolated from the data available. It has been found that the most effective method is to interpolate the data where possible and use result of the nearest available previous acceleration when extrapolation is required. This results in an overall transitional probability as seen in Figure 4.13. In this case, there was no data available for an initial speed of $12ms^{-1}$ and an initial acceleration of $3ms^{-2}$. Therefore, the transitional probabilities for an acceleration of $2ms^{-2}$ have been used. It can be seen that the tendency is for the subsequent acceleration to reduce to $1ms^{-2}$, effectively moving the state of the vehicle away from its limits and therefore reducing the effect of the problem.

Estimating the likely response of the vehicle in undefined states also helps to improve the robustness of the controller. In an ideal situation, the logged data used to generate the Markov model will perfectly define the likely response of the vehicle from every possible initial state. However, in reality, this is very difficult to achieve and would require several hundreds, if not thousands of hours of logged data. As more data are obtained, the likelihood of this occurring becomes smaller; however, there is always a small possibility that the vehicle could enter a state which was not encountered during testing. Given a reasonable estimation the likely response of the vehicle, the resultant strategy should make a sensible decision.

4.4.3 Terminal State

Shortest Path Stochastic Dynamic Programming (SP-SDP) uses a terminal state to define the end of a journey in order to avoid using a discount factor. This has a number of benefits because it allows the optimisation to be aware of when and how likely the drive-cycle is to finish and allows additional costs to be applied to the end of the cycle such as based the terminal battery State of Charge (SoC). For a Charge-Depleting (CD) algorithm, this allows the battery depletion to be managed effectively over the duty cycle and therefore maximise the benefits of being able to charge the vehicle whilst it is parked. For a Charge-Sustaining (CS) algorithm, it allows more fluctuation in the SoC during the cycle, without losing the ability to constrain the final SoC.

The probability of the drive-cycle ending can be calculated in a similar manner to the transitions between other states. The logged data have already been separated into individual trips during the data processing, see Section 4.3.2. Therefore, the probability of the trip finishing can be calculated using the number of times each state was the final state divided by the number of times the state was entered in total.

The definition of the trips in Section 4.3.2 means that the terminal state can only be entered when the vehicle is stationary. As a result, the final acceleration can only be zero or negative. The probability of transitioning to the terminal state for the Loughborough mail room duty cycle can be seen in Figure 4.14. It can be seen that there is a very low overall probability of approximately 0.0012 when the previous acceleration was 0ms^{-2} and no possibility at any other time. The transition to the terminal state does not form part of the main probability matrix in order to allow testing of both SP-SDP and infinite horizon algorithms.

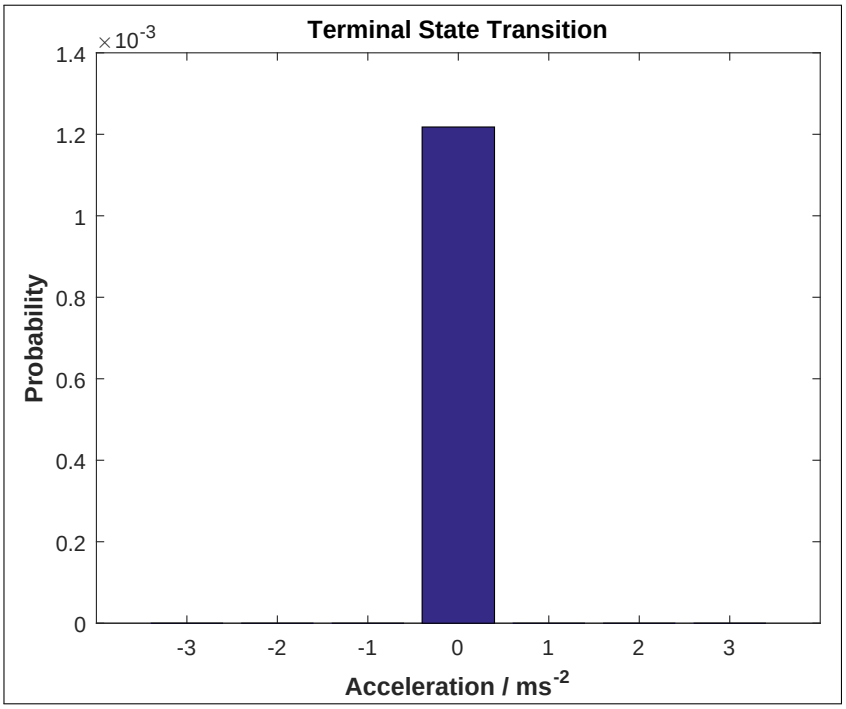

Figure 4.14: Terminal State Transition Probability - Loughborough Mail Room Cycle

4.5 Validation

Some validation of the Markov chain can be achieved using the Monte Carlo method. The vehicle is initialised at zero speed and acceleration and then the transition to the next state is randomly chosen based on the probabilities in the Markov Chain. This process continues until the vehicle transitions into the terminal state. This will generate a random trip based on the transitional probabilities contained in the Markov Chain, which can then be compared to the original logged data, see Figure 4.15. By running a large number of such simulations, the distribution of various parameters can be compared and SAFD analysis can be used to calculate a numerical assessment of correlation. A high correlation will show that the Markov chain effectively models the behaviour of the driver and the vehicle for the assessed duty cycle.

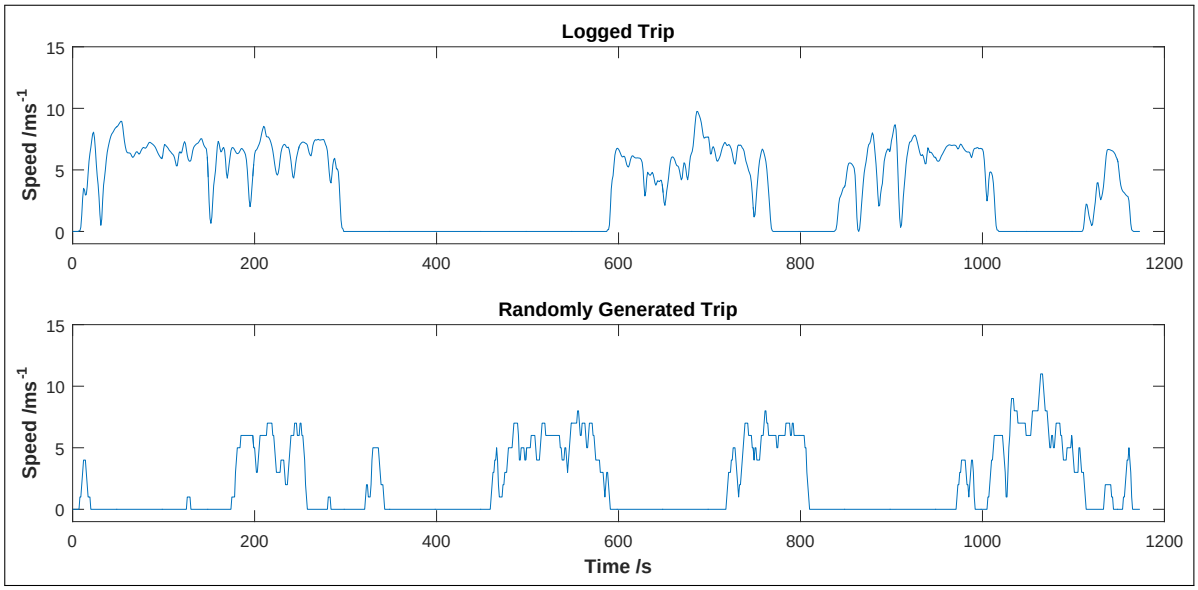

Figure 4.15: Randomly Generated Drive-cycle Comparison

Figure 4.15 shows a comparison between a logged trip and one of a similar length generated using the Markov Chain. It can be seen that the trip generated using the Markov Chain is significantly different to that from the logged data although the generalised behaviour of the vehicle is quite similar. Both trips show similar top speeds of 10ms^{-1} and 11ms^{-1}, and are characterised by a number of journeys at approximately 7ms^{-1} average speed separated by periods where the vehicle is stationary. One significant difference, however, is that the speeds in the logged data are continuous whereas in the randomly generated trip they are not. This is due to the discretization of the data for development of the Markov Chain.

The Monte Carlo method has been used to randomly generate 10,000 trips for a number of the duty cycles logged. This allows the distribution of journey lengths, modal speeds, maximum speeds and peak accelerations to be compared to that of the original logged data. The results of the Loughborough University mail room duty cycle using the rounding method are shown in Figure 4.16. It can be seen that the distribution of journey lengths are quite similar, although the Markov model has produced a number of trips which are longer in length than the original data. As a result, a lower proportion of trips are between 1 and 2km than in the logged data, but this is still the most common length. The peak modal speeds are identical, although the logged data show a greater variation either side of this peak. Both the logged data and randomly generated cycles have a modal maximum speed of approximately 9ms^{-1}, although the proportion of trips with a maximum speed of between 10 and 14ms^{-1} is higher in the randomly generated cycles. The logged data show a peak acceleration of 1ms^{-2} in 40% of the journeys and 2ms^{-2} in the rest. In comparison only 10% of the randomly generated cycles have a peak acceleration of 1ms^{-1}, with approximately 90% reaching 2ms^{-1}. This is perhaps due to the increase in average journey length, meaning that more trips are likely to hit higher maximum speeds.

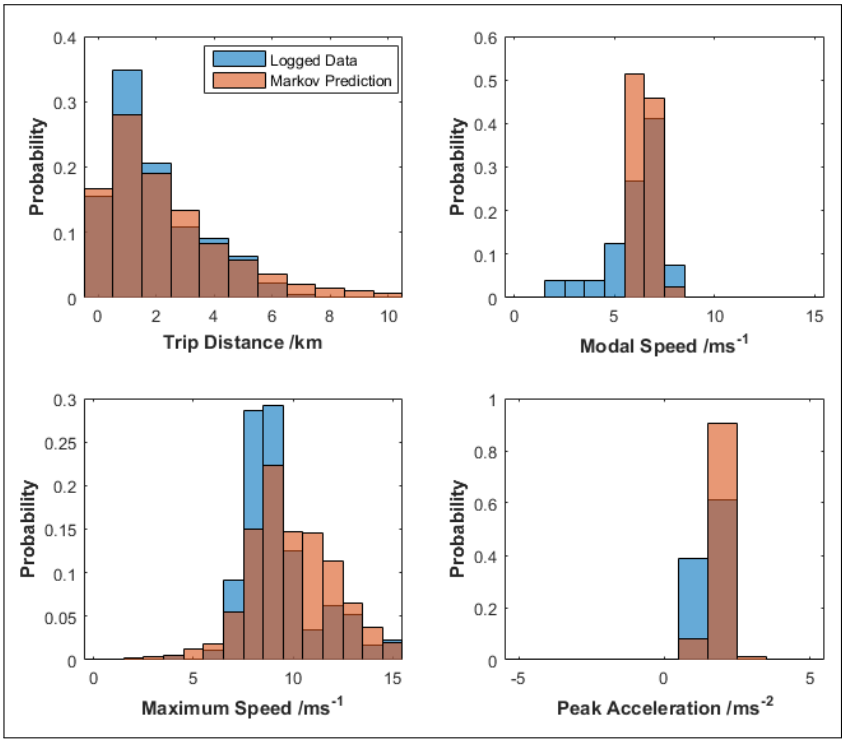

Figure 4.16: Statistical Comparison for Loughborough Mail Room Cycle using Rounding Discretization Method

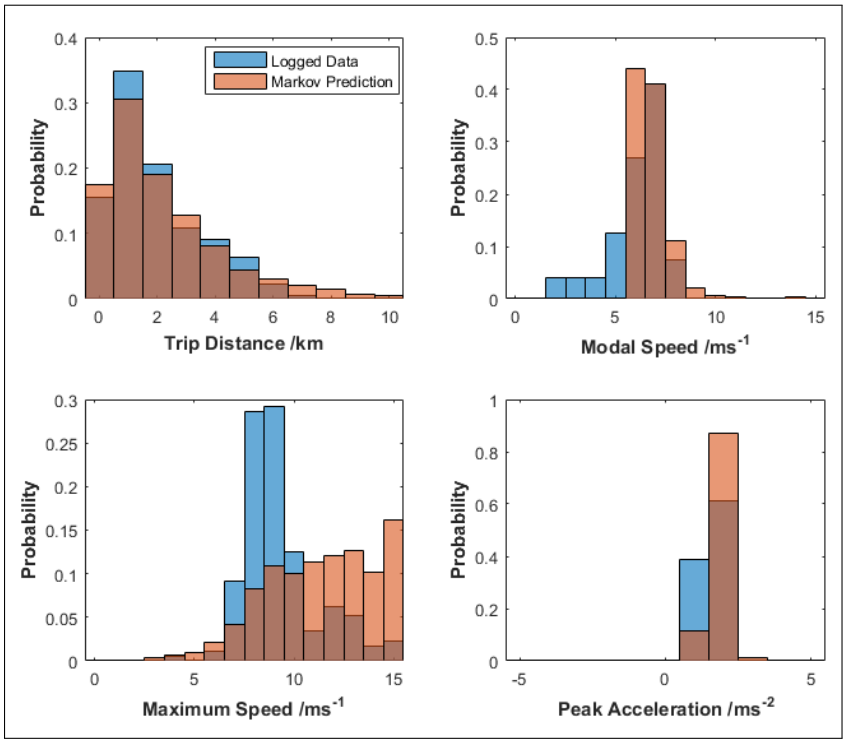

Figure 4.17: Statistical Comparison for Loughborough Mail Room Cycle using Interpolation Discretization Method

In comparison, the results for the same data using the interpolation discretization method are shown in Figure 4.17. In this case, the estimation of journey length and modal speed is slightly improved and the peak acceleration seen is identical to the rounding method. However, it is clear that the interpolation method tends to overestimate the maximum speed. This is likely due to the issue mentioned in Section 4.4.2, leading to a higher usage of extrapolated data. In the Monte Carlo simulation, as in the SDP optimisation, any errors will be cumulative. Another point to note is that the interpolation method may result in impossible accelerations under some circumstances. For example, if the maximum acceleration of the vehicle was 2.1ms^{-2} at a certain speed, the rounding method would give a maximum acceleration of 2ms^{-2}, however the interpolation method would result in some weighting being given to 2ms^{-2} and some to 3ms^{-2}. Although it is possible to have a similar effect for the rounding method at 2.6ms^{-2}, for example, this would occur as often, and would result in a lower over-estimation of the maximum acceleration by the model. Therefore, these results suggest that the interpolation method is not adequate to substitute for higher resolution grid spacing.

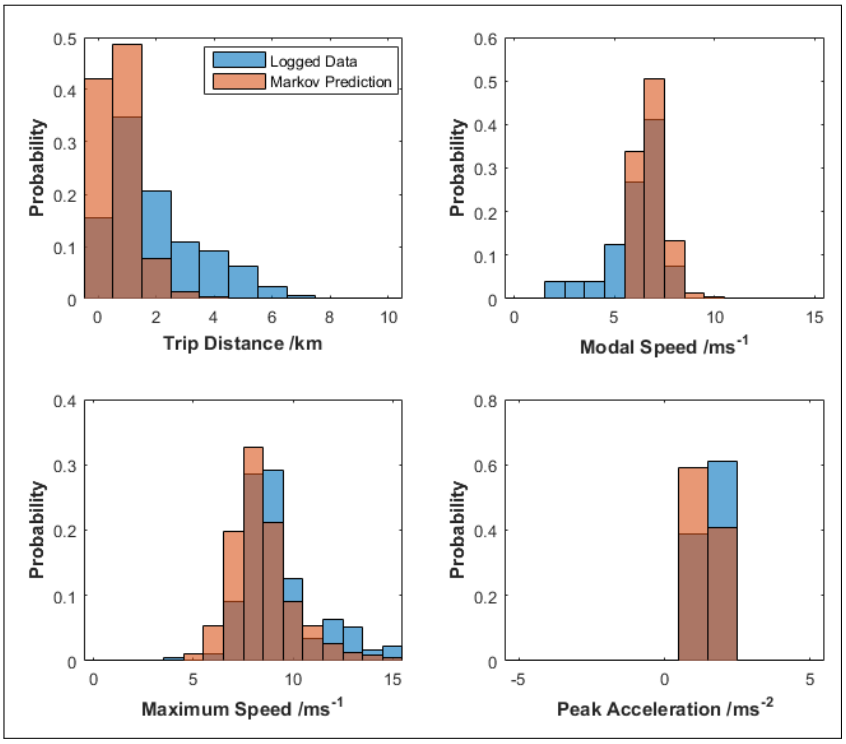

Figure 4.18: Statistical Comparison for Loughborough Mail Room Cycle using Gaussian Discretization Method

Finally, the results for the Gaussian discretization method are shown in Figure 4.18. It can be seen that the maximum speeds reached in the generated trips are much lower than for the other two methods and closer to the original data, although they are approximately $1ms^{-1}$ lower than the original data on average. The estimation of modal speed slightly different, with the approximately 50% of cycles averaging $7ms^{-1}$, and only approximately 30% having a modal speed of $6ms^{-1}$, which is again closer to the original data than the other two methods, although no trips had a modal speed of below $6ms^{-1}$ as was seen in the logged data. The peak acceleration in approximately 60% of the trips was $1ms^{-2}$ and in the rest, it was $2ms^{-2}$. This is the opposite of the distribution seen in the original data and is subject to approximately the same magnitude of error when compared to the other methods. The journey length, however, is vastly underestimated by the Gaussian distribution method with approximately 90% of trips lasting less than 2km and no trips exceeding 4km.

4.5.1 SAFD Analysis

SAFD analysis can be used to numerically compare the randomly generated trips to the original data. This can then be used to examine the performance of the various discretization methods. The Markov chains generated have been used to generate 10,000 random trips and the SAFD has been calculated on each overall dataset. The agreement of each result to the original data has been calculated and is shown in Table 4.4.

	Electrical	Grounds & Gardens	Mail Room	Security	Teaching Support	Microcab Mail Room	Microcab Teaching Support	Microcab Testing
Rounding	97.5	98.2	97.6	98.2	98.0	97.0	90.9	97.5
Interpolation	87.5	83.5	89.1	88.5	90.0	91.2	77.5	86.9
Gaussian	86.9	69.1	84.1	83.0	86.9	86.8	65.8	76.6

Table 4.4: SAFD Agreement for Each Discretization Method (%)

It can be seen in Table 4.4 that the agreement of the cycles generated using the rounding method is very high, with all but the Microcab teaching support cycle having an agreement of above 97%. Duty cycles for which there were more data available, such as for the Loughborough University security and grounds and gardens vehicles, correlated particularly well, although the data appears to be sufficient to accurately model most of the cycles. The agreement of the Microcab teaching support is likely lower due to the fact that very little data were available for this cycle, just one hour and only two trips identified. The interpolation and Gaussian distribution methods also performed relatively well in most circumstances, although the Gaussian method showed considerable variability between 69.1% and 86.9% (neglecting the Microcab teaching cycle). This suggests that this method is not very reliable, and therefore care should be taken to validate the results. Neither method improved on the results of the rounding discretization method however.

Considering both the SAFD agreement and the statistical analysis, the rounding method is the most robust and produces results which correlate with the original data very well despite the inherent loss of information associated with rounding. Although the interpolation method should in theory improve retain more raw information, it has been found that small numerical inconsistencies result as part of the interpolation. These inconsistencies accumulate when the Markov chain is simulated, resulting in significant differences in the generated cycles when compared to the logged data.

It has also been found that the distribution of subsequent acceleration fits a Gaussian distribution under a number of circumstances, especially mid-range speed and low absolute acceleration. However, a single Gaussian distribution at each speed/acceleration pair is insufficient to fully describe every situation. This is especially apparent when the vehicle is stationary, because the modal subsequent acceleration is $0 ms^{-2}$, but further deceleration is impossible. As a result, a different distribution may correlate better with the logged data.

4.6 Conclusions

Overall, the results of the Markov chain using the rounding function compare well to the original data sets, with an agreement of above 97% for all of the logged duty cycles aside from the Microcab teaching support data. The interpolation method also performed reasonably well with agreements of around 90% for many of the duty cycles; however, it did exhibit a tendency to overestimate the maximum speed of the vehicle. Fitting the data to a Gaussian distribution worked reasonably well for a single acceleration, however the Gaussian distribution does not fully describe the probability distribution under all circumstances and leads to much larger errors in the simulation of the Markov model using Monte Carlo simulation due to accumulation. It is expected that the SDP optimisation would be subject to a similar problem. Although the results of the rounding method correlate well with the original data, there are a number of ways the accuracy and reliability of the Markov chain could be improved.

For generation of a Markov chain using historical data there is no substitute for large quantities of high quality data. The quality of the statistical analysis relies heavily on the inclusion of every possible situation to be included in the raw data, and also that the frequency of each subsequent acceleration is appropriately weighted. As the set of input data grows, this becomes more likely and therefore the accuracy of the Markov chain is likely to improve. A larger volume of data allows for more states, by including additional parameters such as the road gradient, or by reducing the grid size of speed and acceleration.

The rounding of the data inevitably results in a loss of information, however attempts to avoid this loss of information by using alternative methods such as interpolation and Gaussian frequency distributions have shown little value due to a reduction in the reliability of the data. Although the effect on a single acceleration is very low, these errors are cumulative as the Markov chain is simulated or the SDP optimisation process takes place and therefore can significantly detriment the final result.

There is room for improvement in the Gaussian distribution method, for example by using multiple overlapping distributions to account for acceleration, steady speed and deceleration. However, this would be non-trivial and require a significantly larger dataset in order to have confidence in the results. As the main benefit of using this method is to reduce the required volume of input data, the value of performing this would be questionable. The Gaussian distribution also has a number of other drawbacks. Firstly, the distribution never reaches zero. As a result, there is always the possibility of an acceleration that the vehicle is incapable of achieving. Although these probabilities are very low, this can lead to significant errors during optimisation if large costs are used to constrain the optimisation. Another issue is that the Gaussian distribution is symmetrical. This works well while the vehicle is moving at low and medium speeds and fits the data well. However, when the vehicle is static and therefore cannot decelerate, the modal subsequent acceleration is often to remain static. As a result, an asymmetrical probability distribution function would fit the data better. This is also the case when the vehicle is close to its maximum speed although the issue is less pronounced.

It has also been found that the 1Hz logging frequency is not ideal for producing a 1Hz model. GPS data are subject to a gradual drift over time and also poor signal can lead to the potential for the occasional incorrect reading. As a result, the raw data requires filtering to reduce the effect of anomalous readings, which inevitably leads to a loss of fidelity of

the data. Logging the location at a higher frequency, such as 10Hz, as used during the Microcab testing data, leads to an increase in the accuracy of the data when filtered and analysed at 1Hz. A similar result could be achieved by using additional sensors on board the vehicle such as an accelerometer. The data from the accelerometer can be combined with the GPS data using a Kalman filter to improve the accuracy of speed, acceleration and gradient measurement.

An additional consideration that was neglected in this analysis is the gradient of the road. This has a significant effect on the power demand of the drive motor and as a result may affect the acceleration of the vehicle. This can introduce significant errors into the optimisation process if the vehicle was assisted by gravity when accelerating especially if the vehicle is not normally capable of this acceleration on flat ground. Unfortunately, the accuracy of GPS altitude data are not sufficient for this purpose, however it may be possible to include information about the gradient based on the vehicles location and map data. If map data are unavailable, additional sensors such as an accelerometer or barometer could be used. The inclusion of gradient data introduces an additional parameter into the model and would therefore require a much larger dataset for statistical analysis.

Finally, all of the data logging collected for this analysis was collected over a period of a few months, and for each usage category, the data collection lasted approximately 1 month. As a result, the long-term usage, including rare trips, is unlikely to be accounted for, and there is also the possibility of seasonal variations. For example, on a university campus, there may be a difference in the usage of the vehicles during term time as opposed to the holidays, and for the Grounds and Gardens vehicles, there could also be significant differences between summer and winter. As a result, there could be an improvement in the accuracy of the data if the collection took place over a longer time period of up to one year.

4.6.1 Suitability for EMS Development

The analysis has been performed specifically with the development of an EMS using SDP in mind. Therefore, the parameters that have been chosen have been picked to best suit this purpose and the resulting Markov model is appropriate for EMS development, especially considering the data that were available and the computational expense of SDP optimisation. For example, from examination of the data and experimentation of the input parameters it has been found that increasing the resolution of the model to 1ms^{-1} and 1ms^{-2} steps to 0.2ms^{-1} and 0.2ms^{-2} would be possible given the quantity of data available. This allows the model to more accurately reproduce the drive-cycles seen during the data collection period, however this would significantly increase (25x) the number of calculations required for SDP optimisation. Therefore, a 1ms^{-1} step has been chosen as a good compromise between accuracy and computational expense.

In an ideal world, one possible improvement would be to include the gradient of the road. As already mentioned, the gradient could significantly affect the power requirements of the vehicle and therefore should be accounted for by the EMS. Unfortunately, introducing an extra parameter to describe the state of the vehicle would require significantly more data and the availability of reliable altitude information. It would also increase the computation time required to solve the SDP optimisation. However, this issue could be avoided by using a single parameter such as the tractive effort or motor power instead of the combination of two states, the acceleration and road gradient. This method would also serve to account

for changes in the mass of the vehicle. One downside of performing this would be that the Markov chain would then be vehicle specific rather than universally suitable for any vehicle over this type of duty cycle.

4.6.2 Suitability for Other Practical Uses

As mentioned at the beginning of this chapter, a Markov chain model has a number of other potential uses outside of EMS development. The Markov model allows estimation of the likely power usage and transient loading when used in combination with a model of the vehicle. Therefore, the model could be used for a variety of design exercises ranging from early design phase sizing exercises all the way up to legislative testing. For this type of usage, the model could be improved by increasing the resolution of the discretisation with respect to both speed and time because it would not have the same requirements for computational efficiency. Given increased resolution, it may also be desirable to improve the accuracy of the data logging by the inclusion of additional sensors such as a barometer for altitude and accelerometers for improving the accuracy of the GPS speed estimation using sensor fusion techniques. This would also likely require a larger volume of data to be collected. For these purposes, it would also be beneficial to extend the data collection period to include seasonal variations in vehicle usage and in order to capture infrequent journeys.

Chapter 5

Controller Development

In this chapter, the design and development of the Energy Management Strategy (EMS) for the Microcab H4 is described in detail. This project uses a Stochastic Dynamic Programming (SDP) optimised controller based on real-world data due to its near-optimal solution of the EMS problem and ease of implementation in real-time for on-board control.

SDP works by minimising the long-term result of a Markov Decision Process (MDP) using a cost function which defines undesirable performance characteristics of the controller. This chapter will begin by formally defining the MDP, including the development of a novel cost function which includes not only the fuel consumption of the vehicle, but also the degradation of the fuel cell in a quantitative sense. Once the problem has been defined, the procedure for solving it using SDP is described in detail, including the exact method and justification of the parameter selection used for the optimisation. The chapter concludes with a brief examination of a typical optimal policy obtained using SDP.

5.1 Introduction

The Energy Management Strategy (EMS) is directly responsible for managing the State of Charge (SoC) of the battery in the Microcab in order to allow the vehicle to take advantage of the hybrid powertrain, and as a result, the actions that are taken by the strategy will have a significant effect on the performance of the vehicle. In particular, the fuel consumption, component degradation and drive-ability are highly dependent of the operating conditions that are chosen by the EMS controller.

There are a number of approaches to the development of an effective EMS, which have been covered in detail as part of the literature review (see Chapter 2). These range from simple heuristic controllers to complex strategies based on machine learning techniques, however this work will focus on optimisation using Stochastic Dynamic Programming (SDP). SDP is by far the most popular technique in recent years due to its near-optimal performance and the ease of implementation of the solution on board the vehicle.

The optimisation of the EMS controller using SDP involves finding the action which minimises the total future anticipated cost incurred for every initial vehicle state. SDP uses a statistical model of the duty cycle and vehicle response in order to estimate the future cost over a set horizon. This may be fixed (finite horizon), infinite (infinite horizon) or determined based on model output (terminal state). This means that although the solution may not be optimal for particular journey, the solution is the optimal time-invariant control policy for the set of journeys used to define the probabilistic duty cycle model. As a result, the policy is entirely causal, depending only on the current state of the vehicle and hence relatively trivial to implement on a real-time controller.

The steps required to develop the controller are shown in Figure 5.1. In order to produce the optimised controller, the first step is to produce a statistical model of the duty cycle. This model describes the probability distribution of the vehicle transitioning from its current state to any other state given each control action. Part of this model (which is independent of the vehicle and control action) has already been created in the form of the Markov chain model developed in Chapter 4. This model can be extended to include the battery SoC and the current EMS power demand which will serve as additional control inputs for the strategy. Concurrently with this, the vehicle model developed in Chapter 3 is used to calculate the cost of each transition. The statistical model and the associated transitional costs can be expressed as two matrices, which form the foundation of the MDP problem.

SDP works to solve this problem by calculating the both the instantaneous cost of performing each action from the current state and the future anticipated cost given the new state of the vehicle and the current control policy. This is an iterative process which is performed in two steps. In the first step, the anticipated costs are calculated given the current control policy (policy evaluation). In the second step, the policy is improved by choosing the set of actions which will minimise the overall costs (policy improvement). This process is iterated until either the cost and/or the policy converges.

The output from the SDP algorithm is therefore the policy which minimises the cost function. This can be applied to the controller as simply a lookup table of control actions based on the inputs to the original MDP problem, see Figure 5.2.

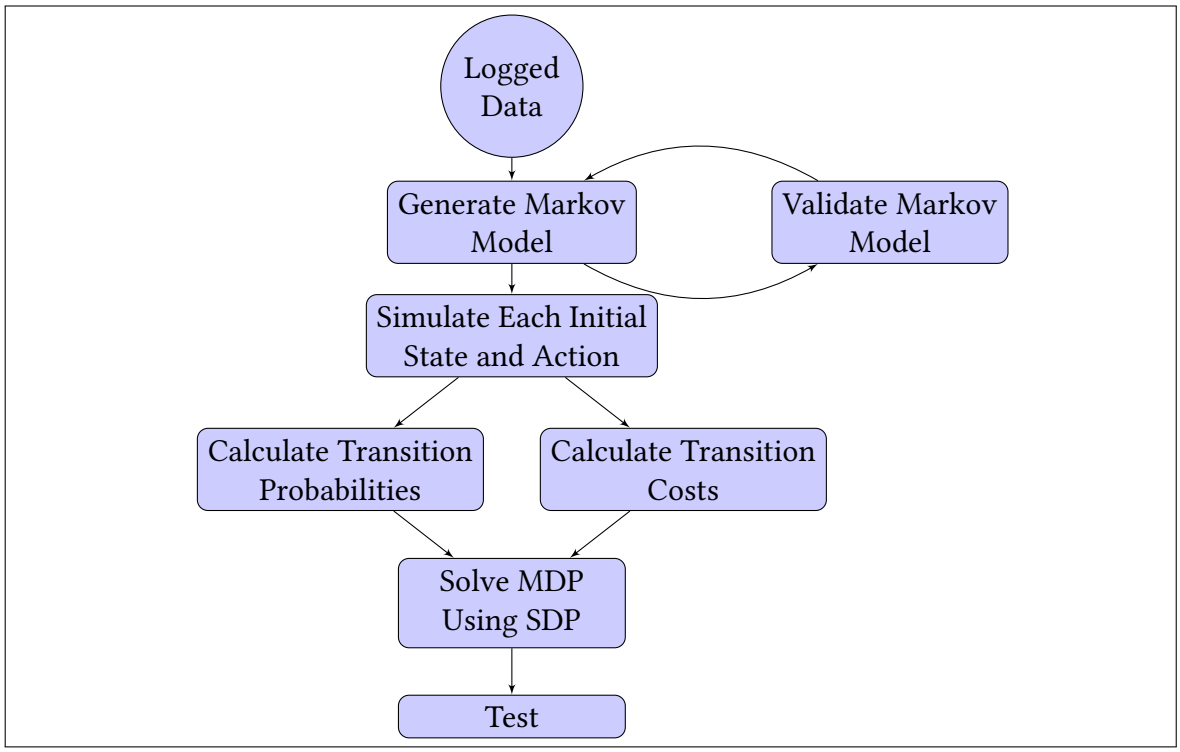

Figure 5.1: Flowchart of the procedure used to generate the real-time controller

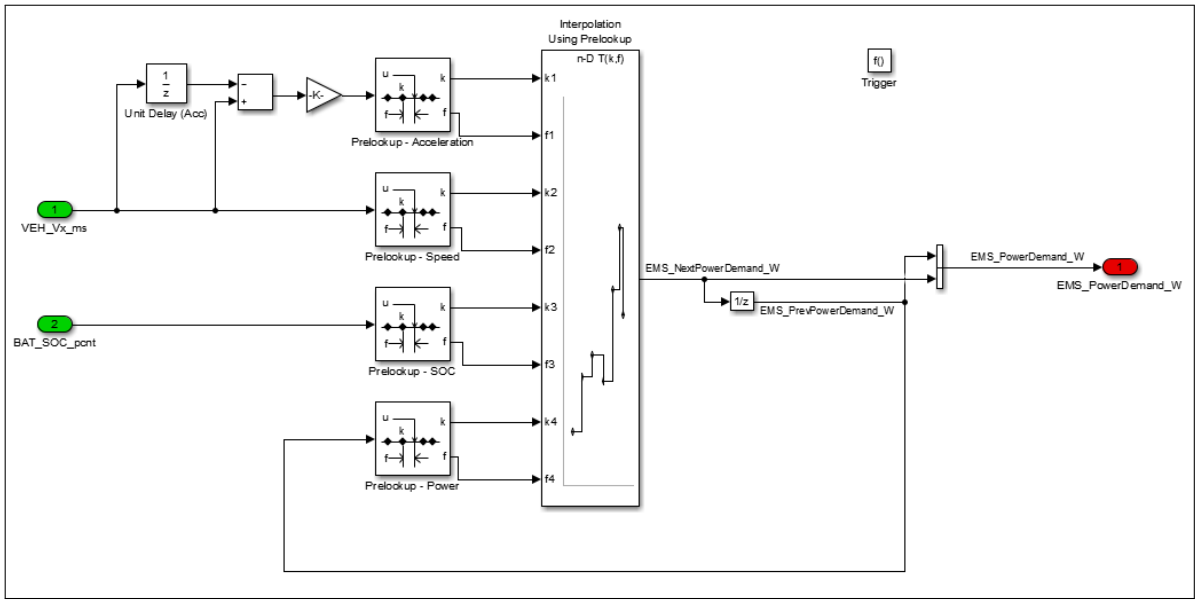

Figure 5.2: EMS Controller Structure - Simulink Model

5.2 MDP Problem Definition

The Markov Decision Process (MDP) problem can be defined by a set of decision epochs, T, a set of Actions, A, a set of States, S, the probabilities of transitioning between each state, $P_{ij,a}$, and the reward or cost of each transition $C_{ij,a}$. The sample rate of much of the logged data is 1 second, and therefore this is the highest rate which can reasonably be used for the time step (Equation 5.2.1). This has been deemed acceptable to use by a number of authors in the literature [45, 64] for the MDP problem since any dynamic effects faster than this can be reasonably ignored.

For the design of an EMS for a Fuel Cell Hybrid Electric Vehicle (FCHEV), the set of actions must determine the operating point of the battery pack and fuel cell and therefore the output power of the main DC/DC converter has been chosen (Equation 5.2.2). This is closely related to the fuel cell power and directly affects the battery current.

$$T = \{0, 1, ...\}\text{s} \tag{5.2.1}$$

$$A = P_{DC,out} = \{0, 200, ..., P_{max}\}\text{W} \tag{5.2.2}$$

The number of states in the problem significantly affects the computational burden, but must be sufficient to allow accurate calculation of the cost function. The states must also be sufficient to model the transitional probabilities accurately enough to provide a reliable estimation of the future states of the vehicle. For this purpose, the speed and acceleration of the vehicle have been chosen, which has been shown in Chapter 4 to be adequate to model the duty cycle of the vehicle. Previous authors [45] have developed strategies based solely on the tractive power demand. As this only uses a single input, it will be must faster to iterate, however this can severely limit the accuracy of future state transitions, especially when applying an infinite horizon solver. Conversely, it may be advantageous to include the incline of the road as an additional input, however this would considerably increase the computational time required. The range of values used has been chosen based on the capability of the vehicle, with a grid spacing of 1ms^{-1} in velocity and 1ms^{-2} in acceleration.

The EMS is directly responsible for managing the SoC of the battery and therefore this must be accounted for in the state definition. This could be achieved by either using the battery voltage as an input vector or the SoC directly, however using the SoC directly has the advantage that this isn't affected by the current loading on the battery. Although mathematically speaking, the optimal policy would give identical results in either case if comparative vectors were used, the final policy is expected to be more closely related to the SoC than the voltage and therefore the size of the input vector can be minimised by using the SoC directly.

Finally, the degradation of the fuel cell is strongly affected by on/off cycling and by transient loading. In order to include the effect of these degradation methods in the calculation of the cost function, the current operating point of the fuel cell should be included in measurement of the vehicle state. This has been achieved by the inclusion of the current demand power from the EMS, which has been chosen because it is already used to define the set of actions. This minimises the size of the sparse matrices used to store the data because the output value of this vector will always be the same as the chosen action. Using the current control action as an input state vector also aids with clarity during examina-

tion of the resultant policy when compared to using equivalent inputs such as the fuel cell power. The complete state of the vehicle can therefore be described using Equation 5.2.3.

$$S = S(a, v, H, P_{EMS}) \tag{5.2.3}$$

5.2.1 Input Grid Resolution

The MDP to be solved is a discrete problem and therefore each of these inputs should be discretized in order to define a fixed number of possible states. The size of each of these inputs will significantly affect the memory usage of the optimisation as well as the computational time required to find the optimal policy. This is due to the high dimensionality of the problem. The total number of states is equal to the product of the sizes of each input vector, and the matrices required to fully define the problem are equal to the number of actions multiplied by the square of the number of states. It is therefore important to select the range, resolution and distribution of the discretization carefully in order to minimise the number of states whilst maintaining accuracy of the solution.

Example selections for the range and resolution of each of these vectors are given in Table 5.1. This gives a total of 142,800 discrete states, and 25 actions. As a result, the full-size probability matrix contains approximately 5×10^{11} individual elements, which would require more than 2TB of storage if stored as a single precision floating point number. This is far more than the memory capacity of even a high performance modern desktop PC. However, this size can be dramatically reduced by the use of sparse matrices in MATLAB by only storing non-zeros elements. As a result, the matrices have approximately 3×10^7 elements and use only 120MB of memory each (using double precision).

Parameter [Unit]	Minimum	Maximum	Spacing
Vehicle Speed, v [ms^{-1}]	0	15	1
Vehicle Acceleration, a [ms^{-2}]	-3	3	1
Battery SoC, H [%]	70	95	0.5
EMS Demand, P_{EMS} [W]	0	1200	50

Table 5.1: Controller State Definition

5.2.2 Cost Function

The objective of the SDP optimisation is to choose actions in order to minimise a future anticipated cost. This cost is calculated by the use of a cost function. The cost function is designed to either reward positive operating conditions or (more frequently) penalise negative conditions. The cost function can be customised in order produce a controller with the desired performance characteristics.

There are two main ways to include operating conditions in the cost function. The first is to use realistic figures for each state in order to optimise a single variable and weighting factors to account for multi-variable optimisation. For example, the hydrogen consumption of the fuel cell can be calculated for each state/action, and using this alone, the optimisation process will produce a controller which provides the optimal performance with regard to fuel economy. Using weighting factors for multiple variables allows each to be "traded off" against each other. For example, the number of gear shifts could be used to optimise the drive-ability. A weighting factor, on either the fuel economy or number of gear shifts, could then be chosen to provide the best compromise between fuel economy and drive-ability.

The second manner in which the cost function can be used is to provide "soft" constraints on the optimisation in order avoid certain conditions. This is often how the limits on the battery SoC are taken into account. Constraints are particularly useful for this purpose due to the fact that it doesn't matter what the SoC is at any point, as long as it is within the acceptable range for the battery pack. By introducing very high penalties to excessively high or low battery SoC and no penalty in between, the controller will attempt to completely avoid these conditions. As long as the SoC stays within the constraints, the cost will not be affected. Theoretically, soft constraints could be used on their own, but usually it is more useful to use them in conjunction with a variable to be optimised. This would, for example, allow the fuel consumption to be optimised whilst keeping the battery SoC within an acceptable range.

As was found in the literature review, the vast majority of previous authors focus on optimising the fuel consumption of the vehicle and use this as the basis for the cost function. Secondary considerations, such as battery SoC maintenance, fuel cell degradation and drive-ability concerns are usually accounted for by constraints on the optimisation. The research for fuel cell vehicles lags behind that for Internal Combustion Engine (ICE) based hybrid vehicles in this regard. More recent work on ICE hybrid vehicles investigates the trade-off between fuel consumption and emissions, or the trade-off between the fuel consumption and drive-ability.

A major concern for fuel cell vehicles is the reliability of the fuel cell itself and therefore it is proposed that this should be included in the optimisation process. A number of authors have proposed strategies that combat fuel cell degradation, mainly focussed on two major causes; the reduction of transient loading, and prevention of reactant starvation. Although there is a great deal of research in the literature into specific degradation methods, no previous work has been found to incorporate this research into SDP controller development. It is therefore proposed that a quantitative analysis of a variety of major degradation methods should be included in the optimisation process and that these could be weighted against the fuel consumption by using their respective monetary values. This would allow the overall running cost of the fuel cell to be minimised by the optimisation process.

The primary cost function developed for this work is made up of three main parts. The controller will be optimised in order to minimise the overall running cost, made up of the

fuel cost, Γ_f and the proportional fuel cell degradation cost, Γ_{FC}. Finally, soft constraints are used in order to maintain the battery SoC, resulting in a penalty cost, Γ_V. Each of these costs is described in detail in the following sections.

5.2.2.1 Fuel Consumption

The fuel consumption of the vehicle is already calculated by the vehicle model developed in Chapter 3 and is based on the operating load of the fuel cell. The output of the model is the fuel consumption, m_f, in mg which can easily be converted into a monetary cost, Γ_f, by multiplying by the value of hydrogen fuel, γ_f, see Equation 5.2.4.

$$\Gamma_f = \gamma_f m_f \tag{5.2.4}$$

5.2.2.2 Fuel Cell Degradation

A number of degradation methods have been identified from the literature review. Although some degradation methods, such as the purity of the fuel, are due to circumstances beyond the control of the EMS, many degradation methods will be directly affected by the operating conditions of the fuel cell and hence can be limited by optimisation of the EMS. A list of potential EMS strategy actions was identified for each method and shown in Table 2.1. There is a lot of overlap in these actions, which can be summarised by four main operating conditions that should be avoided.

1. Low power operation, especially open-circuit
2. High power operation, especially beyond the reactant supply, product removal or heat rejection capability of the stack
3. Transient loading
4. On/Off Cycling

Ideally the voltage degradation rate under each operating condition should be quantified by extensive testing of fuel cell stacks; however, this would be extremely costly and time-consuming and therefore has been deemed out of the scope of this work. Fortunately, there is enough data available in the manufacturer's datasheet [106] and previous literature [13], to make a reasonable estimate. The manufacturer states an expected degradation rate of approximately $11.6\,\mu\mathrm{V/h}$ per cell for the stack at full load, with essentially no degradation below approximately 80 % full load. No low power degradation rates are given; however, these have been obtained from the literature for a similar fuel cell and scaled to match the full load data given by the manufacturer. An estimate for the transient loading degradation has also been obtained from the literature, and the stop-start cycle voltage degradation has been obtained from the manufacturer's specification. These figures are given in Table 5.2.

Operating Conditions	Degradation Rate
Low Power Operation	$10.17\,\mu V/h$
High Power Operation	$11.74\,\mu V/h$
Transient Loading	$0.0441\,\mu V/kW$
Start/Stop	$23.91\,\mu V/cycle$

Table 5.2: PEM Fuel Cell Degradation Rates (per cell)

As shown in Chapter 3, these degradation methods have been incorporated into the vehicle model. The degradation of the fuel cell, D_{FC}, is calculated by the model in mV. This can be divided by the voltage drop at which the fuel cell is said to be fully degraded, D_{max}, to calculate the percentage degradation of the stack. If the degradation rates are assumed to be constant, which should be valid for the short term at least, then the estimated cost, Γ_{FC}, associated with this degradation can be calculated as the percentage degradation multiplied by the monetary value of the stack, γ_{FC}.

$$\Gamma_{FC} = \gamma_{FC} \frac{D_{FC}}{D_{max}} \tag{5.2.5}$$

5.2.2.3 Battery SoC Maintenance

In addition to minimising the total running cost of the fuel cell, the EMS is also responsible for managing the battery. The Microcab H4 does not have an integrated battery charger, and therefore the strategy has been designed to be charge-sustaining. This means there is no need to have a specific final SoC target as long as the SoC stays within the acceptable range to protect the battery from deep-discharge and overcharge throughout any journey. Any deviation in SoC within these bounds will not detriment the performance of the vehicle and hence should not be penalised. Soft constraints are therefore ideal for this purpose.

Battery SoC sustenance can be accomplished by setting constraints on the battery voltage and will prevent the battery from becoming over-charged or deeply discharged. By using the battery voltage, rather than state of charge directly, the battery will also be protected from voltage spikes due to sudden reduction in load from the motors and from voltage drops during periods of high current demand, such as acceleration. In fact, the degradation methods identified in the literature review are more closely related to the cell potential than the SoC directly, and therefore voltage limits will tend to provide better protection than SoC constraints. This soft constraint has been achieved by assigning a cost, α, to extreme cell potentials (above V_{max} and below V_{min}), see Equation (5.2.6).

$$\Gamma_V = \begin{cases} \alpha \int (V_{min} - V_{bat}) dt, & \text{if } V_{bat} < V_{min} \\ \alpha \int (V_{bat} - V_{max}) dt, & \text{if } V_{bat} > V_{max} \\ 0, & \text{otherwise} \end{cases} \tag{5.2.6}$$

Note that the integral of the voltage difference is used in the penalty function. This has been used to ensure that *if* the battery voltage limits are exceeded, then there is a cost incentive for the controller to perform actions which will return the voltage to an acceptable range. If the vehicle components are correctly sized for the application, and the initial SoC of the battery is acceptable, then this detail will have little effect on the results. However, if the control authority is too low (perhaps due to an undersized fuel cell), or if the initial SoC is outside the acceptable range (perhaps due to self-discharge while the vehicle is unused), then the controller will always attempt to return the battery SoC to the acceptable range. This behaviour has been implemented to improve the robustness of the controller under non-ideal circumstances.

A value of 10^4 has been chosen for α. This at least is three orders of magnitude higher than any cost that is likely to occur as a result of hydrogen consumption or voltage degradation of the fuel cell. This means that the voltage management of the battery will over-ride any optimisation if the constraints are exceeded. As a result, the optimisation process will attempt to completely avoid any states outside of the voltage limits of the battery. This is known as a "soft" constraint due to the fact that it is still possible for the constraint to be exceeded if otherwise unavoidable. It would be equally acceptable to choose an even higher value, for example 10^6, however increasing the number too far may lead to computational problems during optimisation. This is because double precision floating point numbers used in the MATLAB algorithm are accurate to approximately 15 significant figures. Given a cost penalty of 10^{10} or higher, the rounding of the floating point numbers, could cause significant errors (in the range 10^{-2} or \$0.01) to accumulate over typical duty cycle lengths of around 10^3 seconds (approximately 15 minutes).

5.2.2.4 Final Cost Function

The final cost function (Equation 5.2.7) is the sum of the three individual components; the monetary cost accumulated due to fuel consumption, the proportional monetary cost due to degradation, and a high penalty due to the battery voltage constraints. This has the net effect of minimising the running cost of the vehicle including fuel cost and degradation, whilst attempting to completely avoid exceeding the voltage limits of the battery.

$$\Gamma_t = \Gamma_f + \Gamma_{FC} + \Gamma_V \tag{5.2.7}$$

5.2.3 Probability & Cost Matrix Generation

The transitional probability matrix describes the statistical chance that the vehicle will transition from any initial state to each subsequent state. Part of the data used to generate this matrix is already available in the form of the Markov chain model developed in Chapter 4. However, the Markov chain model only describes the probabilities of the vehicle transitioning between speed and acceleration pairs. The full state matrix must also include the effect of these transitions on the battery SoC, which will also be dependent on the action of the EMS. This calculation requires the simulation of the vehicle model developed in Chapter 3 from each initial state and for each valid action. The full probability matrix can then be calculated using Equation 5.2.8.

$$\mathbb{P}(S(a,v,H,P_{EMS})^{k+1}|(H^k,P^k_{EMS},u^k)) = \mathbb{P}((a,v)^{k+1}) \times \mathbb{P}((H,P_{EMS})^{k+1}|u^k) \quad (5.2.8)$$

Each time the model is simulated, it is also possible to calculate the cost accumulated, and therefore both the probability and cost matrices can be generated concurrently. In order to produce the results as efficiently as possible the model is simulated in three steps. Firstly, the drag model is used in conjunction with the motor model in order to calculate the electrical power drawn by the motors. Then the fuel cell and DC/DC converter models are used to calculate the power produced by the corresponding EMS action. Finally, the two power vectors are summed and used to calculate the net effect on the battery model, see Figure 5.3.

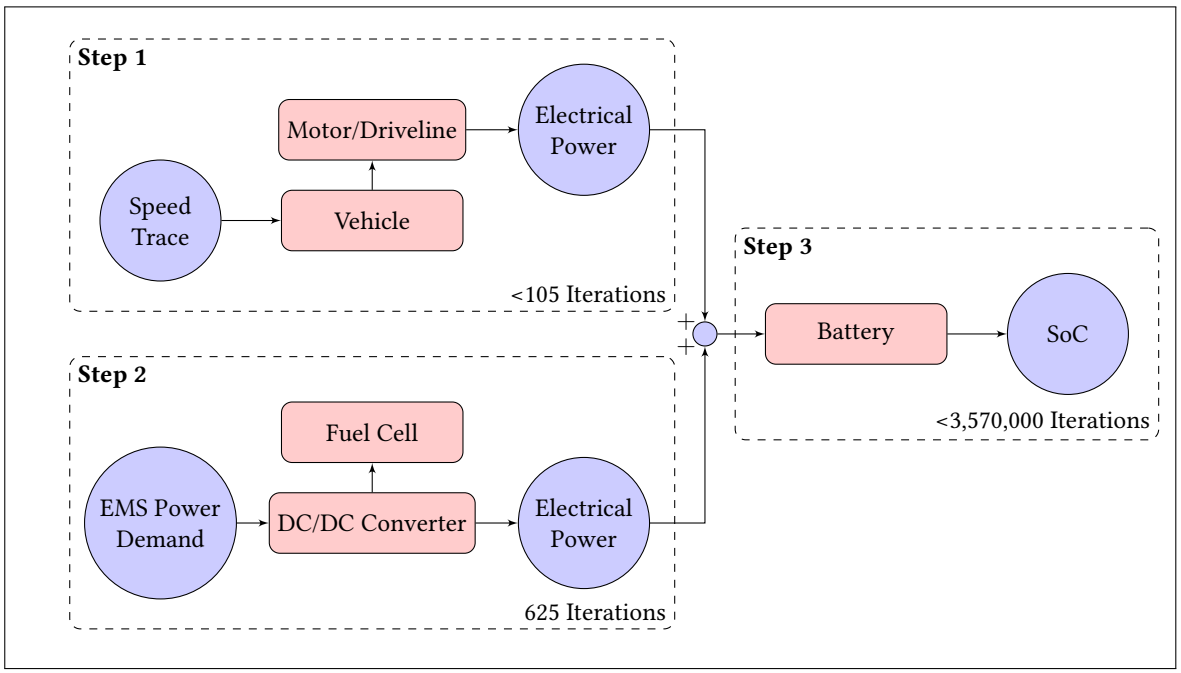

Figure 5.3: Probability & Cost Simulation Steps

This technique improves the speed at which the results can be obtained for two reasons. Firstly, repeated calculations are avoided due to the fact that the drag and motor models need only be simulated for each speed and acceleration pair, not for each additional combination of initial SoC and EMS action. For the grid spacing shown in Table 5.1, this reduces the number of iterations of these models down from a maximum of 3,570,000 to just 105. Equally, the fuel cell and DC/DC converter models are only simulated 625 times. Therefore, only the battery model needs to be simulated for every combination of initial state and potential action. Secondly, the first two models contain no feedback loops which can cause the variable step solver to reduce the time-step of the simulation. As a result, by separating them from the battery model, which contains a feedback loop between the battery voltage and current, they can be simulated much more quickly than if they were contained in the same model.

In addition to this, only valid combinations of initial speed and acceleration are simulated. If the probability of any combination has been calculated to be zero during generation of the Markov chain, then there is no need to perform this simulation. This further reduces the computational burden of the probability matrix.

5.2.3.1 Battery SoC Estimation

The probability and cost matrices are generated using the vehicle model by simulating every valid action from every initial state. The subsequent state and associated cost of performing each action from each initial state is calculated from the simulation results. The cost is easily calculated using the cost function; however, the subsequent state may not match one of the finite states defined in the MDP problem. The problem arises that some actions will result in movement of only a tiny fraction of the grid spacing. This is most apparent with the battery SoC which hardly changes over the time-step of one second and it would be infeasible to reduce the grid spacing enough. In order to alleviate this problem, the subsequent state is represented by a probability distribution split between the grid points. This probability distribution is then multiplied by that of the Markov model in order to generate the full transitional probability matrix for this condition.

5.2.3.2 Cost Calculation

In addition to the electrical power output of the DC/DC converter, the model used in step two of Figure 5.3 also calculates the hydrogen consumption and the fuel cell degradation. This is used with the battery voltage calculated by the battery model to calculate the final cost for each iteration of the model using Equation 5.2.7.

5.2.3.3 Simulation Output

The final output of this calculation is made up of two three-dimensional matrices where the index of the first dimension denotes the initial state, S_k, the second dimension is the final state, S_{k+1} and the third dimension denotes the action, A_k. The data contained in the first matrix is the probability of each transition, and the second matrix is the cost of the transition. Along with knowledge of the states, actions and time-step, these matrices mathematically describe the Markov Decision Process (MDP) problem. More specifically, the problem is to identify which action to take in each state so as to minimise the cost over a certain period of time.

5.2.3.4 Computational Efficiency

Computational efficiency is of paramount importance to dynamic programming optimisation due to the "curse of dimensionality". Dynamic programming techniques explore every possible combination of actions in order to find the optimal solution. As a result, it is very easy to include too many state dimensions, or use too small a grid spacing for the calculations to be performed in a reasonable amount of time. It is therefore extremely important to maximise the efficiency of the computations, and minimise memory usage.

The model performs 1 second of simulation for each iteration in order to generate the transitional probability and cost matrices. During this second the initial speed is given by the initial state, and the acceleration used is the subsequent acceleration expected. Obviously, the combination of initial speed and subsequent acceleration also determines the subsequent speed. The initial DC/DC output power is given by the initial state simulated and the final DC/DC output power determined by the action. During the simulation, the model ramps the DC/DC output power linearly between these conditions. Again, the final state of the model with regards to the DC/DC output power is predetermined by the action taken, due to the fact that this input to the optimisation process is simply the previous output of the controller.

As a result of these two facts, it would be feasible to reduce the size of the matrices significantly by reducing the size of the second dimension (which corresponds to the final state). There is no need to identify the final speed if the acceleration is known, and no need to identify the final DC/DC output power if the action is known. Reduction in the size of these matrices reduces the memory usage, but also reduces the number of calculations required for SDP optimisation.

However, it is not required to do this due to the fact that sparse matrices are used to store these data. As previously mentioned, sparse matrices only store non-zero elements and therefore the additional size of the matrix is not penalised by the consumption of additional memory. In fact, many of the other probabilities in this matrix will also be zero. For example, the final SoC of the battery is represented by a probability distribution between the discrete values above and below the calculated value, as a result, only a maximum of two elements will be non-zero in this dimension. Using sparse matrices also has the advantage that the index of the final state can be used to immediately identify the index of the next initial state with no additional calculations.

Finally, the parallel processing toolbox has been used where possible to improve the speed of the calculations on computers with multiple cores. Due to the high number of independent simulations, this has given a massive benefit, effectively reducing the time required by a factor almost equal to the number of processor cores available. The use of sparse matrices, parallel processing, model reduction, and performing the simulation in stages means that the simultaneous calculation of both the transitional probability and cost matrices takes approximately 24 hours to complete on a desktop PC using a 3.5GHz quad-core processor when using the grid spacing given in Table 5.1, using less than 2GB of memory per worker.

5.3 SDP Solution

Given the probability and cost of each transition it is possible to calculate the statistically optimal action to perform in each state so as to minimise the overall cost. Considering a single time-step, the calculation is very simple. Firstly, the cost and the probability matrices are multiplied on an element-by-element basis. The resulting matrix is a statistical representation of the cost for each transition. The sum of each element in the final state dimension can then be calculated to estimate the stochastic cost of each action for each initial state. The optimal action can be chosen for each initial state as the one that gives the lowest stochastic cost. This set of actions is known as the optimal policy.

If now, a second step is considered, the vehicle would have moved from its initial state. The total cost requires calculation of the cost of the first step, but also the cost of the second step, given the probability of each transition during the first step. The probability distribution of this new state can be calculated using the transitional probability matrix. The cost of performing the optimal action in each new state has already been calculated, as that would be a single time-step problem. Therefore, the cost of the second step can be calculated as the element-by-element product of the probability of each transition during the first step multiplied by the cost of the second step given the single step optimal policy. This can be then added to the stochastic cost of each action for each initial state. The new policy can be calculated as the one that minimises the overall cost over both steps.

The two-step policy may or may not be the same as the single step policy. For example, the single step policy may determine that it is optimal to turn the fuel cell off under almost all circumstances in order to prevent degradation and conserve fuel. However, in the second step, part of this policy may result in the battery voltage penalty being triggered due to demand from the motors. As a result, it would be beneficial to have the fuel cell producing power during the first step in order to prevent this from occurring. Therefore, it may be required to re-calculate the cost of the second step based on the new policy. The total cost would then need to be recalculated, which may result in yet another change to the policy. This process is then repeated until the policy is unchanged.

SDP works by taking this idea of adding the immediate cost of each action to the anticipated future cost due to the probability distribution of each transition and taking it further into the future so as to be representative of the time-scales seen in the real world. There are two main methods, finite horizon and infinite horizon. Finite horizon methods assume a fixed number of time-steps and work in an equivalent way to the example given above. Infinite horizon methods however assume that the process is continued for an infinite number of steps. As this would invariably result in infinite cost, a discount factor is exponentially applied to future steps so as to allow the final cost to converge.

The choice of discount factor will affect both the accuracy of the results and the time required for the cost to converge. A low discount factor may cause the solution to converge very quickly, reducing processing time, but as a result may be unrepresentative of the typical time-scales seen in the real world, and therefore produce a sub-optimal results. Too high a discount factor will cause the convergence to take an excessive amount of time, which may not be necessary to obtain the optimal policy. Often the choice of discount factor is a compromise between calculation time and accuracy.

More recently a number of authors [52, 64] have used an alternative infinite horizon method which does not require a discount factor. This is known as Shortest Path Stochas-

tic Dynamic Programming (SP-SDP) and uses a "terminal state". The terminal state is an additional state added to the model which represents the end of the duty cycle. In order to do this, it has a 100% probability of transitioning to itself with no associated cost. As a result, no cost accumulates once the vehicle has entered the terminal state. This means that the solution will converge for any initial state that has a non-zero probability of eventually entering the terminal state given an infinite number of steps. Therefore, no discount factor (or a discount factor of 1) is required for the infinite horizon cost to converge.

5.3.1 Mathematical Description

Two techniques will be used in this work, the infinite horizon and shortest path SDP. A brief mathematical description of each is given below. Despite its apparent complexity, SDP can be described by two steps. The first is the policy evaluation where the expected costs of performing the current policy are calculated. The second step is the policy improvement step, where the policy is chosen as the set of actions which minimises the expected cost. This process is then repeated until the policy converges.

5.3.1.1 Infinite Horizon

The MDP problem described has been solved using infinite horizon SDP. The objective is to find the optimal control policy, $u = \pi^*(S)$ so as to minimise the total expected cost, $J_\pi(S_0)$, over an infinite time horizon. The total expected cost is calculated using Equation 5.3.9, where $\lambda \in [0, 1)$, represents the one second discount factor.

$$J_\pi(S_0) = \lim_{K\to\infty} E\left\{\sum_{k=0}^{K-1} \lambda^{k-1}\Gamma\left(S_k, \pi(S_k)\right)\right\} \tag{5.3.9}$$

The optimal policy can be found using a policy iteration algorithm. This works by iteratively evaluating the current policy and then improving the policy until the policy converges. The policy evaluation step (Equation 5.3.10), given the current control policy, π is calculated as the cost incurred during the current step added to the expected cost of future steps given the new state, S', that the vehicle has transitioned to.

$$J_\pi^{k+1}(S^i) = \Gamma(S^i, \pi(S^i)) + \lambda E\left\{J_\pi^k(S')\right\} \tag{5.3.10}$$

The policy is then improved by finding the action which will minimise the total expected cost, see Equation 5.3.11.

$$\pi'(S^i) = \underset{a\in A(S^i)}{\operatorname{argmin}} \left[\Gamma(S^i, a) + \lambda E\left\{J_\pi(S^i)\right\}\right] \tag{5.3.11}$$

This process is iterated until the policy remains unchanged for a number of improvement steps. The optimal policy $\pi^*(S)$ is based on the state of the vehicle, and is causal and time-invariant and therefore can be directly implemented in simulation or on board the vehicle.

5.3.1.2 Terminal State

The solution to the terminal state problem is identical except for the fact that now no discount factor is required. That is to say $\lambda = 1$ in the equations above, and therefore the solution can be slightly simplified:

$$J_\pi(S_0) = \lim_{K\to\infty} E\left\{\sum_{k=0}^{K-1} \Gamma\left(S_k, \pi(S_k)\right)\right\} \tag{5.3.12}$$

$$J_\pi^{k+1}(S^i) = \Gamma(S^i, \pi(S^i)) + E\left\{J_\pi^k(S')\right\} \tag{5.3.13}$$

$$\pi'(S^i) = \underset{a\in A(S^i)}{\operatorname{argmin}} \left[\Gamma(S^i, a) + E\left\{J_\pi(S^i)\right\}\right] \tag{5.3.14}$$

This solution will converge given the existence of a terminal state in the model. The terminal state has three requirements. Firstly, every initial state must be able to eventually transition to the terminal state given an infinite number of steps. The terminal state will always transition back to itself. This transition will incur no cost. As a result, the terminal state will be "absorbing". This means that the probability of being in the terminal state will increase as the number of steps increases. As no cost is incurred in the terminal state, the solution will therefore converge.

5.4 SDP Parameter Selection

There are a number of parameters which can be tuned in order to make the compromise between processing time and accuracy. These include the discount factor, the number of policy evaluations, and the criteria for when the solution is said to have converged. Many of these parameters represent a compromise between accuracy and computational burden. This is because increasing the accuracy of the solution will tend to exponentially increase the time required for the solution to converge. Therefore, often the process of parameter selection involves defining a required level of accuracy and selecting the fastest set of parameter values which will achieve this.

5.4.1 Discount Factor Selection

The use of a discount factor artificially forces the solution to converge and has an impact on the effective horizon of the optimisation. A low discount factor will discount future costs relatively quickly and as a result may not compensate for future costs sufficiently. Conversely, a high discount factor will account for future costs more accurately, but will take longer to converge.

This compromise is particularly apparent in this problem due to how the battery SoC is managed. No cost is accumulated whilst the battery voltage is within an acceptable range. Therefore, a strategy which is optimised with a low discount factor will tend towards being charge-depleting in order to minimise the short-term cost of consuming fuel. This means that rate at which the charge is depleted from the battery can be controlled with careful selection of the discount factor. For Charge-Sustaining (CS) strategies, previous authors have compensated for this by using a penalty for deviation from a target or nominal SoC instead of (or in addition to) soft constraints. The weighting on this penalty can severely affect the optimisation process, however, and therefore for a charge sustaining strategy, using a higher discount factor is preferable.

With a high discount factor, the future cost of recharging the battery (in order to avoid the minimum acceptable SoC limit) will be more heavily weighted. This results in an optimisation which is more "aware" of the future cost of recharging and thus will optimise the strategy accordingly, choosing the optimal conditions under which to allow the battery SoC to deplete, and the best times to recharge in order to minimise the overall fuel usage. Unfortunately, the time required for the solution to converge increases exponentially with increasing discount factor. Therefore, it is important to choose a sufficiently high discount factor to ensure charge-sustaining behaviour, but no higher, in order to most efficiently use the computational time. Fortunately, with modern desktop computers, it is possible to obtain a sufficiently accurate solution in a reasonable amount of time without applying a penalty to battery SoC deviation from the nominal value.

More recently, an alternative method to using a discount factor has been developed. This works by using a terminal state which represents the end of the drive-cycle. The terminal state has no on-going cost, and always transitions back to itself. This allows the solution to the optimisation to converge without the use of a discount factor. As a result, the typical length of a journey is accurately represented. For a Charge-Depleting (CD) strategy, the battery SoC will gradually decline to close to the minimum value over the length of a typical journey. For a CS strategy, it is possible to set a final SoC target by applying a penalty to just the transition to the terminal state. This allows the SoC to vary throughout the journey without accumulating any penalty as long as it returns to the target value by the end.

5.4.2 Number of Policy Evaluations

The SDP algorithm has two steps; the first is to evaluate the policy, and the second is to improve the policy. Due to the fact that a single evaluation of the policy is unlikely to result in a policy change (especially as the solution gets close to converging), it is possible to improve the computational efficiency by performing a number of policy evaluations between each improvement step. However, too high a number of evaluations without a policy improvement step may result in unnecessary evaluation calculations which are not representative of the optimal policy. The number of evaluation steps for each improvement step can therefore be optimised in order to minimise the overall computational burden.

5.4.3 Convergence Criteria

The final parameters which require tuning are the convergence criteria. The convergence criteria define the end of the optimisation process, and signify when the optimal policy has been calculated. One method is to define a convergence limit on the final cost. As the optimisation process continues, and the future steps are discounted, the total accumulated cost for each initial condition and action will converge. Future epochs are exponentially discounted and therefore although the cost will never stop increasing, it will each tend towards a final value for each initial state. By checking the matrix of final costs against its previous value, the optimisation process can be stopped once the change in value is smaller than a set limit.

This method is unaffected by the number of evaluation steps in between each improvement step, however it can be difficult to define the convergence limit in advance of the optimisation, as this will be highly dependent on the data in the transition probability and cost matrices. As a result, it is required to set a very small value for this convergence in order to be sure of policy convergence, which in turn will increase the optimisation time.

A better method is to check the policy for any changes since the last improvement step. If the policy is unchanged, then it is said to have converged and the optimal policy has been obtained. This method tends to be more time efficient because it is generally the policy which is of interest rather than the final costs. However, if there are too few evaluation steps then it is possible that the policy could remain unchanged for a number of improvement steps, before changing again later. This problem can be avoided by either increasing the number of evaluation steps or requiring a number of policy improvement steps where the policy remained unchanged.

5.4.4 Summary

In this work, the SDP algorithm was iterated with 100 policy evaluation steps for each improvement step and was deemed to be converged when the policy remained unchanged for 36 improvement steps, representing an hour of drive time. This combination was found to be the most time effective in order to produce reliable results. A value of λ of 0.9999 was chosen for the one second discount factor. This value is relatively high compared to what is found in the literature (0.95-0.995) [44, 47, 51, 52]; however, this was found to be required for charge-sustaining behaviour in the long-term when using only the battery voltage to constrain the SoC. Using these settings, the SDP optimisation took approximately 6 hours to solve on a desktop PC using a 3.5GHz quad-core processor.

5.5 Example Policy

The final output of the SDP optimisation process is the control policy which minimises the cost function over the stochastic duty cycle given by the Markov chain. This can be represented as a four-dimensional lookup table, where each of the four dimensions represents the input vector of one of the input states; speed, acceleration, battery SoC and previous control action. It is therefore very easy to implement this policy in simulation or in a real-time controller for testing purposes.

A cross section of a typical policy is shown in Figure 5.4. This policy was generated using the grid spacing given in Table 5.1 and the SDP parameters given at the end of previous section. It can be seen that the general trends are as expected. For example, the fuel cell will be run at decreasing load as the SoC of the battery increases. There is also a tendency for the fuel cell to be run at a slightly higher load if the previous power demand was higher. This is likely due to the controller attempting to avoid transient loading as much as possible. Finally, it can be seen that the policy has a curved "cliff" edge at the upper end of the battery SoC with regards to the previous power demand. This is likely due to the optimisation of the running cost competing with the requirement to stay within the battery voltage limits. High fuel cell power will likely result in increased battery voltage, and therefore it suddenly becomes favourable to idle the fuel cell in order to avoid the soft constraint.

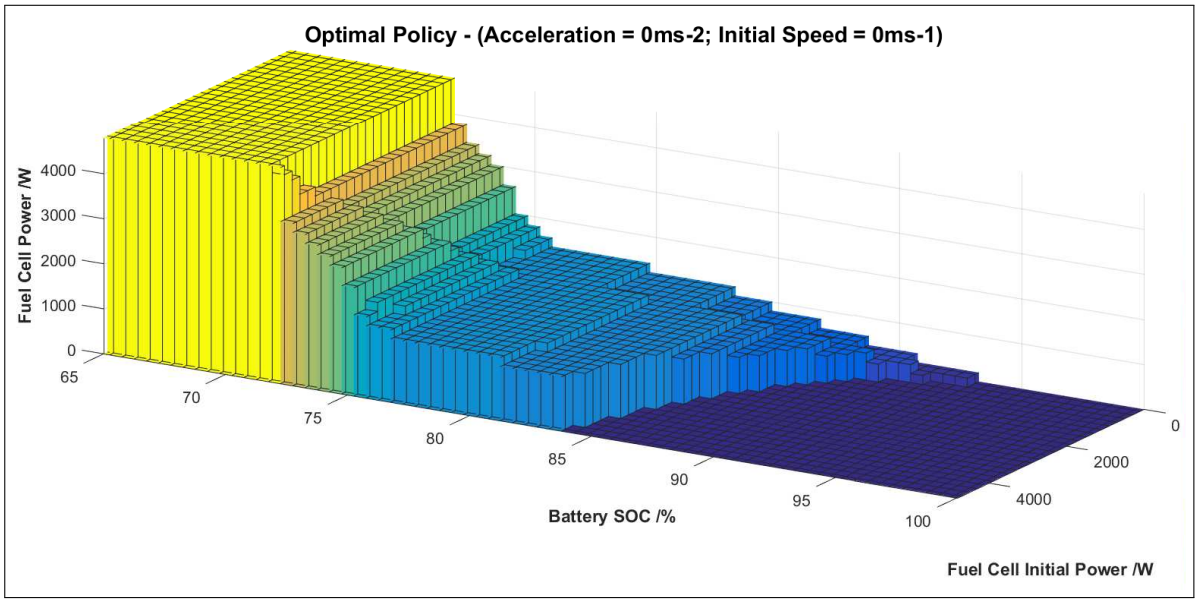

Figure 5.4: Policy Example

It must be mentioned that although the optimal policy is calculated for every state, many of these states will likely never be entered, especially due to the feedback of the previous control action. For example, in the data shown in Figure 5.4, above 75% SoC, the policy never requests more than 3200W. Assuming that the policy is similar at nearby states (i.e., ones that may transition to these states), then it is likely impossible that the previous power would be above 3200W if the SoC is above 75%. This means that detailed examination of the raw policy can be slightly misleading because the optimal action selected in some states will have significantly more effect on the results than the optimal action in other states.

However, although in ideal circumstances some of the states will never be entered, the fact that the policy is calculated for every state is still beneficial. This is because it improves the robustness of the solution for real-world use, given that component failure may occur, or sensor readings may not always be accurate. For example, given an incorrect battery SoC reading, the strategy would be able to recover when the readings become accurate again.

Chapter 6

Strategy Simulation & Analysis

This chapter presents the simulation results of various Energy Management Strategy (EMS) controllers developed using the techniques previously described. The chapter begins with a brief description of how the controllers are tested. Following this, the results of the initial Stochastic Dynamic Programming (SDP) optimised controller are presented and compared firstly to the baseline controller (based on the Microcab H4's current strategy) and also to a controller optimised purely on the fuel consumption.

It is found that for the current design, the 1.2kW fuel cell is insufficient to maintain the battery State of Charge (SoC) under normal usage even when the optimal control strategy is applied. Therefore, the results are recalculated for a 4.8kw stack representative of that in the newer Microcab H2EV. It is found that the current control strategy is no longer appropriate for the system design and that the degradation inclusive controller reduces the estimated degradation by approximately 15% for only a 4% increase in fuel consumption when compared to the strategy optimised purely on the fuel consumption. This gives an overall running cost saving of around 9%.

6.1 Testing Procedure

As mentioned in the previous chapter, the output of the SDP algorithm can be represented by a four-dimensional look up table which can easily be implemented in the full vehicle model developed in Chapter 3. This model can then be used in order to simulate various duty cycles in order to assess the performance of the controller. Initial results are obtained using the grid spacing given in Table 5.1 and the SDP parameters given at the end of previous chapter.

The Microcab H4 is designed for very low speed campus driving and cannot complete any standard drive-cycle. Therefore, logged data of the journeys captured at Loughborough and Birmingham have been used for testing. Individual journeys identified in Chapter 4 have been input as a speed reference into the model. These journeys are then simulated and the EMS is used to control the output power of the DC/DC converter based on the vehicle speed, acceleration, battery SoC and the previous control action. The operating efficiency of various components can then be calculated from the results, along with an estimation of the fuel consumption and fuel cell degradation.

6.1.1 Weighting Factors - Hydrogen and Fuel Cell Stack Cost

In this analysis, the weighting in the cost function associated with the fuel consumption and the degradation have not been chosen arbitrarily, but instead have been chosen based on the monetary value of each. However, the definition of these financial costs is not a trivial task. One potential option is to simply use the purchase cost of each, experienced during the design of the vehicle in question. For an automotive manufacturer, this would be the obvious decision and could be based on highly reliable data, making the cost function extremely relevant to the exact vehicle and therefore the optimisation would minimise the real-world financial running cost.

However, the Microcab H4 is a concept vehicle and thus the purchase cost of the fuel cell is highly inflated compared to that of a production vehicle. Similarly, the hydrogen fuel supply available at Loughborough University is used primarily for research and development purposes and as a result, the associated cost of the supply is not representative of the anticipated "forecourt" cost for such vehicles. The bespoke nature of such vehicles and the manner in which they are used means that there is considerable variability in such cost estimates which depends on the supplier, production quantities and exact system design. Although using such an estimate would be highly justifiable, the results would not translate very well to other vehicle designs, making comparison with similar work difficult.

Instead, it has been decided to consider a scenario in which the fuel cell stack is mass produced, using present day (2015) estimates of mass production costs from the literature. This provides two main benefits compared to using the actual costs experienced with the vehicles. Firstly, as mentioned already, the estimates in the literature for mass produced vehicles are much more consistent allowing for easier comparison to similar work. Secondly, these costs estimates are based on the scaled up manufacturing cost of the fuel cells themselves and thus do not include additional components such as the electronic control unit. These figures are also not subject to supplier profit margins, exchange rate variability and technical assistance which are all but impossible to separate from the purchase prices of "off-the-shelf" stacks such as the Ballard Nexa or Horizon H5000.

The US Department of Energy (DoE) targets a fuel cell cost of $35/kW [12] for fuel cell vehicles to become viable, although recent estimates tend to be marginally higher, in the

range of $50+/kW (2015) [13], $49-53/kW (2015) [107], and $61/kW (2009) [108]. Similarly, dispensed hydrogen costs are expected to be within the range of $2.10/kg to $8.26/kg (2015) [13, 107], depending on the method of production and transportation costs.

Unless otherwise stated, the data shown in this chapter assume a fuel cost of $3/kg of hydrogen and a fuel cell cost of $50/kW. This gives the 1.2kW fuel cell used in the Microcab a replacement cost of $60, and the 4.8kW fuel cell used in later analysis a cost of $240. These figures are clearly much lower than the actual purchase costs associated with the vehicle; however, they have been used for the reasons listed above. These figures are based on recent estimates from the literature for current technology, assuming mass production economy-of-scale. In reality, the prices are likely to be significantly higher for current fuel cell vehicles due to lower production volumes, but are likely to be lower for vehicles released in the future due to more advanced technology. As these prices are used only to weight the degradation and fuel consumption appropriately, the actual magnitudes of the prices are of little importance compared to the ratio between the two.

6.1.2 Controller Design

The primary controller examined has been optimised to minimise the overall running cost inclusive of both fuel consumption and the proportional cost of fuel cell replacement due to voltage degradation. This controller is referred to as the Degradation Inclusive (DI) controller or strategy. This strategy is novel with respect to the inclusion of quantifiable degradation metrics into the cost function. Two other controllers have been developed for comparison purposes; the first is based on the current EMS strategy of the Microcab, and the second is a SDP strategy representative of recent work in the literature.

6.1.2.1 Baseline Controller - Current Microcab Strategy

The baseline controller is the Microcab H4's current control strategy. This strategy attempts to control the DC/DC converter's output power in order to maintain a battery pack voltage of 57.6V. This represents a voltage of approximately 14.4V for each battery, and serves to ensure every battery is fully charged by the fuel cell. The fuel cell will therefore react to both a low battery SoC and the drop in voltage associated with ohmic losses due to high current demand. As the motors may draw more than 10kW of electrical power, and the maximum power output of the DC/DC converter is only 1.2kW, the batteries tend to be depleted while the vehicle is moving, and therefore the voltage will drop below 57.6V. In this case, the DC/DC converter will run at maximum power until the voltage returns to the set point.

6.1.2.2 Minimal Fuel Consumption (MFC) Controller

The second controller developed for comparison is a SDP controller optimised solely to minimise the fuel consumption. This represents recent work in the literature, and serves as a good baseline for comparison to other work in the area. The fuel consumption only SDP controller has been developed using exactly the same methods as the degradation inclusive controller, aside from the removal of second term in the cost function (Equation 5.2.7); that related to the cost of the fuel cell degradation. This comparison allows the effect of the inclusion of degradation metrics into the optimisation to be separated from the normal fuel consumption optimisation.

6.2 1.2kW Fuel Cell

The first test involves simulating the Microcab H4 in its current configuration with a 1.2kW fuel cell. As has been previously mentioned, the fuel cell is relatively undersized for its usage pattern and as a result, it is designed to continue to run for approximately 10 minutes after the vehicle is switched off in order to re-charge the battery pack. Therefore, the vehicle has been simulated over a number of the drive cycles captured in the logged data, each with the addition of a 10-minute stationary period after the main duty cycle to allow the battery SoC to recover.

For each test, the SoC has been initialised so that there is no net change over the complete journey. This avoids any complications involved with accounting for energy stored in the battery and also allows the typical SoC of each strategy to be examined. Other than this, the input to each controller is identical. For each controller, a selection of 10 journeys was tested and the results of one of these were examined in detail. This journey lasts approximately 1 hour and involves four short trips lasting approximately 5-10 minutes each with a stationary period in between. The total distance travelled is approximately 6.0 km with a maximum speed of 6.91 m/s (25 km/h). The mean tractive power required is just 0.35kW, with a peak tractive power of 4.92kW. The full speed trace which represents the duty cycle can be seen in Figure 6.1.

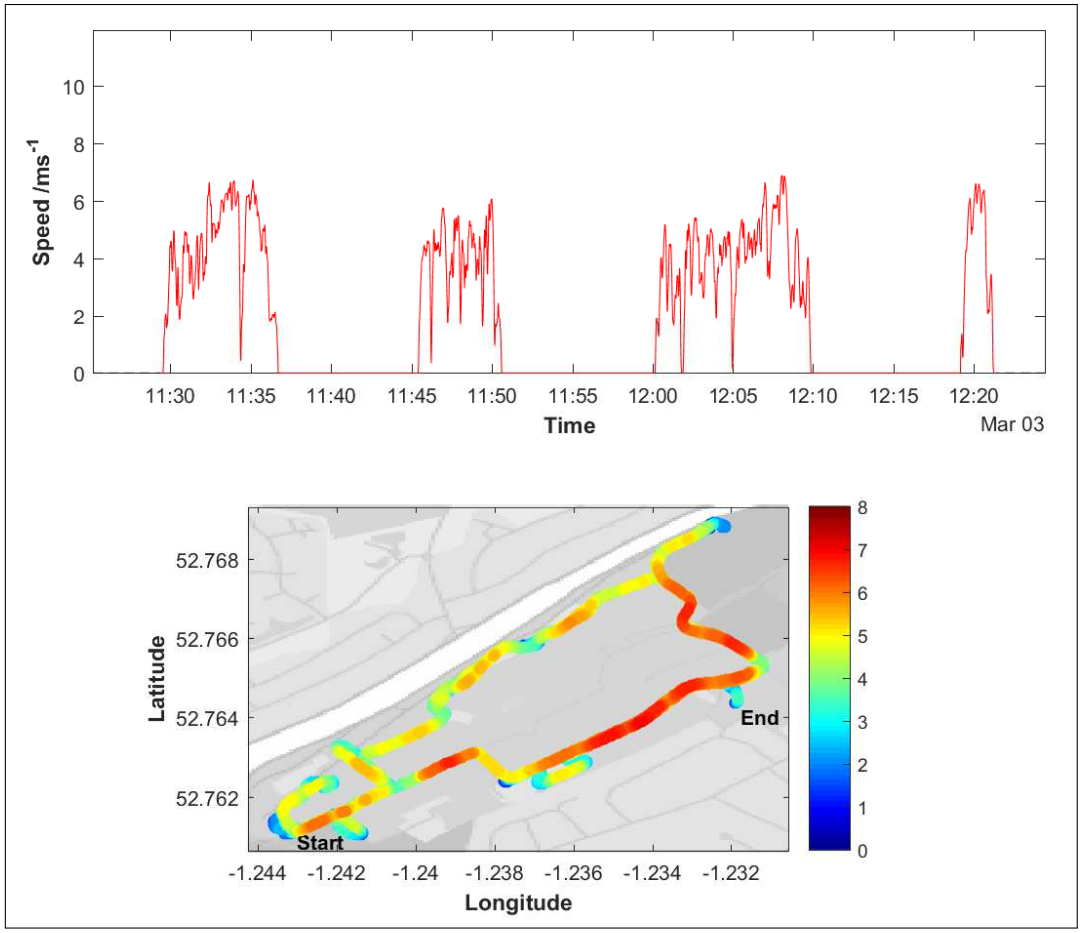

Figure 6.1: Test Journey

6.2.1 Baseline Strategy

The current control strategy on the Microcab operates the fuel cell reactively to the battery voltage. As a result, during periods of high current demand from the motors, the load on the fuel cell also increases. Due to the stop/start nature of urban duty cycles, this puts a highly transient load on the fuel cell. Figure 6.2 shows the results of the simulation using the current control strategy on board the Microcab. The load on the fuel cell can be seen in the second plot.

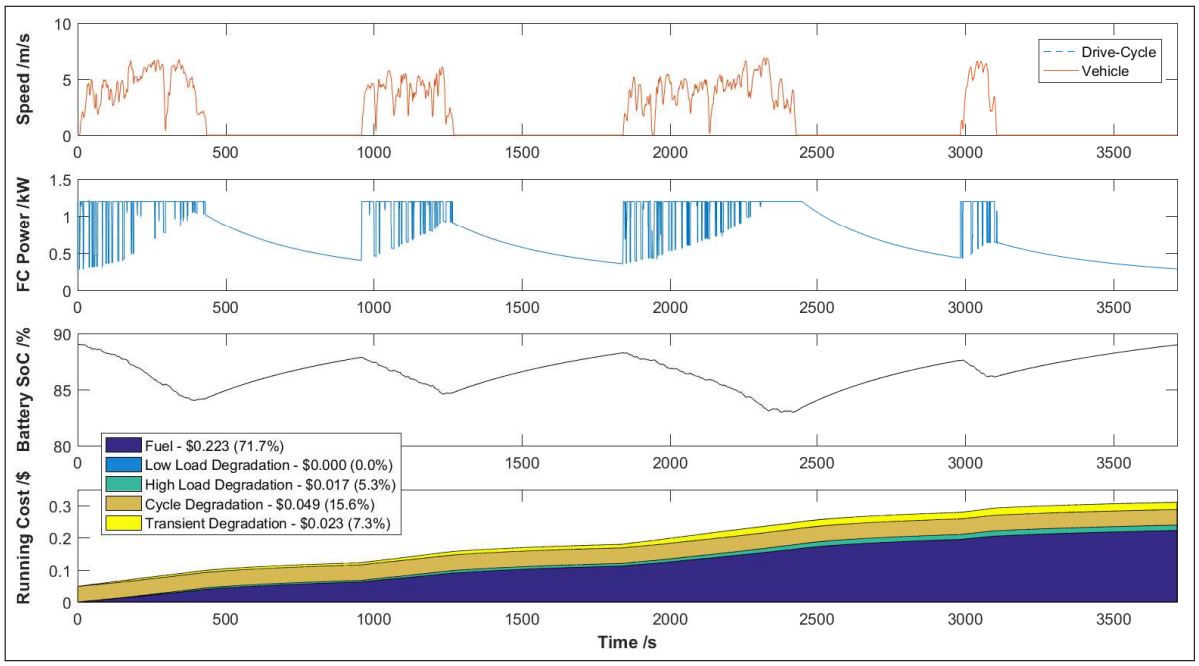

Figure 6.2: Accumulated Running Cost for the Current Microcab Controller (1200W)

During periods of acceleration, the motor draws a high current. This current causes the battery voltage to suddenly drop due to ohmic losses and the fuel cell load increases in order to compensate. When the vehicle subsequently begins to decelerate, the battery voltage recovers, and the load on the fuel cell abruptly drops, see Figure 6.3.

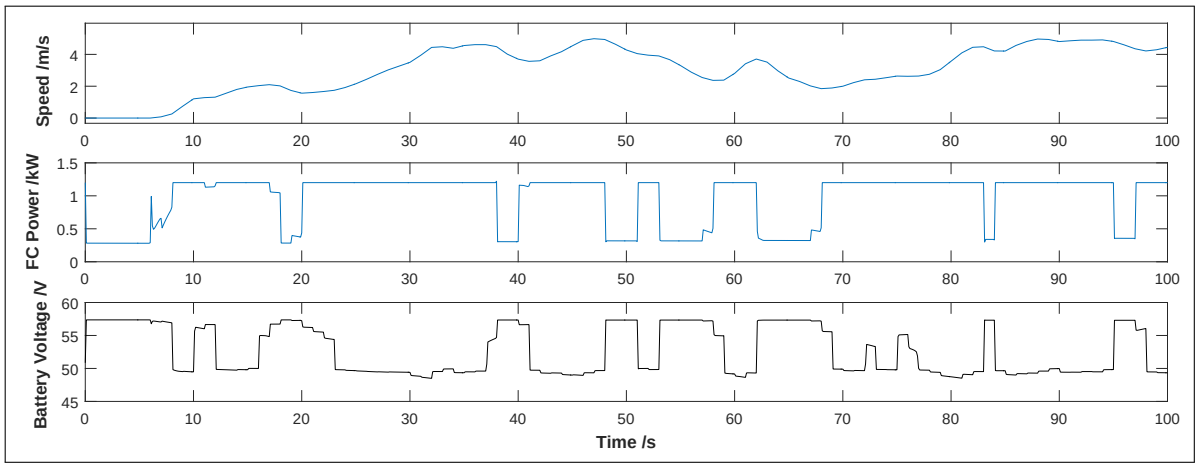

Figure 6.3: Transient loading due to reactive fuel cell load (1200W)

As each trip continues, the battery SoC gradually falls as the fuel cell generally supplies less current than that drawn by the motors. It can be seen in the third trip in Figure 6.2 that during sustained periods of activity, the battery SoC drops significantly enough that the fuel cell begins to run at full power continuously. Despite this, the battery SoC continues to fall. This shows that the fuel cell is undersized for the application, and as a result, is unable to provide enough power to prevent the SoC from decreasing while the vehicle is active. Given a longer period of activity or a journey lasting more than a few minutes, it is likely that the battery would be become discharged well before the fuel cell runs out of fuel.

The lowest plot shows the accumulated running cost as estimated by the model. It can be seen that the fuel consumed accounts for approximately 72% of the total cost of the journey which was around $0.31. The total degradation on the fuel cell is estimated at around 0.15%, representing a proportional cost of $0.09, and putting the estimated lifetime of the fuel cell at around 704 hours (compared to the datasheet estimation of 1500 hours). Just over half of the degradation is due to the single on/off cycle of the fuel cell, 25% due to the transient loading and 20% due to operation of the fuel cell close to full load.

Table 6.1 shows the results for the complete set of tested journeys. It can be seen that the fuel consumption is relatively consistent, ranging between 12.5 g/km to 14.8 g/km, which is approximately proportional to the average power drawn by the motor. The estimated lifetime of the fuel cell varies considerably from 379 hours to 760 hours. This is very closely related to the duration of the journey due to the high on/off cycle degradation cost, and therefore shorter journeys accumulate less time for the same amount of degradation. This suggests that the voltage degradation due to start-up and shut-down is a major cause of fuel cell ageing for this usage pattern.

No	Duration	Distance	Mean Motor Power	Hydrogen Consumption	Estimated Lifetime	Estimated Range	Total Cost
1	3817 s	4.3 km	0.55 kW	13.5 gkm^{-1}	587 h	44.4 km	$0.28
4	3715 s	6.0 km	0.72 kW	12.5 gkm^{-1}	704 h	48.1 km	$0.31
12	2146 s	4.7 km	1.02 kW	13.9 gkm^{-1}	489 h	43.3 km	$0.27
15	2315 s	3.9 km	0.77 kW	12.9 gkm^{-1}	489 h	46.6 km	$0.23
23	2368 s	2.8 km	0.57 kW	13.2 gkm^{-1}	508 h	45.5 km	$0.19
32	1883 s	2.9 km	0.73 kW	13.5 gkm^{-1}	464 h	44.5 km	$0.18
41	1546 s	3.2 km	1.02 kW	14.8 gkm^{-1}	379 h	40.6 km	$0.21
51	4011 s	5.7 km	0.69 kW	13.6 gkm^{-1}	760 h	44.1 km	$0.32
71	2954 s	3.8 km	0.61 kW	12.8 gkm^{-1}	627 h	46.8 km	$0.23
78	2919 s	3.1 km	0.49 kW	12.6 gkm^{-1}	648 h	47.8 km	$0.19
Total	**27674 s**	**40.2 km**	**0.69 kW**	**13.3 gkm^{-1}**	**574 h**	**45.2 km**	**$2.40**

Table 6.1: Performance Summary for the Current Microcab Controller (1200W)

6.2.2 MFC Strategy

The second strategy has been optimised using SDP to minimise the fuel consumption only. The results are shown in Figure 6.4. It can be clearly seen that this strategy puts significantly less transient loading on the fuel cell. Compared to the baseline strategy, the fuel cell power tends to ramp up gradually when the vehicle is moving and as the SoC of the battery decreases. The strategy runs the fuel cell at full power towards the end of each trip, gradually ramping the power down when the vehicle is stationary and as the SoC recovers. In contrast to the baseline strategy, the MFC strategy appears to be more closely related to the SoC of the battery than the voltage.

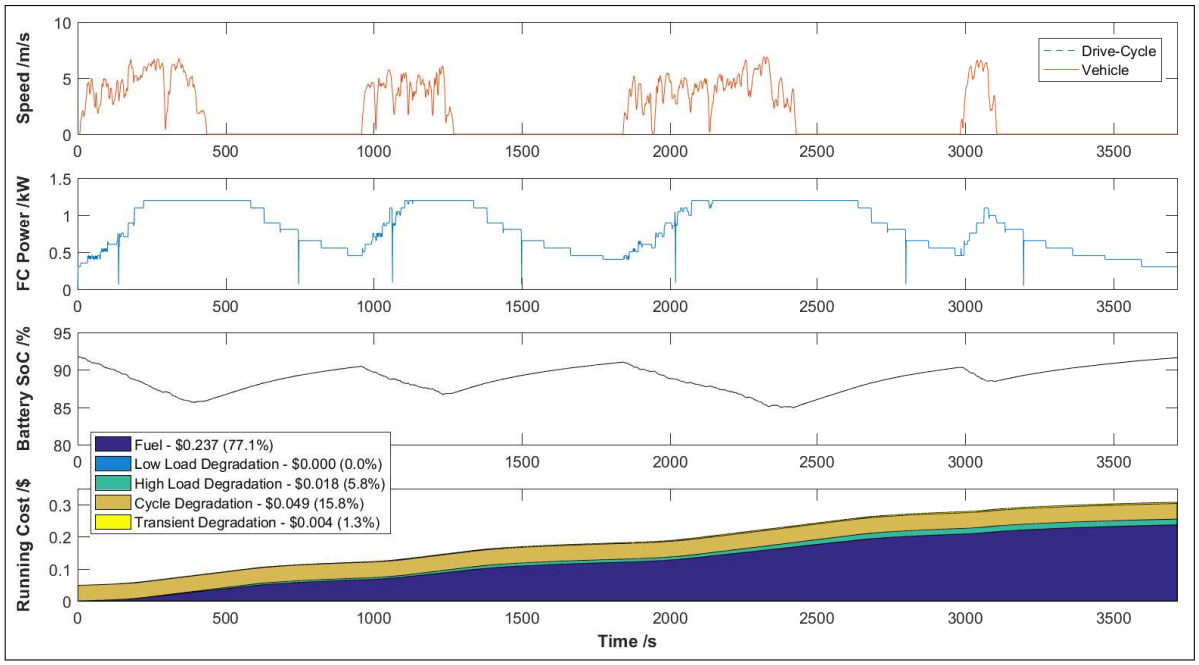

Figure 6.4: Accumulated Running Cost for the Fuel Only Optimised Controller (1200W)

Although the SDP strategy uses the SoC as an input rather than the voltage, it could still react to the battery voltage indirectly by responding to changes in the vehicle speed and acceleration. These will affect the current drawn by the motors, and hence the voltage of the battery due to its internal resistance. The algorithm does not appear to do this however, and seems to vary the load inversely proportionally to the SoC. This has the indirect effect of reducing the transient loading on the fuel cell, however, the MFC strategy is not optimised to do this, and therefore there must be another reason why it makes these control decisions.

At high SoC, the battery voltage risks hitting the upper constraint on the optimisation and therefore the optimisation is minimising the probability of this happening despite an increased load from the duty cycle. As the SDP optimisation uses the transitional probability matrix to generate its policy, it is "aware" of the possibility that the load may decrease in the future and the effect that this will have on the battery voltage. Due to the highly transient loading pattern from the campus journeys there is almost always a relatively high possibility for the vehicle to begin to decelerate, regardless of its current trajectory. Therefore, in order to protect the battery from its upper voltage constraint, the fuel cell load only begins to increase once the battery SoC has begun to deplete. By doing this, it is much less

likely that the increased current from the fuel cell will cause the battery voltage to suddenly spike above the maximum voltage constraint.

Despite this, there are a number of sharp downward spikes seen in the fuel cell demanded power. These generally occur at the beginning of decelerations in the duty cycle and are therefore likely due to the controller attempting to avoid the maximum battery voltage constraint. This suggests that even though the fuel cell power is only increased once the SoC has dropped, there is still the possibility that the maximum voltage constraint could be breached. Given that there is an extremely high penalty if this occurs, it is unlikely that the MFC controller is taking this risk in order to optimise the fuel consumption. It is much more likely that if a lower power was demanded, the battery voltage would risk breaching its minimum limit. This suggests that the fuel cell is compromising its overall strategy in order to avoid the penalties associated with the voltage constraints. This is likely due to the low maximum power of the fuel cell. As a result, the strategy tends to operate the battery very close to its maximum voltage constraint in order to allow for sustained periods of high current demand from the motors.

Compared to the baseline strategy an increase in fuel cost of approximately 6.5% is observed. As the MFC strategy is optimised to give the minimal fuel consumption, this again suggests that the strategy is compromised by the battery voltage constraints. The fuel cell is run at less efficient operating points in order to minimise the possibility of the battery reaching its minimum voltage limit during a sustained period of activity. In contrast, the baseline strategy aggressively targets a high battery SoC, but is not actually constrained by the battery voltage. As a result, the fuel cell is run at lower overall power for the same battery SoC, which results in a minor fuel saving at the risk of causing damage to the battery due to deep-discharge. Figure 6.5 shows a detailed comparison of the battery SoC for both controllers. It can be seen that both controllers follow relatively the same pattern, however the MFC controller maintains a SoC which is consistently around 2.5% higher.

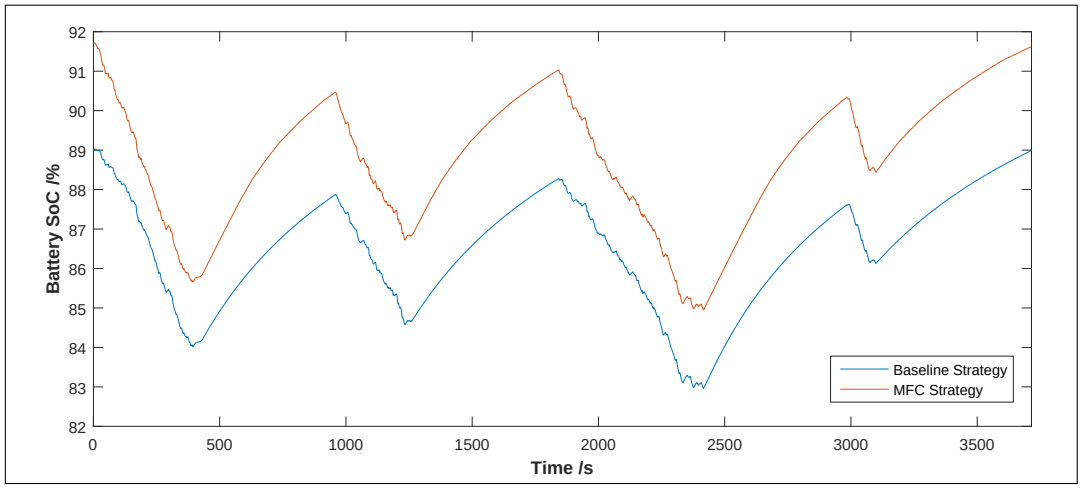

Figure 6.5: Detailed Comparison of baseline and MFC Strategies

The reduction in transient loading does have an indirect benefit however, in that the fuel cell degradation is reduced. The overall degradation using this controller is estimated at approximately 0.12% representing a saving of around 20%. For the MFC controller, approximately 70% of the degradation is due to the single on/off cycle of the fuel cell which cannot be avoided. There is a 10% increase in the degradation associated with operating the fuel cell at high load; however, an 80% reduction in the cost of transient loading causes a 161 hour (24%) increase in the expected lifetime. As a result, the overall estimated cost of the drive-cycle ($0.31) is identical to that calculated for the baseline strategy.

The results for all ten tested cycles are shown in Table 6.2. As before, the fuel consumption is relatively consistent and now even more closely related to the average motor power. The fuel consumption is approximately 5% higher than the baseline strategy on average. Similarly, the estimated lifetime varies considerably and is most correlated to the duration of the journey. This is because the degradation due to the single on/off cycle is consistently the most significant degradation method due to the reduction in transient loading on the fuel cell. Compared to the baseline strategy, the overall cost is approximately 3.6% lower despite the increase in fuel consumption.

No	Duration	Distance	Mean Motor Power	Hydrogen Consumption	Estimated Lifetime	Estimated Range	Total Cost
1	3817 s	4.3 km	0.55 kW	13.7 gkm^{-1}	1058 h	43.7 km	$0.24
4	3715 s	6.0 km	0.72 kW	13.3 gkm^{-1}	878 h	45.2 km	$0.31
12	2146 s	4.7 km	1.02 kW	14.4 gkm^{-1}	490 h	41.7 km	$0.28
15	2315 s	3.9 km	0.77 kW	13.7 gkm^{-1}	603 h	43.7 km	$0.22
23	2368 s	2.8 km	0.57 kW	13.6 gkm^{-1}	721 h	44.0 km	$0.17
32	1883 s	2.9 km	0.73 kW	14.6 gkm^{-1}	518 h	41.2 km	$0.19
41	1546 s	3.2 km	1.02 kW	15.3 gkm^{-1}	390 h	39.2 km	$0.21
51	4011 s	5.7 km	0.69 kW	14.4 gkm^{-1}	976 h	41.8 km	$0.31
71	2954 s	3.8 km	0.61 kW	13.6 gkm^{-1}	806 h	44.0 km	$0.22
78	2919 s	3.1 km	0.49 kW	13.2 gkm^{-1}	868 h	45.4 km	$0.18
Total	**27674 s**	**40.2 km**	**0.69 kW**	**14.0 gkm^{-1}**	**727 h**	**43.0 km**	**$2.32**

Table 6.2: Performance Summary for the Fuel Only Optimised Controller (1200W)

6.2.3 DI Strategy

The final controller is designed in order to minimise the overall running cost of the fuel cell inclusive of both hydrogen consumption and degradation. As can be seen in Figure 6.6, the DI strategy behaves almost identically to the MFC strategy. As a result, the costs are largely similar; both the fuel consumption and estimated degradation costs are identical to 3 significant figures.

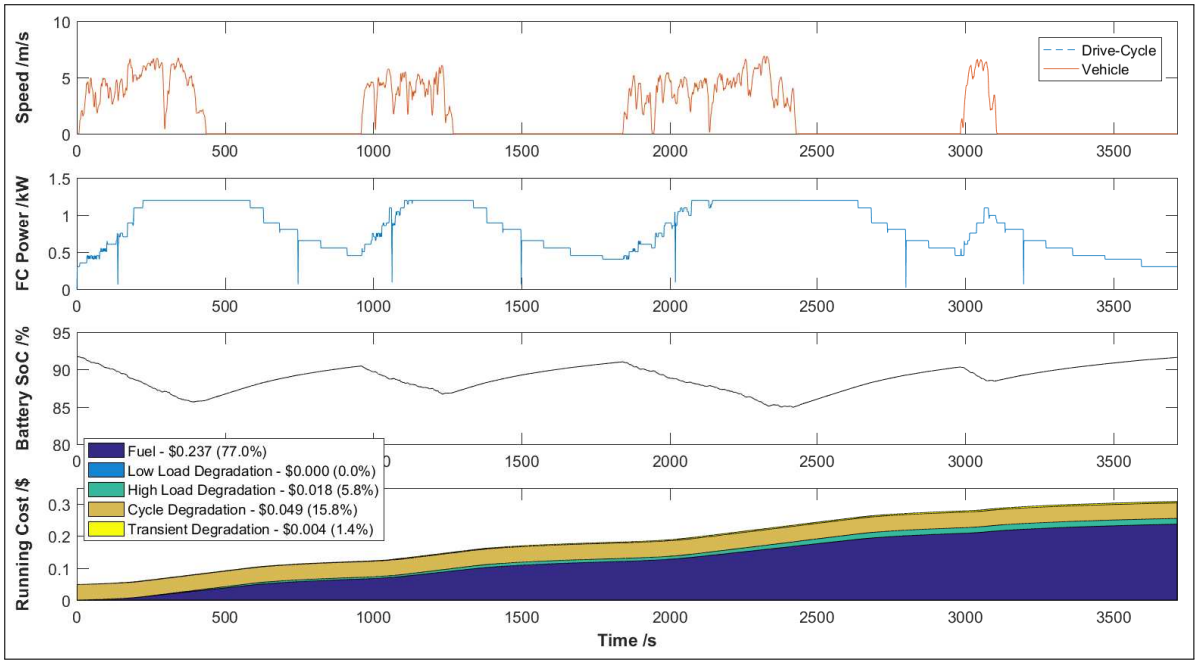

Figure 6.6: Accumulated Running Cost for the Degradation Inclusive Optimised Controller (1200W)

The fact that both controllers behave very similarly suggests that the control authority of the EMS is very low, probably due to the low maximum power of the fuel cell. It is likely that the constraints on the battery voltage are dominating the optimisation process due to the possibility of a sustained journey which will deplete the battery even if the fuel cell is run at maximum power. As a result, the SDP optimised controllers tend to run the fuel cell in such a way as to maintain high battery SoC. If this is the case, they would behave almost identically to each other because they are both subject to the same voltage constraints, and the minimisation of fuel consumption and degradation are having negligible effect on the optimisation.

It can be seen in Table 6.3 that the results for all 10 journeys are again almost identical to those for the MFC strategy. The fuel consumption and total cost of each journey were almost identical. The estimated lifetime varies very slightly however. The overall degradation of the DI strategy was on average approximately 0.2% higher, although it varies between 0.7% better and 1.3% worse depending on the journey. Although this shows the that degradation was not reduced by the SDP algorithm, this result is well within the variation expected due to the stochastic nature of the optimisation process. As has been mentioned before, the SDP gives the statistically optimal policy for the transitional probabilities defined in the Markov chain model, but may or may not give the optimal results for a single journey (or a small sample) when taken in isolation.

No	Duration	Distance	Mean Motor Power	Hydrogen Consumption	Estimated Lifetime	Estimated Range	Total Cost
1	3817 s	4.3 km	0.55 kW	13.7 gkm^{-1}	1044 h	43.7 km	$0.24
4	3715 s	6.0 km	0.72 kW	13.3 gkm^{-1}	874 h	45.2 km	$0.31
12	2146 s	4.7 km	1.02 kW	14.4 gkm^{-1}	490 h	41.7 km	$0.28
15	2315 s	3.9 km	0.77 kW	13.7 gkm^{-1}	603 h	43.7 km	$0.22
23	2368 s	2.8 km	0.57 kW	13.6 gkm^{-1}	723 h	44.0 km	$0.17
32	1883 s	2.9 km	0.73 kW	14.6 gkm^{-1}	522 h	41.2 km	$0.18
41	1546 s	3.2 km	1.02 kW	15.3 gkm^{-1}	390 h	39.2 km	$0.21
51	4011 s	5.7 km	0.69 kW	14.4 gkm^{-1}	970 h	41.8 km	$0.31
71	2954 s	3.8 km	0.61 kW	13.6 gkm^{-1}	806 h	44.0 km	$0.22
78	2919 s	3.1 km	0.49 kW	13.2 gkm^{-1}	865 h	45.4 km	$0.18
Total	**27674 s**	**40.2 km**	**0.69 kW**	**14.0 gkm^{-1}**	**726 h**	**43.0 km**	**$2.32**

Table 6.3: Performance Summary for the Degradation Inclusive Optimised Controller (1200W)

6.2.4 Comparison and Summary

The final cost of fuel and proportional degradation for each controller is summarised in Figure 6.7, where in each group of bars, the left bar refers to the baseline controller, the middle is the MFC strategy, and the right bar is the DI strategy. It can be seen that the performance of all 3 strategies was very similar overall, and the performance of each of the SDP optimised strategies almost identical in every case. The fuel consumption of the baseline strategy was lower for every journey, although the overall cost of the baseline strategy was higher for 7 out of the 10 journeys, mainly due to the degradation cost associated with transient loading. On average, the fuel consumption was 5.1% higher for both optimised strategies compared to the baseline; however, the degradation was on average 21% lower resulting in an overall cost saving of 3.6% and an increased estimated lifetime of around 26.5%.

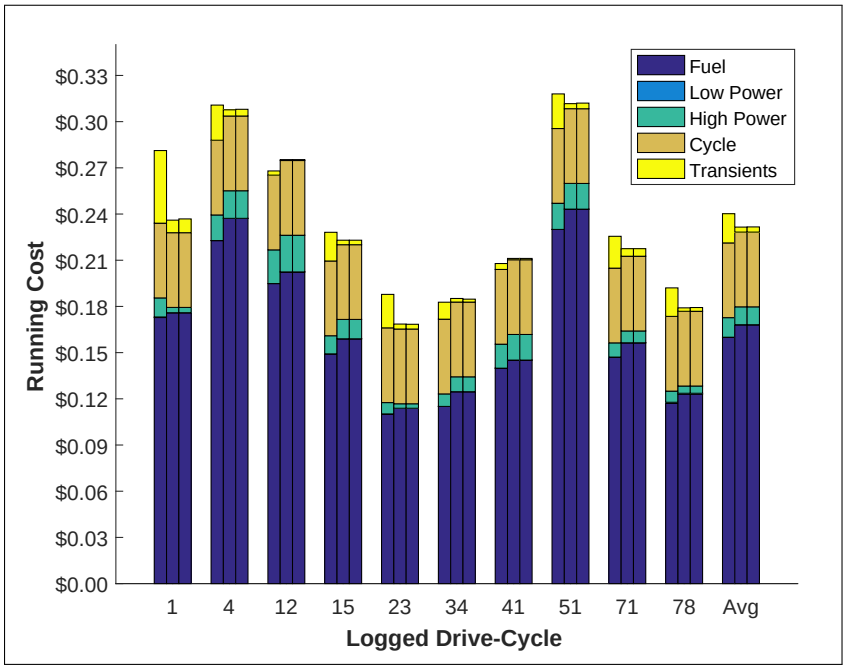

Figure 6.7: Cost Comparison (1200W), Left Bar = Baseline, Middle = MFC, Right = DI

It has already been found at the University of Birmingham [4, 6] that the fuel cell is generally quite undersized even for low speed campus journeys and as a result requires approximately 7 minutes [4] in order to replenish the batteries after the vehicle has been used. As a result, it is fitted with a 10-minute timer relay which keeps the fuel cell operational after the vehicle ignition has been switched off. The low maximum power of the fuel cell results in the gradual depletion of the battery SoC during usage, despite the fuel cell operating at maximum power. This has resulted in a high stack utilisation of 68% [6], maximising the benefit of the fuel cell for a low mass and packaging cost. The downside, however, is that the vehicle has reduced driving range for a single journey because the batteries will almost certainly become discharged before the hydrogen fuel in the tank is used up. If the vehicle is driven non-stop, the batteries will become depleted after approximately 15 to 25 minutes which results in a range of just 8km. However, with the intermittent cycles typically seen on campus, during testing the range has been shown to be approximately 30

to 45 km [6].

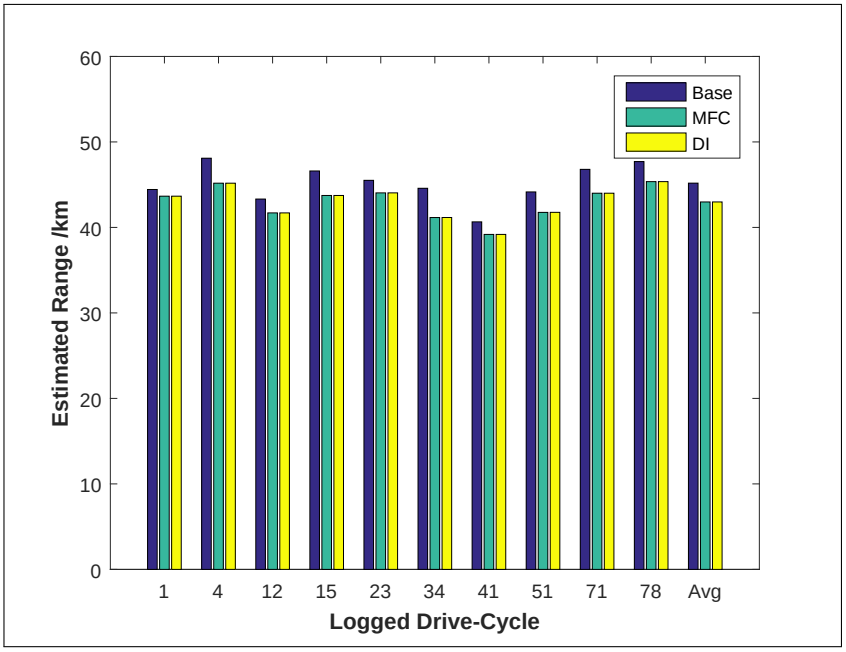

Figure 6.8: Range Comparison (1200W)

This correlates well with the results of the simulations, shown in Figure 6.8, where the average range was around 45km for the journeys tested. In comparison, the SDP controllers only achieved an average range of around 43km, a slight reduction. This is a direct result of the increase in the fuel consumption for these controllers, see Figure 6.9. It can be seen that the fuel consumption for the two SDP controllers was consistently higher than that of the baseline, which was mainly due to these strategies spending less time running the fuel cell at its optimal efficiency operating point.

The low maximum output power of the fuel cell does mean that a relatively simple control algorithm can be used. This control algorithm is designed to run the fuel cell so that the batteries are kept fully charged. Because the maximum power of the fuel cell is too low in order to achieve this during driving, the fuel cell runs at maximum power for a substantial proportion of its time, and the batteries are used to absorb transient loading of the duty cycle. As a result, the fuel cell runs at a fairly steady load, and experiences fewer transients than it would do otherwise with this strategy. Unfortunately, the high power operation results in some degradation of its own, although this is significantly less than would be caused by a continuously changing load. Despite this, the fact that the fuel cell is being run reactively to the vehicle load means that there is still considerable transient degradation when compared to the SDP controllers, which in turn results in a lower average estimated lifetime of the stack, see Figure 6.10.

This is because the baseline strategy manages the SoC using the battery voltage as its only input. In contrast, the SDP controllers vary the load on the fuel cell in response to the SoC. For the DI strategy, one reason for this could be the small effect of the transient load cost, however the MFC strategy behaves in an identical manner, therefore this is unlikely to be the reason. More likely, it is because the SDP algorithm takes the probabilities of future changes in load into account and the battery is less likely to be overcharged if the fuel cell power is only increased once the SoC has fallen.

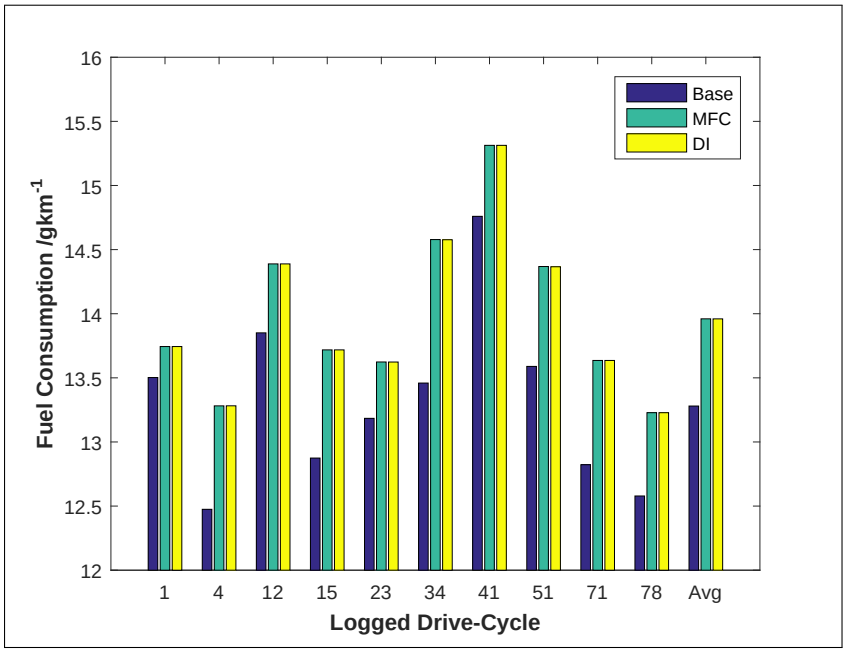

Figure 6.9: Fuel Consumption Comparison (1200W)

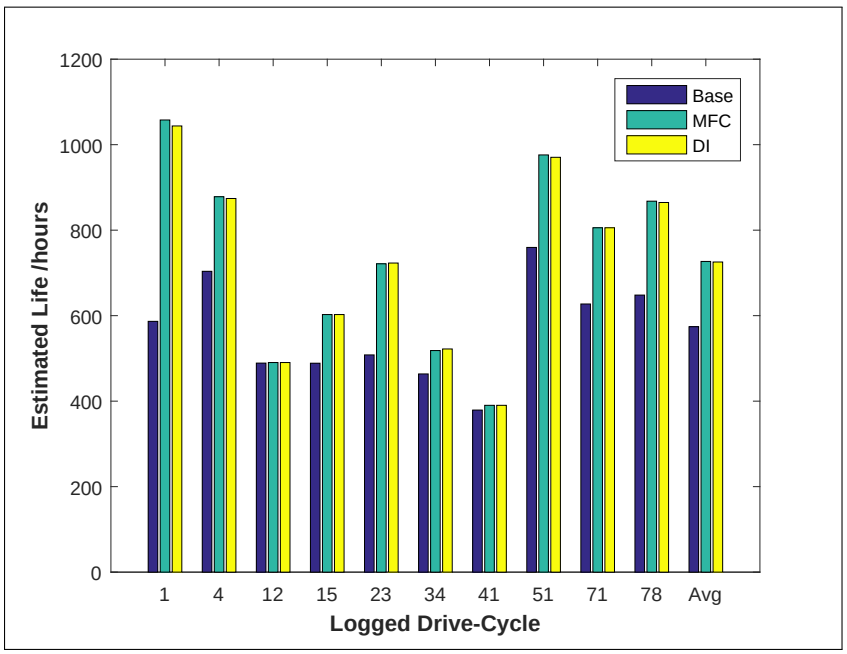

Figure 6.10: Estimated Lifetime Comparison (1200W)

Despite these differences, the SDP optimisation results in a very similar strategy to the baseline controller, and both the MFC and the DI optimisations produce almost identical results to each other. Both of these facts suggest that battery voltage constraints dominating the optimisation. The "soft" constraints are implemented by assigning a very high cost, orders of magnitude higher than the variables to be optimised, to any transition which would result in these limits being exceeded. Under normal conditions this effectively reduces the number of valid actions to those which would keep the battery voltage within

the acceptable range. This is because any action which could potentially allow the constraints to be exceeded will have an extremely high cost compared to that associated with the fuel consumption and stack degradation and therefore should be completely avoided. For any initial state for which there is no action that will prevent the battery voltage limits from being exceeded, the optimal action will be the one that most effectively minimises the penalty for exceeding these constraints, attempting to bring the state back to one within the constraints. In this case, as the costs associated with the main optimisation function are orders of magnitude lower, they will have negligible effect on the overall cost.

Using a 1.2kW fuel cell, it is not possible to guarantee that the battery voltage constraints will never be exceeded under normal use. For every possible state of the vehicle, even those in the middle of the acceptable voltage range, there exists a significant probability that the battery could be depleted (or would be over-charged) even if the fuel cell is run at maximum power. As a result, the high penalty associated with the constraints affects every initial state, and therefore the costs associated with fuel consumption and stack degradation have minimal effect on the optimised strategy. In other words, the control authority of the EMS is too low to ensure the protection of the battery which takes priority over the minimisation of running cost. The optimal strategy is therefore the one that minimises the possibility of the voltage limits from being exceeded whether or not the fuel cell degradation is included in the cost function.

In conclusion, the 1.2kW fuel cell stack used in the Microcab H4 is generally undersized for its application. As a result, it is required to run at full power for almost all of the time that the vehicle is active just to maintain the battery SoC. The current strategy is designed to run the fuel cell in order to keep the batteries fully charged at all times, only letting the battery to act as a buffer when the current demand from the motors exceeds the maximum power of the fuel cell. Due to the low maximum power of the fuel cell, the SDP optimisation results in a similar strategy. The excessive cost associated with the battery voltage penalties dominates the optimisation process, meaning that the optimisation of both fuel consumption and fuel cell degradation have insignificant effect. As a result, the optimised strategies show only a marginal benefit over the current strategy with regards to the minimisation of these targets.

6.3 4.8kW Fuel Cell

It has been observed in previous work by Kendall *et al.* [4] and by Staffell *et al.* [6], and confirmed in the first half of this chapter that the fuel cell in the Microcab H4 is undersized for its duty cycle when it was used at the University of Birmingham. Although the Microcab provided acceptable performance for short trips, extended journeys tended to deplete the battery pack faster than it could be charged by the fuel cell. Therefore, one of the improvements for the next generation of the Microcab, the H2EV, is to increase the maximum power of the fuel cell stack. One of the options for the Microcab H2EV is a 5kW fuel cell. In order to model this, the 1.2kW fuel cell in the Microcab H4 has been scaled-up by a factor of 4 to a nominal 4.8kW. This new model now simulates four identical 1.2kW fuel cells operating in parallel. This will give the EMS much more control authority, and allow for much more flexibility with regards to the load on the fuel cell at any time. As a result of this additional control authority, the optimisation of the fuel consumption and degradation should be improved and the benefits of the SDP optimisation should be clearer.

Each controller has been simulated over the same selection of logged journeys in order to assess its performance with the larger fuel cell stack. Because the size of the stack has been increased, it is also no longer necessary to include the 10-minute stationary period after each logged journey.

6.3.1 Baseline Strategy

It can be clearly seen in Figure 6.11 that the baseline strategy would result in significantly more degradation due to transient loading if the size of the fuel cell were to be increased. This is because the current control strategy aggressively targets a high battery SoC.

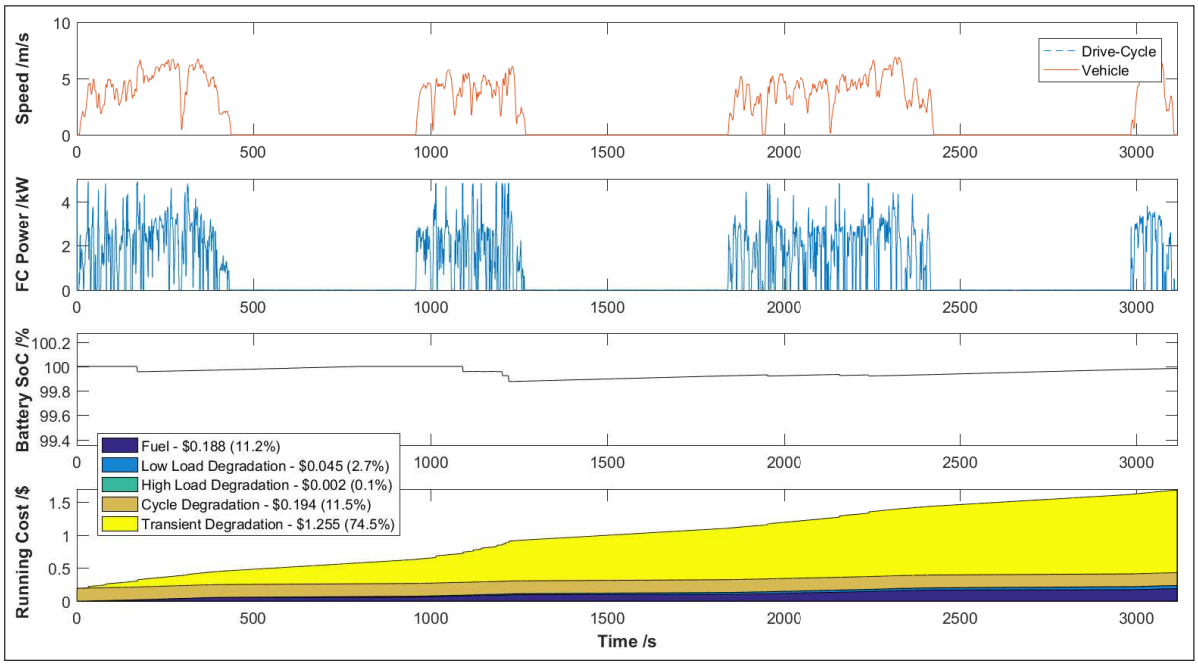

Figure 6.11: Accumulated Running Cost for the Current Microcab Controller (4800W)

The strategy behaves in a similar way to before, increasing the load on the fuel cell as the vehicle accelerates or is moving at a relatively constant speed, and reducing it when the vehicle decelerates or stops. However, the increased size of the fuel cell now means that the battery SoC is managed much more effectively and as a result it can be seen that it does not significantly change throughout the journey. As the SoC does not drop during active periods, the voltage of the battery remains relatively high and therefore the fuel cell does not need to run at the limit of its capacity for prolonged periods of time in order to recharge the battery. This means that the fuel cell is always running reactively to the electrical load from the motors and as a result, it experiences a highly transient loading pattern.

Figure 6.12 shows a close-up of the operating power of the motor, battery pack and fuel cell for a section of the journey shown in Figure 6.11. It can be seen that the fuel cell operating power closely follows the electrical demand from the motors, different only due to the efficiency of the DC/DC converter. This results in very little net current on the battery pack, and a highly transient load on the fuel cell. In fact, the batteries are only really used during an acceleration at the end of this section of the data, where the power drawn by the motor exceeds the capability of the stack for just one second. Obviously, using a 4.8kW fuel cell, this occurs much less frequently than it did with the 1.2kW stack.

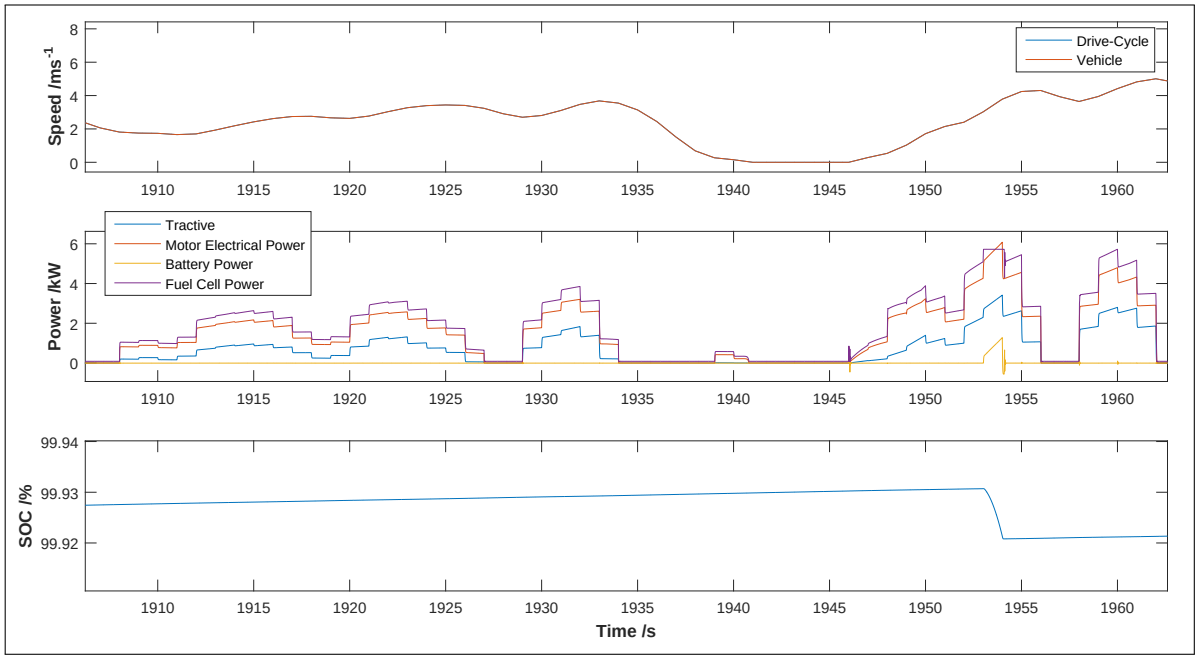

Figure 6.12: Baseline Controller Energy Management (4800W)

Overall, the 4.8kW fuel cell stack operates more efficiently (45%) than the 1.2kW stack (41%); this is because it spends more time operating at part load where it is more efficient. In addition to this, much less energy (99%) is lost due to cycling losses in the battery. This results in an overall 16% reduction in the fuel consumed, reducing the fuel consumption from 12.5g/km to 10.5g/km. Unfortunately, the fuel consumption only counts for approximately 11% of the total cost of this journey. The highly transient load and the increased cost of the stack, result in an estimated proportional cost due to degradation of $1.50, meaning that the overall cost of the journey is increased by around 540% and the estimated lifetime of the stack is now just 139 hours.

The results for all ten of the tested journeys are shown in Table 6.4. It can be seen that the trend continues across the range. The fuel consumption is reduced on all journeys by between 9% and 22%, resulting in an average fuel consumption of 11.3 g/km, 15% lower than the 1.2kW fuel cell. However, the estimated cost of degradation is increased massively by almost a factor of 10 due to the highly transient loading on the fuel cell, reducing the lifetime of the fuel cell down from an estimated 574 hours to just 166 hours. The degradation due to operation at very low loading is also increased; however, the degradation due to operation at high load is reduced by approximately 79%. The reduced lifetime of the stack as well as its increased cost result in an overall cost increase of 318% when compared to the 1.2kW fuel cell.

No	Duration	Distance	Mean Motor Power	Hydrogen Consumption	Estimated Lifetime	Estimated Range	Total Cost
1	3217 s	4.3 km	0.66 kW	11.9 gkm^{-1}	140 h	50.6 km	\$1.69
4	3115 s	6.0 km	0.86 kW	10.5 gkm^{-1}	139 h	56.9 km	\$1.68
12	1546 s	4.7 km	1.41 kW	11.0 gkm^{-1}	223 h	54.6 km	\$0.62
15	1715 s	3.9 km	1.05 kW	10.6 gkm^{-1}	110 h	56.7 km	\$1.16
23	1768 s	2.8 km	0.76 kW	11.5 gkm^{-1}	128 h	52.0 km	\$1.01
32	1283 s	2.9 km	1.08 kW	11.5 gkm^{-1}	188 h	52.2 km	\$0.55
41	946 s	3.2 km	1.67 kW	11.5 gkm^{-1}	178 h	52.3 km	\$0.46
51	3411 s	5.7 km	0.81 kW	11.8 gkm^{-1}	270 h	50.9 km	\$1.04
71	2354 s	3.8 km	0.76 kW	11.4 gkm^{-1}	334 h	52.7 km	\$0.60
78	2319 s	3.1 km	0.62 kW	11.4 gkm^{-1}	137 h	52.7 km	\$1.23
Total	**21674 s**	**40.2 km**	**0.88 kW**	**11.3 gkm^{-1}**	**166 h**	**53.2 km**	**\$10.05**

Table 6.4: Performance Summary for the Current Microcab Controller (4800W)

Obviously, it would be necessary to modify the current strategy if a larger fuel cell were to be fitted to the Microcab in order to achieve acceptable rates of degradation. The current strategy is designed around the current vehicle specification and it is unlikely that the fuel cell would be upgraded without consideration of the EMS. It can be seen from these results that there is potential to improve the fuel consumption of the vehicle if a larger fuel cell were to be used. This is because the current 1.2kW fuel cell runs at full load for a high proportion of its operating time. Fuel cells suffer from significant ohmic losses a high load due to the increased current, but may also suffer from mass transport limitations which can lead to reduced efficiency as well as possible voltage degradation. Using a larger stack allows the fuel cell to be run at a more efficient operating point whilst still providing enough power to maintain the battery SoC.

It is clear however, that the increased rates of degradation would be unacceptable for a production vehicle, and would lead to significant maintenance costs. This is because the EMS no longer takes advantage of the battery pack in order to absorb the transient loading inherent in vehicle duty cycles. It would therefore be necessary to design a strategy which would allow a greater degree of battery SoC deviation during the cycle while still maintaining the fuel economy of using the larger fuel cell. This could dramatically reduce the transient loading on the fuel cell. One way to achieve this would be to set a rate of change limit on the fuel cell load as has been performed previously in the literature by Thounthong *et al.* [109].

6.3.2 MFC Strategy

The results for the MFC strategy are shown in Figure 6.13. It can be seen that the strategy runs the fuel cell near to 800W for much of the time that the vehicle is stationary, increasing to around 2.0kW while the vehicle is moving.

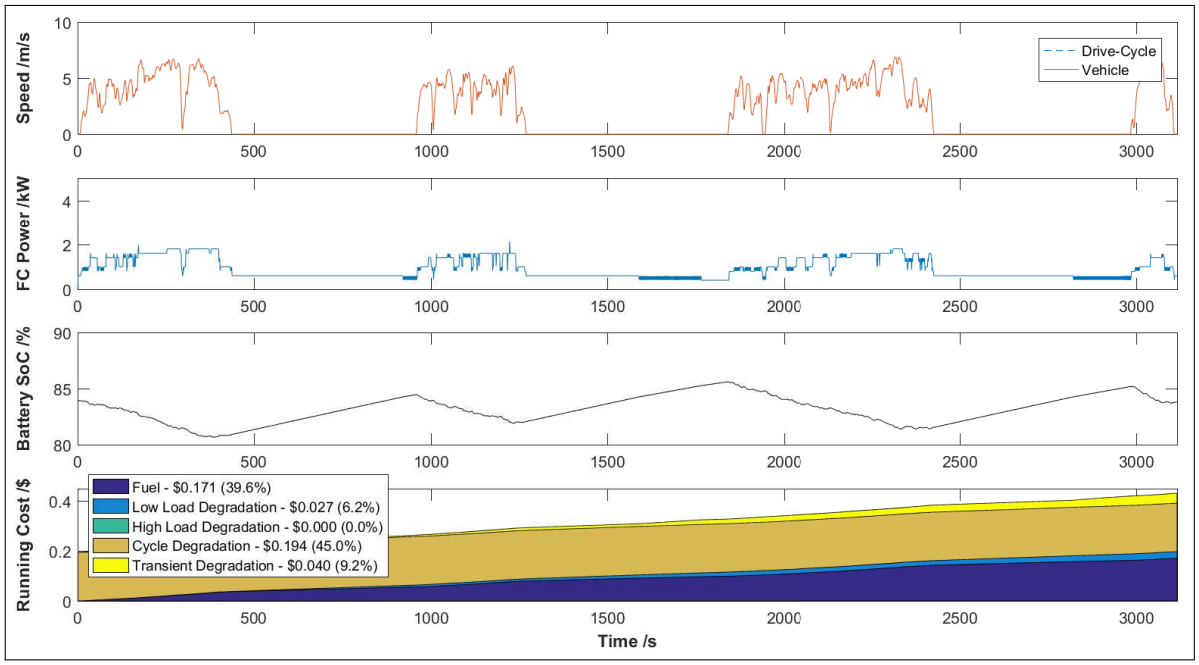

Figure 6.13: Accumulated Running Cost for the Fuel Only Optimised Controller (4800W)

In contrast to the baseline strategy, the battery SoC is much lower throughout the cycle and also tends to fluctuate significantly more. The increased size of the fuel cell allows the MFC optimised strategy to utilise the capacity of the battery to a much greater effect. This is because if high power is required by the motors for a sustained period, the fuel cell would be able to generate much more power in order to prevent the SoC of the battery from dropping too low. It is also worth noting that no downward spikes are present in the fuel cell power, due to the fact that the strategy no longer operates the battery close to its upper voltage constraint. Therefore, sudden deceleration no longer threatens to cause the battery voltage to rise above this constraint and as a result, the load on the fuel cell is more stable.

The fuel cell tends to operate in or around its maximum efficiency for almost the entire journey; allowing the battery SoC to fluctuate in order absorb the transient loading of the duty cycle. This results in a further fuel saving of approximately 9% when compared to the baseline strategy for the 4.8kW fuel cell. Significant degradation savings are also seen; the transient loading is reduced by approximately 96%, and the low load degradation is reduced by approximately 40%. This represents a total reduction in voltage degradation of 83%. Even though this strategy does not take into account any degradation metrics, the improvement is seen due to the tendency to operate the fuel cell close to its maximum efficiency. This operating region results in minimal degradation, and there is also an inherent reduction in transients by running the fuel cell consistently in its maximum efficiency region, rather than reactively to the load.

In contrast to the MFC strategy for the 1.2kW fuel cell, this strategy seems to be more closely related to the vehicle speed and acceleration than the battery SoC. The fuel cell is generally run at high power when the vehicle is moving and lower power during stationary periods. This is likely due to the fact that there is a reduced risk of the battery voltage from exceeding its limits due to the increased control authority of the EMS. This means that the battery SoC can be allowed to fluctuate more in order to act as an energy buffer. This allows the operating point of the fuel cell to be chosen to be the one that is most likely to minimise the long-term fuel consumption.

This strategy is designed to minimise the fuel economy as much as possible, and therefore is constantly updating the operating point in order to do this. Unfortunately, the SDP optimisation requires discretization of the fuel cell operating points. Therefore, there are times when the optimal strategy results in oscillations between two discrete operating points in order to achieve the optimal fuel economy. This results in some unnecessary transient loading on the fuel cell. In addition to this, small spikes in the fuel cell load are seen during active periods, especially when the vehicle accelerates. Although this may give the optimal fuel efficiency, this also results in some unnecessary transient loading.

Table 6.5 shows the results of the MFC across all 10 journeys tested. It can be seen that the degradation is lower than the baseline strategy for all journeys, ranging between 6.9% and 11.4% with an average reduction of 9.9%. This represents a reduction of 27.2% when compared to the SDP strategies optimised for the 1.2kW fuel cell. The biggest cost saving when compared to the baseline strategy however, is the reduction in transient loading which increases the estimated lifetime by a factor of 2.5 times, from 166 hours on average up to 583 hours. This means that the overall cost of the 10 journeys is reduced by 66% when compared to the baseline strategy; however, the increased cost of the fuel cell means that this is approximately 60% higher than the MFC strategy designed for the 1.2kW fuel cell.

No	Duration	Distance	Mean Motor Power	Hydrogen Consumption	Estimated Lifetime	Estimated Range	Total Cost
1	3217 s	4.3 km	0.66 kW	10.7 gkm^{-1}	693 h	55.9 km	\$0.45
4	3115 s	6.0 km	0.86 kW	9.6 gkm^{-1}	797 h	62.7 km	\$0.43
12	1546 s	4.7 km	1.41 kW	9.9 gkm^{-1}	471 h	60.7 km	\$0.36
15	1715 s	3.9 km	1.05 kW	9.7 gkm^{-1}	515 h	61.8 km	\$0.33
23	1768 s	2.8 km	0.76 kW	10.4 gkm^{-1}	507 h	57.8 km	\$0.32
32	1283 s	2.9 km	1.08 kW	10.3 gkm^{-1}	392 h	58.4 km	\$0.31
41	946 s	3.2 km	1.67 kW	10.7 gkm^{-1}	279 h	56.1 km	\$0.33
51	3411 s	5.7 km	0.81 kW	10.5 gkm^{-1}	846 h	57.2 km	\$0.45
71	2354 s	3.8 km	0.76 kW	10.1 gkm^{-1}	614 h	59.5 km	\$0.37
78	2319 s	3.1 km	0.62 kW	10.2 gkm^{-1}	576 h	59.1 km	\$0.36
Total	**21674 s**	**40.2 km**	**0.88 kW**	**10.2 gkm^{-1}**	**583 h**	**59.0 km**	**\$3.70**

Table 6.5: Performance Summary for the Fuel Only Optimised Controller (4800W)

6.3.3 DI Strategy

The results of the DI strategy can be seen in Figure 6.14. It can be seen that this strategy again performs quite similarly to the MFC controller, but with a few important differences. The similar behaviour results from the fact that both controllers have costs associated with the fuel consumption, but also shows that the optimisation of degradation does not directly compete with that of the fuel economy. This is because the fuel cell experiences little degradation at its optimal operating point, and therefore it is beneficial for both fuel consumption and degradation to operate the fuel cell consistently at this point. The most significant difference between the strategies is that the fuel cell tends to operate at an even more consistent load than before, and with no oscillations between discrete operating points. This is likely as a result of the cost associated with the transient loading, which causes the DI optimal policy to show some degree of hysteresis on the fuel cell demand.

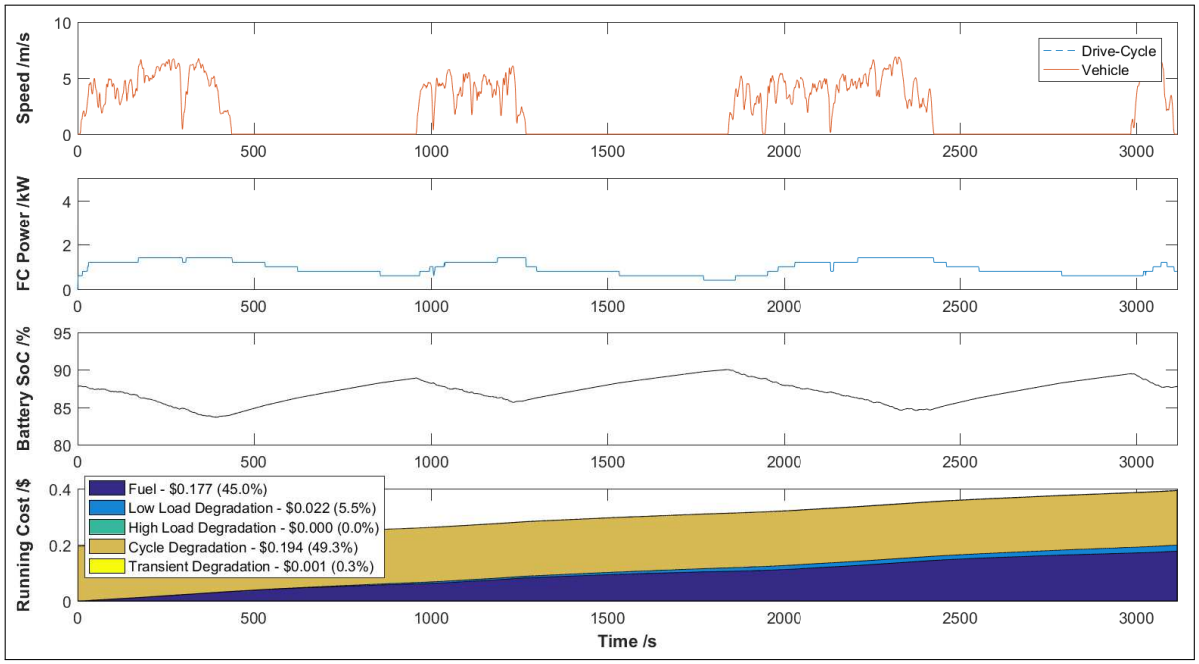

Figure 6.14: Accumulated Running Cost for the Degradation Inclusive Optimised Controller (4800W)

The effect of this cost can be clearly seen at in the region of 1000-1800 seconds into the journey, see Figure 6.15. Firstly, between 1000 and 1250 seconds into the journey, the vehicle is moving. The MFC controller varies the fuel cell power demand dynamically in response to the varying speed and acceleration throughout the trip. In contrast, the DI strategy maintains a relatively steady load on the fuel cell gently adjusting the demand as the trip continues.

The oscillation between operating points performed by MFC strategy is very apparent between approximately 1580 and 1750 seconds, when the vehicle is stationary. The initial load on the fuel cell was at 600W when the vehicle first stopped at around 1250 seconds. As the battery begins to recharge, the load on the fuel cell decreases, down to 400W by the time the vehicle begins to move again at 1820 seconds. Between these separate operating points, there is a region of oscillation lasting approximately 3 minutes. In contrast, the

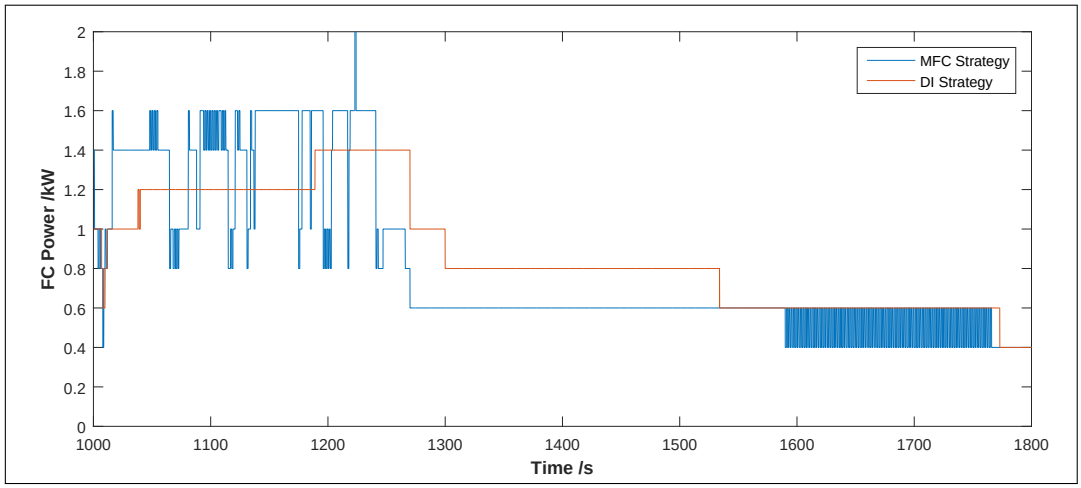

Figure 6.15: Detailed Comparison of MFC and DI Strategies

DI controller stays at the upper operating point during this period, before dropping down permanently to the lower operating point until the vehicle begins to move again. A final point to notice from Figure 6.15 is that the fuel cell demand from the DI controller tends to lag behind that of the MFC controller, acting almost like a low pass filter. This is likely due to the hysteresis in the strategy, as a result, the fuel cell power is generally lower for the DI controller at the beginning of active periods, and higher at the beginning of stationary periods.

For the DI strategy, the overall cost of the journey is estimated at \$0.39 with approximately \$0.18 (45%) due to the fuel consumption. The vast majority of the degradation (90%) was due to the single on/off cycle of the fuel cell, with the majority remaining cost due to fuel cell operation at very low current loading. As no cost is associated with operation at high current loading, this suggests that the 4.8kW fuel cell may now be oversized for the application.

As a result of relatively minor changes to the strategy, the degradation due to transient loading is reduced by 97% when compared to the MFC controller. Along with a 20% reduction in degradation due to low current loading, this results in an overall 17% decrease in degradation for this strategy and a 20% increase in the estimated fuel cell lifetime. As both optimisation targets are largely complimentary, the fuel consumption is only marginally increased (3.7%), meaning the overall estimated cost of the journey is reduced by more than 8%. This suggests that there is a significant benefit to the inclusion of degradation metrics in the cost function despite their relatively small effect on the policy.

It can be seen in Table 6.6 that, similar to the baseline and MFC strategies, the fuel consumption is relatively consistent across all journeys, ranging between 9.9g/km and 11.2g/km. On average, the fuel consumption is 6.9% lower than that of the baseline strategy, and only 3.2% higher than that of the MFC strategy. The degradation however is much lower than for both other strategies due to a massive reduction (95.7% on average compared to the MFC strategy) in transient loading. This results in an overall reduction in the proportional cost of the degradation of 75.7% when compared to the baseline strategy and 14.9% when compared to the MFC strategy. The reduced degradation means that the estimated lifetime of the fuel cell is now 685 hours, 18% higher than the MFC strategy, and the overall cost of the 10 journeys is reduced by approximately 8.9%.

No	Duration	Distance	Mean Motor Power	Hydrogen Consumption	Estimated Lifetime	Estimated Range	Total Cost
1	3217 s	4.3 km	0.66 kW	11.2 gkm^{-1}	934 h	53.6 km	$0.37
4	3115 s	6.0 km	0.86 kW	9.9 gkm^{-1}	958 h	60.5 km	$0.39
12	1546 s	4.7 km	1.41 kW	10.0 gkm^{-1}	526 h	60.3 km	$0.34
15	1715 s	3.9 km	1.05 kW	10.0 gkm^{-1}	566 h	60.0 km	$0.32
23	1768 s	2.8 km	0.76 kW	10.8 gkm^{-1}	560 h	55.5 km	$0.30
32	1283 s	2.9 km	1.08 kW	10.6 gkm^{-1}	430 h	56.8 km	$0.29
41	946 s	3.2 km	1.67 kW	10.7 gkm^{-1}	320 h	56.0 km	$0.30
51	3411 s	5.7 km	0.81 kW	10.9 gkm^{-1}	1021 h	54.9 km	$0.41
71	2354 s	3.8 km	0.76 kW	10.5 gkm^{-1}	729 h	57.0 km	$0.34
78	2319 s	3.1 km	0.62 kW	10.6 gkm^{-1}	700 h	56.5 km	$0.32
Total	**21674 s**	**40.2 km**	**0.88 kW**	**10.5 gkm^{-1}**	**685 h**	**57.2 km**	**$3.37**

Table 6.6: Performance Summary for the Degradation Inclusive Optimised Controller (4800W)

6.3.4 Comparison & Summary

Increasing the stack size from 1.2kW to 4.8kW now means that the battery SoC can be effectively managed by the EMS. This is because the maximum power of the fuel cell stack now exceeds the mean electrical power drawn by the motor during normal vehicle usage. As a result, the range of the vehicle is determined by the capacity of the hydrogen tank rather than the battery capacity and the vehicle no longer requires stationary periods in between journeys in order to recharge its battery pack. The increased fuel cell stack size also now means that it is possible to operate the fuel cell in its optimal operating region for a higher proportional of time which leads to significant fuel saving and a further increase in the vehicles operational range. For the baseline strategy designed for the smaller stack, the fuel consumption is reduced by approximately 16%, and further fuel saving is achieved using the SDP optimised strategy. Figure 6.16 shows a comparison of each strategy.

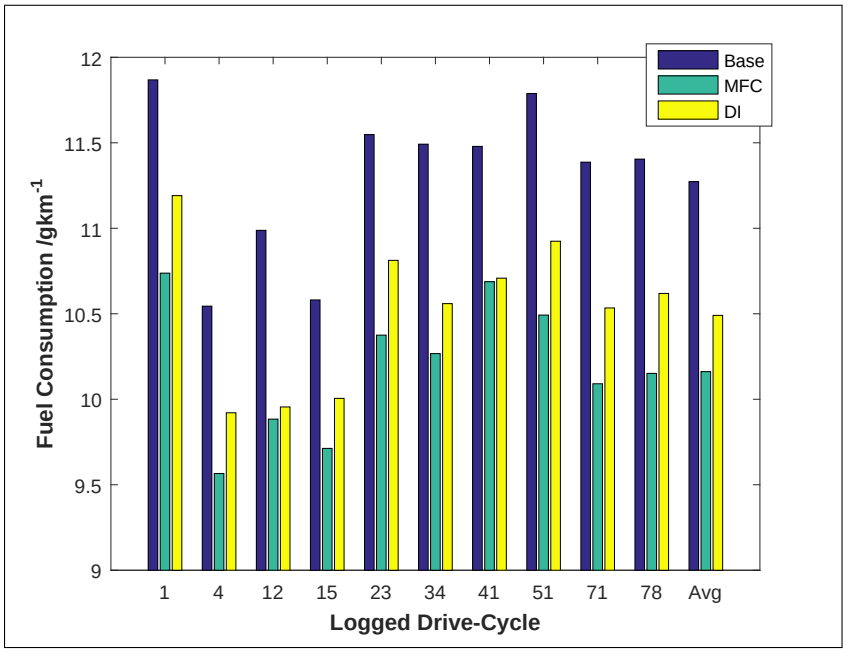

Figure 6.16: Fuel Consumption Comparison (4800W)

It can be seen that the fuel consumption for the MFC strategy is the lowest overall, averaging approximately 9.9% lower than that for the baseline strategy. This is to be expected due to the fact that this strategy has been optimised to minimise the fuel consumption of the vehicle. The DI controller also performs well, achieving an average fuel consumption just 3.2% higher than the MFC. Another advantage of reducing the fuel consumption is that the vehicles range is also increased. This is because the vehicle will be able to travel further on the same mass of fuel. Range can be a particular problem for Fuel Cell Hybrid Electric Vehicles (FCHEVs) due to the packaging concerns of hydrogen storage mentioned in Chapter 1. It can be seen in Figure 6.17, that the range of the vehicle is increased from 53.2km for the baseline controller to around 59km for the MFC controller, an increase of 10.9%. The range for the DI was also only 3.2% lower on average than that of the MFC controller.

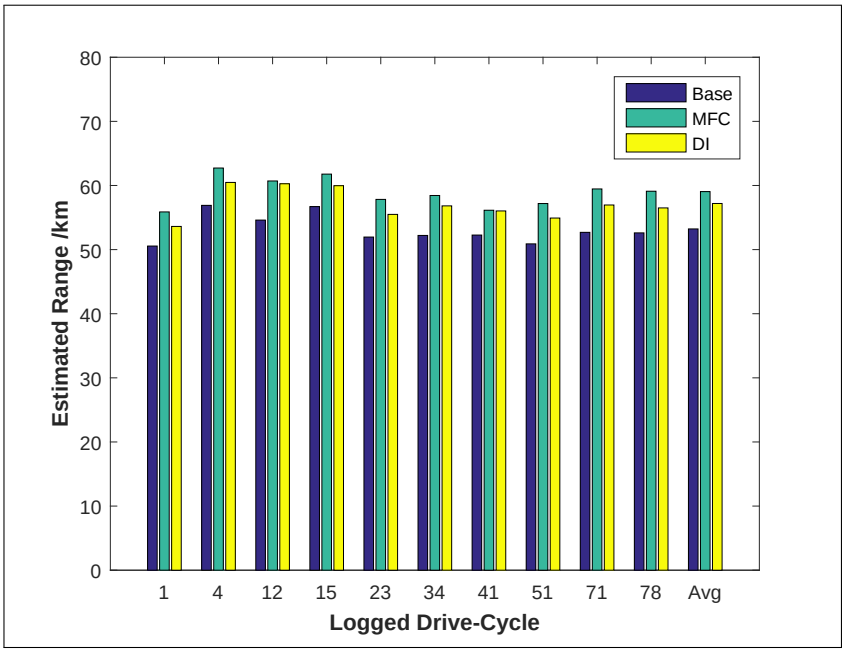

Figure 6.17: Range Comparison (4800W)

However, if the fuel cell size were to be increased to 4.8kW, the baseline strategy would no longer be appropriate due to in a massive increase in fuel cell degradation caused by transient loading. This is because the current strategy aggressively attempts to maintain the battery at a high SoC. Using a fuel cell with a maximum power of 1.2kW results in a strategy which runs the fuel cell at maximum power for a high proportion of its operational time; effectively limiting the transient loading on the fuel cell. However, a larger fuel cell is able to maintain the battery SoC during typical usage patterns, and therefore runs almost entirely reactively to the current demand from the motors so that the net battery current is approximately zero. As a result, the battery is no longer used as an energy buffer and the fuel cell absorbs much of the transient loading associated with urban duty cycles.

It would be possible to generate a new heuristic strategy which takes into account the change in system performance characteristics associated with a larger fuel cell. This could be achieved by various methods, one of simplest being to limit the rate of change of fuel cell load [109]. This would reduce the transient loading on the fuel cell significantly, using the batteries more effectively to manage the transient nature of the duty cycle. However, this type of strategy would require significant testing in order to choose the maximum rate of change of power in order to achieve optimal performance. Too high a limit and the transient degradation would not be reduced significantly, but too low a limit and the SoC would not be effectively sustained. Further performance gains could be made adding additional rules to the controller, for example, by favouring more efficient operating points or allowing a higher rate of change on the fuel cell load if the SoC was particularly low. However, this would further increase the complexity of the strategy and therefore development and testing time. If the powertrain were to be changed again or the duty cycle varied, these parameters would need to be re-tuned.

In contrast, the SDP optimisation process takes into account these changes and it is relatively trivial to re-optimise the strategy for a different powertrain design or duty cy-

cle. It may even be feasible to continually re-optimise the controller on board the vehicle, given an initial optimisation performed offline. Not only this, but the resultant policy is not constrained by heuristic rules, which may or may not be applicable to the particular configuration or duty cycle. It is therefore perhaps unfair to compare the results of the SDP optimised strategies directly to the current strategy which was designed for an earlier version of the vehicle, especially in regard to the degradation associated with transient loading.

Figure 6.18, therefore, shows a comparison of the costs associated for both SDP control strategies, but not that for the baseline strategy. In this chart, the left bar represents the MFC controller, and the right bar in each group is the DI controller. It can be seen that the fuel consumption of the MFC controller is consistently lower than that of the DI controller. This is to be expected as minimisation of the fuel consumption is the sole target of the MFC optimisation. However, the fuel consumption only represents approximately 33% of the estimated cost on average. The other two thirds are represented by the proportional cost of the fuel cell degradation.

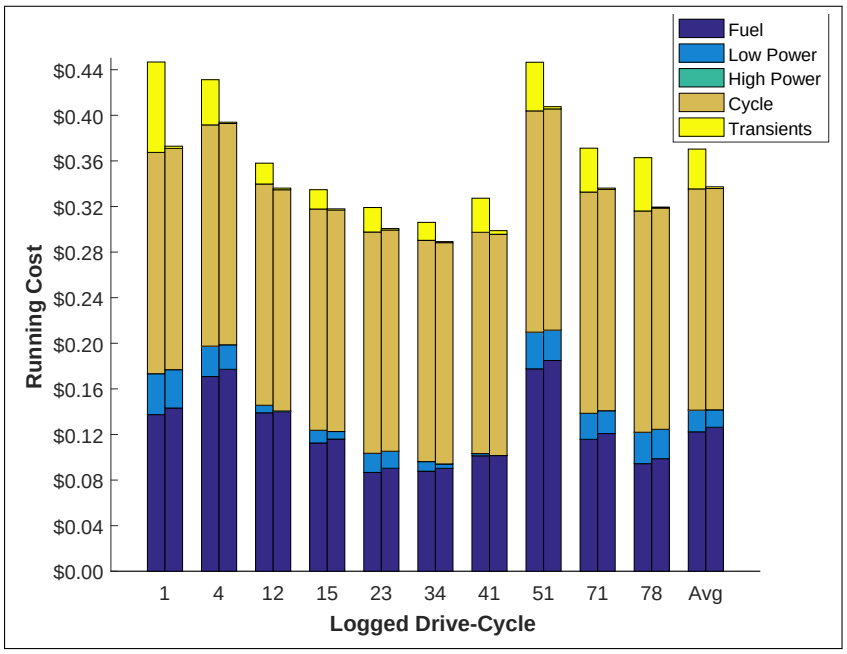

Figure 6.18: Cost Comparison (4800W), Left Bar = MFC, Right = DI

The vast majority of the degradation for both strategies is due to the start-up and shut-down of the fuel cell. For the MFC controller, this represents on average 52.4% of the cost of each journey, and for the DI this is even higher at approximately 57.6%. Obviously, this must occur at least once for each journey and therefore the voltage degradation due to this method cannot be reduced any further. For the MFC strategy it may be possible to save additional fuel by shutting down the fuel cell during stationary periods, however for this fuel cell, this would increase the degradation massively and is also unlikely to be performed in reality. For this reason, the fuel cell has been assumed to be running throughout each test, and a single on/off cycle is included as an unavoidable degradation cost.

The most significant differences between the strategies are the ageing due to transient loading and low load operation. The DI strategy optimisation results in an average reduction in degradation of 95.7% for transient loading and 19.1% for low load operation. As a result, the degradation costs of the DI strategy are approximately 14.9% lower, giving an overall cost reduction of around 8.9% on average when accounting for the 3.2% increase in fuel consumption. The reduced degradation means that the fuel cell stack is estimated to last an additional 102 hours (18%) on average, see Figure 6.19. There is obviously a huge benefit to the inclusion of the degradation metrics into the cost function for the SDP optimisation.

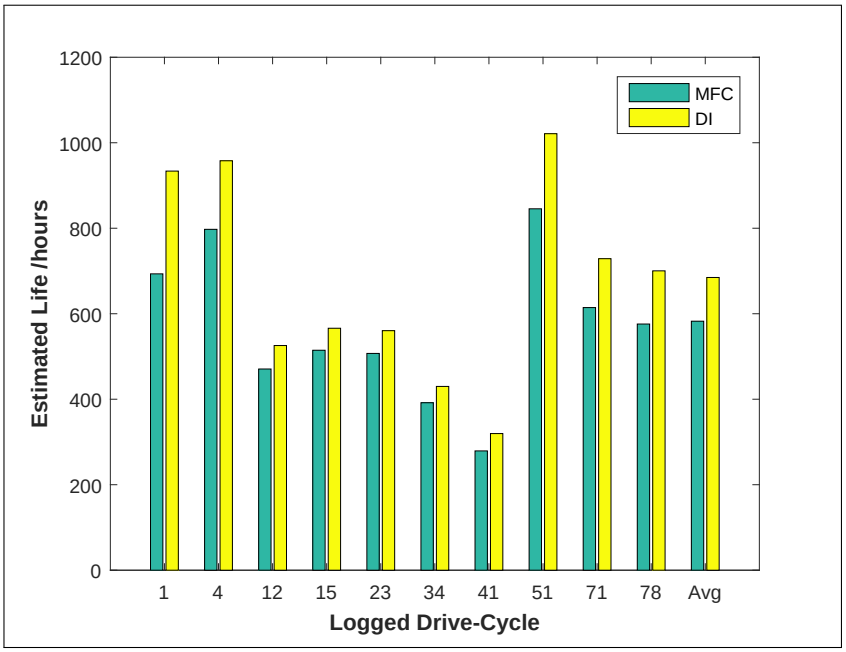

Figure 6.19: Estimated Lifetime Comparison (4800W)

Comparing to the results of the SDP optimised strategies for the 1.2kW fuel cell stack, it is possible to see that the fuel consumption has been reduced significantly by around 27.2% for the MFC controller and by around 24.9% for the DI controller. Similar to the results for the baseline controller, this is most likely due to the running of the fuel cell at a more efficient operating point. Using the 1.2kW fuel cell, the average operating efficiency was 41%, but using the 4.8kW stack, the efficiency increased to above 52%. In addition to this, there was a 27% reduction in the energy lost to cycling the battery for the DI strategy and 60% reduction for the MFC strategy although this only represents relatively small saving overall.

Both strategies saw an increase in the cost of the degradation however, mainly due to the increased cost of the stack. For the MFC strategy, for both stack sizes, approximately 80% of the degradation was due to the single on/off cycle of the stack. The increased stack size reduced the degradation due to high load operation down to zero from 0.193%, but introduced a low load degradation of 0.079% and increased the degradation due to transients from 0.055% to 0.145%. Overall, the increase in low load degradation and transient degradation was a little more than offset by the reduction in high load operation meaning that the total degradation seen across all ten journeys was reduced from approximately 1.05%

for the 1.2kW fuel cell, to around 1.03% for the 4.8kW stack. However, the increased size of the stack (by a factor of 4) means that the total cost of the degradation was increased by a similar amount, from $0.64 to $2.48.

For the DI strategy, the increased control authority and the optimisation of the degradation resulted much less transient degradation (0.006%), and slightly less low load degradation (0.064%). As a result, the total estimated degradation was just 0.88% across all ten journeys for the 4.8kW stack, representing a reduction of around 17% compared to the 1.2kW stack. However, the increased cost of the 4.8kW stack meant that the projected cost due to degradation was increased by approximately 3.3 times from $0.64 to $2.11.

Although the degradation rates for both strategies were slightly lower, the estimated lifetimes of the stacks are shown to be slightly shorter. For the MFC strategy, the lifetime reduced from 727 hours to 583 hours (19.8%), and for the DI strategy the projected lifetime was reduced from 726 hours to 685 hours (5.6%). This is due to the 10-minute recharging period included for the 1.2kW stack simulations. During this period, the vehicle is not being used for transport purposes, and therefore it is perhaps more appropriate to compare the useful life of each stack. If the 10-minute recharging period is not included as part of the useful operational time (but the degradation accumulated is included as it is necessary to recharge the battery), the estimated useful lifetime for the 1.2kW stack is around 569 hours for the MFC strategy and 568 hours for the DI strategy. The 10-minute recharging time is not required for the 4.8kW stack, and therefore the useful lifetime is unchanged. In this case, the estimated lifetime of the 4.8kW stack is approximately 2.4% higher for the MFC strategy and 20.5% for the DI strategy when using the larger stack.

Finally, it must be noted that for both optimised strategies, the 4.8kW fuel cell was never run in the high power region. In fact, the peak demand across all journeys was 3.8kW for the MFC strategy and just 3.2kW for the DI controller. In addition to this, some degradation was seen due to operation in the low load region for both controllers. This is the opposite situation to the 1.2kW fuel cell and suggests that the larger fuel cell is now somewhat oversized for the vehicle's duty cycle. Although the increased fuel cell size shows better fuel economy and a longer lifetime, the increased size directly results in an increase in the cost of the stack. The running cost of the vehicle would therefore be reduced by using a smaller stack. The optimal stack size, which minimises the running cost of the vehicle while still maintaining the battery SoC during long journeys is likely to lie somewhere in between 1.2kW and 4.8kW. This is investigated more thoroughly in Chapter 7.

In conclusion, all three controllers show effective management of the battery SoC due to the introduction of a larger fuel cell. This increases the control authority of the EMS enough so that the vehicle is able to operate continuously without depleting the battery pack. However, changes to the vehicle specification or to the duty cycle often require the EMS to be re-optimised. For a heuristic strategy such as that currently used in the Microcab H4, this can mean significant testing is required, and often means new rules are required in order to combat performance issues introduced by the new specification. One of the advantages of the SDP technique is that it is relatively trivial to re-run the optimisation of a SDP strategy in order to account for these changes. As a result of increasing the fuel cell size from 1.2kW to 4.8kW, the current strategy employed by the Microcab is no longer viable due to significant transient loading on the fuel cell. The SDP algorithms, however, are able to take advantage of this new degree of control authority in order to effectively manage the battery SoC and allow for optimisation of their respective cost functions.

Degradation of the fuel cell accounts for a substantial proportion of the running cost of a fuel cell vehicle due to the high cost of the stack as well as its relatively poor reliability when compared to conventional technology. As a result, the DI control strategy showed significant improvement on current state-of-the-art EMSs due to a 14.9% reduction in projected degradation cost for only a 3.5% increase in fuel consumption. As a result, the running cost of this strategy has been found to be on average 8.9% lower than that of a strategy optimised solely for minimisation of the fuel consumption. The DI controller also shows a 17.5% increase in the projected lifetime of the fuel cell. The vast majority of this increase in projected lifetime is due to a significant (95.7% on average) reduction in the transient loading experienced by the fuel cell. Careful examination of the behaviour of the strategy shows that this has been achieved by the introduction of hysteresis in the fuel cell load demand by the EMS.

Chapter 7

Optimisation of Hybrid Component Sizes

This chapter examines the effect of changing the fuel cell maximum power and the battery capacity on the performance of the vehicle with regards to the fuel consumption and range, and the degradation of the fuel cell and its anticipated lifetime.

The Stochastic Dynamic Programming (SDP) algorithm has been used to generate an Energy Management Strategy (EMS) for each combination of fuel cell size and battery capacity. Each of these strategies has been subsequently simulated over the same 10 journeys used in the previous chapter, in order to assess the performance of the vehicle.

It is found that the running cost of the vehicle is minimised by using the smallest possible fuel cell stack that will satisfy the average power demand of the duty cycle and that increased battery size up to double the current capacity results in reduced fuel consumption and degradation.

7.1 Introduction

One of the advantages of SDP is that the optimisation process results in a strategy which is statistically optimal for the vehicle. This means direct comparisons can be made between different system designs in order to assess their potential performance benefits. Many sizing exercises in the literature use identical control strategies for comparing different system architectures. At first glance, this would seem to be the fairest way to make a comparison, however the control strategy can have a significant effect on the results. For example, Rousseau *et al.* [5] find that by increasing the minimum fuel cell power threshold in their control strategy, more energy tends to be lost due to the fuel cell efficiency losses (due to generally higher operating point), and less energy lost during braking (due to a generally lower battery State of Charge (SoC)). As a result, a different combination of fuel cell maximum power and battery size is preferable when compared to a lower threshold.

In contrast, the SDP optimisation process can be performed for each individual system design, producing a strategy which will give the statistically optimal performance for that design. Each resultant strategy will therefore be unique, but will represent the best-case performance of its respective vehicle specification. In this way, a system design which is focussed on minimal battery cycling (for example, by using a small battery) can be directly compared to another focussed on good fuel cell operating point efficiency (for example, by using a larger battery) without concern of any bias due to the choice of control strategy.

In order to perform this analysis, almost 1300 simulation journeys have been performed, representing 128 different system configurations; varying the maximum power of the fuel cell and the capacity of the battery. For each system configuration, the reduced vehicle model has been simulated in order to produce the transitional probability and cost matrices, which have then been solved using SDP as described in Chapter 5. Each vehicle has then been simulated over the same 10 drive-cycles used in the previous chapter in order to calculate the typical fuel consumption, range, fuel cell lifetime and operating cost when used on a university campus.

Due to the considerable number of system designs analysed, and the varied sizes of the battery, the input states have been modified slightly from the values mentioned in Table 5.1. The primary reason for this is to ensure that the range of input states is representative of the full range of operating states that the vehicle will enter. The vehicle speed and acceleration states have not been modified due to the fact that the duty cycle is unchanged, however the range of the battery SoC and fuel cell power demand have been increased. The range of battery SoC has been increased because a larger capacity battery is able to provide more current at the same SoC, see Figure 3.13. As a result, larger battery capacities are able to run to a lower overall SoC while still providing the same tractive power. In order to prevent the optimisation process from taking too much time, the spacing of each has been marginally reduced so that the overall number of states is approximately the same.

Parameter (Unit)	Minimum	Maximum	Spacing
Vehicle Speed, v (ms^{-1})	0	15	1
Vehicle Acceleration, a (ms^{-2})	-3	3	1
Battery SoC, H (%)	40	100	1
EMS Demand, P_{EMS} (W)	0	P_{max}	$P_{max}/20$

Table 7.1: Controller State Definition

For comparison purposes, both SDP strategies have been simulated. The Minimal Fuel Consumption (MFC) strategy represents recent work in the literature where the strategy is optimised purely to minimise the fuel consumption, and the fuel cell Degradation Inclusive (DI) strategy represents the novel strategy designed to concurrently minimise the fuel cell degradation alongside the fuel consumption. The comparison of these results not only demonstrates the benefits of the novel DI strategy presented in this thesis, but also allows the strategy characteristics associated with the optimisation of the degradation to be identified separately from those associated with minimisation of the fuel consumption.

7.2 Sweep of Fuel Cell Maximum Power

It has been found in Chapter 6 that the 1200W fuel cell fitted to the Microcab H4 is relatively underpowered for a campus duty cycle, and tends to drain the battery while the vehicle is in use. In contrast, the 4800W fuel cell planned for the Microcab H2EV is somewhat oversized for journeys tested; leading to fuel cell degradation caused by operation at very low current loading, and increased running cost. Therefore, a sweep of various fuel cell sizes has been performed in order to find the optimal fuel cell maximum power output required for campus usage patterns. The following values have been tested;

Parameter (Unit)	Minimum	Maximum	Spacing
Fuel Cell Maximum Power, $P_{FC,max}$ (W)	600	4800	600
Battery Capacity, C_n (Wh)	2112	2112	-

Table 7.2: Fuel Cell Sweep Values

As in the previous chapter, the assumption has been made that the fuel cell maximum power output is modified by scaling the output current, so that the nominal voltage is kept the same. This has been achieved by assuming a number (0.5 to 4) of stacks running in parallel. Although in reality, the performance characteristics of the stack (efficiency, degradation rates) may be affected by its size, this would significantly increase the complexity of the sizing exercise, and is likely to have only a small effect on the overall results when compared to the difference in stack size.

It is expected that as the fuel cell stack size is increased, the performance of each strategy will be improved due to the increased control authority of the EMS. The EMS should be able to maintain the battery SoC as long as the fuel cell is at least equal to the average power demand over the journey, and this would represent the minimum heuristic design criteria for the fuel cell size. It is likely that by over-sizing the fuel cell above this minimum level, that the fuel cell will be able to run at a more optimal efficiency region, improving both the fuel consumption and reducing the degradation, and therefore reducing the overall running cost despite the increased cost of a larger fuel cell. As the fuel cell maximum power is increased further, the benefits are likely to become gradually less significant, and at some point, the increased cost of the fuel cell will become the dominant factor. This will lead to the calculation of an optimal size of fuel cell for this type of duty cycle.

7.2.1 SoC Sustenance

In this work, battery SoC sustenance is managed by the EMS through the use of constraints on the optimisation. These constraints are implemented using a very high cost penalty for exceeding them, which is orders of magnitude higher than the values to be optimised. This is known as a "soft constraint", and therefore it is possible to breach the constraint by incurring a very high cost penalty. In general, the optimisation will avoid the possibility of exceeding these limits when at all possible, however, if this is unavoidable for any reason, the penalty associated with avoiding the constraints will tend to dominate the optimisation process, leading to poor performance with regard to the targets to be optimised.

As in Chapter 6, the SoC has been initialised individually for each controller so that minimal net change is seen over the cycle. The reason for this is due to the way that the battery SoC is managed. As result, there is no explicit target value and each controller will find its own "natural equilibrium" in order to produce the desired charge-sustaining behaviour. Therefore, starting both controllers from the same initial value will generally lead to different final values. Accounting for this change in SoC is notoriously difficult.

Another way of thinking about this is to consider the battery SoC range as a feature of the control strategy rather than an input to it. As long as each strategy shows negligible net SoC change over the cycle the results are comparable with regards to fuel consumption and fuel cell degradation due to the fact that the stored energy in the battery is unchanged. Any differences resulting from the different overall SoC, such as battery cycling efficiency, are representative of the decisions that the optimisation process has taken in order to optimise its cost function.

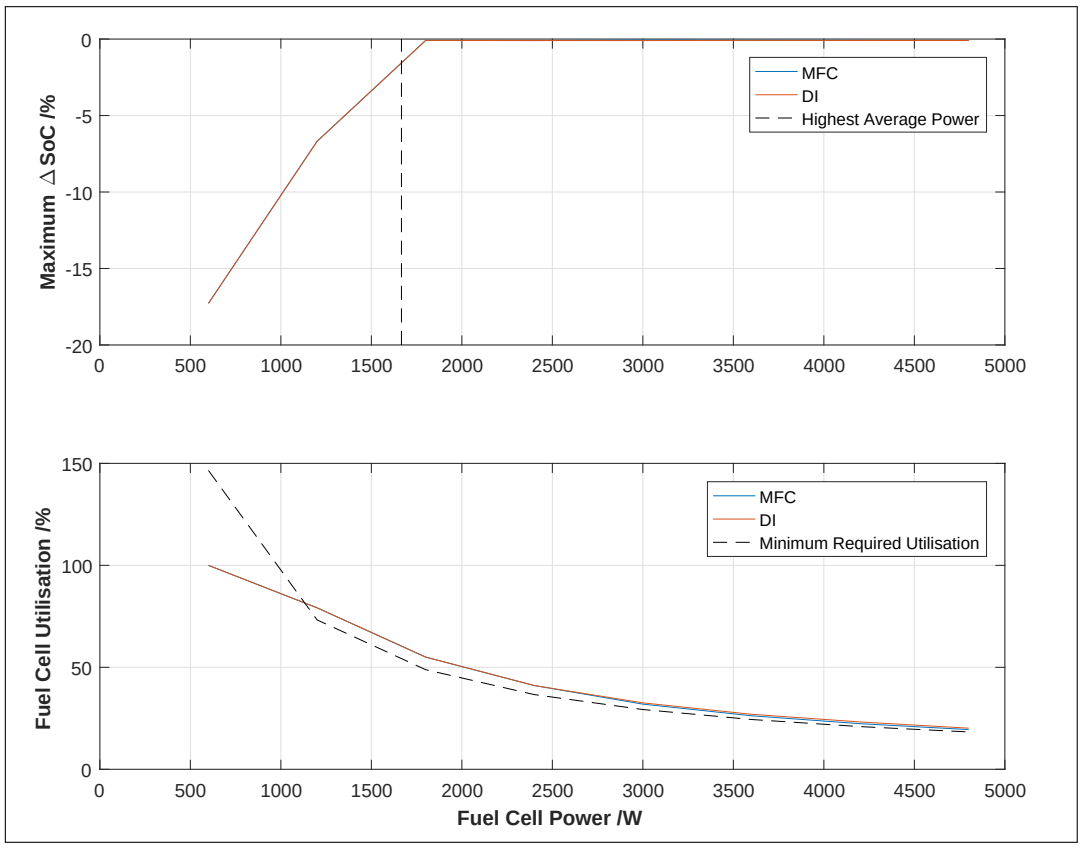

Figure 7.1: SoC Sustenance vs. Fuel Cell Size

Figure 7.1 shows the maximum change in SoC over a single journey and average fuel cell utilisation over the set of 10 journeys for each size of fuel cell. It can be seen clearly from the top plot that a fuel cell of 1800W is required for every journey to be completed without a net fall in battery SoC. This is unsurprising; the highest average power over a single journey was around 1650W, which shown as a dashed black line. Therefore, care should be taken when comparing the results of simulations of fuel cells below this size. The second plot shows the fuel cell utilisation. This is the average power supplied by the fuel cell, divided by its maximum power. As would be expected, the utilisation decreases as the maximum power of the fuel cell increases. The black dashed line in this plot represents the fuel cell utilisation required in order to meet the average electrical power demand over the complete set of journeys (approximately 880W).

It can be seen that a fuel cell of 600W is unable to maintain the battery SoC for this type of usage pattern, despite running at full power throughout every journey. In fact, a utilisation of 146% would be required in order to meet the overall average power demand, which is obviously not possible. As a result, the battery SoC falls by an average of 9.1% on each journey and therefore the fuel consumption and fuel cell degradation are likely to be under-estimated when compared to that of larger fuel cells.

A fuel cell of 1200W requires a utilisation of at least 73% in order to meet the average power requirement over the set of journeys, and therefore the 1200W fuel cell would likely be able to complete the set of journeys as a whole. However, there is variation in the average power requirement of each journey when considered individually, and two of the journeys have a requirement of more than 1200W. Therefore, a vehicle with a 1200W fuel cell would experience a drop in SoC for these two journeys even if it ran at maximum power throughout. In this analysis, each journey has been examined individually and therefore the average change in SoC for the 1200W is slightly below zero due to SoC drops over these two journeys. Again, this means that care must be taken when comparing to the results of larger fuel cells as the fuel consumption and fuel cell degradation are likely to be underestimated.

The highest average power demand over a single journey was approximately 1650W, which is represented by the black dashed line in the top plot. This represents the lowest peak power requirement of the fuel cell in order to complete every journey without requiring additional energy from the battery. It can be seen that all vehicles fitted with a fuel cell larger than this value were able to complete every journey without a net change in battery SoC. As a result, these results are directly comparable.

It can be seen that both SDP strategies perform almost identically with regards to SoC sustenance and overall fuel cell utilisation. This is important because it shows that the constraints are working as expected and dominating the optimisation for smaller fuel cells. For larger fuel cells, the SoC is being managed successfully and therefore it has been possible to simulate the journeys with zero net change in battery SoC. This means that the energy stored in the battery is unchanged and the fuel consumption and degradation figure are representative of the long-term average values for both controllers.

Figure 7.2 shows the minimum, maximum, and average initial SoC of the battery across all journeys for each size of fuel cell. It can be seen that both strategies are almost identical up to 2400W. Above this, the DI controller tends to maintain a slightly higher SoC in general, although up to 4200W, the minimum value is the same as the MFC controller. In general both policies tend to utilise a lower SoC as the size of the fuel cell increases.

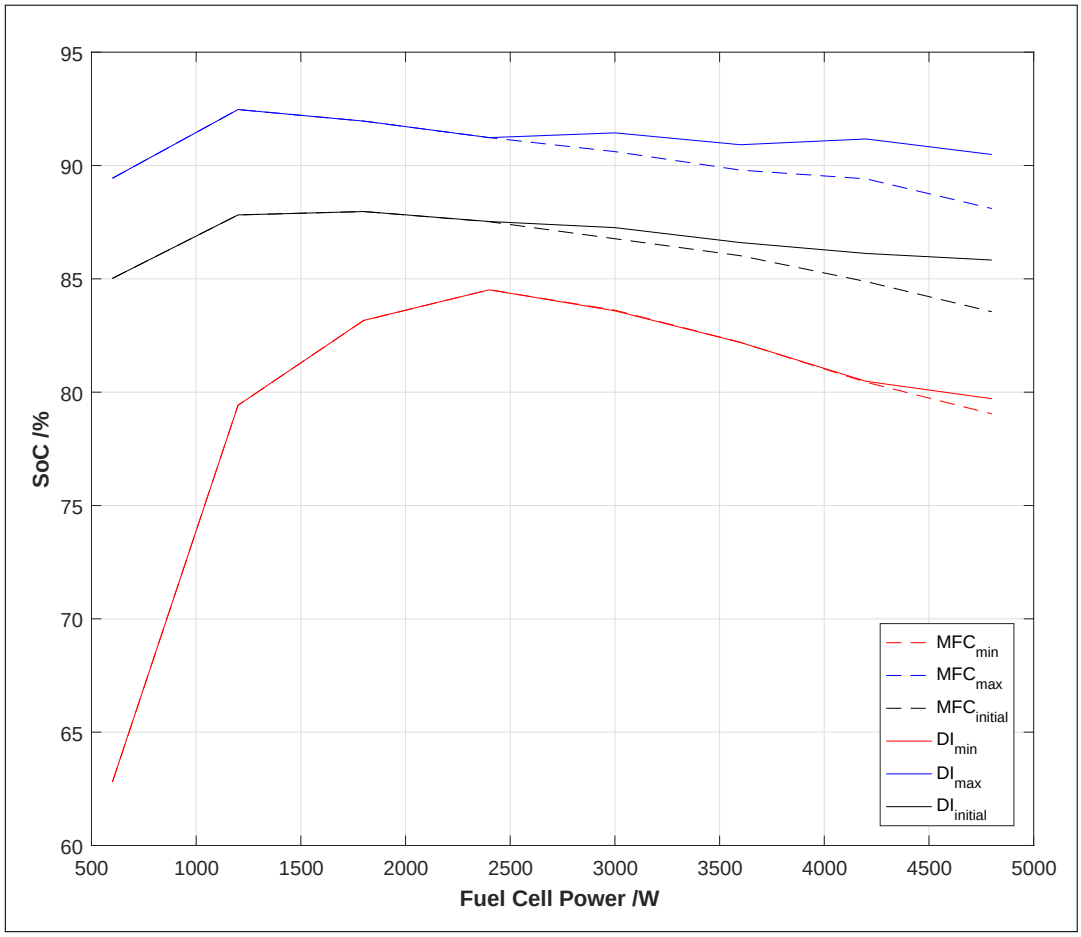

Figure 7.2: Minimum, Maximum and Initial SoC vs. Fuel Cell Size

Both strategies perform almost identically up to a fuel cell maximum power of 2400W. This is likely due to the fact that the battery voltage constraints are dominating the optimisation process, suggesting that a fuel cell power of at least 2400W, and preferably above this value, is required for the optimisation to produce meaningful results. As described in the previous chapter, if the fuel cell is undersized, the battery voltage constraints will tend to dominate the optimisation.

As the maximum power of the fuel cell increases, the battery SoC can be allowed to drop lower without the risk of the lower battery voltage constraint being compromised. This is because, if required, a larger fuel cell can supply more power should a sudden acceleration occur. This is beneficial because it allows the EMS to operate further from the upper voltage constraint, and with a larger SoC range. This means that more operating points are able to be used without compromise to the battery voltage constraints and in effect the control authority of the EMS is greater.

For the DI strategy however, the initial value and maximum values do not fall as quickly as its minimum value or that of the MFC strategy, and hence it tends to utilise a larger SoC range than that of the MFC strategy. This is likely caused by the hysteresis effect of this strategy as described in the previous chapter. The reluctance to change its operating point in order to avoid transient degradation causes the DI strategy to have a slower response to changes in load. As a result, the battery is required to act as an energy buffer and a greater range in the SoC utilisation is observed.

7.2.2 Fuel Consumption

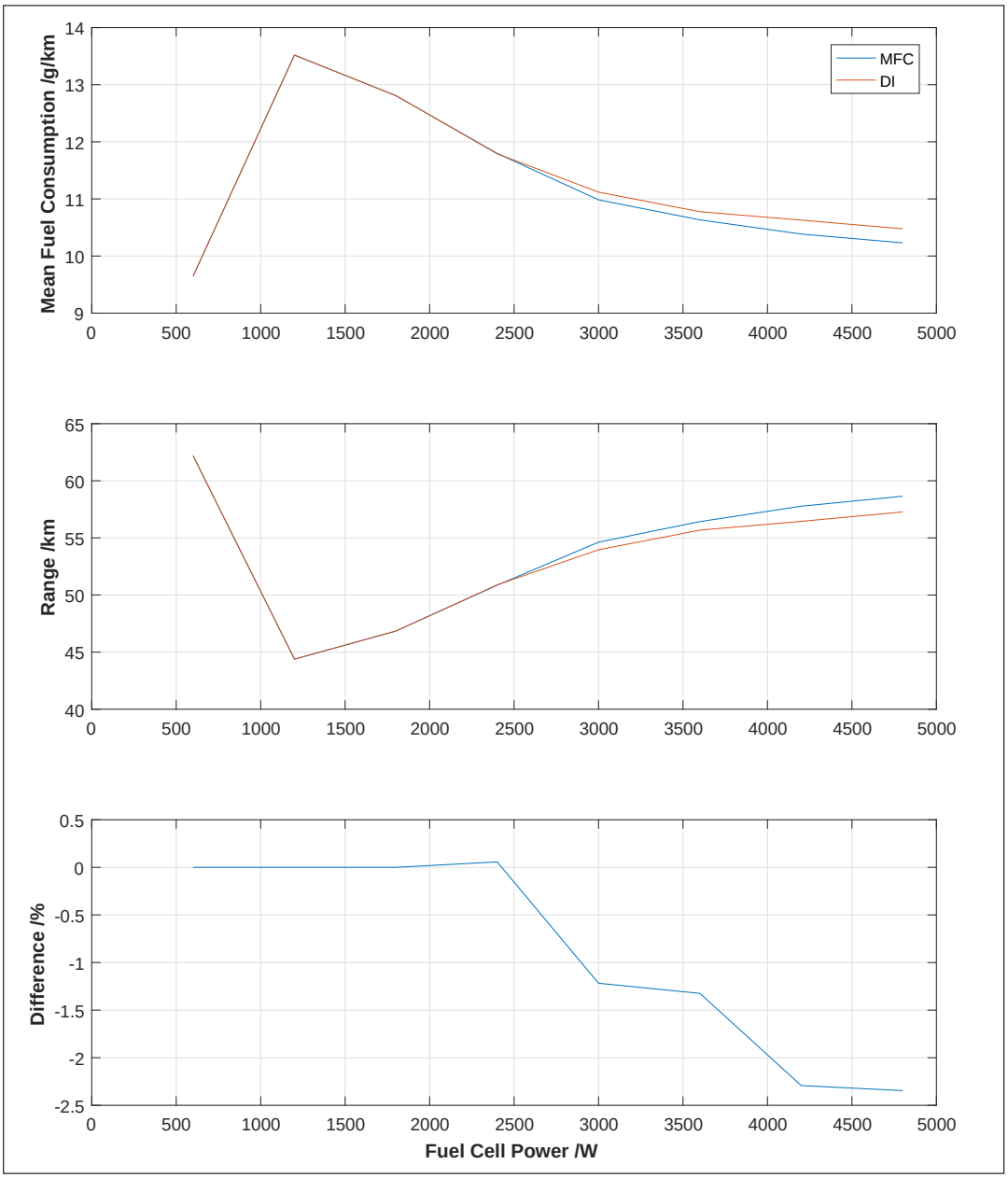

Figure 7.3: Fuel Consumption vs. Fuel Cell Size

Figure 7.3 shows the average fuel consumption across all 10 logged journeys for each fuel cell size. It can be seen that the fuel consumption for the 600W fuel cell is lowest at approximately 9.6 g/km. Fuel consumption sharply rises to a peak of 13.5 g/km for the 1200W controller, and then gradually decreases down to around 10.4 g/km for the DI strategy and 10.2 g/km for the MFC strategy. It can be seen that both strategies produce almost identical results up to approximately 2400W. Above this, the DI controller shows marginally higher fuel consumption. The estimated vehicle range follows an identical pattern albeit inverse. This is because the range is calculated directly from the fuel consumption and the size of the fuel storage (which is constant).

The low fuel consumption at 600W is purely due to the small size of the fuel cell. Even running at maximum power where the efficiency is relatively poor, the low maximum power output means that the fuel consumption is also very low. However, this size of fuel cell was unable to maintain the battery SoC so this does not constitute a comparable result. Consequently, when the fuel cell maximum power output is increased to 1200W, the fuel consumption also increases, even though the 1200W fuel cell was also unable to maintain the battery SoC for all journeys. Above 1200W, the fuel consumption begins to decrease. This suggests that at 1800W and higher, the EMS has gained enough control authority in order to begin to optimise the operating point of the fuel cell and hence reduce the fuel consumption.

At 3000W and higher, the fuel consumption further continues to decrease and the strategies begin to diverge, resulting in a maximum difference of 2.4%[1] between the two strategies at 4800W. This suggests that the control authority of the EMS is therefore high enough for the addition of the fuel cell degradation estimation to make a difference to the overall strategy. The fact that both strategies still perform very similarly suggests a good alignment between the targets of minimising the fuel consumption and minimising the degradation.

Overall, ignoring the result at 600W, the fuel consumption gradually decreases as the maximum power of the fuel cell increases. This is likely due to the increasing control authority of the EMS meaning that the fuel cell spends more time operating at or near to its peak efficiency region. The larger the fuel cell, the more likely it is that the vehicle is able to cope with a sudden increase in tractive effort due to a sudden acceleration, for example. As a result, it is able to utilise a higher SoC range, without risk of breaching the battery voltage constraints. This leads to a higher overall operating efficiency. This trend is unlikely to continue indefinitely however, and it can be seen in Figure 7.3 that the fuel consumption is beginning to level out. It is expected that for larger fuel cells, the fuel consumption will begin to increase again. This will occur for a variety of reasons.

Firstly, the grid spacing between the twenty discrete operating points increases as the maximum power increases; this will have an adverse effect on the fine control of the fuel cell in the range of desired operating points. It is also possible that some higher operating points may not be used at all due to the risk of breaching the upper voltage limit. Even if the grid spacing were to be kept constant (increasing the number of states and therefore the computational effort to complete the SDP optimisation), the fuel consumption would still begin to increase for larger fuel cells. This is because the average power required to complete the duty cycle will remain constant, meaning that at some point the fuel cell will be required to operate below its optimal region. Below approximately 30% of maximum power, the fuel cell efficiency sharply decreases due to the current required to drive the ancillary devices connected to the fuel cell. Finally, although it has not been modelled here, the increase in fuel cell size will also cause an increase in its mass, for large fuel cells, this will significantly affect the mass of the vehicle, leading to an increase in the electrical power drawn by the motor.

[1]Note that this value is slightly different to that calculated in Chapter 6 (3.2%) due to the increased grid spacing of the SoC and fuel cell power demand

7.2.3 Fuel Cell Lifetime

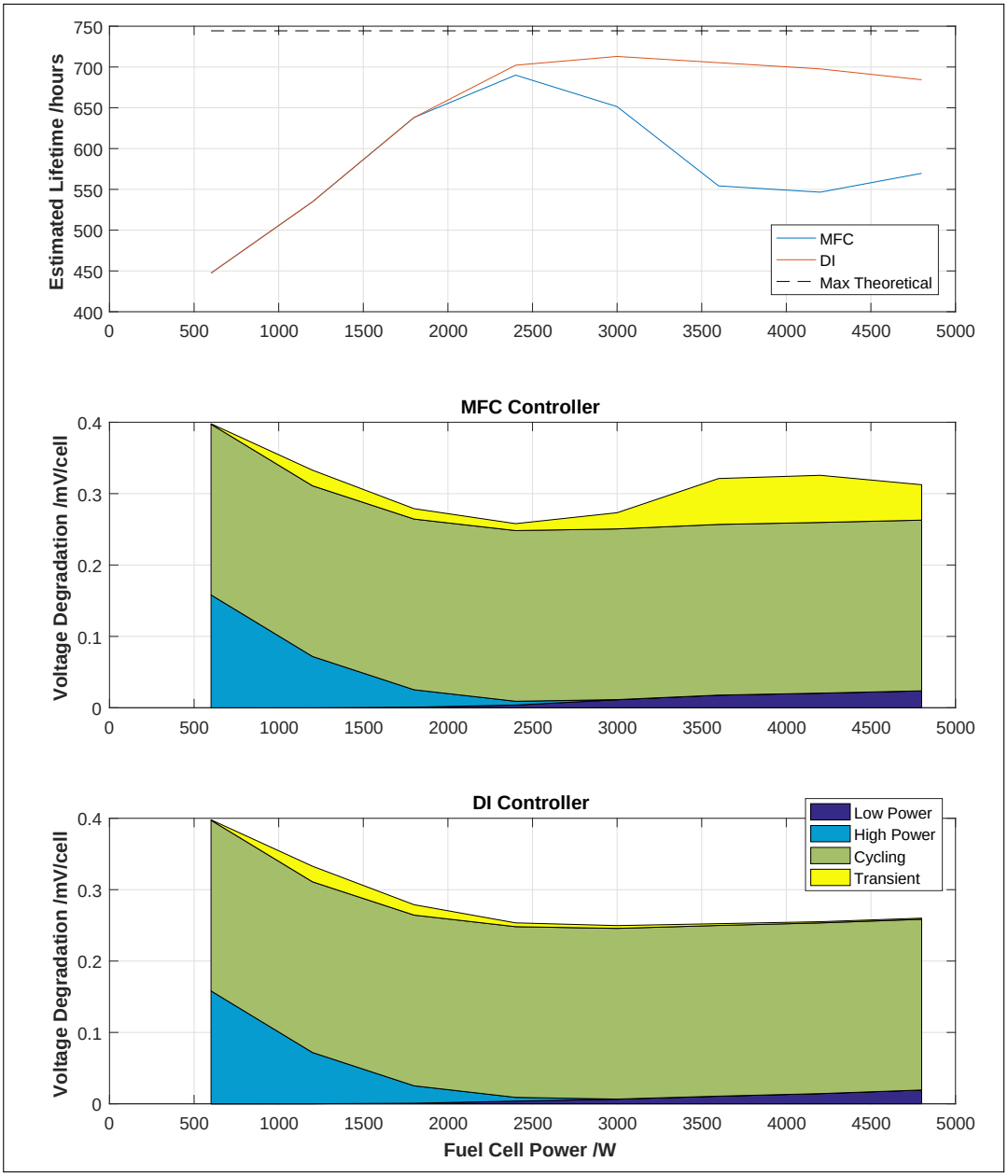

Figure 7.4: Fuel Cell Degradation vs. Fuel Cell Size

Figure 7.4 shows the estimated fuel cell lifetime and voltage degradation for both controllers. It can be seen that the estimated fuel cell lifetime for both controllers tends to increase approximately linearly up to 2400W, above which they begin to diverge significantly. The estimated lifetime for the DI controller levels off above 2400W, peaking at 3000W with a value of 713 hours and then gently falling to 684 hours at 4800W. In contrast, the estimated lifetime of the fuel cell controlled using the MFC strategy falls significantly above 2400W, to just 546 hours at 4200W, increasing slightly to 569 hours at 4800W. The reason for this difference is quite clear in the plots below. The MFC controller suffers from much more transient voltage degradation above 2400W when compared to the DI strategy.

As was seen with the fuel consumption, both strategies result in almost identical estimated fuel cell lifetimes up to a maximum fuel cell power of around 1800W. This is again most likely due to the domination of the battery voltage constraints on the optimisation. However, in contrast to the fuel consumption, the estimated lifetime of the fuel cell for each strategy differs significantly above 2400W. As a result, the DI controller sees a 27.6% increase (Figure 7.3) in estimated fuel cell lifetime at 4200W. This is due to a small reduction in degradation caused by running at low load, and a massive reduction in the transient loading of the fuel cell.

7.2.3.1 Transient Degradation

For the MFC strategy, transient voltage degradation represents up to 20% of the ageing of the fuel cell (at 3600W and 4200W). A large proportion of this is caused by oscillations in the demanded fuel cell load as a result of the strategy attempting to run between discrete operating points (as was described in Chapter 6) however additional transient loading is seen due to the transient nature of transportation duty cycles, especially those experienced during stop/start urban driving such as on a university campus. The transient loading increases as the maximum power of the fuel cell increases, up to around 4200W, and then begins to fall again. This is likely due to the increased control authority of the EMS, meaning more operating points are available for the optimisation and will not cause the battery voltage constraints to be breached. As the maximum power of the fuel cell increases, grid spacing between the fixed number of operating points also increases. This means that it becomes even more desirable for the MFC strategy to oscillate between the points in order to optimise the fuel consumption. As the maximum power of the fuel cell increases further, some operating points will be more likely to cause the upper battery voltage constraint to be breached, and therefore there are fewer valid actions for the EMS. As a result, the transient loading on the fuel cell is reduced when the largest fuel cells are tested.

In contrast, the DI controller experiences almost no voltage degradation due to transient loading. This is because the DI strategy optimisation takes the cost associated with fuel cell degradation into account and therefore shows no tendency to oscillate between discrete operating points. It appears to achieve this by introducing some hysteresis with respect to the current operating point, as seen in Chapter 6 (Figure 6.15). A minor negative side effect of this strategy is that the response of the DI controller is slightly slower than that of the MFC strategy resulting in a larger SoC utilisation.

7.2.3.2 Operating Point Degradation

Both strategies show similar trends in the voltage degradation due to the operating point of the fuel cell. For small fuel cells up to around 2400W, the strategies are almost identical to one another and show excessive amounts of degradation due to operation at or close to full load. This is due to the fact that the fuel cells are required to run in this operating region due to their small maximum power output. As the size of the fuel cell increases, the degradation caused by low power operation increases. This is caused by the increased size of the fuel cell, which is required to run at a proportionally lower load in order to generate the same average power. Both of these trends are what would be expected.

Even though there is a large region at mid load (between 25% and 80% of full load) that the fuel cell experiences no degradation due to its operating point; there is no size of fuel

cell that would not see any degradation caused by this. In fact, there is overlap between the two modes, and fuel cells between 1200W and 3000W are likely to see some degradation caused by both high and low load operation. This is likely due to the fact that this size of fuel cell requires its full range of operating points in order to manage the battery voltage.

Much less degradation due to the operating point is seen in larger fuel cells when compared to smaller fuel cells, despite the fact that the raw degradation rates are similar. This is likely because the control authority of the EMS is higher for larger fuel cells and the operation at low load is only used when it is beneficial to do so. For the larger fuel cells tested (up to 4800W), and likely some slightly larger than this, the degradation due to operation at low load is likely caused by competition with the fuel economy optimisation. It is likely that the proportional cost of the degradation is lower than the increased fuel consumption which would be caused by avoiding this region altogether. As the size of the fuel cell increases further, low load operation will become unavoidable in the same way that high load operation is unavoidable for smaller fuel cells. Therefore, fuel cells significantly larger than 4800W are likely to see much higher rates of degradation due to operation at low loading.

For fuel cells larger than 3000W, the DI strategy sees between 20 - 40% less degradation than the MFC strategy due to operation at low load. This is likely due to two main factors. Firstly, the DI strategy optimisation applies a cost due to this degradation and therefore has some incentive to avoid it. However, it is also likely caused as a side effect of the avoidance of transient loading. The DI strategy tends to avoid transient loading by applying some hysteresis on its response to changes in load, and therefore tends to have a slightly slower response than the MFC strategy. As a result, it tends to operate at a more consistent load, closer to the average power demand, hence often avoiding short periods of low power operation experienced by the MFC strategy.

7.2.3.3 Cycling Degradation

Cycling degradation is largely caused by the inhomogeneous distribution of reactants and products during start-up and shut-down in addition to operation outside normal temperature, pressure and humidity conditions, see Section 2.2.2.6. Although it would be possible to allow the EMS strategy to determine when the fuel cell should be started and shut-down, it has been found that the MFC strategy tends to cause a high number of cycling events resulting in levels of degradation unlikely to be acceptable in the real world. As a result, it has been assumed that the simulation of each journey will result in a single cycling event.

It can be seen that the degradation due to this single unavoidable start-stop cycle represents a large proportion of the degradation for a fuel cell of any size. This is most apparent for the DI strategy at 3000W, where it represents 96% of the estimated degradation. The fuel cell used in the Microcab H4 shows a rate of degradation due to start-stop cycling of approximately $23.91\,\mu\mathrm{V/cycle/cell}$. This means that even with no degradation from other methods, the fuel cell would only last approximately 1200 cycles before being considered at the end of its useful life. As the drive-cycle lengths average approximately 37 minutes, this represents a theoretical maximum of lifetime of only 744 hours if no degradation was seen due to other causes, shown as a dashed black line in the uppermost plot. At 3000W, the MFC strategy results in a deficit of 99 hours compared to this figure, whereas the new controller reduces this deficit by 63 % to just 37 hours by minimising the voltage degradation due to other causes.

In comparison to a more recent fuel cell used by Chen *et al.* [13], the fuel cell in the Microcab exhibits quite high degradation due to cycling. Chen *et al.* used a figure of $13.79\,\mu\mathrm{V/cycle/cell}$. If this number were to be used instead of that from the Ballard datasheet, the degradation due to cycling would still represent approximately 80 % for the baseline controller and 93 % for the degradation optimised controller. This increases the predicted lifetime of the fuel cell to 1035 hours for the baseline controller and 1199 hours for the optimised controller. In this case the lifetime of the fuel cell has been increased by 16 % due to the DI optimised control; however, it is still well below the 5000 hour US Department of Energy (DoE) target for vehicular applications. As there is nothing that the EMS can do to further reduce the number of cycling events, this suggests that the degradation caused by cycling is an critical area of focus for future research.

7.2.4 Running Cost

Figure 7.5 shows the average running cost over the 10 journeys for each size of fuel cell. A comparison of the two strategies is shown in the top plot, with a breakdown of the costs for each of the strategies shown in the centre and lower plots. It can be seen that there is a clear correlation of monotonically increasing cost with increased size of fuel cell, although the trend is not linear. Comparing the two strategies, the costs for both strategies are almost identical up to 2400W; however, there is a clear reduction in running cost by using the DI controller above 2400W.

The lowest running cost is achieved by the 600W fuel cell, although this is almost certainly due to the fact that the maximum power of the fuel cell is unable to provide enough power to maintain the battery SoC. Therefore, these results do not provide a fair comparison with regards to the cost. Following this, there is a sharp rise from \$1.56 at 600W up to \$2.30 for 1200W. The 1200W fuel cell was also not capable of completing all of the cycles, however its average utilisation was well below 100% overall (Figure 7.1), and therefore the cost is likely to be only slightly underestimated. The first truly valid point for comparison is 1800W, due to the fact that this controller was able to complete all journeys successfully.

The increase in running cost as the size of the fuel cell increases can be directly attributed to the increased overall value of the fuel cell with size. As explained at the beginning of Chapter 6, a fuel cell cost of \$50/kW has been assumed. These figures are based on recent estimates from the literature for current technology, assuming mass production economy-of-scale. It has been assumed that the fixed costs of the fuel cell are negligible compared to the variable costs due to the high price of materials (e.g., platinum catalyst) and the economy-of-scale afforded by mass production. This means that a 4800W fuel cell will cost four times as much as a 1200W fuel cell and therefore assuming identical rates of voltage degradation, the cost associated will also be four times as much. This increase in fuel cell value can be seen to be the main contributor to the trend between fuel cell size and running cost.

However, unlike the increase in estimated fuel cell value, the relationship between the running cost and the size of the fuel cell is not linear. As the size of the fuel cell increases, the control authority of the EMS is also increased, and the operating point of the fuel cell becomes closer to optimal. This results in a reduction in both the fuel consumption and the rates of degradation for the DI strategy, which significantly offset the increase in the value of the fuel cell. As a result, the DI strategy sees only a 47% increase in running cost between 1200W and 4800W despite a 300% increase in the value of the fuel cell.

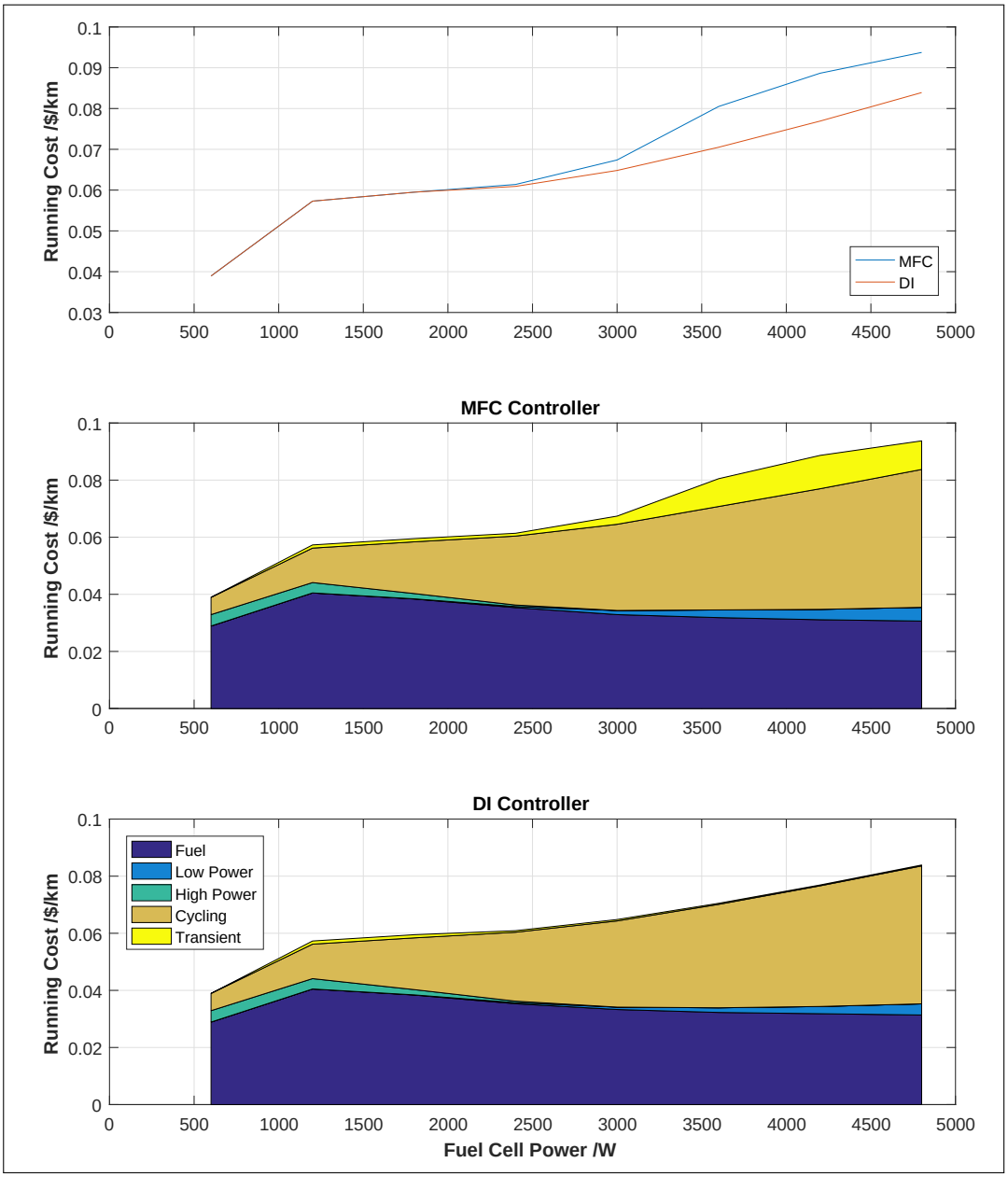

Figure 7.5: Running Cost vs. Fuel Cell Size

Examining the breakdown of the running cost in more detail, it can be seen that it is dominated by two main factors; the cost of the fuel and the cost of the degradation due to cycling. The cost of the fuel is reduced by 24% between 1200W and 4800W for the MFC controller and 23% for the DI controller. However, the increase in the cost of the degradation due to cycling increases much more than this, resulting in an overall cost increase over the same range. Due to the fact that only a single on/off cycle is considered for each journey, the rate of voltage degradation due to start-stop cycling is fixed. As a result, it increases proportionally with the fuel cell size. This means that although it only represents approximately 21% of the running cost at 1200W, it is responsible for 52% of the cost at 4800W for the MFC strategy and 58% for the DI strategy. Much of the reduction in fuel consumption is achieved well below 4800W, and diminishing gains are observed as the

size of the fuel cell increases. This results in a curve in the relationship between running cost and fuel cell maximum power, although the gradient always remains positive.

Comparing the two strategies, it is possible to see that the reduction in transient loading on the fuel cell results in a significant cost saving for fuel cells larger than 3000W. For the MFC strategy, degradation due to transient loading represents up to 13% of the cost (at 4200W), whereas for the DI strategy it is consistently below 1% of the overall running cost. Despite a slight increase in fuel consumption (2.4%), the overall running cost of the DI strategy is up to 15% lower (at 4200W) when considering the proportional cost of fuel cell degradation.

7.2.4.1 Sensitivity to Fuel Cell Cost

If a fixed cost of fuel cell manufacturing or replacement was considered, and the cost of the fuel cell assumed to follow a linear (y=mx+c) relationship, a doubling of the fuel cell size would not result in a doubling of the cost. Therefore, it may be possible that the reduction in fuel consumption would outweigh the increase in cycling degradation cost. Unfortunately, it is not easy to test this hypothesis due to the fact that the cost associated with degradation would be changed and therefore the SDP strategy would need to be re-optimised. However, a change in the associated cost of cycling would not affect the strategy. This is due to the fact that the EMS can do nothing else to further optimise the start-stop cycling.

As previously mentioned, the fuel cell in the Microcab experiences especially high rates of degradation due to cycling when compared to values in the literature. If the rate of degradation used by Chen *et al.* [13] of $13.79\,\mu\mathrm{V/cycle/cell}$ were to be used instead of $23.91\,\mu\mathrm{V/cycle/cell}$ as quoted in the Ballard datasheet, the relationship between the running cost and fuel cell size would be changed considerably. This is shown in Figure 7.6. It can be seen that in this case, the reduction in fuel consumption between 1200W and 2400W more than offsets in the increase in degradation cost. As a result, discounting the 600W fuel cell, a 2400W fuel cell becomes the optimal size. Above this, diminishing returns in fuel economy mean that the running cost begins to rise again.

This shows that the choice of the fuel cell size is quite sensitive to the rate of the fuel cell degradation. There are a number of factors which are involved in the calculation of the overall running cost, which tend to compete with each other as the size of the fuel cell is varied. Whereas the fuel consumption and the voltage degradation will tend to decrease as the fuel cell maximum power increases, the absolute cost of the fuel cell increases. Therefore, it has been found that from a purely cost perspective, a larger fuel cell is only justified when the reduction in fuel consumption and voltage degradation observed exceeds its increase in replacement cost.

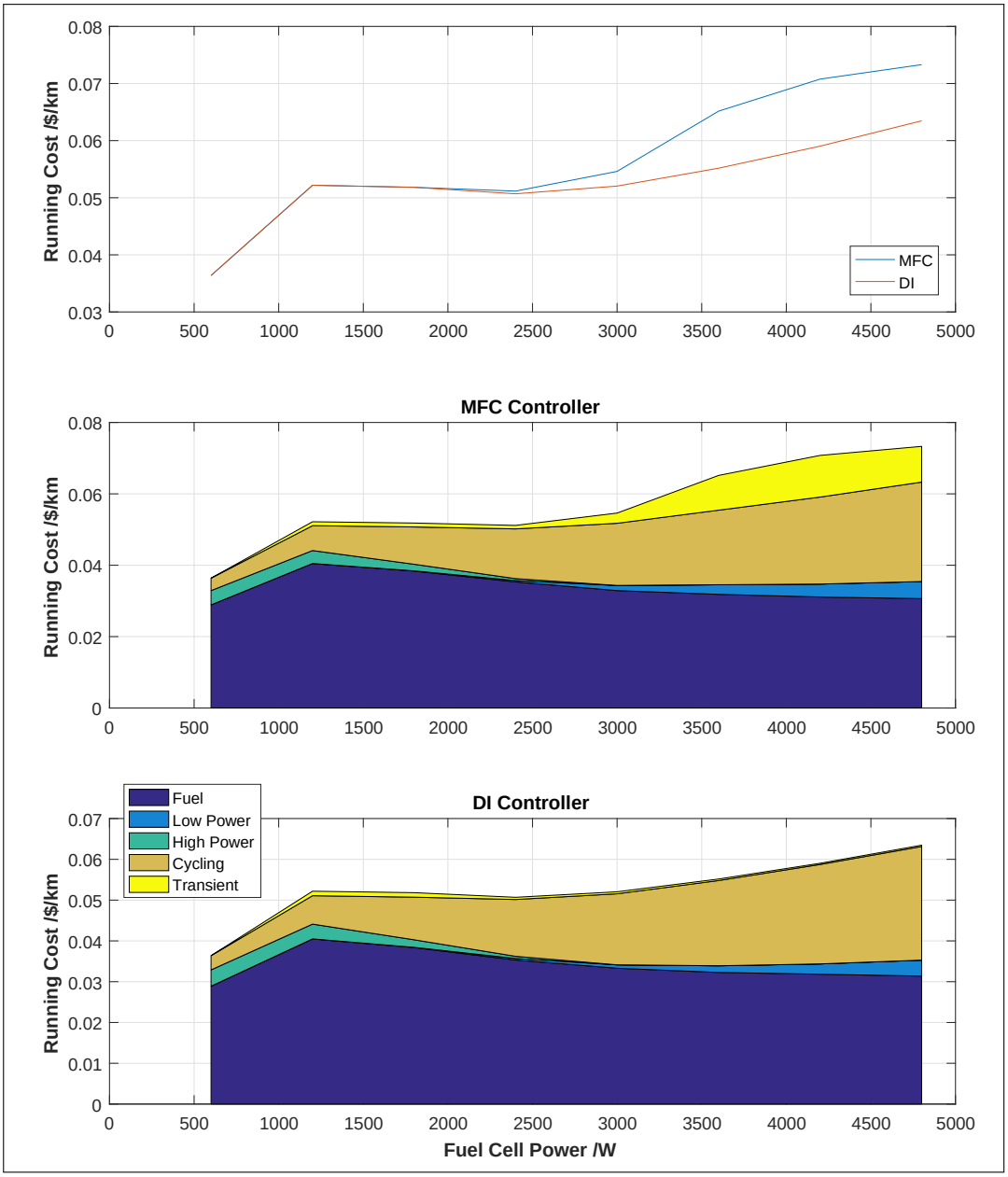

Figure 7.6: Running Cost vs. Fuel Cell Size (assuming lower rate of cycling degradation)

7.2.5 Summary

"The cost of the system could be reduced by using a smaller stack and running it at a higher relative power, however this will also tend to reduce the operating efficiency and is likely to increase the rates of degradation, reducing the lifetime of the system. This means that it is hard to gauge whether the initial cost saving of a smaller stack will be outweighed by the increased maintenance cost due to reduced reliability." - Chapter 1 - Introduction

The short answer to the above question can be found in Figure 7.5. The running cost of the fuel cell is minimised by using the smallest possible fuel cell that will meet the average power requirements of its usage pattern and running it at close to full load. This results in higher fuel consumption, and higher rates of degradation than using a larger fuel cell, however the reduced cost of the stack more than outweighs the costs associated with these downsides.

However, the long answer is more complicated. In actual fact, the benefits of the smaller stack are marginal, and the balance could easily be shifted in favour of a slightly larger stack by relatively minor changes in the calculation. For example, if the cost due to start/stop cycling was lower (as shown in Figure 7.6), or if the fixed costs were assumed in addition to the variable costs of the fuel cell with size, it may mean that a larger stack may be preferable.

In addition to this, there are a number of additional benefits to using a larger stack that are unrelated to the cost. For example, the cost associated is not the only concern with regard to the fuel consumption. The packaging requirements of hydrogen storage for transportation are not trivial, meaning that often a compromise is made with regard to its capacity. This usually means that the fuel consumption has a direct effect on the range of the vehicle, because lower fuel consumption means that the vehicle can travel a greater distance on the same amount of fuel. The 4800W fuel cell is shown to have reduced the fuel consumption by almost 30% when compared to a 1200W stack, resulting in a proportional increase in the vehicles range. Similarly, the reliability of the stack will also affect the customer's perception of the vehicle, which can be a crucial factor for emerging technologies. The larger 4800W stack is shown to have a 28% increase in lifetime (for the DI strategy) when compared to the 1200W system.

However, increasing the size of the stack indefinitely would not indefinitely improve the fuel consumption and reliability. Diminishing returns are seen in regard to the fuel consumption up to 4800W, and further increases are likely to cause the fuel consumption to begin to increase as the power requirements of the duty cycle move past the optimal operating points of the fuel cell. Similarly, the estimated degradation reaches a minimum value at 3000W for the DI controller, above which it begins to increase again as the time spent operating at low power tends to increase. It is therefore important to consider the vehicle's targets as whole rather than to focus on a single objective, such as the minimisation of cost.

It is therefore the author's opinion that a fuel cell of approximately 2400W offers the most beneficial performance with regards to the cost, range and fuel cell lifetime. Compared to a 1800W fuel cell stack (minimum cost system which would successfully complete all tested journeys), the range is approximately 8.6% higher, the estimated lifetime is 10% higher, and the overall operating cost is only 3% higher. It is also very likely that the 10 journeys tested do not fully cover all possible likely circumstances, and the additional power availability may be required to complete more demanding journeys that the vehicle is likely to encounter.

7.3 Effect of Battery Capacity

The capacity of the battery will also have a significant effect on the performance of the vehicle. The battery is generally used as an energy buffer which gives the EMS the flexibility to run the fuel cell at a different load to that required for traction. This means that the transient loading on the fuel cell can be reduced, but also allows the EMS to run the fuel cell closer to its optimal operating point, resulting in higher fuel economy and reduced voltage degradation. Up to a point, the larger the battery capacity, the greater the flexibility in fuel cell operating point and therefore the higher the gains. However, diminishing returns are expected as the battery capacity increases, and the benefits are expected to level off once the capacity of the battery reaches a point where the fuel cell is able to run at an approximately constant load.

The effect of the increase in mass of the battery has not been included in this analysis due to the small size of the battery pack in comparison to the mass of the vehicle. However, very large battery packs would also increase the mass of the vehicle significantly and therefore would begin to detriment the overall fuel economy by increasing the mechanical energy required to complete the journeys.

The procedure for the battery capacity sweep is the same as for the fuel cell sweep. The following values have been tested;

Parameter (Unit)	Minimum	Maximum	Spacing
Fuel Cell Maximum Power, $P_{FC,max}$ (W)	2400	2400	-
Battery Capacity, C_n (Wh)	568	4224	568

Table 7.3: Battery Capacity Sweep Values

7.3.1 SoC Sustenance

A fuel cell with a maximum power of 2400W has been chosen for the battery size sweep which is more than that required to complete every journey (approximately 1650W). Therefore, as shown in Figure 7.7, the maximum net change in battery SoC for both controllers was within 0.1%. This means that unlike the fuel cell size sweep, the fuel consumption, stack degradation and running cost for every simulation are directly comparable.

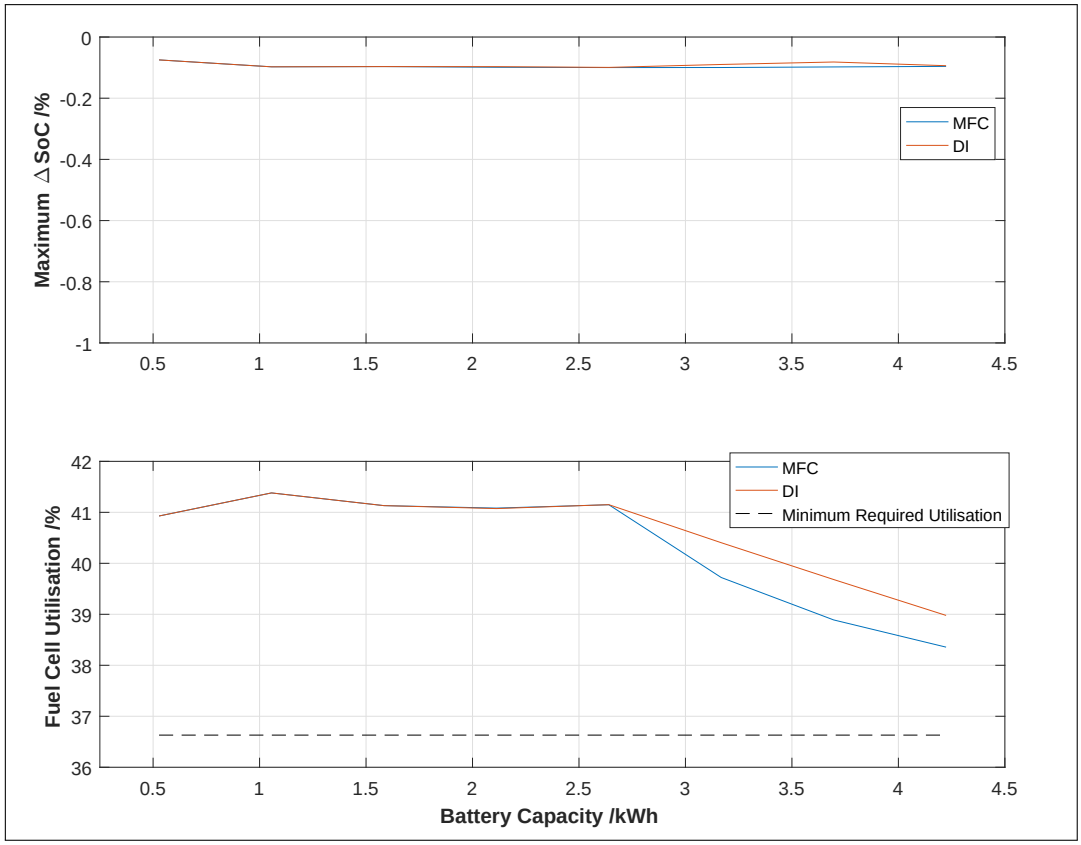

Figure 7.7: SoC Sustenance vs. Battery Capacity

Also shown in Figure 7.7 is the stack utilisation. In this plot, the dashed black line represents the average utilisation required to drive the traction motors (36.6%), which accounts for all efficiency losses aside from cycling losses in the battery. It can be seen that for battery capacities up to approximately 2.6kWh, the fuel cell utilisation is approximately constant at around 41%. Above this value, the utilisation drops approximately linearly for the DI controller to around 39% at 4.2kWh. For the MFC controller the utilisation falls slightly further to around 38.4%.

The cycling losses in the battery are largely due to charging and discharging at high "C-rates", where "C" is defined as the current divided by the battery capacity. Discharging at high C-rates will cause the voltage of the battery will be pulled down significantly, and similarly, charging at a high C-rate will cause the battery voltage to be pulled up. This is due to the internal resistance of the battery and the over-voltage effects associated with the Shepherd coefficient. Power is the product of voltage and current, and therefore even assuming 100% charge transfer efficiency, less energy is able to be extracted from the battery than was required to charge it. This effect is relatively small at low C-rates where the

internal resistance is the dominant factor, but can be significant at high C-rates where the effect of over-voltage coefficient becomes much higher (see Figure 3.13).

As mentioned, the C-rate is inversely proportional to the battery capacity. This means that small batteries will experience proportionally higher C-rates assuming the same current loading. The fact that the cycling losses are approximately constant for battery capacities up to 2.6kWh suggests that in this region, the battery spends a considerable proportion of time close to the voltage constraints. Therefore, even though the fuel cell is large enough to maintain the battery SoC over all of the journeys, it has limited control authority and the optimisation is unlikely to show much benefit. Above 2.6kWh, however, the fuel cell utilisation (and therefore cycling losses) begins to fall. This shows that the battery is most likely operating for more time in regions where the effect of over-voltage coefficient is negligible, and hence is further from its constraints. As a result, the optimisation of fuel economy and fuel cell degradation is likely to be more effective in this region.

Above 2.6kWh, the DI strategy shows approximately linear decrease in cycling losses. This is likely a direct result of the increase in battery capacity and hence the proportional reduction in the C-rate. Comparing the MFC and DI strategies in this region shows that the MFC strategy results in significantly fewer cycling losses in the battery. This is likely due to the fact that the reduction in battery cycling losses will compete directly with the DI strategy objective to minimise transient loading on the fuel cell. As the MFC strategy does not include this objective, further gains can be achieved in this regard by passing transient loading inherent in the duty cycle onto the fuel cell.

For lead acid batteries, the effect of the increase in battery capacity is compounded when the battery voltage is used as a constraint as was performed here. This is because the increased battery capacity means that the same current results in a proportionally lower C-rate. In turn, the voltage deviation from open-circuit is proportionally reduced when in the region dominated by internal resistance and exponentially reduced when in the region dominated by the over-voltage coefficient. This means that more charge can be withdrawn from the battery (and hence a lower SoC can be achieved) before the voltage constraints are exceeded. As a result, the effective useful capacity of the battery is increased by far more than the increase in actual capacity.

Another way of explaining this is that the useful capacity of the battery is related to the current loading it experiences. The Odyssey PC1200 batteries used in the Microcab have a capacity of 30Ah when discharged at 41A, but only 26Ah when discharged at 78A. By increasing the capacity of the battery pack, the current is shared between more cells, hence the load on each cell is lower and a higher useful capacity is available. In this case, if the battery capacity is increased by a factor of 1.9 so that the average current on each 12V battery is reduced from 78A down to 41A, the effective capacity is increased by additional 15%, resulting in an overall increase of around 2.2 times. This means that significant gains can be made with only a slight increase in battery capacity.

7.3.2 Fuel Consumption

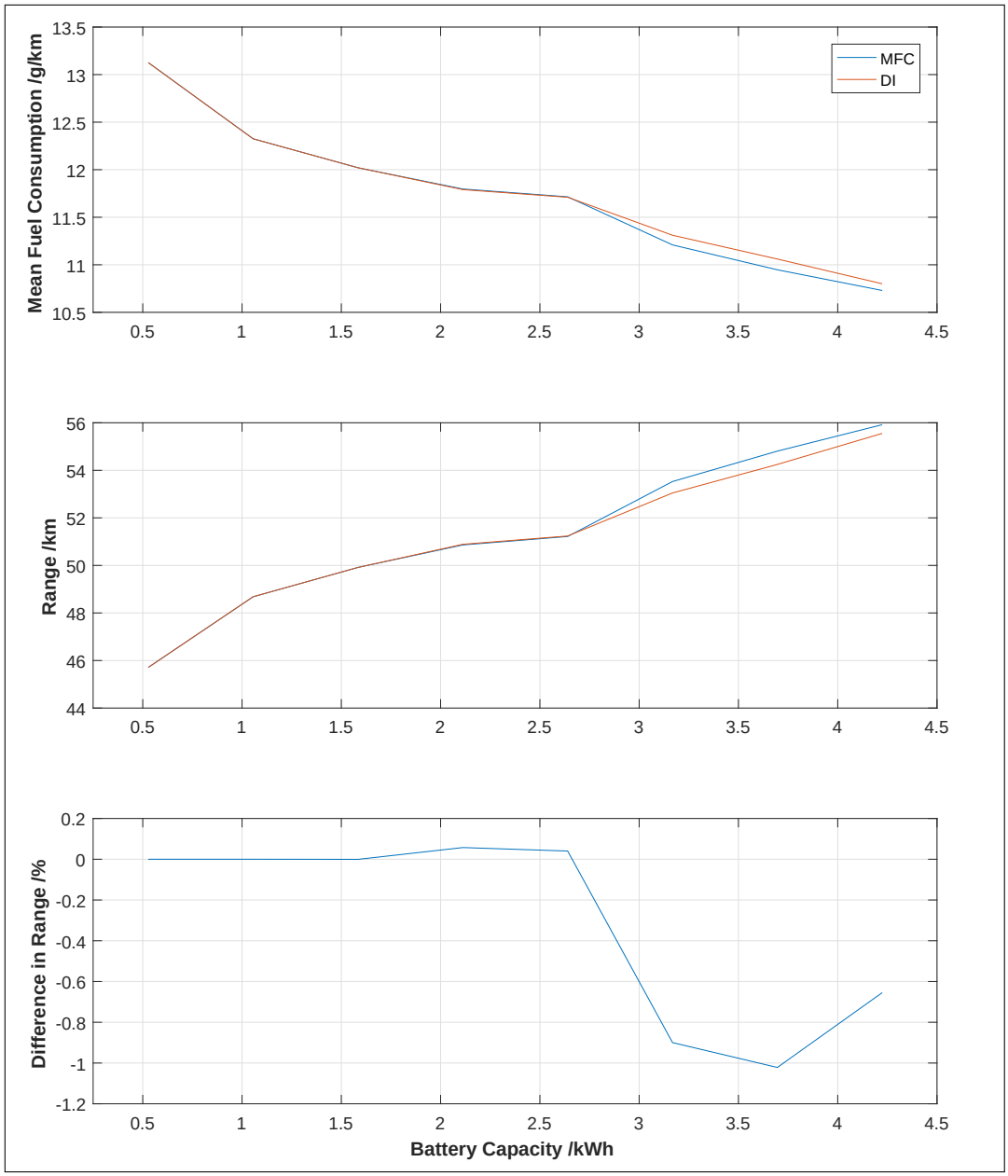

Figure 7.8: Fuel Consumption vs. Battery Capacity

Figure 7.8 shows the variation of fuel consumption and range with regards to the battery capacity. It can be seen that in general, the fuel consumption falls as the battery capacity is increased. As with the SoC, both strategies perform almost identically up to approximately 2.6kWh. Above 2.6kWh, there is a slight difference, with the MFC strategy achieving a slightly lower overall fuel consumption of 10.7g/km at 4.2kWh, compared to the DI strategy which achieves a minimum consumption of 10.8g/km.

The fuel consumption is expected to reduce as the battery size increases due to the additional control authority that is afforded to the EMS. This allows the EMS more flexibility with regards to the fuel cell operating point without risk of compromising the battery volt-

age constraints. As a result, the EMS is able to run the fuel cell for more time in its most efficient operating region and therefore produce the same amount of electrical power while consuming less fuel. In addition to this, the increase in battery capacity also means that the C-rate of the batteries is reduced, which in turn means that the cycling losses in the battery are reduced as mentioned in the previous section. This means that the average electrical load on the fuel cell is lower and therefore less fuel is consumed.

Comparing the optimised strategies, the MFC strategy shows a fuel consumption which is around 1% lower for any battery capacity above 2.6kWh. This is to be expected because the MFC strategy is optimised purely in order to minimise the fuel consumption, without regard to any degradation. It has been noted in the previous section that the MFC strategy tends to show fewer cycling losses in the battery which would account for a large proportion of this difference. This results in a lower fuel consumption, but likely causes additional transient loading on the fuel cell. Aside from this however, both strategies perform very similarly, which suggests that the objective of minimising the degradation is largely complimentary to optimisation of the fuel consumption.

It can be seen that aside from the result for a 2.6kWh battery, there is a slight curve in the trend. This is because as the battery capacity is increased, diminishing performance gains are achieved. As a result, it is expected that for much larger batteries, the curve will begin to level out, reaching a limit where the load on the fuel cell is approximately constant at the average power demand. Although the mass of the batteries has been neglected in this analysis, at this point the mass increase would become significant eventually causing the trend to reverse as the increased vehicle mass means that additional electrical power is required to drive the vehicle. It must also be noted that the additional cost of significantly larger batteries would also cease to become negligible compared to the overall cost of the vehicle.

7.3.3 Fuel Cell Lifetime

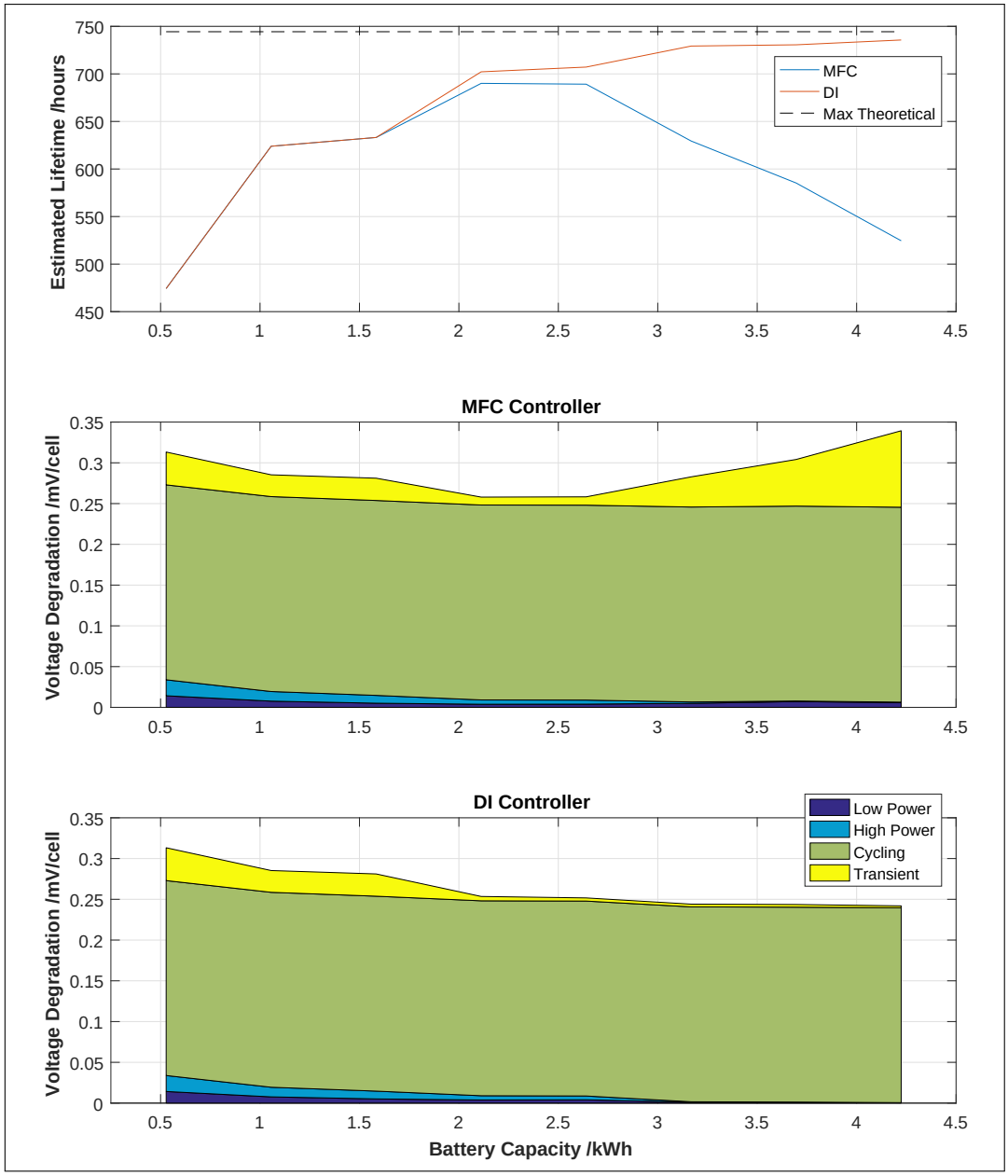

Figure 7.9: Fuel Cell Degradation vs. Battery Capacity

Figure 7.9 shows the estimated lifetime for both SDP optimised controllers. In the centre and lower plots, the breakdown of degradation methods is shown for each strategy. The top plot in Figure 7.9 also shows the theoretical maximum fuel cell lifetime based on the rate of degradation due to cycling. This is shown as a dashed black line. Each journey must start and stop the fuel cell at least once; therefore, even if no degradation is seen due to any other methods, the fuel cell will have a finite lifetime of approximately 744 hours. It can be seen that the estimated lifetime using MFC strategy peaks at 690 hours (93% of maximum) for a battery capacity of 2.1kWh. However, the estimated lifetime of the fuel cell using DI strategy continues to rise as the battery capacity is increased and reaches a maximum of 736 hours, 99% of the theoretical maximum at 4.2kWh.

In general, the lifetime of the fuel cell for both strategies rises as the battery capacity increases up to 2.6kWh. It can be seen that both controllers follow almost identical patterns up to approximately 1.6kWh, at which point the DI controller begins to show marginally less voltage degradation. Above 2.6kWh, the lifetime of the DI controller continues to increase, however the lifetime of the fuel cell for the MFC strategy begins to fall relatively sharply to just 525 hours at 4.2kWh.

7.3.3.1 Transient Degradation

In the region below approximately 2.1kWh, the transient degradation for both strategies is approximately equal and follows the trend that as the battery capacity increases, the transient degradation decreases. This is due to the increased control authority of the EMS. Below approximately 2.6kWh, the battery capacity is only marginally large enough for the battery to operate as an energy buffer to the fuel cell. This means that although the fuel cell is able to maintain the net battery SoC over the drive-cycle, its operating point is directly affected by the instantaneous load from the traction motor for a large proportional of the time. In this region, as the battery capacity increases, the number of options available to the EMS gets larger, and as a result the EMS is able to choose the actions which will best optimise its objectives. Below approximately 2.1kWh, the largest advantage is gained by running the fuel cell close to its most efficient operating point for more time. This has the added advantage that it also reduces the transient loading on the fuel cell, and hence the behaviour of both strategies is similar.

Between 2.1kWh and 2.6kWh, the results of the strategies begin to diverge. It can be seen that, in this region, the DI strategy continues to reduce the transient degradation, down to just 3.8μV/cell over the entire set of 10 journeys. Above 2.6kWh, the two strategies diverge considerably. The vast majority of this difference is due to the much higher degree of transient loading seen with the MFC strategy. In this region, it becomes advantageous from the fuel consumption perspective to prevent cyclic loading on the battery in order to minimise cycling losses in the battery. This is achieved by passing the transient loading on to the fuel cell, which in turn tends to degrade the fuel cell. The DI strategy on the other hand, penalises this transient loading in its cost function and therefore this situation is avoided. Because the DI strategy is designed to optimise the degradation as well as the fuel consumption, the associated costs of each target are traded off against each other. It can be seen that the increased fuel consumption caused by avoiding this transient loading is very small, and therefore the DI strategy is able to significantly reduce the transient loading for only a marginal increase in the fuel consumption. As the battery size increases up to around 4.2kWh, the battery is better able to act as an energy buffer to the fuel cell and therefore the transient loading on the fuel cell can be further reduced.

For the DI strategy, degradation due to transient loading is further reduced down to just 2.2μV/cell for the largest battery capacity of 4.2kWh. In contrast, the transient degradation MFC controller does not reduce by as much in the region between 1.6kWh and 2.6kWh, and even begins to increase for batteries larger than this. This results in a significantly lower estimated lifetime of the fuel cell for the largest battery capacities.

7.3.3.2 Operating Point Degradation

The battery capacity obviously has a large effect on the degradation due to operating point. It can be seen that for both controllers, the degradation due to operating point reduces by around 75% from the 0.5kWh battery up to the 2.6kWh battery. This is because the battery acts as a buffer to the fuel cell. Smaller batteries will be less able to absorb loads, meaning that the full range of fuel cell operating point is required in order to maintain the battery within its voltage limits. As the battery capacity increases, the battery is able to absorb transient loads for longer periods of time allowing the fuel cell to operate at a time-averaged load. This means that it is not required to operate at its extreme limits of power as often and as a result, the degradation due to operating point is reduced.

Above 2.6kWh, the two strategies behave slightly differently to each other. The degradation due to operation point for the DI strategy continues to decrease to an almost negligible level for a battery capacity of 4.2kWh. In fact, the degradation due to the operating point is reduced from 4.7μV/cell when using a 2.6kWh battery down to just 0.6μV/cell when using a 4.2kWh battery. In contrast, the MFC strategy shows a relatively constant level of operating point degradation, at approximately 8.0μV/cell, although the balance shifts from 50:50 (low:high) degradation for a 2.6kWh battery to 90:10 for a 4.2kWh battery. This shows that although the battery capacity is large enough to avoid low load operation, the MFC chooses to operate in this region to optimise the fuel consumption. In contrast, the DI strategy does not operate in this region suggesting that the fuel consumption benefit is outweighed by the potential degradation. This behaviour is also likely to be related to the avoidance of transient degradation. The DI strategy penalises transient loading on the fuel cell, instead operating the stack at a more averaged load; which will inherently mean that it spends less time at the extreme limits of load.

7.3.3.3 Cycling Degradation

In line with previous results, the degradation due to cycling is the dominant mode of ageing seen. For the DI strategy, this represents 76% of the degradation seen for the smallest battery size, and up to 99% for the 4.2kWh battery due to the effective management of the other methods. As before, there is very little that the EMS can do to further reduce this method degradation. For the MFC strategy, there is more degradation due to other methods with the largest fuel cell, but cycling is still responsible for 70% of the fuel cell degradation.

It must be noted that the fuel cell in the Microcab H4 does experience a particularly high cycling degradation rate compared to figures from the literature, however even using a smaller estimate based on the figure used by Chen *et al.* [13] of $13.79\,\mu\mathrm{V/cycle/cell}$, the cycling would still be responsible for up to 98% of the degradation for the DI strategy and 58% for the MFC strategy with a 4.2kWh battery.

7.3.4 Running Cost

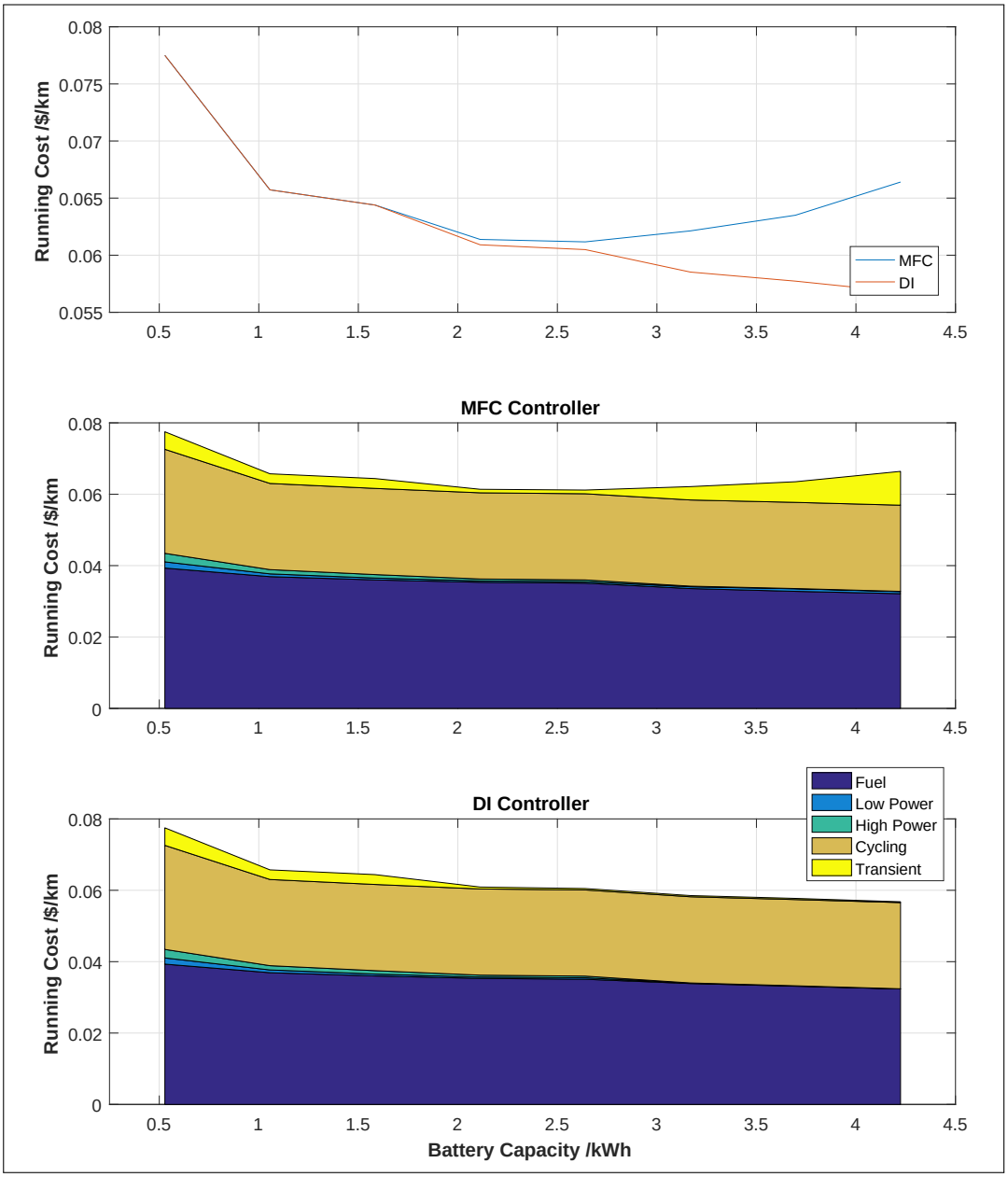

Figure 7.10: Running Cost vs. Fuel Cell Size

When optimising the DI controller, the fuel consumption and stack degradation are weighted using their respective costs, and the SDP algorithm is used to minimise the overall running cost. This means that although the MFC strategy is expected to outperform the DI controller with respect to the fuel consumption, the reduction in cost associated with degradation for the DI strategy should mean that its overall running cost should be lower. The top plot in Figure 7.10 shows the comparison between the two strategies. It can be clearly seen that as before, both strategies perform almost identically for battery capacities up to 1.6kWh. Between 1.6kWh and 2.6kWh, the strategies begin to diverge slightly due to slightly reduced degradation seen when using the DI strategy. For battery capacities greater than 2.6kWh, the DI strategy results in significantly lower running costs due to a massive reduction in degradation for only a marginal increase in the fuel consumption.

It can be seen that for both strategies and throughout the range of battery sizes, the dominant factors associated with the running cost are the fuel consumption and the cycling degradation. This correlates with the results found in the fuel cell sizing exercise. The degradation due to cycling has been minimised using the assumption that each strategy will only start and stop the fuel cell once, and therefore there is nothing that either optimisation can do to further reduce this. As a result, it is constant throughout the exercise. The fuel consumption on the other hand generally reduces as the battery capacity increases due to the increased control authority of the EMS.

Below 2.6kWh, both strategies perform almost identically, however above this value, the DI strategy clearly results in a lower overall running cost. This difference increases as the capacity of the battery is increased, and results in a maximum reduction in running cost of 15% for a battery capacity of 4.2kWh. This is reduction can be attributed to a 98% reduction in the transient loading on the fuel cell and a 90% reduction in the degradation due to the operating point. This results in a 40% increase in the estimated lifetime of the stack, which far outweighs the increase in the fuel consumption of just 0.7%.

7.3.5 Summary

The optimisation of the strategy for various battery capacities has shown that as the battery capacity increases, the fuel consumption is reduced. This is to be expected due to the fact that the battery acts as a buffer on the fuel cell and can absorb sudden loads which would otherwise cause the fuel cell to operate far from its peak efficiency. As the battery capacity increases, this buffer becomes larger and the EMS is afforded more flexibility with which to choose its optimal action. As a result, the performance of both strategies improves as the battery capacity increases.

The MFC strategy optimises the fuel consumption in two ways. Firstly, the operating point of the fuel cell is chosen so that its average operating efficiency is improved; this is generally performed by running the fuel cell closer to its optimal operating point and allowing the battery to absorb sudden loads. As the battery capacity increases up to around 2.6kWh, this results in both reduced fuel consumption and reduced transient degradation. Above 2.6kWh, diminishing returns are seen by performing this as the fuel cell spends most of its time close to optimal operating efficiency; where the curve of efficiency against load is relatively flat. However, for battery capacities above 2.6kWh, the MFC also begins to minimise the overall load on the fuel cell by reducing the cyclic loading on the battery. As transient loading on the battery causes cyclic losses in the battery, the MFC strategy tends to transmit these higher frequency transients onto the fuel cell. This doesn't significantly detriment the fuel cell efficiency due to the fact that the operating efficiency curve is relatively flat in this region and the change in load is quite small. As a result, the fuel consumption is further reduced; however, this is now at the expense of fuel cell degradation. This means that although the fuel consumption is optimised, excessive transient degradation on the fuel cell means that the overall running cost begins to increase for larger battery sizes.

In contrast, the DI strategy is designed to minimise the overall running cost of the fuel cell inclusive of the degradation. With battery capacities up to 2.6kWh, this strategy behaves similarly to the MFC strategy, reducing both fuel consumption and degradation by running the fuel cell with a steady load close to its optimal operating point. Its performance

increases as the increased capacity of the battery allows. However, with battery capacities above 2.6kWh, this strategy begins to diverge from the MFC strategy. As the battery capacity increases, the cyclic loss in the battery naturally decreases due to the reduction in C-rate (defined by current/capacity). However, unlike the MFC strategy, the DI strategy does not transmit the high frequency transient loading to the fuel cell in order to further reduce these losses. In fact, the DI displays some degree of hysteresis on the fuel cell load and further reduces the transient loading on the fuel cell in order to minimise the cost associated with the transient loading degradation. Although this results in a marginally higher fuel consumption (0.7% for 4.2kWh battery), the reduction in the cost associated with the fuel cell degradation (approximately 40% for a 4.2kWh battery) massively outweighs this. As a result, the overall running cost is approximately 15% lower for the 4.2kWh battery.

For a battery capacity of 2.6kWh, both strategies show very similar behaviour and achieve similar performance in terms of fuel consumption (0.04% difference), range (0.04%), lifetime (2.4%) and overall running cost (1.1%). This capacity battery could be said to be the minimum which provides acceptable degree of control authority for the SDP optimisation to show its benefits. However, for larger capacities, the DI controller shows a much higher degree of robustness. Whereas both strategies show continuous improvements in the fuel consumption, the MFC strategy results in significantly increased degradation as the capacity of the battery increases beyond 2.6kWh.

Finally, it must be noted that the mass of the battery pack has not been included in this analysis. This assumption has been made due to the fact that the battery pack is relatively small in comparison to the total mass of the vehicle and therefore is not likely to significantly affect the results for the range of capacities examined. However, it must be noted that the improvement in both fuel consumption and fuel cell degradation seen with increasing battery size will gradually become less prominent for larger sizes of battery pack. As the battery capacity increases past 4.2kWh, the gains observed are likely to become even smaller and it is likely that the increased mass of the battery will become the dominant factor, resulting in the fuel consumption and fuel cell degradation beginning to increase.

7.4 Conclusions

This chapter has analysed the effect of changing both the fuel cell maximum power and the battery storage capacity with regards to the fuel consumption, vehicle range, fuel cell lifetime and vehicle running cost. For each system design, two strategies have been optimised using Stochastic Dynamic Programming (SDP); the first is designed to minimise the fuel consumption (MFC strategy) and the second is designed to minimise the overall running cost, inclusive of both fuel consumption and fuel cell degradation (DI strategy). The advantage of optimising the controller for each individual design is that near-optimal performance of each design is achieved and therefore system designs which offer advantages in different areas can be compared without the possibility of the results being compromised by a strategy which favours one particular benefit.

It has been found that on a purely running cost basis, the optimal design is the one that minimises the fuel cell maximum power and maximises the battery capacity. This is largely due to the fact that the cycling degradation rates seen on the Microcab contribute very strongly to its overall running cost. As a result, it is beneficial to minimise the cost of the fuel cell as much as possible despite this causing an increase in the fuel consumption and fuel cell degradation. The minimum fuel cell power required to complete every examined journey without a net change in battery SoC was 1800W, although the current fuel cell stack size of 1200W would be sufficient to maintain the battery SoC on an average journey. This means that although the battery would be depleted over some particularly harsh journeys, it could be recharged during milder trips, assuming its capacity was large enough.

In reality, there are other aspects to consider in addition to the cost. The hydrogen storage capacity of Fuel Cell Hybrid Electric Vehicles (FCHEVs) tends to be limited by the packaging requirements. This means that a reduction in the fuel consumption will most likely result in a direct increase in the range of the vehicle in addition to the reduced running cost. In addition to this, the reliability of the stack will also affect potential customer's perception of the vehicle, which is a highly important area for emerging technologies such as fuel cell vehicles. Therefore, it may be beneficial to use a slightly oversized stack in order to balance these objectives as a whole. During this exercise, it has been found that a 2400W fuel cell has a range that approximately 9% higher than the 1800W system and an estimated lifetime that is 10% higher for only a 3% increase in running cost.

With regards to the battery size, larger batteries tended to show a significant reduction in the fuel consumption and fuel cell degradation when tested using a 2400W fuel cell. It has been found that for a 2400W system, a battery capacity of at least 2.6kWh is required in order to ensure that the battery voltage constraints would not be compromised. This would result in a fuel consumption of around 11.7g/km, an estimated range of approximately 51km and an estimated fuel cell lifetime of around 705 hours, resulting in an overall running cost of approximately $0.06/km for the DI strategy. Increasing the battery capacity further to double (4.2kWh) its current size allows the fuel consumption to be reduced further to around 10.8g/km, and increases the lifetime by another 30 hours (4%).

Comparing the two strategies, there is a clear benefit to the inclusion of the estimated fuel cell degradation into the cost function. It has been found that the MFC controller tends to subject the fuel cell to a high amount of transient loading, especially for large fuel cell sizes and high battery capacities, where the control authority of the EMS is high. In comparison, the DI is able to reduce the transient loading by up to 99% in these cases,

which results in a significant (approximately 40%) increase in the estimated lifetime of the fuel cell. In doing so, the fuel consumption is only marginally increased, by around 1% for an over-sized battery and around 2.5% for an over-sized fuel cell. For systems which would be marginally capable of sustaining the battery SoC, the advantages of the DI controller are much less pronounced due to the low control authority of the EMS. This is due to the fact that the EMS is only just able to avoid the voltage constraints and therefore the behaviour of both strategies is very similar. However, there is often still a distinct reduction in overall running cost for these systems when compared to the MFC strategy.

The main difference between the strategies is that the MFC controller tends to pass high frequency, low amplitude transient loading onto the fuel cell in order to minimise the cycling losses in the battery. This reduces the average load on the fuel cell and results in a small, but significant reduction in the fuel consumption. This is particularly apparent when the ideal load on the fuel cell is in a region between the discrete operating states defined in the SDP optimisation. In this situation, the MFC strategy will tend to oscillate between these discrete states rapidly, massively increasing the transient loading on the fuel cell. In contrast, the DI strategy tends to show some degree of hysteresis on the fuel cell load. As a result, the transient degradation is massively reduced. This does have the minor downside that the response of the DI tends to be slower, resulting in a larger range of battery SoC being utilised and hence greater cycling losses in the battery.

Throughout this exercise, one of the major contributors to the running cost is the degradation associated with start-stop cycling of the fuel cell. This was responsible for up to 99% of the degradation cost for some system designs when using the DI strategy and for most realistic designs it was responsible for more than 50% of the running cost for both strategies. Although theoretically it would be possible to allow the EMS to control the fuel cell start-up and shut-down, in this work it has been found that the fuel cell should be started at the beginning of the journey and shut down at the end in order to force each controller to only cycle the fuel cell once. This minimises the cost associated with this degradation method and there is very little that the EMS can do to further reduce this. As a result, this highlights that this area is an key area for future research.

Finally, it must be noted that this exercise did not account for the change in the mass of the vehicle associated with the different system designs. This assumption has been made on the basis that the range of values used in this exercise is relatively small, and therefore will result in negligible change to the overall vehicle mass. However, if the exercise were to be repeated, especially for a larger range of battery capacities, then the inclusion of this change in mass should be accounted for. In this case, it is likely that for battery capacities much above 4.2kWh, the fuel consumption and fuel cell degradation is likely to begin to increase. This would allow the optimal battery capacity to be found.

Chapter 8

Conclusions and Further Work

This chapter summarises the report and identifies the key finding in relation to the issues introduced at the beginning of the report. The output of the project is compared to the objectives listed in the introduction, and research questions highlighted in the literature review. The chapter ends with a critical analysis of the project, including issues encountered and reflections on the broader research value of the findings. Finally, o0pportunities for further development are identified as well potential applications of the novel strategy optimisation.

8.1 Summary

Fuel Cell Hybrid Electric Vehicles (FCHEVs) have been seen as the "silver bullet" which could solve a number of issues to do with transportation for a number of decades now. This is because they do not rely on diminishing fossil fuel reserves. As a result, a hydrogen fuel cell vehicle will produce no emissions from the vehicle and therefore do not contribute to localised air pollution. In fact, if run on hydrogen produced by renewable means, a fuel cell vehicle will not produce any carbon emissions at all. As the global population continues to increase and the on-growing growth of developing nations puts ever-increasing pressure on the need for a low carbon solution, hydrogen powered vehicles become increasingly attractive.

Unfortunately, hydrogen FCHEVs have a number of significant drawbacks especially in regard to their cost, durability and hydrogen storage which as yet have prevented them from being competitive with conventional vehicles. When considered separately, the latest research purports to show that many of these issues are very nearly overcome. For example, General Motors (GM) estimate that by 2020 to 2025 only 5-10g of platinum will be required for catalysis by using a platinum-alloy shell on a more affordable core [1]. This is comparable to the amount used in the catalytic converters of conventional vehicles. However, when these issues are considered concurrently this is not always the case. For example, reduced platinum loading has been shown to significantly increase the rate of degradation due to Electro-Chemical Active Surface Area (ECASA) reduction.

It is therefore important to consider the vehicle in a holistic sense in order to examine the trade-off between these targets and the effect that different design ideas have on the effect of the vehicle as whole rather than the particular benefit in one area. That way, the true overall benefit of each new development can be truly assessed. One of the areas that can have a significant effect on the performance of the vehicle as a whole is the Energy Management Strategy (EMS). The EMS is responsible for choosing the operating conditions of the fuel cell and as a result contributes significantly to the overall fuel consumption, reliability and drive-ability of the vehicle. Therefore, when examining the trade-off between these issues, it is extremely important to consider the behaviour of the EMS.

In the first part of this thesis, a novel EMS has been developed which optimally trades off the hydrogen consumption and fuel cell degradation. It has been found that it is possible to increase the lifetime of the fuel cell on the Microcab H4 by approximately 15% for only a 3.5% increase in fuel consumption. This corresponds to a reduction in the overall running cost of approximately 9% when compared to a strategy based solely on optimising the fuel consumption. The vast majority of this improvement was due to a massive reduction (approx. 95%) in the transient loading of the fuel cell.

In addition to the immediate effects of its implementation, there is another significant benefit to this strategy when compared to the latest research in the literature. This optimisation process can be performed on any vehicle design to analyse the real-world benefits of any potential design improvements. Because the optimisation process produces the statistically optimal strategy for that vehicle, the performance can be directly compared to alternative designs without concern that the results are affected by any bias in the EMS. Each design will therefore have a unique strategy which maximises its individual benefits and represents the best performance that it can achieve.

This allows alternative designs, such as the introduction of a reduced platinum catalyst,

to be analysed in a holistic sense and identify their real-world benefits as well as any potential drawbacks. The penultimate chapter of this thesis presents an example of this type of usage where a component sizing exercise has been performed to identify the optimal fuel cell stack size and battery capacity for campus driving patterns. This is common exercise which is often performed in the early design stages of a new hybrid vehicle, and provides a significant contribution in its own right; however, it only scratches the surface of the potential applications of the novel strategy optimisation developed.

8.2 Optimal Control of the Microcab H4

The Microcab H4 is a lightweight vehicle designed specifically for the transportation of people and goods around the University of Birmingham's campus. It has been designed to replace diesel vehicles which were used previously and suffered from poor efficiency and high emissions due to the low speeds required. The Microcab has been designed to be low cost, costing just £250,000 to fully manufacture five prototype vehicles and is fitted with a relatively small 1.2kW fuel cell and a 2.1kWh battery pack. It has a top speed of approximately 30mph and a peak acceleration of just 3m/s. The vehicles were used on campus for approximately 2 years and accumulated around 4000km of usage, consuming about 68kg of hydrogen. During this time, the performance of the vehicles was studied and it was found that the vehicles suffered from relatively poor efficiency which would be improved by examination of the vehicle from a systems level in addition to the implementation of a more advanced EMS control algorithm.

The current control algorithm on board the Microcab H4 is a heuristic strategy designed to maintain the batteries at 100% State of Charge (SoC). A thorough examination of the literature in Chapter 2 revealed that there are a number of significant improvements that can be made to this type of design. The strategy is extremely simple and based solely on maintaining the battery SoC, therefore efficiency gains could be made by the introduction of a number of rules designed to optimise the operating point of the fuel cell and other components on board the vehicle. In this way, these components could be run at a higher overall operating efficiency. However, although "rule-based" controllers tend to be robust and easy to implement on board a vehicle, they do not tend to take advantage of all the potential benefits of a hybrid powertrain, meaning that further gains can be made by using more complex control algorithms. Careful examination of a number of different techniques, ranging from more complex "rule-based" controllers to machine learning techniques such as neural networks, highlighted two potential candidates; Stochastic Dynamic Programming (SDP) and Adaptive Equivalent Consumption Minimization Strategy (A-ECMS).

Equivalent Consumption Minimization Strategy (ECMS) is a heuristic technique which involves the calculation of the equivalent fuel consumption related to variation in the battery SoC. The strategy then minimises the instantaneous cost calculated as the sum of the actual fuel consumption and the equivalent fuel consumption relating to the use of the battery. A-ECMS is a development of this strategy which involves the real-time adjustment of the equivalence factor based on recent driving history. SDP on the other hand involves the generation of a stochastic model of the duty cycle. This stochastic model is then used in combination with a vehicle model in order to calculate the cost of each potential action from each potential vehicle state. The strategy is then determined by the set of actions which will minimise the cost over an infinite horizon. Although the optimisation of the

SDP strategy is extremely computationally expensive, the final strategy is captured in a lookup table which can easily be implemented on board the vehicle.

Both techniques show significant performance benefits (around 15-20%) when compared to "rule-based" controllers and are able to replicate the performance of the optimal solution to within 1-2% for the minimisation of the fuel consumption. However, SDP has been chosen because it is much more straight-forward to optimise the strategy for more complex cost functions involving not just the fuel consumption, but other performance metrics such as drive-ability, component degradation and emissions. In this situation, ECMS strategies tend to require additional correction factors in order to constrain the SoC deviation in the long-term which can significantly impair their performance.

During the course of the literature review, it was also found that much of the research into the optimisation of the EMS for fuel cell vehicles focuses solely on the fuel consumption. In this regard, research for FCHEVs lags behind that for Internal Combustion Engine (ICE) based hybrids which tends to consider a number of additional factors in the cost function such as drive-ability, battery ageing and emissions. Although many of these metrics, such as the number gear shifts, are not relevant for single gear power-trains such as in FCHEVs, the degradation of the fuel cell can be significant and is heavily affected by the EMS. It was therefore decided to design a novel EMS that could concurrently optimise both hydrogen consumption and stack degradation.

The strategy uses a number of metrics in order to quantify the major causes of fuel cell degradation which are under control of the EMS. These include penalties for operation at low loading and idle, at high current loading, transient loading and on/off cycling. In an ideal case, these figures would be obtained from extensive testing, however due to the time and budget restrictions on the project, this has been deemed out of the project scope. Instead, the figures used to quantify the degradation are derived from numbers given in the fuel cell datasheet, along with additional information from the literature. The finalised strategy weights the fuel consumption and degradation using their respective costs and is constrained by the battery voltage in order to ensure charge-sustaining behaviour.

8.2.1 1.2kW Fuel Cell

In Chapter 6, the novel Degradation Inclusive (DI) controller is compared to both the current heuristic strategy and a Minimal Fuel Consumption (MFC) strategy representative of recent work in the literature. The MFC strategy is identical in all respects aside from the exclusive of degradation from the cost function. It is initially found that the 1.2kW fuel cell in the Microcab H4 is generally quite undersized for its application and as a result is unable to maintain the battery SoC under all conditions. This means that both controllers optimised using SDP perform identically due to the voltage constraints dominating the cost function. As a result, the fuel consumption of the vehicle is increased by approximately 5% compared to the current strategy; however, the degradation due to transient loading is significantly reduced, leading to an increase in the estimated lifetime of approximately 27% and an overall cost saving of approximately 3.6%.

The results for the current strategy, however, do help to validate the vehicle model used by replicating the results seen during the vehicles usage at Birmingham. It was found by Staffell *et al.* [6], that the vehicle's traction battery would tend to deplete if the vehicle was driven non-stop, giving a maximum range for a single journey to be approximately

8km. However, with intermittent usage typical of campus driving patterns, the fuel cell could maintain the battery SoC, tending to recharge it while the vehicle was stationary, and giving a range up to 45km. In comparison, this strategy achieved an estimated range of approximately 45km over the cycles simulated for this chapter. The SDP strategies achieved a slightly lower range of 43km due to the increased fuel consumption. This difference can largely be attributed to the fact that the optimised strategies run the fuel cell at maximum power and hence a lower efficiency in order to recharge the battery more quickly during stationary periods. In contrast, the baseline strategy allows the fuel cell power to gradually reduce as the battery charge increases, which is more efficient, but increases the possibility of the batteries being depleted if the vehicle were to begin being used again after a brief period of time.

8.2.2 4.8kW Fuel Cell

Overall, it was concluded that the 1.2kW fuel cell was generally quite undersized for the application. This correlates with previous findings by Kendal *et al.* [4] and Staffell *et al.* [6] and means that the current control strategy of running the fuel cell near to maximum power for almost all of the time is the only viable option in order to attempt to maintain the battery SoC. As a result, the SDP optimised strategies tended to produce very similar behaviour to the current strategy. Therefore, it was decided to repeat the analysis for one of the options for the newer Microcab H2EV, a 4.8kW fuel cell. This would allow the potential benefits of the novel control strategy to be examined in detail.

With a 4.8kW fuel cell, the current strategy causes the fuel cell to suffer from a very high amount of transient loading due to the fact that stack is now able to maintain the battery at 100% SoC. With the 1.2kW fuel cell, the batteries tended to be gradually depleted over a single journey meaning that the fuel cell load was relatively stable at 100% power for much of time, however with a 4.8kW fuel cell, all of the transient loading inherent in the duty cycle is now passed directly onto the fuel cell and the estimated lifetime of the fuel cell is reduced down from approximately 574 hours to just 166 hours. This is an inherent problem with heuristic strategies; what works well on one system design may not necessarily translate well to another, meaning that direct comparison between system designs can be very difficult without concern of bias from the strategy. Although it would be possible to improve the results with the introduction of a few simple rules, this may negatively affect the results for the 1.2kW fuel cell.

Conversely, it is relatively trivial to re-optimise the SDP strategies for the changes in the system design. Because the fuel cell is now able to maintain the battery SoC, the optimisation is no longer dominated by the voltage constraints and the differences between the MFC and DI strategies are apparent. As would be expected, it is found that the MFC strategy results in the lowest fuel consumption, approximately 9.9% lower than the baseline strategy and 3.7% lower than the DI strategy. However, the MFC strategy introduces in a number of oscillations in the fuel cell load in order to minimise the fuel consumption. As a result, it also suffers from a high degree of transient loading. The DI strategy, overall, behaves very similarly, but avoids this type of transient loading due to some hysteresis on the fuel cell loading. This means that transient loading is decreased by approximately 96% when compared to the MFC strategy leading to an increase in the estimated lifetime of around 18%. This results in an overall running cost reduction of approximately 9%.

8.2.3 Key Findings

In general, the findings of Chapter 6 correlate well with the theory and previous literature. It has been found that the performance of the vehicle is heavily reliant on both the system design and the control strategy. An undersized fuel cell leads to generally deficient performance due to the reduced control authority of the EMS, however for an appropriately sized fuel cell, the differences between the strategies is apparent. As would be expected, the MFC strategy resulted in the lowest fuel consumption and the DI strategy resulted in the lowest overall running cost. The key findings can be summarised as follows;

1. **Control Authority:** The degree of control authority of the EMS is crucial for optimisation of the strategy. If the system is unable to stay within its constraints, then the cost penalty associated with these constraints will dominate the optimisation process, and as a result, inferior performance is observed. The 1.2kW fuel cell is unable to maintain the battery voltage within its constraints under all circumstances. Because the cost associated with these constraints is so high, the cost associated with fuel consumption and degradation is negligible and the performance of the strategy with regard to these targets is poor.

2. **Fuel Consumption:** Both SDP strategies tended to show relatively similar performance with regard to the fuel consumption. As would be expected the MFC strategy shows the best overall performance for the 4.8kW fuel cell stack, but for the DI strategy the fuel consumption was only 3.2% higher, which was still approximately 7% lower than for the baseline strategy.

3. **Operating Point Degradation:** In general, optimisation of the fuel consumption coincides with minimisation of the operating point degradation. It is beneficial for both strategies to run the fuel cell at its optimal operating point for as much time as possible. This inherently means that extreme loading conditions tend to be avoided in order to optimise the fuel cell efficiency. However, it may be beneficial from a fuel consumption point of view to run at low loading conditions under some circumstances, especially if this means a reduction in the energy losses in other parts of the system, such as DC/DC converter efficiency or battery cycling. As a result, the DI strategy reduced the operating point degradation by approximately 19% for the 4.8kW fuel cell.

4. **Transient Degradation:** Minimisation of the fuel consumption can compete heavily with minimisation of the transient loading on the fuel cell. In order to minimise cycling losses in the battery, the MFC strategy tends to introduce an oscillating load on the fuel cell under some circumstances. This leads to significant transient degradation, which can substantially reduce the lifetime of the fuel cell. The DI strategy however, avoids transient loading almost entirely by introducing some hysteresis into its strategy, massively improving the reliability of the fuel cell for only a marginal increase in the fuel consumption.

5. **Cycling Losses:** For both the MFC and DI strategies, the start/stop cycling degradation was the highest contribution to the overall running cost, at 52% and 58% respectively. There is very little that the EMS can do to further reduce this type of degradation and therefore it represents a significant area for further research.

8.3 System Design Using Optimal Control

The performance of any hybrid powertrain depends heavily on the control strategy of the EMS. This is because the EMS chooses the operating point of the various components involved which determines whether or not they operate efficiency. It is therefore important to consider the design of the EMS when comparing different system designs. SDP is an ideal candidate for this type of analysis because each strategy can be optimised individually for every particular design. This means that the maximum performance of each alternative is given, and the results are directly comparable without concern as to bias in the strategy.

An interesting question that arises in the literature regards the benefit of using an over-sized fuel cell in order to limit the degradation. Is it more cost effective to use a marginally sized fuel cell which would need to run close to full power and hence suffer from high rates of degradation, or an over-sized fuel cell which would be able to run at a more optimal operating point and therefore experience significantly less degradation? Chapter 7 analyses the effect of changing the fuel cell maximum power and the battery capacity on the performance of the vehicle with regard to the fuel efficiency, operating range, fuel cell lifetime and operating cost. For each design, both MFC and DI strategies have been optimised using SDP. Overall, it is found that in order to minimise the absolute running cost of the vehicle, the smallest fuel cell that is capable of maintaining the battery SoC should be used in conjunction with a relatively large capacity battery. It must be noted however that the degradation and cost of the battery were not taken into account due to the assumption that they would be negligible compared to the relatively high cost of both the hydrogen fuel and fuel cell stack.

Of the fuel cell sizes tested, it was found that the 1800W fuel cell stack was the smallest stack which was able to successfully maintain the battery SoC over all of the tested journeys. This was to be expected due to the fact that the highest average power on a single journey was approximately 1650W, and the maximum power of the fuel cell would need to be at least as high as the average power demand in order to ensure no net change in the battery SoC. For fuel cell stacks of this size and higher, the results were therefore directly comparable, and it was found that the smallest size (1800W) was the one that minimised the overall running cost for both the MFC and DI strategies. This can be attributed to the excessive cost of start-stop cycling and the linear increase in the value of the fuel cell as the stack size increases.

Given a linear approximation of the fuel cell cost as used in this analysis, as the fuel cell size increases, so does its value, so although the hydrogen consumption and degradation rates for larger fuel cell stacks tended to be smaller than that for 1800W, the overall running cost will still increase with size. However, the results are marginal, and it is shown that a stack with a lower start/stop cycling degradation rate, as used by Chen *et al.* [13], would have a larger optimal stack size of 2400W. This is because the reduction in fuel consumption and degradation in the region between 1800W and 2400W more than compensates for the increase in the value of the fuel cell.

However, it is also concluded in this analysis, that there are significant benefits to using a slightly larger fuel cell stack than that with the lowest running cost. By increasing the stack size to 2400W, the running cost is increased by approximately 3%, however the estimated range is increased by approximately 9% and the estimated lifetime is around 10% longer. The fuel consumption is a crucial factor to consider for FCHEVs, because on-board hydrogen

storage can be an issue with regard to packaging, and therefore increased fuel efficiency also often directly correlates to an increase in the vehicle range. The reliability of fuel cells is also often cited as a concern for this type of vehicle and can have significant impact on consumer's perception of the technology which can be a crucial factor for emerging technologies.

With regard to the battery capacity, for a fuel cell of 2400W, it is found that the fuel consumption generally decreases as the battery capacity increases. This is because the EMS is afforded a larger range of fuel cell operating points which will not exceed the battery voltage constraints. Both strategies perform very similarly up to a capacity of around 2.6kWh due to the low control authority of the EMS. Below this point, the choice of fuel cell operating point is largely determined by that which will minimise the risk of exceeding the constraints on the battery voltage. Above 2.6kWh however, there is a clear benefit to the DI strategy, which, despite showing a marginally higher (0.7%) fuel consumption, suffers from significantly less degradation (40%) when used with a 4.2kWh battery. This results in a significantly reduced running cost of around 15%.

8.3.1 Key Findings

Chapter 7 demonstrates the use of the novel control strategy in order to compare different systems designs. This is achieved by producing a number of optimal strategies considering vehicle designs with a variety of fuel cell sizes and battery capacities. The results largely correspond to the trends one might expect from the theory; however, the analysis quantifies the real-world trade-off between the fuel cell cost and reliability. The key findings can be summarised as follows;

1. **Control Authority** Again, the control authority of the EMS has an enormous impact on the results and it is shown that systems with undersized fuel cell or battery capacities tend to produce significantly inferior results due to the poor optimisation of the targets. This analysis compares two slightly different strategies, each of which are constrained identically. This allows the identification of areas where the constraints are dominating the optimisation as regions where the two strategies behave almost identically. It is shown that for undersized systems, the control authority of the EMS is relatively low and no significant benefit is seen by inclusion of the degradation into the cost function. However, as the stack size and battery capacity is increased, the DI strategy tends to show massive reduction in the degradation for only a minor increase in fuel consumption.
2. **Fuel Cell Size** In order to minimise the running cost of the fuel cell vehicle with regard to both fuel consumption and degradation, it is optimal to choose the fuel cell with the lowest maximum power that exceeds the average power required over the worst-case duty cycle. This is largely due to the excessive cost of start-stop cycling degradation which cannot be mitigated by the EMS, and due to the increase in the value of the fuel cell with size. However, the results are marginal and it is shown that a fuel cell with a lower start-stop cycling degradation rate will benefit from a slightly oversized fuel cell. As the size of the stack becomes larger however, the benefits tend to reduce and the value of the stack again becomes the dominate factor. Therefore, in some cases, it may be beneficial to oversize the stack slightly, but it is unlikely to be economical to over-size the stack significantly.

3. **Battery Size** The battery capacity can have a significant effect on both the fuel consumption and the fuel cell degradation. Increasing the battery capacity allows the EMS a higher degree of control authority with which to optimise the strategy. As a result, significant benefits are observed which can be attributed to the fuel cell being run at a higher overall efficiency and a significant reduction in the transient loading for the DI controller.

8.4 Research Questions

As part of the literature review a number of research questions were raised. In particular, six specific questions were highlighted in Section 2.4.1 for further study as part of this work. An attempt at answering these questions follows below;

1. **How can these degradation methods [see Section 2.2.2.6] be quantified so as to be used in a degradation inclusive cost function?**

   As was shown in the literature review, there are a number of known degradation methods for fuel cells, mostly due to deviation of temperature and chemical species concentration, either across the whole cell, or in a localised area. Due to the complex interactions between the electrical, chemical and thermodynamic processes involved, examination at a high level requires either a complex mathematical model or a significant degree of abstraction. For the purposes of developing an EMS using SDP, complex mathematical models would be unsuitable and therefore simplification of the degradation methods was chosen. In order to achieve this, four main operating conditions/events, were highlighted as causing elevated rates of degradation and the fuel cell datasheet was used in order to estimate their effect. These were; high power operation, low power/idle operation, transient loading and on/off cycling.

   The values used for the cost function were based on figures from the manufacturers datasheet [106], cross referenced with figures quoted in the literature [13]. For more information on the details of the cost function, see Section 5.2.2.

2. **To what extent can the fuel cell ageing be reduced by optimising the EMS with regard to known fuel cell degradation causes?**

   The EMS can reduce fuel cell degradation via two methods. Firstly, it can be used to stabilise the load on the fuel cell when it is in use. It has been found in Chapter 6 that transient degradation can be reduced by around 99% with very minimal (3-5%) in the fuel consumption. This also serves to reduce the degradation due to operating point by ensuring that the fuel cell runs at a more consistent load and is therefore less likely to operate at the extremes of its loading range.

   Secondly, the EMS can be used to turn off the fuel cell when it is not required. By allowing the EMS to power on the fuel cell only when required, it is theoretically possible to balance the on/off cycling degradation with that caused by its operating point. However, it was found that the degradation due to cycling was so high that it is never beneficial to cycle the fuel cell more than absolutely necessary. The optimal policy is to turn the fuel cell on at the beginning of a journey and off again at the end, allowing it to operate continuously in between even if this means that it would suffer elevated rates of ageing due to operation at idle/low loading.

3. **Under real-life driving scenarios, which degradation methods are the most significant?**
   Transient loading of fuel cells in automotive applications is a much-discussed topic in the literature and is often quoted as an important reason to hybridise a fuel cell vehicle's powertrain by using an ultracapacitor or a battery pack. As a result, there is previous work which incorporates load stabilisation of the fuel cell into the control strategy. However, no research was found that specifically examines typical transient loads found during transportation usage and their effect on the lifetime of the fuel cell. For other methods of fuel cell aging, such as that due to cycling or the operating point, there are even fewer mentions.

   The work in Chapter 6 examines this area in significantly more detail than has been done in the past. It was found that for control strategies which do not avoid for transient loading, this method of degradation accounts for around 0-15% of the ageing of the fuel cell. For the vehicle considered in Chapter 6, using a 4.8kW fuel cell, operating point degradation accounts for approximately 8-10% of the fuel cell aging depending on the type of control strategy. However, it was found in Chapter 7 that the degree operating point degradation is much more dependent on the size of the fuel cell chosen. Finally, the degradation due to on/off cycling was found to be most significant, contributing to around 75-96% of the ageing process depending on the control strategy and size of the fuel cell. As a result, it also contributed to more than 50% of the running cost of the vehicle in some cases. In summary, it was found that transient degradation can be easily avoided by design of the supervisory EMS controller and operating point degradation is largely dependent on the size of the fuel cell chosen and the average power requirements of the vehicle. As a result, on/off cycling was found to be the most significant unavoidable contribution and therefore represents a critical area for further research.

4. **How should the degradation of the fuel cell be weighted fairly against more traditional optimisation metrics such as the fuel consumption?**

   The fuel cell degradation was weighted against the fuel consumption by using their relative monetary values. It was decided to do this so that it was possible to calculate overall running cost of the vehicle inclusive of both factors and that this would be the value to be minimised by the optimisation process. This technique could also be extended to include other factors such as the degradation of the battery pack and/or mechanical drivetrain components. However, it was found that defining the cost of the fuel cell was not a trivial task due to the small size of the fuel cell and the limited production numbers of the vehicle in question, and that using the actual replacement cost of the fuel cell would heavily weight (200:1) the degradation over the fuel consumption. Instead it was chosen to use estimated mass-production figures from the literature in order to allow fairer comparison between the two. For more information on the cost function weighting, see Section 6.1.1.

5. **What effect does each of these choices have on the performance and reliability of the vehicle as a whole?**
   The work in this thesis is for a small niche vehicle, designed specifically for campus usage, however, it is possible to extrapolate from the results in Chapter 7 in order to estimate what they would mean for full-scale passenger vehicles.

   a) A fuel cell with a maximum power equivalent to an ICE For fuel cell vehicles, as well as ICE hybrid vehicles, consumers are likely to be concerned with the power output of the prime fuel converter. This has lead manufacturers to tend to provide hybrid vehicles with ICEs of a comparable size to their non-hybrid counterparts. As an example, the Toyota Mirai is fitted with a 114kW (153hp) fuel cell stack, similar in maximum power to an equivalent ICE used in this type of vehicle, which is hybridised with a relatively small 1.6kWh NiMH battery pack. It would be fair to say that this configuration puts the Mirai into the "Mild" hybrid category where the vast majority of the tractive power comes from the prime fuel converter (rather than the energy buffer). This may be compared to the results for a large fuel cell and small battery pack in Chapter 7.

   Fuel cells tend to run at their optimum efficiency at around 30-40% of their maximum power in contrast to ICEs which reach maximum efficiency at 50-90% of the peak power output [5]. As a result, from a fuel consumption perspective it is more beneficial to oversize a fuel cell than an ICE. The results in Chapter 7 confirm this, suggesting that a large fuel cell will tend to give the best fuel consumption figures. The fuel consumption could, however, be improved by also increasing the size of the battery pack. From a fuel cell degradation perspective, using a large fuel cell will tend to mean that the fuel cell will experience more transient loading, especially if the supervisory EMS is not designed to minimise this. This issue is also compounded by the fact that the larger fuel cell will cost more to replace, meaning that the degradation will contribute significantly to the running cost of the vehicle. Even with a degradation "aware" controller, the fuel cell is likely to experience significant transient loading due to the small size of the battery pack, see Figure 7.9.

   b) A fuel cell with peak efficiency at the average power demand

   As mentioned in part a), fuel cells tend to reach peak operating efficiency at around 30% of their maximum power. Therefore, this heuristic design criteria would likely result in a fuel cell which is around or possibly slighter smaller than that used in the Toyota Mirai and the overall effect would be similar. The fuel cell would run very efficiently resulting in optimal fuel consumption, however the fuel cell would be, in general, quite large and therefore expensive. As a result, the cost of the degradation would still be fairly significant. If the battery pack was also sized for optimal fuel consumption, it would likely be larger than that in the Mirai. As a result, the degradation could be less of an issue due to the battery pack absorbing some of the transient loading, especially if the EMS had be designed to consider this. The net effect would be an expensive vehicle, for which the reduction in long term running cost may or may not out outweigh the upfront cost.

c) A fuel cell with a maximum power slightly higher than the power required to cruise at maximum cruising speed

Overall, this method would be the most sensible way to choose the size of the fuel cell. The maximum power of the fuel cell defines the maximum cruising speed of the vehicle due to the fact that if the vehicle exceeds this speed, the battery pack would gradually be depleted over time and therefore the vehicle would, at some point, have to slow down. Considering a maximum cruising speed of around 110km/h (70mph), this would require the fuel cell to produce around 90-110kW. Purely by coincidence, this is a similar size of fuel cell to that of the previous two answers and as a result, the effects would be similar to those already described.

6. **What effect would different system designs have on the control decisions made by an EMS designed using optimal control?**
The answer to this question is covered in detail in Chapter 7 for assorted sizes of fuel cell and battery pack. In particular, it can be seen in Figure 7.2 that in general, a larger fuel cell means that the EMS will tend to allow the battery pack to drop to a lower level while running. This is because a larger fuel cell is able to handle sudden high load demands better without the battery voltage dropping below the minimum limit. For the MFC controller, this has the net effect of running the battery pack at a lower nominal SoC due to the fact that the maximum SoC tends to fall also. For the DI controller, the nominal battery SoC tends to fall only slightly, and the maximum SoC tends to remain fairly high. This is because the DI controller uses the additional capacity of the fuel cell to smooth out transient loading whereas the MFC controller tends to use it to maximise the fuel consumption by running the battery at a flatter part of the battery polarisation curve and hence minimising cycling losses.

   One issue that was not encountered in this work is the effect of regenerative braking, however the behaviour of the controller can be analysed in order to estimate what the effect of regenerative braking would be.

8.5 Conclusions

"The overall goal of this work is to identify the best methods in which to optimise the holistic design of a FCHEV using pre-existing or already available components." - Introduction (Chapter 1)

The work in this thesis began with a review of the design requirements of a FCHEV, considering the overall requirements of individual components, their interactivity and a critical analysis of state-of-the-art supervisory control techniques. It was concluded in the literature review that Stochastic Dynamic Programming (SDP) and Equivalent Consumption Minimization Strategy (ECMS) represented the forefront of technology, both in popularity and consistency of performance. A number of other techniques were also identified, some of which are deserving of further research (see Section 2.4.1), such as Game Theory (GT) and Model Predictive Control (MPC), however it was decided to focus on well-known techniques for generic hybrid vehicles and how these could be adapted for use on fuel cell vehicles in particular. Using the Microcab H4 as a baseline, a novel EMS strategy was developed using SDP that concurrently optimises both the fuel consumption and fuel cell degradation. These areas were chosen in order to broaden the research value of the work because they had been identified as specific areas for which further research was required for FCHEVs. Improvements in fuel efficiency serve to alleviate issues due the fuel storage limitations of FCHEVs (see Section 1.3.2), and reduction of degradation serves to increase the longevity and long term running costs of such a vehicle, also highlighted as a major limitation of current FCHEVs.

The project encountered a number of minor issues. The first was which was due to the limited availability of data from the Microcab's usage at the University of Birmingham meaning that it was necessary to examine techniques in order improve the quality of the Markov chain model of the duty cycle. Rather than simply rounding the data in order to discretize the speed trace, it was theorised that if the data was interpolated and weighted, or fitted to a known distribution, more information would be retained during the discretisation process. Although, this was almost certainly the case, both new techniques encountered a new issue in that it became possible for the vehicle to enter a state which was not encountered in the test data. This resulted in a Markov chain that could not produce satisfactory results when simulated. Although, these new techniques were unsuccessful, the validation procedure of the Markov model did serve well to highlight this efficiently. In fact, the same technique (Speed-Acceleration Frequency Distribution (SAFD) analysis) as used for validation was successfully used to identify similar data captured at Loughborough University that could be used to generate a high-fidelity model of a campus duty cycle, closely correlated with the original data.

Another issue that was encountered was that the initial performance of the SDP optimised strategy was much below expectations. Close examination of the data showed that the fuel cell was in fact too small to guarantee that the battery SoC could be maintained even over a relatively mild "campus based" duty cycle. This correlated with previous findings [4, 6] from when the vehicle was used at the University of Birmingham. Although, these findings were known in advance, it was hoped that the optimised control strategy would improve the efficiency of the system such that the issue would be overcome. However, the fact that even an optimal control policy could not overcome this issue serves to prove that it is due to a system design flaw rather than poor control. The issue was over-

come by increasing the size of the fuel cell in the model so that the model would represent the newer Microcab H2EV which is fitted with a 5kW fuel cell.

Finally, although the small size of the Microcab H4 limits the broader research value of the specific controller design, the techniques that have been developed and demonstrated using this vehicle could be equally well applied to a larger vehicle which is more representative of a typical modern passenger vehicle and similar results would be expected. In fact, due to the higher mass of such a vehicle, as well as a greater range of speeds, it may be theorised that such a controller could produce even more noteworthy results.

Despite these issues, the SDP controller worked as expected and the overall objectives (Section 1.6) of the project were met. There were a number of key findings which have already been described in this Chapter, however, there are two that deserve special mention due to their significance to FCHEVs in general. Firstly, it was found that it is possible to significantly improve the lifetime of the fuel cell with very little penalty to the fuel consumption. It was shown that by including the fuel cell degradation in the cost function for SDP, it was possible to reduce the degradation of the fuel cell by around 19% for only a 3.2% increase in the fuel consumption. Secondly, it was found that the degradation cost of on/off cycling was perhaps the most significant degradation method which could not be further reduced using supervisory control. As a result, it was found that, from a system design perspective, very is important not to oversize the fuel cell more than is absolutely necessary. It has also been highlighted that this is a key area for further research.

8.6 Recommendations for Further Work

There are number of areas for further work from this thesis. These can be separated into two categories; firstly there are a number of areas in which the SDP optimisation process can be developed to improve its accuracy as well its usefulness. Secondly, the use of this strategy optimisation opens up a vast range of potential applications for the comparison of different vehicle designs, as well as the analysis of FCHEV performance in a holistic sense. Each of these categories has been considered individually in the following sections.

8.6.1 Development of the Strategy

This research is the first to quantifiably analyse the trade-off between hydrogen consumption and fuel cell stack degradation using optimal control. As a result, there are a number of ways in which this technique can be developed further to improve both its accuracy and extend its relevance to real-world vehicles. The strategy optimisation in this work has focussed on areas of particular importance to FCHEVs, such as the fuel cell stack degradation and the vehicle range. However, many of the factors that influence ICE hybrid vehicle EMS optimisation, such as battery degradation and power availability, are equally important to FCHEVs. There is already a significant amount of research in these areas and quantification methods already developed in the literature could be included in the cost function alongside the fuel consumption and fuel cell degradation.

1. **Battery Degradation** There are a variety of ways that the battery degradation could be included. One of the simplest methods would be to include a cost associated with the accumulated charge transfer as performed by Moura *et al.* [64]. This would allow the lifetime of the battery to be estimated, as well as its influence on the running cost of the vehicle. This has not been included in this thesis, so as to be able to isolate the effect of the fuel cell degradation methods on the optimisation and also due to the low cost of lead acid batteries which would not be expected to significantly affect the results. However, more advanced battery technology, such as lithium-ion, tends to be significantly more expensive and more sensitive to its operating conditions. Therefore, investigation into the three-way trade-off between hydrogen consumption, stack degradation and battery degradation may produce significant results. This work could then be further extended to investigate the benefits of including capacitors to protect the battery.
2. **Power Availability** Many of the drive-ability aspects considered for ICE vehicles are of little importance to fuel cell vehicles due to their low noise and vibration, and the lack of requirement for a gearbox. However, some aspects such as power availability could be included in the cost function. The low size of the battery and marginal size of the fuel cell in the Microcab H4 means that the straight-line performance of the vehicle can be significantly affected by the SoC of the batteries. Therefore, it may be desirable to include a cost associated with the power availability as described by Vidal-Naquet and Zito [62] when using this technique for development of a production vehicle.
3. **Fuel Cell Degradation Metrics** The fuel cell degradation metrics used in this thesis are relatively simple ways of accounting for the many degradation methods apparent in FCHEVs based on the figures available from the fuel cell datasheet and the

literature. However, for a more accurate estimation of the stack lifetime for a particular, it would be possible to improve the quantification of these estimations using experimental testing. By testing a large number of sample cells and stacks, the accuracy of the parameters could be improved alongside identification of additional metrics that could be used to quantify the degradation of the fuel cell stack.

4. **Model Development** In the same vein to the previous point, the vehicle model used in the work has been kept relatively simple. This has been done deliberately in order to reduce its complexity and ensure that it is suitable for running multiple SDP optimisations; however, there is potential for improvement in this regard. For example, it would be interesting to investigate the effect of the fuel cell temperature on the results. This could be achieved by the inclusion of the fuel cell temperature as an additional state of the vehicle. Both the efficiency of the fuel cell and the rate of fuel cell degradation would be dependent on this, especially during the warm-up period.
5. **Comparison to A-ECMS** SDP was chosen as the basis for this control strategy due to its robustness with regards to the cost function in comparison to ECMS. This is because strategies based on ECMS often require some sort of regulation factor in order to account for other costs such as that associated with the fuel cell degradation. However, it may be possible to develop a novel adaptive strategy which accounts for both fuel consumption and fuel cell degradation using online learning such as that used in A-ECMS. This would allow potential benefits such as real-time adjustment of the degradation estimation algorithm based on feedback from the fuel cell management system.
6. **MPC** The development of MPC for hybrid vehicles is a currently rapidly developing area in the literature, especially the use of *a priori* information available from connected devices such as GPS navigation, traffic information and Intelligent Transport System (ITS). The cost function developed in this thesis could be used in conjunction with this type of strategy in order to further optimise the strategy.

8.6.2 Applications of the Strategy

The previous chapter in this thesis demonstrates an example application of this strategy optimisation in order to assess the comparative benefits of a variety of fuel cell stack sizes and battery capacities. However, there is a vast number of potential applications, some of which would require further development such as mentioned in the previous section. These include the comparison of more detailed design changes such as the platinum loading on the catalyst or the effect of the introduction of lithium-ion batteries.

1. **Experimental Testing** The work in this thesis consists solely of simulation using validated models, however further work could involve some form of experimental testing. Although Hardware-in-the-Loop (HIL) testing of the fuel consumption estimation would be relatively easy to perform using the equipment available, validation of the degradation estimation would be a complex and time-consuming task, possibly requiring the use of multiple vehicles. It has therefore been decided that it would not be feasible to achieve significant validation with the resources available to this project.

2. **Platinum Loading of the Catalyst** Another question that arose in the introduction is the effect of reducing the platinum loading on the catalyst. This has obvious benefits in reducing the cost of the fuel cell; however, it can also affect the durability of the stack. This work could be used to quantifiably assess benefits and costs of reduced platinum loading in order to identify the optimal balance between cost and durability.
3. **Vehicle Configuration Changes** The Microcab H4 is a relatively old FCHEV developed almost 10 years ago using a minimal cost philosophy. This work could be used to assess the potential benefits of updating various components individually. For example, the introduction of a brushless DC electric motor, as used on the newer Microcab H2EV, would significantly reduce the loading on the fuel cell due to its higher efficiency. As a result, it may be more economical to use this type of motor than to increase the size of the fuel cell to 2400W. Similarly, lithium-ion batteries have a significantly higher energy density than lead acid and it would be interesting to investigate if their increased cost is justified by the reduced mass of the vehicle.
4. **A More Conventional Passenger Vehicle** Finally, this work has focussed on the application of the strategy for a relatively specialised vehicle. It would be interesting to investigate the results when considering a more conventionally sized vehicle such as the Toyota Mirai, or the Hyundai ix35 Fuel Cell. This would allow for examination using standardised test cycles such as the New European Driving Cycle (NEDC), US federal drive-cycles and Artemis.

References

[1] Ulrich Eberle, Bernd Müller, and Rittmar von Helmolt. Fuel cell electric vehicles and hydrogen infrastructure: Status 2012. *Energy & Environmental Science*, 5(10):8780–8798, 2012.

[2] S.H. Mohr, J. Wang, G. Ellem, J. Ward, and D. Giurco. Projection of world fossil fuels by country. *Fuel*, 141:120 – 135, 2015.

[3] Nan Qin, Ali Raissi, and Paul Brooker. Analysis of fuel cell vehicle developments. Technical report, Florida Solar Energy Center, 2014.

[4] K. Kendall, B.G. Pollet, A. Dhir, I. Staffell, B. Millington, and J. Jostins. Hydrogen fuel cell hybrid vehicles (HFCHV) for Birmingham campus. *Journal of Power Sources*, 196(1):325 – 330, 2011.

[5] A. Rousseau, P. Sharer, and R. Ahluwalia. Energy storage requirements for fuel cell vehicles. Technical Report 2004-01-1302, SAE, 2004.

[6] Iain Staffell. Results from the microcab fuel cell vehicle demonstration at the University of Birmingham. *International Journal of Electric and Hybrid Vehicles*, 3(1):62–82, 2011.

[7] Paul Ruetschi. Aging mechanisms and service life of lead acid batteries. *Journal of Power Sources*, 127:33 – 44, 2004. Eighth Ulmer Electrochemische Tage.

[8] P. Pisu, K. Koprubasi, and G. Rizzoni. Energy management and drivability control problems for hybrid electric vehicles. In *Decision and Control, 2005 and 2005 European Control Conference. CDC-ECC '05. 44th IEEE Conference on*, pages 1824–1830, Dec 2005.

[9] Wei-wei Xiong, Yong Zhang, and Cheng-liang Yin. Configuration design, energy management and experimental validation of a novel series-parallel hybrid electric transit bus. *Journal of Zhejiang University - Science A*, 10:1269–1276, 2009.

[10] C.C. Chan. The state of the art of electric, hybrid, and fuel cell vehicles. *Proceedings of the IEEE*, 95(4):704 –718, April 2007.

[11] Yongling Sun, Joan Ogden, and Mark Delucchi. Societal lifetime cost of hydrogen fuel cell vehicles. *International Journal of Hydrogen Energy*, 35(21):11932 – 11946, 2010. Symposium of the Mexican Hydrogen Society.

[12] M Dresselhaus, G Crabtree, and M Buchanan. Basic research needs for the hydrogen economy: Report on the basic energy sciences workshop on hydrogen production, storage, and use. *Office of Science, US Department of Energy*, 2004.

[13] Huicui Chen, Pucheng Pei, and Mancun Song. Lifetime prediction and the economic lifetime of proton exchange membrane fuel cells. *Applied Energy*, 142:154 – 163, 2015.

[14] Bruno G. Pollet, Iain Staffell, and Jin Lei Shang. Current status of hybrid, battery and fuel cell electric vehicles: From electrochemistry to market prospects. *Electrochimica Acta*, 84:235 – 249, 2012.

[15] Boucar Diouf and Ramchandra Pode. Potential of lithium-ion batteries in renewable energy. *Renewable Energy*, 76:375 – 380, 2015.

[16] Christopher Vagg. *Optimal Control of Hybrid Electric Vehicles for Real-World Driving Patterns*. PhD thesis, Department of Mechanical Engineering, University of Bath, 2014.

[17] Craig Marks, Edward A Rishavy, and Floyd A Wyczalek. Electrovan - a fuel cell powered vehicle. Technical report, SAE Technical Paper, 1967.

[18] Ferdinand Panik. Fuel cells for vehicle applications in cars - bringing the future closer. *Journal of Power Sources*, 71(1-2):36 – 38, 1998.

[19] Rittmar von Helmolt and Ulrich Eberle. Fuel cell vehicles: Status 2007. *Journal of Power Sources*, 165(2):833 – 843, January 2007.

[20] Chuck Shulock, Ed Pike, Alan Lloyd, and Robert Rose. Vehicle electrification policy study - Task 1 report: Technology status. Technical report, ICCT: The International Council on Clean Transportation, 2011.

[21] IEA. Technology roadmap: Hydrogen and fuel cells. Technical report, International Energy Agency, 2015.

[22] Kathleen O'Malley, Grace Ordaz, Jesse Adams, Katie Randolph, Channing C. Ahn, and Ned T. Stetson. Applied hydrogen storage research and development: A perspective from the US Department of Energy. *Journal of Alloys and Compounds*, 645, Supplement 1:S419 – S422, 2015. Supplement Issue: Proceedings from the 14th International Symposium on Metal-Hydrogen Systems: Fundamentals and Applications, 2014 (MH2014).

[23] IEA. Prospects for hydrogen and fuel cells. Technical report, International Energy Agency, 2005.

[24] K. Kendall, B. Pollet, and J. Jostins. Hydrogen hybrid vehicles for University of Birmingham campus. In *IET HEVC 2008: Hybrid and Eco-Friendly Vehicle Conference*, pages 1 –3, December 2008.

[25] Tim O. Deppen. *Optimal Energy Use in Mobile Applications with Storage*. PhD thesis, University of Illinois at Urbana-Champaign, 2013.

[26] D.F. Opila, X. Wang, R. McGee, R.B. Gillespie, J.A. Cook, and J.W. Grizzle. An energy management controller to optimally trade off fuel economy and drivability for hybrid vehicles. *IEEE Transactions on Control Systems Technology*, 20(6):1490–1505, 2012.

[27] Rajit Johri and Zoran Filipi. Self-learning neural controller for hybrid power management using neuro-dynamic programming. Technical Report 2011-24-0081, SAE Technical Paper, 2011.

[28] Y. Guezennec, Ta-Young Choi, G. Paganelli, and G. Rizzoni. Supervisory control of fuel cell vehicles and its link to overall system efficiency and low-level control requirements. In *American Control Conference, 2003. Proceedings of the 2003*, volume 3, pages 2055–2061, June 2003.

[29] J. Schiffer, O. Bohlen, R.W. De Doncker, D.U. Sauer, and Kyun Young Ahn. Optimized energy management for fuelcell-supercap hybrid electric vehicles. In *2005 IEEE Conference Vehicle Power and Propulsion*, pages 341 – 348, September 2005.

[30] Andreas Schell, Huei Peng, Doanh Tran, Euthie Stamos, Chan-Chiao Lin, and Min Joong Kim. Modelling and control strategy development for fuel cell electric vehicles. *Annual Reviews in Control*, 29(1):159 – 168, 2005.

[31] Chan-Chiao Lin, Min-Joong Kim, Huei Peng, and Jessy W. Grizzle. System-level model and stochastic optimal control for a PEM fuel cell hybrid vehicle. *Journal of Dynamic Systems, Measurement, and Control*, 128(4):878–890, 2006.

[32] A. Vahidi, A. Stefanopoulou, and Huei Peng. Current management in a hybrid fuel cell power system: A model-predictive control approach. *IEEE Transactions on Control Systems Technology*, 14(6):1047 –1057, November 2006.

[33] Aymeric Rousseau, Thomas Wallner, Pagerit Sylvain, and Henning Lohse-Busch. Prospects on fuel economy improvements for hydrogen powered vehicles. Technical report, SAE, 10 2008.

[34] Minjin Kim, Young-Jun Sohn, Won-Yong Lee, and Chang-Soo Kim. Fuzzy control based engine sizing optimization for a fuel cell/battery hybrid mini-bus. *Journal of Power Sources*, 178(2):706 – 710, 2008.

[35] Tatsuaki Yokoyama. Progress and challenges for Toyota's fuel cell vehicle development. In *California Air Resources Board ZEV Symposium, Sacramento CA. Sept*, volume 21, 2009.

[36] E. Schaltz, A. Khaligh, and P.O. Rasmussen. Influence of battery/ultracapacitor energy-storage sizing on battery lifetime in a fuel cell hybrid electric vehicle. *IEEE Transactions on Vehicular Technology*, 58(8):3882 –3891, October 2009.

[37] Ashley Kells and Oliver Jackson. Simulation of a fuel cell hybrid London taxi. Report / study, Intelligent Energy, The Innovation Centre, Lotus Engineering, 2009.

[38] Shinobu Sekine and Koichi Kojima. Progress and challenges in Toyota's fuel cell vehicle development. Technical report, SAE, October 2011.

[39] Peter Fisher, John Jostins, Stuart Hilmansen, and Kevin Kendall. Electronic integration of fuel cell and battery system in novel hybrid vehicle. *Journal of Power Sources*, 220(0):114 – 121, 2012.

[40] Mehdi Ansarey, Masoud Shariat Panahi, Hussein Ziarati, and Mohammad Mahjoob. Optimal energy management in a dual-storage fuel-cell hybrid vehicle using multi-dimensional dynamic programming. *Journal of Power Sources*, 250:359 – 371, 2014.

[41] K.B. Wipke, M.R. Cuddy, and S.D. Burch. ADVISOR 2.1: A user-friendly advanced powertrain simulation using a combined backward/forward approach. *IEEE Transactions on Vehicular Technology*, 48(6):1751 –1761, November 1999.

[42] Valerie H. Johnson, Keith B. Wipke, and David J. Rausen. Hev control strategy for real-time optimization of fuel economy and emissions. Technical Report 2000-01-1543, SAE, 2000.

[43] B.M. Baumann, G. Washington, B.C. Glenn, and G. Rizzoni. Mechatronic design and control of hybrid electric vehicles. *Mechatronics, IEEE/ASME Transactions on*, 5(1):58–72, Mar 2000.

[44] I. Kolmanovsky, I. Siverguina, and B. Lygoe. Optimization of powertrain operating policy for feasibility assessment and calibration: Stochastic dynamic programming approach. In *Proceedings of the 2002 American Control Conference*, volume 2, pages 1425–1430, 2002.

[45] Chan-Chiao Lin, Huei Peng, J. W. Grizzle, Jason Liu, and Matt Busdiecker. Control system development for an advanced-technology medium-duty hybrid electric truck. Technical Report 2003-01-3369, SAE, 2003.

[46] Chan-Chiao Lin, Huei Peng, J.W. Grizzle, and Jun-Mo Kang. Power management strategy for a parallel hybrid electric truck. *IEEE Transactions on Control Systems Technology*, 11(6):839 – 849, November 2003.

[47] Chan-Chiao Lin, Huei Peng, and J.W. Grizzle. A stochastic control strategy for hybrid electric vehicles. In *Proceedings of the 2004 American Control Conference*, volume 5, pages 4710 –4715, July 2004.

[48] A. Sciarretta and L. Guzzella. Control of hybrid electric vehicles: Optimal energy management strategies. *IEEE Control Systems*, 27(2):60–70, 2007.

[49] F.R. Salmasi. Control strategies for hybrid electric vehicles: Evolution, classification, comparison, and future trends. *Vehicular Technology, IEEE Transactions on*, 56(5):2393–2404, Sept 2007.

[50] P. Pisu and G. Rizzoni. A comparative study of supervisory control strategies for hybrid electric vehicles. *Control Systems Technology, IEEE Transactions on*, 15(3):506–518, May 2007.

[51] L. Johannesson, M. Asbogard, and B. Egardt. Assessing the potential of predictive control for hybrid vehicle powertrains using stochastic dynamic programming. *IEEE Transactions on Intelligent Transportation Systems*, 8(1):71–83, 2007.

[52] Edward Dean Tate, Jessy W. Grizzle, and Huei Peng. Shortest path stochastic control for hybrid electric vehicles. *International Journal of Robust and Nonlinear Control*, 18(14):1409–1429, 2008.

[53] D.F. Opila, D. Aswani, R. McGee, J.A. Cook, and J.W. Grizzle. Incorporating drivability metrics into optimal energy management strategies for hybrid vehicles. In *Decision and Control, 2008. CDC 2008. 47th IEEE Conference on*, pages 4382–4389, Dec 2008.

[54] S. Kermani, S. Delprat, R. Trigui, and T.-M. Guerra. Predictive energy management of hybrid vehicle. In *Vehicle Power and Propulsion Conference*, pages 1–6, 2008.

[55] Georgios Fontaras, Panayotis Pistikopoulos, and Zissis Samaras. Experimental evaluation of hybrid vehicle fuel economy and pollutant emissions over real-world simulation driving cycles. *Atmospheric Environment*, 42(18):4023 – 4035, 2008.

[56] Pei-zhi Zhang, Cheng-liang Yin, Yong Zhang, and Zhi-wei Wu. Optimal energy management for a complex hybrid electric vehicle: Tolerating power-loss of motor. *Journal of Shanghai Jiaotong University (Science)*, 14:476–481, 2009.

[57] Anthony M. Phillips, Ryan A. McGee, J. Tony Lockwood, Ray A. Spiteri, Judy Che, John R. Blankenship, and Ming L. Kuang. Control system development for the dual drive hybrid system. *SAE International Journal of Engines*, 2(1):114–122, 2009.

[58] Lars Johannesson, Stefan Pettersson, and Bo Egardt. Predictive energy management of a 4QT series-parallel hybrid electric bus. *Control Engineering Practice*, 17(12):1440 – 1453, 2009.

[59] G. Ripaccioli, D. Bernardini, S. Di Cairano, A. Bemporad, and I.V. Kolmanovsky. A stochastic model predictive control approach for series hybrid electric vehicle power management. In *American Control Conference*, pages 5844–5849, 2010.

[60] Marco Sorrentino, Gianfranco Rizzo, and Ivan Arsie. Analysis of a rule-based control strategy for on-board energy management of series hybrid vehicles. *Control Engineering Practice*, 19(12):1433 – 1441, 2011.

[61] A. Chasse and A. Sciarretta. Supervisory control of hybrid powertrains: An experimental benchmark of offline optimization and online energy management. *Control Engineering Practice*, 19(11):1253 – 1265, 2011.

[62] F. Vidal-Naquet and G. Zito. Adapted optimal energy management strategy for drivability. In *Vehicle Power and Propulsion Conference (VPPC), 2012 IEEE*, pages 358–363, Oct 2012.

[63] Hongtao Zhang, Yanzhou Qin, Xianguo Li, and Xinzhi Liu. Driver-oriented optimization of power management in plug-in hybrid electric vehicles. In *EIC Climate Change Technology Conference 2013*, number 1569730735 in CCTC 2013, pages 1–12, 2013.

[64] S.J. Moura, J.L. Stein, and H.K. Fathy. Battery-health conscious power management in plug-in hybrid electric vehicles via electrochemical modeling and stochastic control. *Control Systems Technology, IEEE Transactions on*, 21(3):679–694, May 2013.

[65] Ganesh Mohan, Francis Assadian, and Stefano Longo. An optimization framework for comparative analysis of multiple vehicle powertrains. *Energies*, 6(10):5507–5537, 2013.

[66] S. Di Cairano, Wei Liang, I.V. Kolmanovsky, M.L. Kuang, and A.M. Phillips. Power smoothing energy management and its application to a series hybrid powertrain. *IEEE Transactions on Control Systems Technology*, 21(6):2091–2103, 2013.

[67] Clement Dextreit and Ilya V. Kolmanovsky. Game theory controller for hybrid electric vehicles. *IEEE Transactions on Control Systems Technology*, 22(99):652–663, April 2013.

[68] Frederick G. Harmon, Andrew A. Frank, and Sanjay S. Joshi. The control of a parallel hybrid-electric propulsion system for a small enmanned aerial vehicle using a cmac neural network. *Neural Networks*, 18(5-6):772 – 780, 2005.

[69] J. Sun and I.V. Kolmanovsky. Load governor for fuel cell oxygen starvation protection: a robust nonlinear reference governor approach. *Control Systems Technology, IEEE Transactions on*, 13(6):911–920, Nov 2005.

[70] Phatiphat Thounthong, Stephane Raël, and Bernard Davat. Energy management of fuel cell/battery/supercapacitor hybrid power source for vehicle applications. *Journal of Power Sources*, 193(1):376 – 385, 2009.

[71] Min-Joong Kim and Huei Peng. Power management and design optimization of fuel cell/battery hybrid vehicles. *Journal of Power Sources*, 165(2):819 – 832, 2007.

[72] Ying Wu and Hongwei Gao. Optimization of fuel cell and supercapacitor for fuel-cell electric vehicles. *IEEE Transactions on Vehicular Technology*, 55(6):1748 –1755, November 2006.

[73] J. Bauman and M. Kazerani. A comparative study of fuel-cell-battery, fuel-cell-ultracapacitor, and fuel-cell-battery-ultracapacitor vehicles. *IEEE Transactions on Vehicular Technology*, 57(2):760 –769, March 2008.

[74] Delphine Sinoquet, Gregory Rousseau, and Yohan Milhau. Design optimization and optimal control for hybrid vehicles. *Optimization and Engineering*, 12:199–213, 2011.

[75] Xiao-Zi Yuan, Hui Li, Shengsheng Zhang, Jonathan Martin, and Haijiang Wang. A review of polymer electrolyte membrane fuel cell durability test protocols. *Journal of Power Sources*, 196(22):9107 – 9116, 2011.

[76] Jay T. Pukrushpan, Huei Peng, and Anna G. Stefanopoulou. *Control of Fuel Cell Power Systems*. Springer, 2008.

[77] Shengsheng Zhang, Xiaozi Yuan, Haijiang Wang, Walter Mérida, Hong Zhu, Jun Shen, Shaohong Wu, and Jiujun Zhang. A review of accelerated stress tests of MEA durability in PEM fuel cells. *International Journal of Hydrogen Energy*, 34(1):388 – 404, 2009.

[78] Latevi Placca and Raed Kouta. Fault tree analysis for PEM fuel cell degradation process modelling. *International Journal of Hydrogen Energy*, 36(19):12393 – 12405, 2011.

[79] J.T. Pukrushpan, A.G. Stefanopoulou, and Huei Peng. Control of fuel cell breathing. *Control Systems, IEEE*, 24(2):30–46, Apr 2004.

[80] D. Liu and S. Case. Durability study of proton exchange membrane fuel cells under dynamic testing conditions with cyclic current profile. *Journal of Power Sources*, 162(1):521 – 531, 2006.

[81] Yuyan Shao, Geping Yin, and Yunzhi Gao. Understanding and approaches for the durability issues of Pt-based catalysts for PEM fuel cell. *Journal of Power Sources*, 171(2):558 – 566, 2007.

[82] Wolfgang Schmittinger and Ardalan Vahidi. A review of the main parameters influencing long-term performance and durability of PEM fuel cells. *Journal of Power Sources*, 180(1):1 – 14, 2008.

[83] Jinfeng Wu, Xiao-Zi Yuan, Jonathan J. Martin, Haijiang Wang, Daijun Yang, Jinli Qiao, and Jianxin Ma. Proton exchange membrane fuel cell degradation under close to open-circuit conditions: Part i: In situ diagnosis. *Journal of Power Sources*, 195(4):1171 – 1176, 2010.

[84] Suk Joo Bae, Seong-Joon Kim, Jong In Park, Chan Woong Park, Jin-Hwa Lee, Inseob Song, Naesung Lee, Ki-Bum Kim, and Jun-Young Park. Lifetime prediction of a polymer electrolyte membrane fuel cell via an accelerated startup/shutdown cycle test. *International Journal of Hydrogen Energy*, 37(12):9775 – 9781, 2012.

[85] V.B. Avakov, V.A. Bogdanovskaya, A.V. Kapustin, O.V. Korchagin, A.V. Kuzov, I.K. Landgraf, M.M. Stankevich, and M.R. Tarasevich. Lifetime prediction for the hydrogen-air fuel cells. *Russian Journal of Electrochemistry*, 51(6):570–586, 2015.

[86] P. Thounthong, V. Chunkag, P. Sethakul, B. Davat, and M. Hinaje. Comparative study of fuel-cell vehicle hybridization with battery or supercapacitor storage device. *IEEE Transactions on Vehicular Technology*, 58(8):3892 –3904, October 2009.

[87] Haroune Aouzellag, Kaci Ghedamsi, and Djamel Aouzellag. Energy management and fault tolerant control strategies for fuel cell/ultra-capacitor hybrid electric vehicles to enhance autonomy, efficiency and life time of the fuel cell system. *International Journal of Hydrogen Energy*, 40(22):7204 – 7213, 2015.

[88] Jay T. Pukrushpan, Huei Peng, and Anna G. Stefanopoulou. Control-oriented modeling and analysis for automotive fuel cell systems. *Journal of Dynamic Systems, Measurement, and Control*, 126(1):14–25, 2004.

[89] Liangfei Xu, Jianqiu Li, Minggao Ouyang, Jianfeng Hua, and Geng Yang. Multi-mode control strategy for fuel cell electric vehicles regarding fuel economy and durability. *International Journal of Hydrogen Energy*, 39(5):2374 – 2389, 2014.

[90] Gustav Boehm, David P Wilkinson, Shanna Knights, Reinhold Schamm, and Nicholas J Fletcher. Method and apparatus for operating a fuel cell, October 8 2002. US Patent 6,461,751.

[91] M.A. Roscher, J. Assfalg, and O.S. Bohlen. Detection of utilizable capacity deterioration in battery systems. *IEEE Transactions on Vehicular Technology*, 60(1):98 –103, January 2011.

[92] K. Nakamura, M. Shiomi, K. Takahashi, and M. Tsubota. Failure modes of valve-regulated lead acid batteries. *Journal of Power Sources*, 59:153 – 157, 1996.

[93] J. Vetter, P. Novak, M.R. Wagner, C. Veit, K.-C. Moller, J.O. Besenhard, M. Winter, M. Wohlfahrt-Mehrens, C. Vogler, and A. Hammouche. Ageing mechanisms in lithium-ion batteries. *Journal of Power Sources*, 147:269 – 281, 2005.

[94] Scott B. Peterson, Jay Apt, and J.F. Whitacre. Lithium ion battery cell degradation resulting from realistic vehicle and vehicle-to-grid utilization. *Journal of Power Sources*, 195(8):2385 – 2392, 2010.

[95] Yancheng Zhang, Chao-Yang Wang, and Xidong Tang. Cycling degradation of an automotive LiFePO4 lithium-ion battery. *Journal of Power Sources*, 196(3):1513 – 1520, 2011.

[96] C. Vagg, S. Akehurst, C. J. Brace, and L. Ash. Stochastic dynamic programming in the real-world control of hybrid electric vehicles. *IEEE Transactions on Control Systems Technology*, PP(99):1–14, 2016.

[97] R. Boris, C. Vermillion, and K. Butts. A comparative analysis of electronic pedal algorithms using a driver-in-the-loop simulator and system identification of driver behavior. In *American Control Conference (ACC), 2010*, pages 682–687, June 2010.

[98] A. Brahma, Y. Guezennec, and G. Rizzoni. Optimal energy management in series hybrid electric vehicles. In *Proceedings of the 2000 American Control Conference*, number 6 in 2000 American Control Conference, pages 60–64, 2000.

[99] G. Paganelli, M. Tateno, A. Brahma, G. Rizzoni, and Y. Guezennec. Control development for a hybrid-electric sport-utility vehicle: strategy, implementation and field test results. In *American Control Conference, 2001. Proceedings of the 2001*, volume 6, pages 5064–5069 vol.6, 2001.

[100] Cristian Musardo, Giorgio Rizzoni, Yann Guezennec, and Benedetto Staccia. A-ECMS: An adaptive algorithm for hybrid electric vehicle energy management. *European Journal of Control*, 11(4-5):509 – 524, 2005.

[101] USDOT-FHWA. National household travel survey, Washington, DC. http://nhts.ornl.gov/index.shtml, Accessed 07/2014, 2009.

[102] Jonathon Mansell. Testing and modelling the microcab. 2012.

[103] Ritchie Daniel, Thomas Brooks, and David Pates. Analysis of US and EU drive styles to improve understanding of market usage and the effects on OBD monitor IUMPR. Technical Report 2009-01-0236, SAE Technical Paper, 2009.

[104] Harry Charles Watson. Vehicle driving patterns and measurement methods for energy and emissions assessment. Technical report, Bureau of Transport Economics, Canberra, 1978.

[105] Michel André. The ARTEMIS european driving cycles for measuring car pollutant emissions. *Science of The Total Environment*, 334-335:73 – 84, 2004. Highway and Urban Pollution.

[106] Ballard Power Systems Inc. *Nexa (310-0027) Power Module User's Manual*, June 2003.

[107] U.S. Department of Energy's Office of Energy Efficiency and Renewable Energy (EERE). The fuel cell technologies program multi-year research, development, and demonstration plan (MYRD&D plan), 2016.

[108] Yun Wang, Ken S. Chen, Jeffrey Mishler, Sung Chan Cho, and Xavier Cordobes Adroher. A review of polymer electrolyte membrane fuel cells: Technology, applications, and needs on fundamental research. *Applied Energy*, 88(4):981 – 1007, 2011.

[109] Phatiphat Thounthong, Viboon Chunkag, Panarit Sethakul, Suwat Sikkabut, Serge Pierfederici, and Bernard Davat. Energy management of fuel cell/solar cell/supercapacitor hybrid power source. *Journal of Power Sources*, 196(1):313–324, 2011.

Appendix A

Drive-cycle Trip Analysis Plots

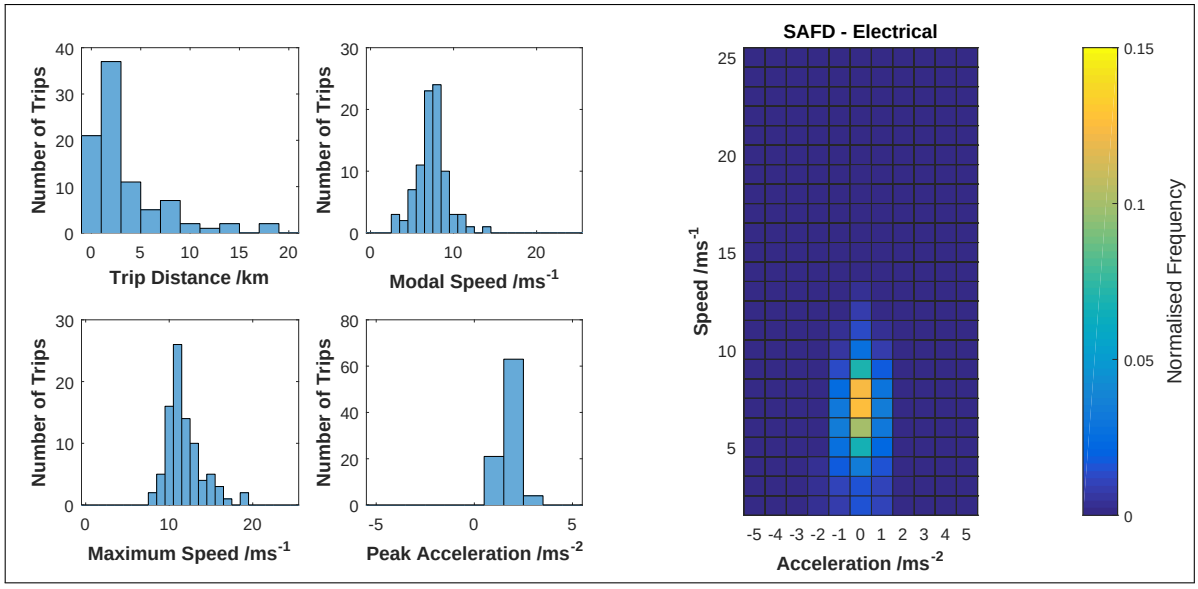

Figure A.1: Loughborough Electrical Trip Analysis

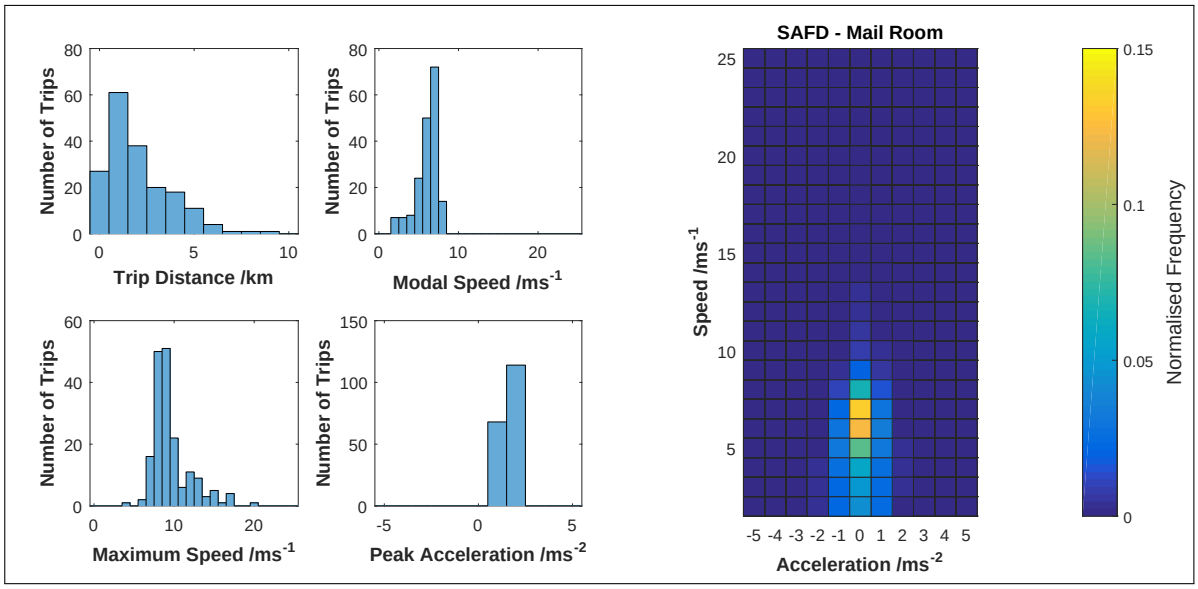

Figure A.2: Loughborough Mail Room Trip Analysis

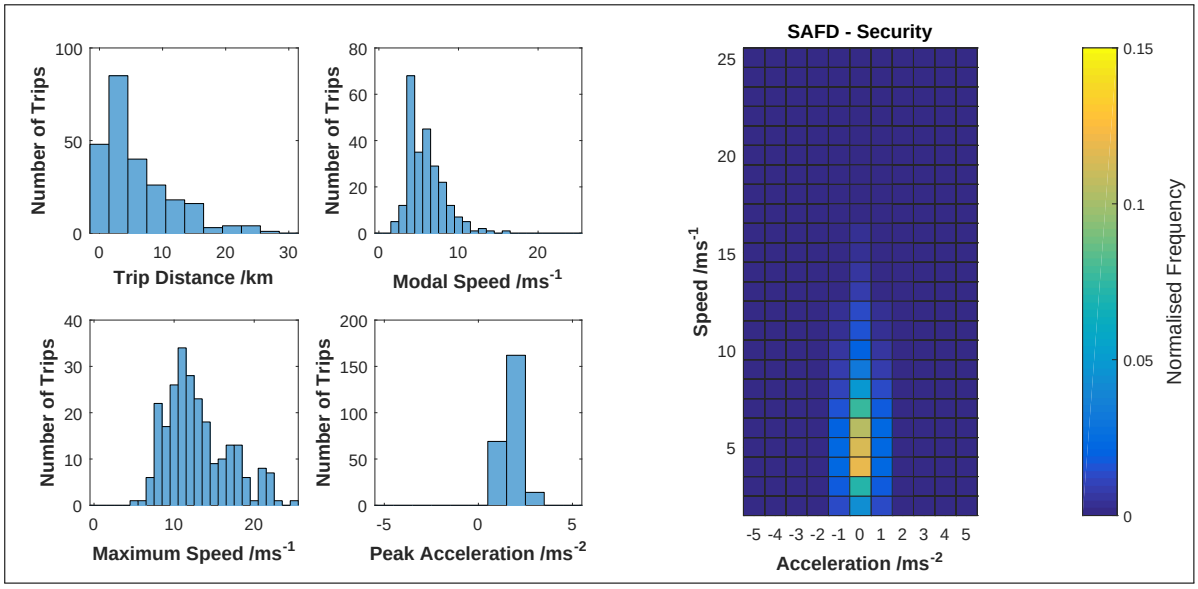

Figure A.3: Loughborough Security Trip Analysis

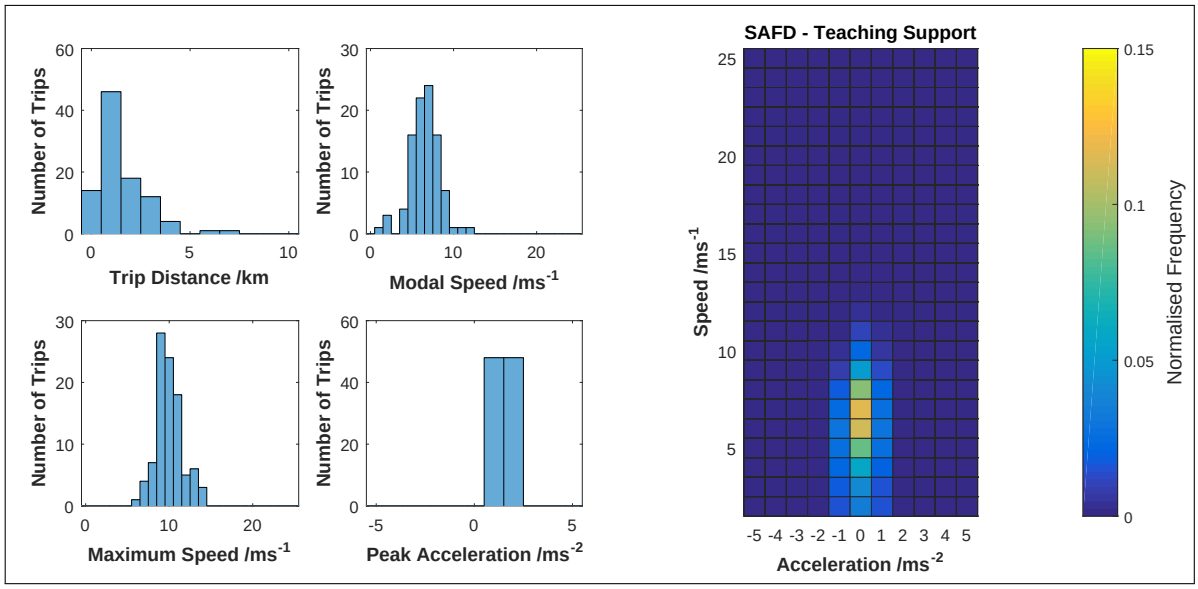

Figure A.4: Loughborough Teaching Support Trip Analysis

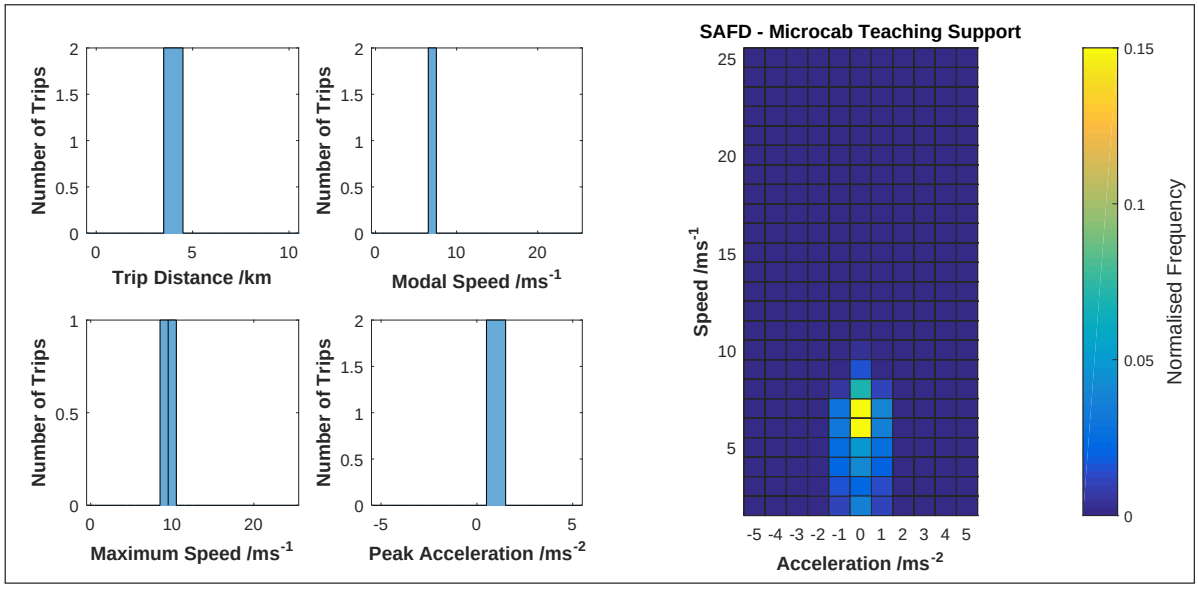

Figure A.5: Microcab Teaching Support Trip Analysis

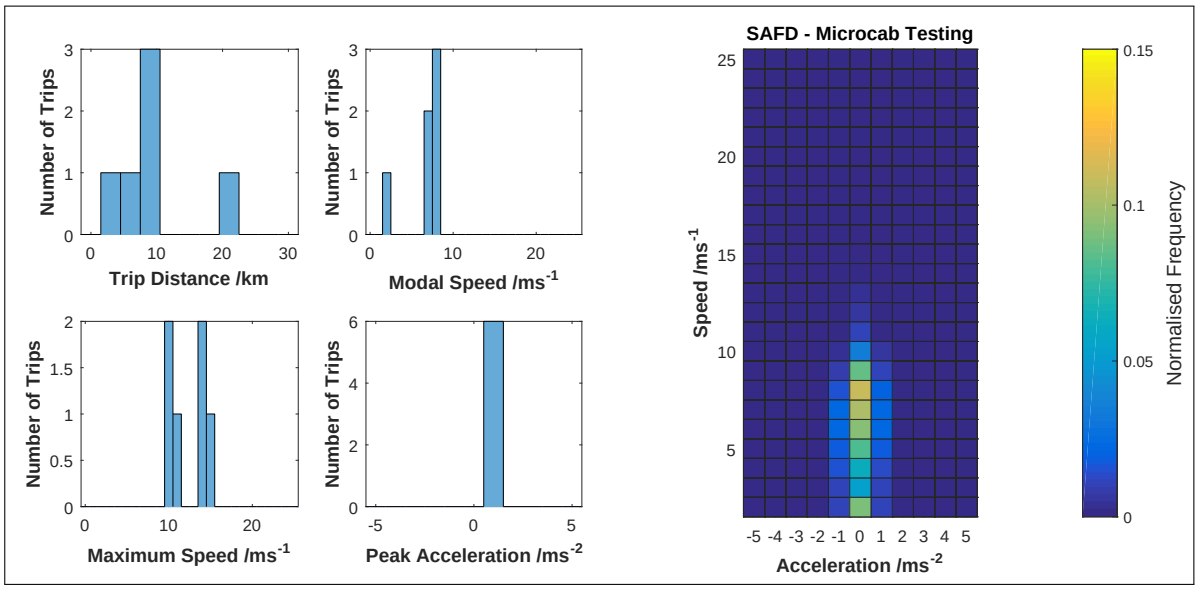

Figure A.6: Microcab Testing Trip Analysis